



Cessna Aircraft Company Raytheon Missile Systems AIAA Foundation

The 2011 Cessna Aircraft Company/Raytheon Missile Systems Design/Build/Fly Competition Flyoff was held at TIMPA Field in Tucson, AZ on the weekend of April 15-17, 2011. This was the 15th year the competition was held. Of the record 94 entries this year, 82 teams submitted written reports to be judged. 70 teams attended the flyoff, all of which completed the technical inspection. Over 700 students, faculty, and guests were present. The weather was sunny and warm allowing for non-stop flying. Of the 207 official flight attempts, 133 resulted in a successful score divided among 55 teams. Thirty-three teams successfully completed all three missions. The quality of the teams, their readiness to compete, and the execution of the flights continues to improve each year. This year's requirement to pre-inspect the airplanes with an advisor before the competition sped up the technical inspections and expedited teams getting to a flight attempt.

The contest theme this year was a Soldier Portable UAV. The airplane had to fit in a commercially available suitcase meeting airline carry-on requirements. The first mission was a "dash to critical target" with no payload followed by an Ammo Re-supply mission (steel bar payload) and a Medical Supply mission (golf balls). As usual, the total score is the product of the flight score and written report score. More details on the mission requirements can be found at the competition website: <http://www.aiaadb.org>.

First Place went to Georgia Tech University Team *ThereWillBeBuzz*, Second Place went to University of Southern California Team *The RFB* and Third Place went to Purdue University Team *Golfstream*. A full listing of the results is included below. The Best Paper Award, sponsored by the Design Engineering TC for the highest report score, went to Technion University Team *GolfiTech* with a score of 98.50.

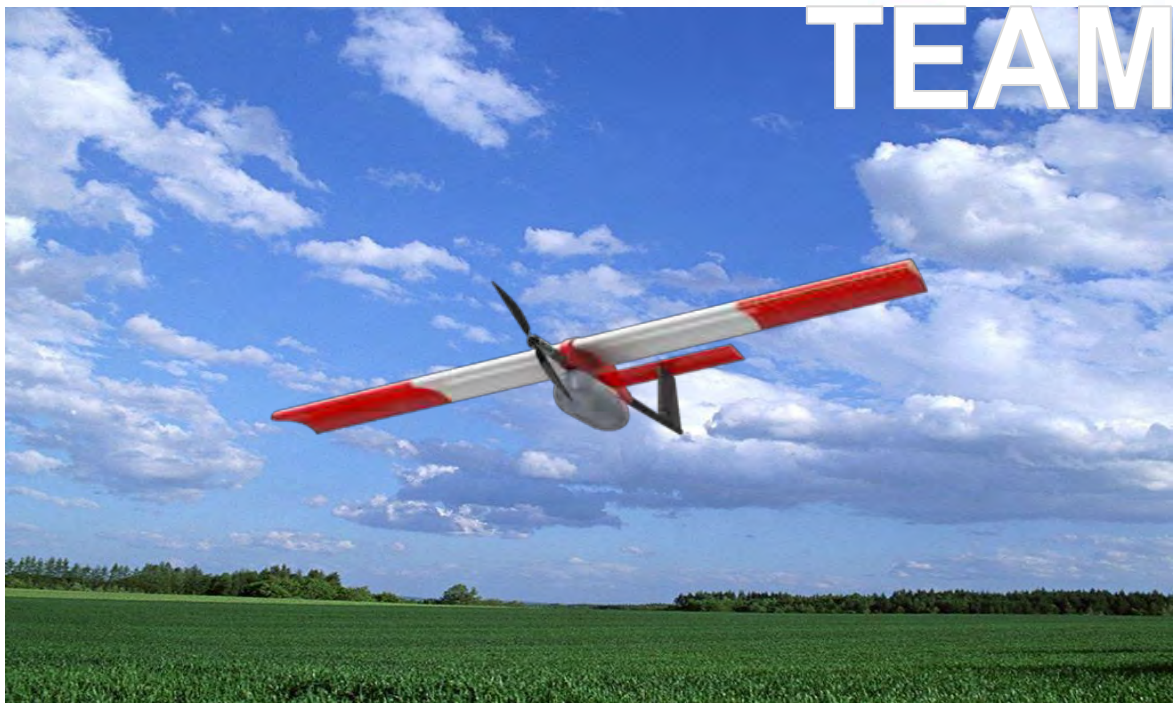
We owe our thanks for the success of the DBF competition to the efforts of many volunteers from Cessna Aircraft, Raytheon Missile Systems, and the AIAA sponsoring technical committees: Applied Aerodynamics, Aircraft Design, Flight Test, and Design Engineering. These volunteers collectively set the rules for the contest, publicize the event, gather entries, judge the written reports, and organize the flyoff. Thanks also go to the corporate Sponsors: Raytheon Missile Systems and Cessna Aircraft Company, and also to the AIAA Foundation for their financial support. Special thanks go to Raytheon Missile Systems for hosting the flyoff this year.

Finally, this event would not be nearly as successful without the hard work and enthusiasm from all the students and advisors. If it weren't for you, we wouldn't keep doing it.

Russ Althof
For the DBF Governing Committee

Technion - Israel Institute of Technology

G IfiTech



Design/Build/Fly 2011

Table of Contents

| | |
|---|-----------|
| 1. Executive Summary | 3 |
| 2. Management Summary | 4 |
| 2.1 Organization of the design team: | 4 |
| 2.2 Design personnel and assignment areas:..... | 5 |
| 2.3 Working plan | 6 |
| 3. Conceptual Design | 7 |
| 3.1 Mission requirements | 7 |
| 3.2 Design requirements deriving from mission requirements..... | 9 |
| 3.3 Solution concepts/configurations considered..... | 10 |
| 3.4 Concept weighting, selection process and results | 11 |
| 4. Preliminary Design | 15 |
| 4.1 Design/analysis methodology | 15 |
| 4.2 Design/sizing trade offs..... | 16 |
| 4.3 Mission model | 16 |
| 4.4 Aircraft estimated lift, drag and stability characteristics | 17 |
| 4.5 Propulsion | 22 |
| 4.6 Aircraft mission performance | 25 |
| 5. Detailed Design | 26 |
| 5.1 Dimensional parameters | 27 |
| 5.2 Structural characteristics / capabilities..... | 27 |
| 5.3 Systems and sub-systems design, component selection, integration and architecture | 28 |
| 5.4 Weight and balance | 31 |
| 5.5 Flight performance parameters..... | 33 |
| 5.6 Mission performance..... | 33 |
| 5.7 Drawing Package | 35 |
| 6. Manufacturing Plan and Processes | 41 |
| 6.1 Process selected for manufacture of major components and assemblies | 41 |
| 6.2 Manufacturing processes selection..... | 44 |
| 6.3 Manufacturing work plan | 47 |
| 7. Testing Plan | 47 |
| 7.1 Objectives..... | 47 |
| 7.2 Test Schedule and check list | 51 |
| 8. Performance Results | 52 |
| 8.1 Performance of key subsystems | 52 |
| 8.2 Performance of the complete aircraft..... | 55 |
| 9. Bibliography | 59 |

1. Executive Summary

It was a great challenge to participate in the Design/Build/Fly competition. For all team members it was the first time to be part of an aircraft evolution process, from design and up to flight tests. This report describes the whole process beginning with the competition rules publication and up to flight tests.

The objective of this year's competition was to simulate a small, light, soldier assistance UAV. Initially the competition rules were carefully studied, in order to determine the effect of different aircraft aspects on the score. This revealed that the payload weight has the biggest effect. Hence the design process aimed for payload maximization. The team decided to use all available space in the suitcase, and design a modular aircraft that will have to be assembled on site. The aircraft was designed to be statically stable, hence it had a conventional geometry of main wing, and back tail. Due to hand launch, the aircraft had to use landing gear only upon landing. In order to reduce weight, as it strongly affected the score, the team decided to eliminate the need for landing gear by designing the bottom of the aircraft to absorb impact energy allowing the aircraft to land safely on its belly.

The aircraft's main structure was based on carbon fiber tubes, which have the highest strength to weight ratio. The main wing had a carbon fiber tubular spar as well. This makes it both light and simple to assemble. The payload compartment was built as a separate structure, which was not part of the aircraft body. This specific design allowed easy aircraft loading with its third mission payloads.

This year's competition includes three different missions. In each mission the aircraft will be judged by different parameters.

The first mission scores the speed and maneuverability of the aircraft. Many laps have to be flown around the flight path, including a full outside 360 degrees turn. In order to ease maneuverability, the center of gravity of the empty aircraft was placed closer to the neutral point, enabling the aircraft to enter faster into the turns. In order to fly as fast as possible, a suitable propeller was chosen, providing the best efficiency at high speeds.

However, the aircraft was not designed for high airspeeds, but for high lifting capabilities, as more points could be collected during the payload missions.

The second mission scores the ratio between payload weight and the empty aircraft weight. Design and construction of a light aircraft enables the lifting of relatively heavy payloads, weighing about the same as the whole aircraft.

The third mission is very similar to the second, as in this mission also a heavy payload has to be carried. The most significant design goal for increasing lifting abilities is the stall speed. As the aircraft has no runway, in order to gain sufficient speed, it must be able fly at hand launch speed. Not only is the hand launch airspeed low, the thrower has to release the aircraft in a

controlled manner, avoiding wing stall, thus reducing the launch speed even more. In order to overcome this problem, especial care was given both to profile selection and to wing area maximization. Moreover, mounting a suitable propeller able to accelerate the aircraft beyond the stall speed limit very rapidly, should reduce launch crash danger.

The designed aircraft is able to lift 3.8 lb, approximately 43% of its maximum takeoff weight. The aircraft should be able to fly when fully loaded, complete three laps around the flight path and complete the payload missions without running out of battery. The airplane's payload compartment is designed to carry 28 golf balls, and 3.75 lb square metal bar.

The maximum airspeed that can be achieved when flown without payloads is 80 ft/sec, and the cruise speed of this configuration is 75 ft/sec, enabling completion of almost seven laps in 4 minutes. Although the aircraft has so far demonstrated very good performance and can successfully complete all three missions, more improvements will be added to the design in order to lighten the next two planned aircraft. Lighter aircraft will enable the loading of a heavier metal bar and increase golf balls number, thus increasing the flight score.

2. Management Summary

2.1 Organization of the design team:

From experience a multiplicity of opinions generally contributes to better engineering solutions. Therefore, the team decided to assign more than one person to almost every design area of the project. Due to lack of manpower, every person took part in more than one design area.

The team divided the aircraft design into 7 sub areas listed in Fig. 1. In addition, there were three management positions, which were also performed by team members: ordering parts, budget monitoring and writing reports.

2.2 Design personnel and assignment areas:

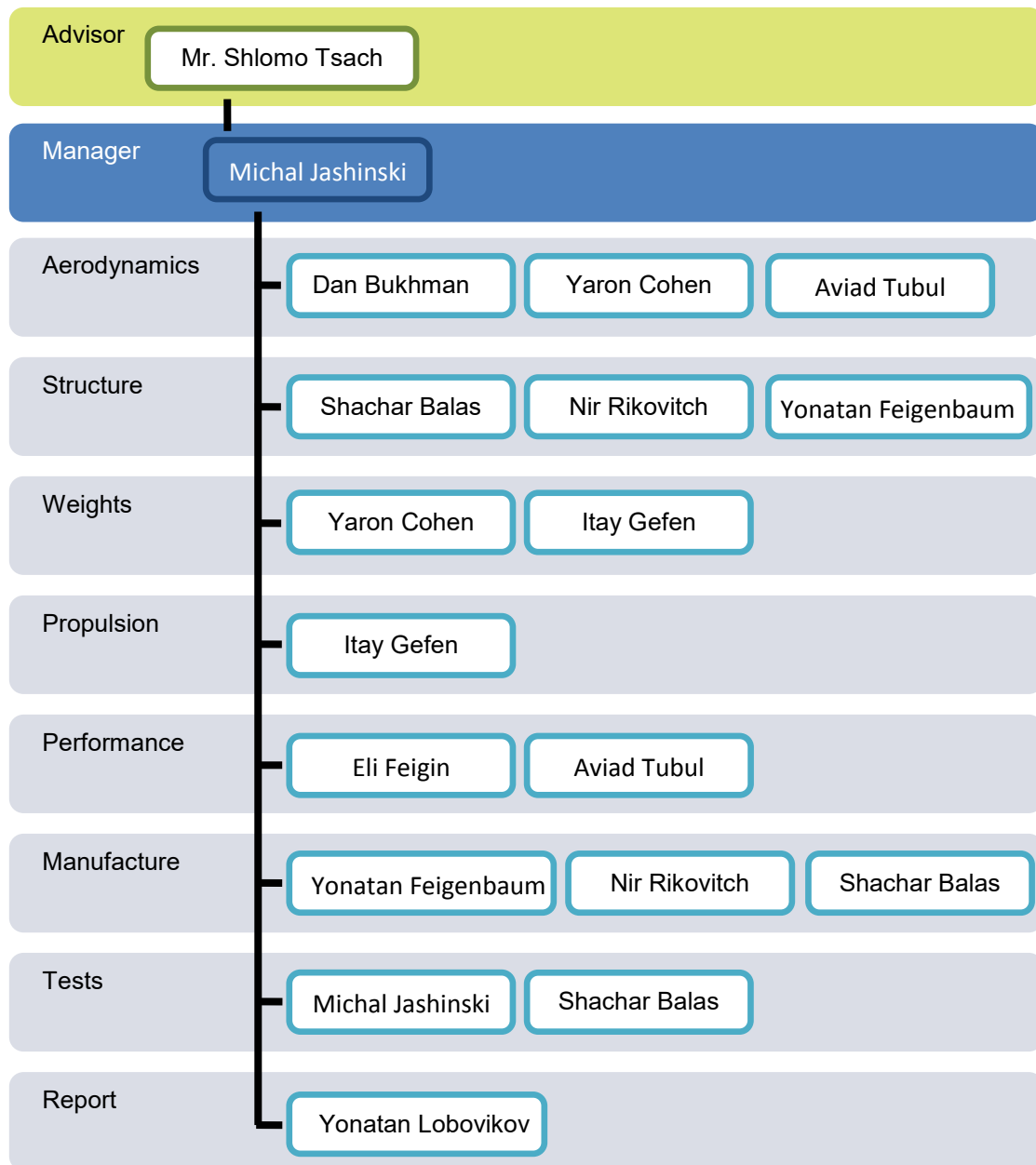


Figure 1: Design team organization.

2.3 Working plan

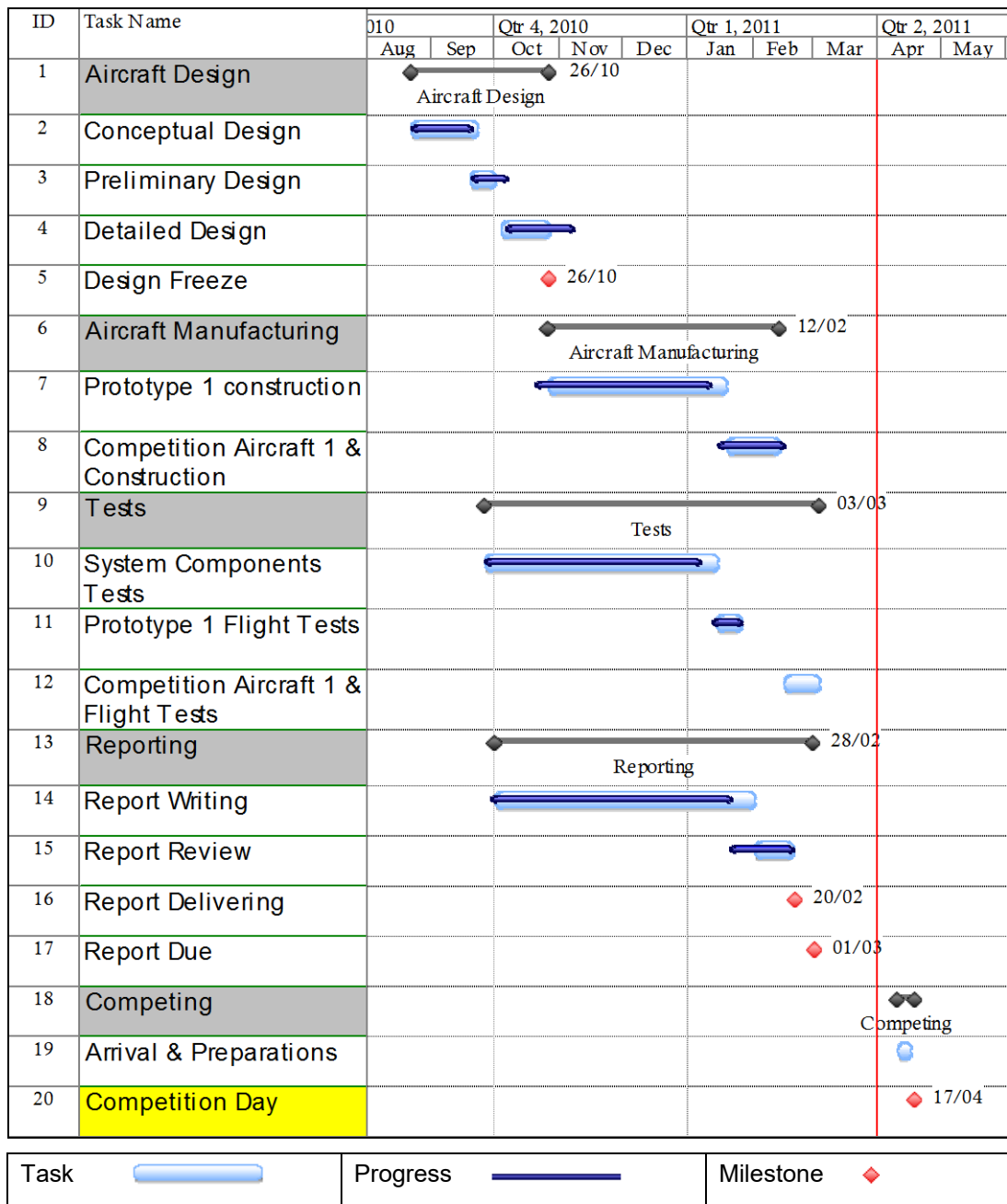


Figure 2: Design progress schedule.

3. Conceptual Design

At this early stage of design the team learned the rules, and converted them into design requirements by calculating the most suitable design parameters in order to increase the total score. Afterwards, a few different geometrical configurations were investigated, and the best aircraft configuration was selected. The conceptual design did not deal with exact aircraft dimensions as these were calculated at later stages of the design process.

3.1 Mission requirements

This year's competition simulates a real life scenario of soldiers in the field needing a quick resupply of ammunition and medical support. The missions and restraints of the present year represent different aspects of a suitable military assistance aircraft:

- Aircraft to be carried in a bag by the soldier.
- No need for runway to launch.
- Aircraft that can lift payloads with substantial weight and volume relative to its own weight.
- Rapid deployment of the payloads.

Any aircraft built to participate in the competition and perform the missions must be designed under the following restraints:

- The aircraft must be packed into a commercially produced suitcase whose total dimensions of length, width and height does not exceed 45 inches.
- The aircraft must be extracted from the case, and mounted at the launch site within less than 5 minutes, by only one individual.
- The aircraft must be electrically powered and the electrical current must not exceed 20 amps. Also, the batteries supplying the power must be of a NiCad or NiMH type, and weigh no more than 9 oz.
- Prior to the flight, the aircraft must withstand a safety test to be conducted by lifting the whole plane structure from its main wing tips.

After preflight inspection test approval, the UAV has to fly around the course according to the geometry shown in Fig. 3 for all three missions.

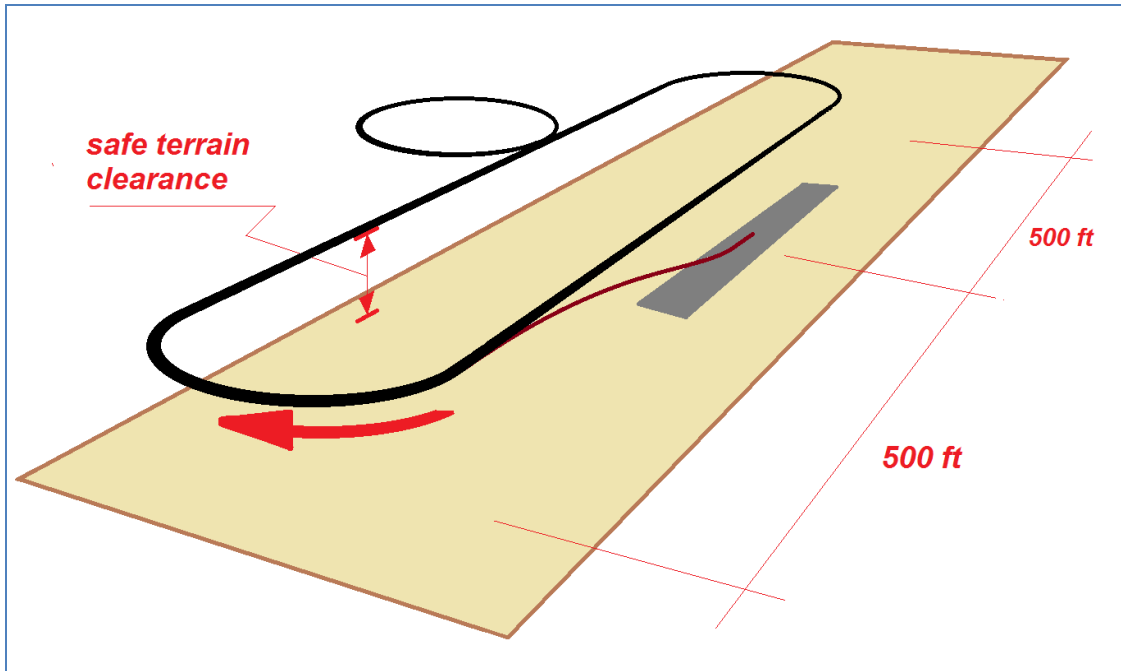


Figure 3: Flight course.

The required missions and objectives for this year's competition are described at Table 1:

| Mission | Mission Objective | Mission description |
|------------------------------------|--------------------------------------|--|
| Mission 1: Dash to critical target | Test UAV speed | Complete as many laps as possible during a 4 minute flight time |
| Mission 2 - Ammo Re-Supply | Test UAV payload weight to RAC ratio | Complete 3 laps carrying a heavy metal bar of given minimum dimensions |
| Mission 3 - Medical Supply | Test UAV payload capabilities | Complete 3 laps carrying as many golf balls as possible |

Table 1: Description of missions

The contest score for this year is:

$$Total\ score = \frac{\text{report score}}{\sqrt{RAC}} \left[\frac{N}{N_{\max}} + 3 \frac{W_p}{W_0} + 2 \frac{N_{ball}}{N_{ball_{\max}}} \right]$$

Where:

- RAC - maximum of empty weights measured after each successful scoring flight
- N - number of complete laps performed by the team
- N_{\max} - maximum number of complete laps performed by any team
- W_p - payload weight
- W_0 - flight weight
- N_{ball} - number of golf balls flown by the team
- $N_{ball_{\max}}$ - maximum number of golf balls flown by any team

3.2 Design requirements deriving from mission requirements

The combined mission requirements of this contest dictate an aircraft designed for speed, efficiency and high payload-carrying ability.

- To successfully complete the first mission the aircraft must have the ability to fly sufficiently fast without any loads. Hence the main wing must have a profile of high aerodynamic efficiency for low lift coefficient. In addition, a propulsion system designed to produce high propulsive power at high airspeeds is required.
- To gain a high score for the second mission, the aircraft design must be light, but strong enough to be able to carry a heavy payload. Hand launch of the heavy loaded aircraft requires a peak thrust during launch, and a low stall speed that can be achieved with low wing loading, and airfoils designed for high lift production at low speeds.
- In addition to the 2nd mission requirements, the 3rd mission combines a heavy load with space demands. In order to accomplish this mission successfully, the baggage compartment of the airplane must be spacious enough to carry the balls, but carefully designed, in aspects of weight and drag reduction.

It would appear a few requirements contradict each other in some aspects, and the team had to consider where to prefer certain design parameters over others. In order to make the best decisions, some simple calculations were made, predicting the effect of every mission on the final score. The calculations assumed best figures achieved for the first and the third missions, and a simple correlation between gross weight and payload-carrying ability. As derived from Fig. 4, the plane able to lift the heaviest payload will significantly increase the total team score.

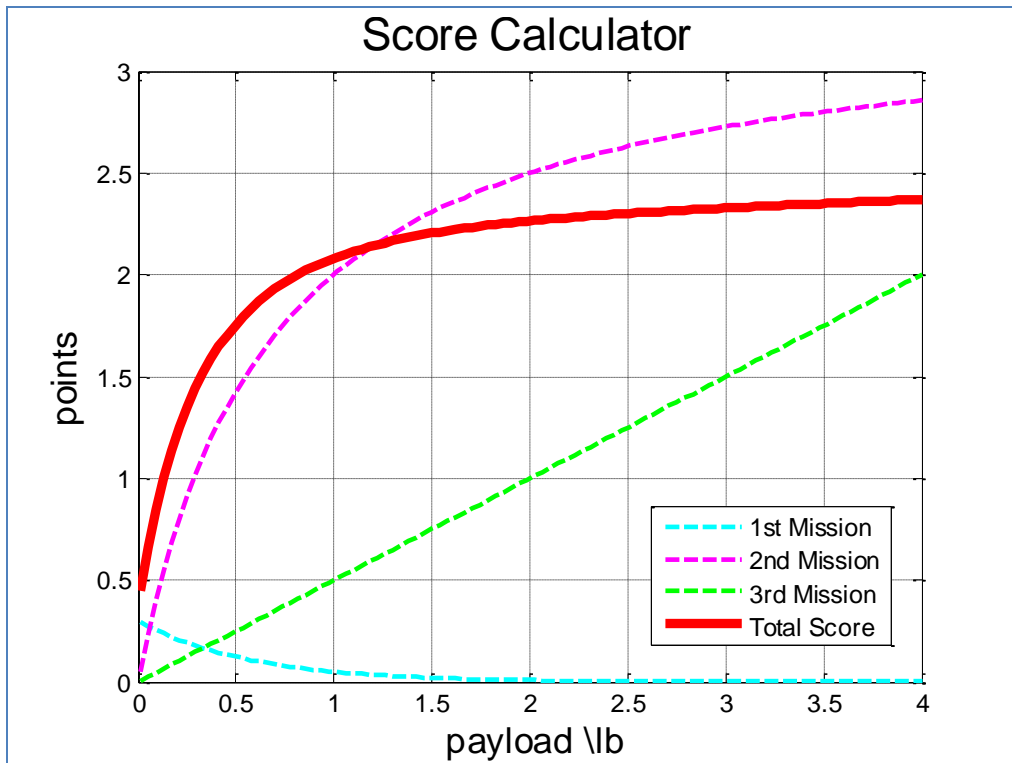


Figure 4: Score model.

3.3 Solution concepts/configurations considered

Four basic airframe configurations were considered in the design of the UAV. Every design was judged by 5 main characteristics: Empty system weight, liftability, manufacturability, stability and control, and aerodynamic performance. The team consisted of 10 people; hence manufacturing rated relatively low, together with stability and controllability of the vehicle that in the worst case scenario could be easily solved by electronic means. However, from the design requirements detailed above, derives that the score of the contest was affected greatly by the payload to RAC ratio, as from the RAC itself. Therefore those parameters affected the selection the most. Another criteria derived from the mission requirements was the ability to complete the

lap as fast as possible, hence the aerodynamic performance affected the comparison as well. The summation of the basic aircraft design appears in Table 2, where five was the best and one the worst.

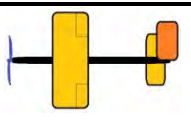
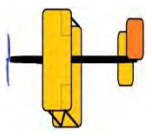
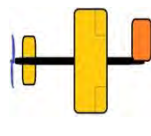
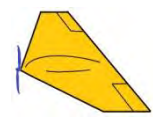
| Figure of Merit | Weight | Conventional | Biplane | Canard | Flying wing |
|-------------------------|--------|---|--|---|---|
| | |  |  |  |  |
| System weight | 0.3 | 3 | 2 | 3 | 4 |
| Liftability | 0.3 | 4 | 5 | 4 | 2 |
| Aerodynamic Performance | 0.2 | 5 | 4 | 2 | 4 |
| Stability and Control | 0.1 | 5 | 2 | 5 | 2 |
| Manufacturability | 0.1 | 4 | 3 | 4 | 2 |
| Total | 1 | 4 | 3.4 | 3.4 | 3 |

Table 2: Basic design configuration comparison.

From the comparison above the team chose to focus on designing a conventional shape UAV, as this appears to be the most suitable choice.

3.4 Concept weighting, selection process and results

After the general configuration of the airplane was determined, the team made a few decisions about the configurations of specific parts. The selection process was considered the most critical for the success of the design. Hence a long period of time was dedicated to this.

Moreover, in order to increase the score as much as possible, both aerodynamics and weight reduction affected configurations selection the most.

3.4.1 Payload area geometry and location

It was desirable to design the payload compartment in such a way that the CG location will not vary with different loadings of the airplane. At first, a decision had to be made about the geometric place of the payloads in the airplane. A few alternatives were investigated: baggage area inside the plane, or an outer pod, mounted beneath the airframe. Or a combination of two

small pods to reduce separation and turbulence drag was checked. In Table 3, four figures of merit were considered, where the most significant was the drag caused by the payload area, reducing speed limit, and the ability to grip and successfully launch the airplane.

| Figure of merit | weight | Inside the body | Central pod | Two symmetrical tanks |
|-------------------|--------|---|--|---|
| | |  |  |  |
| Drag | 0.4 | 5 | 4 | 3 |
| Modularity | 0.2 | 3 | 5 | 3 |
| Manufacturability | 0.1 | 4 | 5 | 3 |
| Ease of Launch | 0.3 | 4 | 5 | 2 |
| Total | 1 | 4.2 | 4.6 | 2.7 |

Table 3: Payload configuration decision matrix.

The best solution, although not from an aerodynamical point of view, but from consideration of all aspects was one central pod, which is highly modular, and the easiest to launch by hand.

Carrying the payload inside an external pod enables flexibility and modularity of the design by allowing future changes of the CG location and compartment size. A round sectioned cylindrical shape was chosen for the pod mainly because of manufacturing considerations. A front dome and a narrowing at the back of the pod were designed in order to reduce pressure drag, and lower the downstream turbulence. The main aspects of payload arrangements were:

- Total number of golf balls – the most spacious pod would be able to carry the highest number of golf balls. However, restricted by the suitcase for its length, the only variable that could change was its diameter.
- Drag – in opposition to the previous demand, a larger pod diameter created more pressure drag and downstream turbulence. As described earlier, proper design has to minimize the drag in order to gain a higher score for the first mission.
- Grip ability – in order to safely and successfully launch the airplane, the pod should enable good hand grip ability for the thrower during the launch. This is mainly affected by the pod outer diameter.
- Loading time – Although loading time does not affect the score directly, the assembly time limits do require a quick loading ability of the golf balls.

The payload arrangement considerations are summarized in Table 4:

| Figure of Merit | Weight | 3.3" | 3.6" | 4" | 4.7" |
|-----------------|--------|------|------|------|------|
| No. Golf Balls | 0.3 | 4 | 3 | 5 | 5 |
| Drag | 0.3 | 5 | 4 | 4 | 2 |
| Grip Ability | 0.25 | 4 | 4 | 3 | 2 |
| Loading Time | 0.15 | 2 | 4 | 4 | 4 |
| Total | 1 | 4 | 3.7 | 4.05 | 3.2 |

Table 4: Payload configuration decision matrix.

In conclusion, it was decided to place 4 balls in a profile, as the best compromise between drag reduction and number of golf balls carried.

3.4.2 Main wing geometry and location

Hand-Launch of the aircraft was the main reason for mounting the wing as high as possible on the fuselage in order to allow a comfortable grip of the UAV body near the CG while keeping a good clearance between the launchers head and the wing. Locating the wing above the CG also improved the lateral stability creating a pendulum effect.

A rectangular wing shape was chosen. This is considerably easier to manufacture though not ideal in terms of induced drag. The outer wing sections are designed with a small dihedral angle which improves the lateral stability.

Wing area was determined according to a Wing Loading parameter. The launch speed of the UAV appears to be below its stall speed, and the aircraft gains more speed while descending. Hence, it was important to lower the stall speed by keeping the wing loading relatively low.

Wing Aspect Ratio was determined according to aerodynamic issues and suitcase constraints. It was preferred to choose a high AR in order to optimize the airplanes aerodynamic efficiency, despite some spoiling of the liftability at low speeds.

3.4.3 Control surfaces geometry and location

Flaps and ailerons – in order to maximize the takeoff weight, the team decided to use flaps. It was decided to use the same control surfaces as ailerons and flaps, to be called flaperons. This

reduces the total number of control surfaces and servos, making the aircraft simpler, and lighter. Mixing the pilot inputs of flaps and ailerons adds a little complexity, but was resolved by adequately programming the transmitter.

The flaperons were located at the outward wing sections to increase the arm of the roll moment.

Tail - Three tail arrangements were considered from several aspects:

- Conventional Tail - simple, easy to build, and usually provides adequate stability and control with a light structure weight. However, one must consider its vulnerability during belly landings, possible loss of effectiveness due to wing wake effects and problematic clearance between the horizontal control surface and the thrower body during hand launch.
- V-Tail - overcomes the problems mentioned above, and also offers reduced wetted area. Nevertheless, the use of the same control surfaces as elevator and rudder involves some control actuation complexity. Additionally, moving the control surfaces toward one side to act as a rudder produces an undesirable rolling moment in opposition to the desired direction of turn.
- T-Tail - usually heavier, necessitating a sturdier vertical tail to structurally support the horizontal tail. However, it is simple to build and control, and also offers a few prominent advantages. Locating the horizontal surface upward diminishes the wing wake effects, increasing its effectiveness and allowing reduction of its size, hence its weight. Moreover, the horizontal surfaces high position prevents it from touching the ground during belly landings and guarantees a very good clearance from the thrower's upper body during hand launch.

As shown in Table 5, the T-Tail was chosen as the most appropriate design for the aircraft.

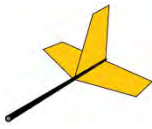
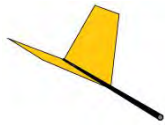
| Figure of Merit | Weight | Conventional | T-Tail | V-Tail |
|-----------------------|--------|---|--|---|
| | |  |  |  |
| Landing Durability | 0.25 | 2 | 5 | 5 |
| Launch Clearance | 0.25 | 2 | 5 | 3 |
| Weight | 0.20 | 5 | 3 | 5 |
| Stability and Control | 0.15 | 5 | 5 | 3 |
| Drag | 0.15 | 3 | 4 | 4 |
| Total | 1.00 | 3.2 | 4.45 | 4.05 |

Table 5: Tail design configurations summary.

3.4.4 Propeller location selection

Propeller location was mostly affected by aerodynamic and power considerations. However, other aspects like the safety of the person who launches the UAV affected the design as well. For example, a pusher propeller could reduce body drag, but would also be unsafe for use. The use of two propellers offers better ground clearance due to smaller diameter of the propellers. However, smaller propellers are generally less efficient, and the necessity to balance both propellers RPM adds complexity to the system. Another aspect was the propulsion system's weight. Using two propellers requires extra motor, a speed controller and additional wiring, making it heavier. The above is summarized in Table 6.

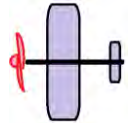
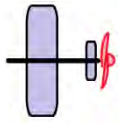
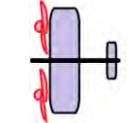
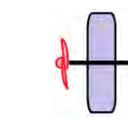
| Figure of Merit | Weight | tractor | pusher | side by side | tractor & pusher |
|-------------------|--------|---|---|---|---|
| | |  |  |  |  |
| Weight | 1.4 | 5 | 5 | 3 | 2 |
| Launch & Landing | 1.3 | 4 | 2 | 5 | 2 |
| Aerodynamics | 1.0 | 4 | 5 | 4 | 3 |
| Manufacturability | 1.0 | 5 | 5 | 2 | 4 |
| Efficiency | 1.0 | 5 | 4 | 3 | 2 |
| Total | 0 | 4.6 | 4 | 3.6 | 2.3 |

Table 6: Propeller location selection.

4. Preliminary Design

At this stage of the design process exact sizing of the aircraft was decided. The general geometry of every airplane part was established. Also, main components of the power system were chosen. However, no structural investigation was carried out yet, as the inner, physical components of the structure were to be determined at a later design stage.

4.1 Design/analysis methodology

The preliminary design was carried out iteratively, in order to maximize the team's score at the competition. The first iteration started with an initial intelligent guess of the geometry size, and

weight, followed by aerodynamic calculations and an accurate mission model, which used the aerodynamical figures achieved earlier. The mission model was programmed to simulate different flight aspects and combine them together. The simulation yielded number of laps completed for the light configuration, load factor, and ability to take off successfully after the hand launch for the heavy configuration. The design process ended when the iterations showed convergence. Although the process was carried out very accurately, the team was aware at every stage of the uncertainties involved in these theoretical calculations. To overcome this uncertainty, and verify the abilities of the design, flight tests were planned and carried out, by means of a specially designed performance demonstrator, to be described later.

4.2 Design/sizing trade offs

As mentioned before, in order to gain as high a score as possible, the team aimed for an aircraft that would be able to carry as much payload as possible. Therefore, maximizing the payload compartment and wing area was most important. Driven by this motive, all the design process was channeled to increase to the maximum those parts of the UAV, and decrease or eliminate at all if possible other components. Also, later decisions about the main wing best operational point had to be made in order to maximize the ratio between gained score by speed and by payload missions.

4.3 Mission model

As part of the iterative design process, a performance analysis was made in order to estimate the aircraft capabilities and to assess the aircraft performance in the competition. A Matlab simulation program was written, integrating all aircraft parameters calculated in the design process, mainly polar drag, UAV estimated weight, thrust, and current draw.

Due to the rules, allowing no changes of the outer airplane geometry between the missions, polar drag and lift were the same for every mission. The main differences that mattered during the simulation were different UAV weights, and parameters affected by this, i.e. power and propulsion characteristics. As mentioned before, the team decided to carry the maximum payload weight possible in both payload carrying missions. Hence, although the competition was composed of three different missions, only two different simulation profiles were required: one for “dash to critical target” mission, and one for payload supply missions.

All missions were modeled using the following phases:

- Launch – when releasing the aircraft from the thrower's hand at full throttle initial speed was approximated as 12 ft/sec.
- Climb – this stage starts right after the release and ends when the aircraft is at its safe terrain clearance, which was decided to be 50 feet. The whole stage was flown at a 15 degrees climb angle and the motor would be set to full throttle, neglecting motor acceleration.
- Acceleration after climb – occurs only at the first lap of every mission. After the aircraft reaches its desired flight height, it maneuvers to horizontal flight and accelerates to its top speed.
- Turns – there are two kinds of turns in the mission, half turn (180°) and full turn (360°). Turns in all three missions will be performed with a load factor of 3, while the other parameters vary. Despite the fact that lower velocities guarantee faster turns, further analysis showed that deceleration before the turn influences complete turn time as well, and due to relatively short flight time this influence was not negligible. Hence, a decision was made to enter the turn at the fastest speed possible.
- Accelerations after the turns – as the aircraft turns, its flight speed decreases due to increase of induced drag. Thus, after the turn is completed, the flight speed starts to rise back to its cruise value. Later performance analysis showed that the acceleration lasted during almost the whole of the straight passes.

The main uncertainties of the mission model were:

- Wind regime, including cross winds. This was neglected.
- A few aircraft parameters such as its aerodynamic characteristics were based on estimated calculations, and were not necessarily the exact true ones.
- Nominal battery voltage was considered constant during the whole flight.

As advised by previous Technion DBF teams, proper sets of propellers, batteries and payload arrangements had to be prepared prior to the competition, according to flight tests, in order to be prepared for every wind condition.

4.4 Aircraft estimated lift, drag and stability characteristics.

4.4.1 Airfoil selection

Wing airfoil – The airfoil's selection process was derived from the unique demands set by the competition rules. Due to the need to launch the UAV as heavy as possible for the payload missions, special attention was paid to high lift foils at low Re numbers.

Nevertheless, in order to fulfill the first mission requirement the foil must not produce too much drag. In particular, the following parameters were examined:

| Objective | Requirement | Parameter |
|---------------------------|---------------------------------|---------------|
| Reduce the stall velocity | Highest lift coeff. At low Re | C_L |
| Achieve best performance | Highest aerodynamic efficiency. | L/D |
| Drag reducing | Low lift coeff. at max. L/D | C_L Vs. L/D |

Table 7: Foil parameters and requirements.

High performances at low Reynolds numbers foils were searched using the UIUC foil data base and comparing foils by Eppler, NACA and Gottingen. After the initial survey, four foils were selected for further review: NACA 9412, S1223, FX 63-137 13.7% smoothed and GO233 airfoil. The selected airfoils' performances were simulated at $Re=75K$ and the obtained data is displayed below.

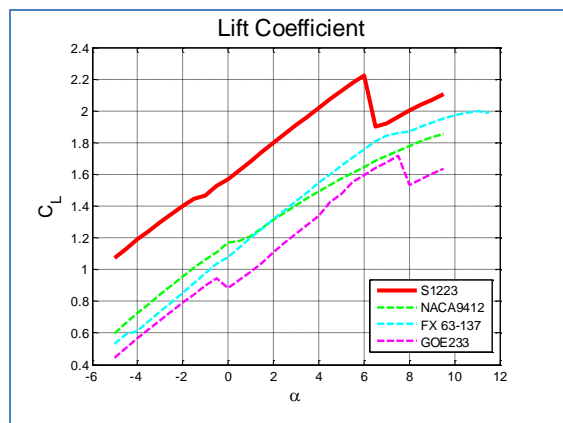


Figure 5: Foil lift comparison.

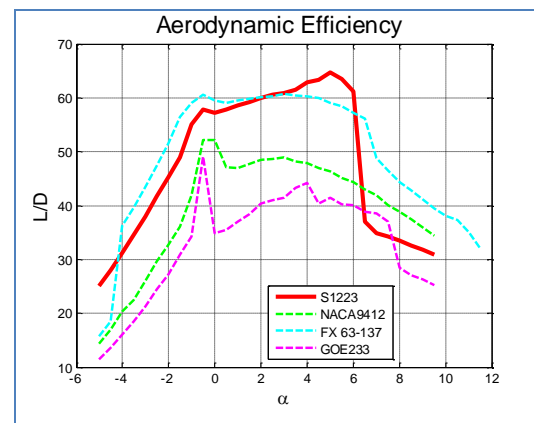


Figure 6: Foil efficiency comparison.

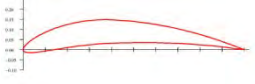
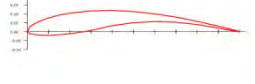
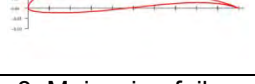
| | Airfoil | $(L/D)_{\max}$ | $C_{L,\max}$ | $C_L @ (L/D)_{\max}$ |
|---|----------|----------------|--------------|----------------------|
|  | S1223 | 64 | 2.2 | 2.0 |
|  | NACA9412 | 52 | 0.7 | 1.9 |
|  | GOE233 | 49 | 0.85 | 0.0 |
|  | FX63-137 | 61 | 2 | 0.6 |

Table 8: Main wing foils considered.

Table 8 shows that the S1223 foil has a significant advantage over other foils at all examined parameters above. Hence it was chosen to be the foil for the main wing.

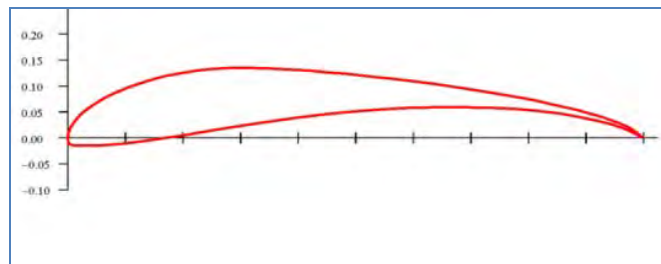


Figure 7: Chosen foil for main wing.

Horizontal stabilizers foil – For the horizontal stabilizer, there were four main options: thin or thick, symmetric or semi-symmetric foils. The thickness of the airfoil determined its drag and lift characteristics. Thicker airfoil could produce more lift but also more drag. Because the stabilizer’s purpose is to provide moments only, a thin airfoil was chosen due to its relatively low drag, while relatively low lift force was compensated by designing a slightly longer arm.

A symmetric foil is commonly used in UAV's, gliders, and light aircraft, providing the vehicle more stability and identical pitch moment for both positive and negative AOA of the stabilizer. On the other hand a semi-symmetric foil could theoretically achieve a slightly higher total lift coefficient for the whole airplane, allowing the vehicle to reach a higher pitch-up moment. Also, a semi-symmetric foil based wing is easier to manufacture.

Because the symmetric foil adds stability, and because possible lift addition from the horizontal stabilizer would be negligible due to its relatively small surface area in comparison to the main wing surface area, it was decided to choose the NACA 0012 foil.

Vertical stabilizer – This shares the same foil design, although in order to prevent yaw moments in straight flight this was immediately chosen to be symmetrical.

4.4.2. Aerodynamic performance prediction

Preliminary aerodynamic performance predictions were based on airfoil data and parasite drag buildup using handbooks and simple computational programs. Results were obtained for $Re=75k$.

| Component | C_{D0} | % of total |
|-----------------------|----------|------------|
| Wing | 0.0070 | 65 |
| Vertical Stabilizer | 0.0005 | 4 |
| Horizontal Stabilizer | 0.0013 | 12 |
| Tower | 0.0008 | 7 |
| Boom | 0.0002 | 2 |
| Shell | 0.0009 | 8 |
| Engine | 0.0002 | 2 |
| Total | 0.0108 | 100 |

Table 9: Parasite drag distribution.

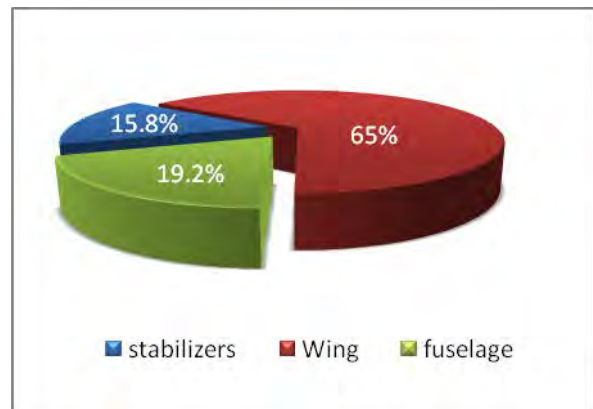


Figure 8: Drag distribution.

Due to relatively successful pod and fuselage design, the total drag contribution of the payload compartment is relatively low, and above 80% of the plane's drag is caused by the lifting and control surfaces. The theoretical parameters obtained by the team are summarized in Figs. 9-10.

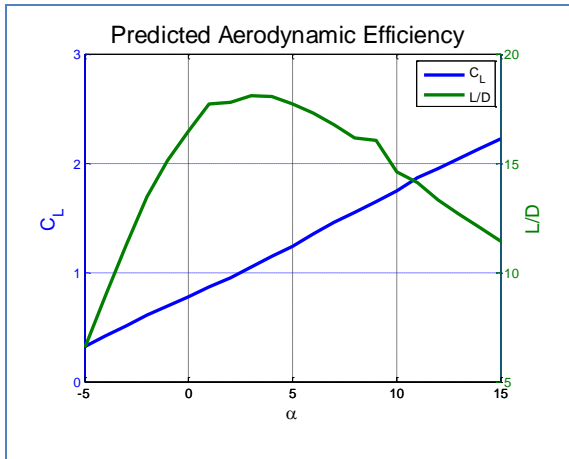


Figure 9: Lift coeff. and flight efficiency.

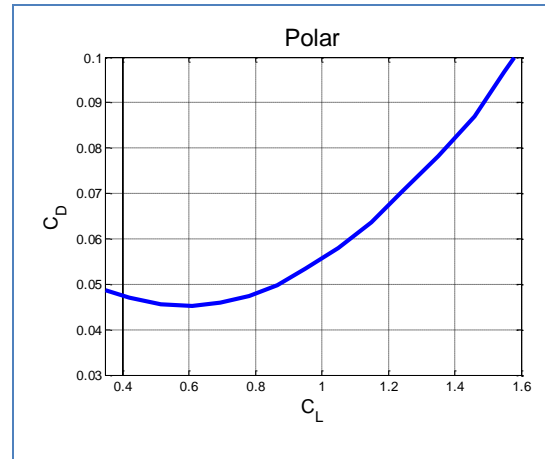


Figure 10: Drag Polar.

4.4.3 Stability characteristics

This year's missions does not require maneuvers, therefore the team aimed for built in stability. Moreover, in order to save weight the objective was to eliminate the pilot's need for a computerized control system. To design a stable aircraft, the team conducted a thorough literature study to determine the parameters influencing stability. Based on this study, the design process followed a few guide lines in order to achieve stability:

- The center of gravity had to be slightly forward to the center of pressure, which is placed approximately by the main wing center of pressure.
- The stabilizers were placed after the main wing, creating built in stability, the vertical tail volume was designed to be 0.3 and the horizontal tail volume 0.01.
- The payload compartment was designed to be mounted under the main wing, providing dumping moment stall resistance or uncontrolled dive.
- The propeller was placed in line with the C.G. in order to lower its pitch moment. Also the propeller was mounted in the front of the airplane, ensuring a yaw damping moment.
- The flaperons were placed on the outer side of the wing, increasing roll moment. They occupied about 50% of the span, and 20% of the chord.

In order to obtain stability and control derivatives, overall airplane dimensions had to be calculated, both from the assumption about its weight distribution and lift surfaces functionality. The following table presents the main stability derivatives.

| | | | | | |
|---------------|-------|--------------|-------|----------|-------|
| $C_{L\alpha}$ | 6.39 | $C_{Y\beta}$ | -0.25 | C_{Lp} | -0.57 |
| $C_{M\alpha}$ | -0.61 | $C_{L\beta}$ | -0.02 | C_{Yr} | 0.25 |
| C_{Lq} | 6.83 | $C_{N\beta}$ | 0.01 | C_{Nr} | -0.14 |
| C_{Mq} | -4.81 | C_{Yp} | -0.09 | C_{Lr} | 0.26 |

Table 10: Stability derivatives in [1/rad].

The figures in Table 10 describe a stable airplane in each and every aspect of lateral and longitudinal dynamics, according to well-known aeronautical criteria for stability.

4.5 Propulsion

4.5.1 An examination of missions' objectives from the aspect of propulsion yields the following requirements:

- Dash to critical target mission – High and continuous thrust is necessary for maximizing airspeed during flight. This requires maximizing available power and consequently maximizing the batteries' stored energy. Designing a propulsion system which can be efficient at high airspeeds is essential to convert as much stored energy in the batteries as possible to available power.
- Ammo re-supply and medical supply missions – Successful hand launch of the heavily loaded aircraft is dependant on its ability to accelerate fast enough, gain speed and lift in order to avoid collision with the ground collision. Hence maximizing thrust at low airspeeds is required to increase liftability of the UAV. Generating high thrust requires a peak input power during takeoff. Unlike the first mission, the possibility to fly at low average airspeed during these missions diminishes the need for maximizing energy on board.

The selection of the electrical components was primarily affected by two factors:

- Weight minimization - Minimizing the weight of the propulsion system components would yield a higher score as it lowers the RAC and enables the carrying of heavier payloads.
- Overheating prevention - Overheating of motor or battery can decrease the performance significantly and even burn out the motor. It is necessary to ensure safe working temperatures of the components by choosing electrical components designed for higher currents than expected and also designing adequate cooling.

Sizing – The estimated flight weights considered as a baseline for the preliminary design were 5.5 lb for the first mission and 7.5 lb for second and third missions. The initial approach

to propulsion system sizing was based upon values of power to weight and thrust to weight ratios which are common in radio-controlled sport model airplanes.

A ratio of 40 Watts of input power per pound of airplane, considered as a minimum requirement, yields 220 Watts for the first mission, and 300 Watts for the second and third missions. Although a static thrust to weight ratio of 1/4 was considered to be a minimum, a relatively large ratio of 1/2 was chosen in order to provide sufficient acceleration, required after hand launch.

4.5.2 Battery optimization – The chosen battery type was NiMH which had higher specific energy density and was less sensitive to memory effect than the NiCad type. A study of the subject concluded that the nominal cell capacity specified by the manufacturers may vary considerably under different working conditions. Furthermore, the high current draw expected from the battery, decreases the cell's usable capacity in accordance with Peukert's Law and this has to be taken into consideration. Competition rules limit battery current to 20 amps. Therefore the battery voltage has to be higher than a certain level in order to achieve the desirable power within the current limits.

To enable input power higher than 300W at 20 amps, a battery of more than 15V is required. Using more than 220W of average input power during the 4-minute-flight of the first mission determined the minimum battery energy at ~15Wh. According to the above estimations, a battery review was held in order to choose the optimal battery pack for each mission. The review included cell types which are designed for high currents.

| Cell Type and Capacity [mAh] | # Cells | Voltage [V] | Energy [Wh] | Max. Power [W] | Weight [lb] |
|------------------------------|---------|-------------|-------------|----------------|-------------|
| KAN 400 | 36 | 43.2 | 17.3 | 346 | 0.75 |
| ELITE 1500 | 14 | 16.8 | 25.2 | 336 | 0.73 |
| Intellect 1600 | 12 | 14.4 | 23.0 | 288 | 0.72 |
| ELITE 1700 | 11 | 13.2 | 22.4 | 264 | 0.75 |
| ELITE 2000 | 10 | 12 | 24.0 | 240 | 0.75 |
| ELITE 2200 | 7 | 8.4 | 18.5 | 168 | 0.71 |

Table 11: Battery packs comparison.

According to this review, it was decided to use the ELITE 1500 14-cell battery pack for all three missions, as it provides the maximum energy, but can also generate very high power due to its high number of cells. The battery energy happened to be higher than minimal

requirement, but it allowed higher performance and had a safety margin against uncertainties related to cell usable capacity that were previously mentioned.

4.5.3 Motor selection – Motor selection process focused on highly efficient electric brushless motors within the designed working range of ~300 Watts. The intention to use a large diameter propeller together with the relatively high battery voltage required a motor with a low RPM/Volt constant. Special computer calculations narrowed the selection to a Kv range of 400-500 RPM/Volt, mainly found on out-runner motors, or a combination of an in-runner motor and a gearbox. While the first type might be more efficient due to gearbox absence, the second type weighs less.

A review was conducted and covered relevant motors of four leading manufacturers. The most competitive motors are shown at Table 12:

| Motor | Weight [Oz.] | Kv [RPM/Volt] | Power Limit [W] |
|--------------------------------------|--------------|---------------|-----------------|
| Neu 1107/6D + Maxon Gear 4.4:1 | 5 | 432 | 600 |
| Hacker B40 21S + Maxon Gear 4.4:1 | 6.1 | 461 | 500 |
| Hacker B40 16L + Maxon Gear 4.4:1 | 7.2 | 426 | 700 |
| Hacker A40 14S V2 14- Pole | 7.3 | 530 | 900 |
| Neu 1907/3Y | 8.3 | 480 | 1800 |

Table 12: Motors comparison.

The motor chosen was the Neu1107/6D combined with a Maxon 4.4:1 planetary gearbox. The decision was made mainly because of its exceptionally light weight and its small case diameter which fitted the aircraft design the best.

4.5.4 Propeller optimization – Propeller performance varies greatly with flight speed. Hence propeller selection involves a major compromise. Fitting different propellers for every mission by the rules, enabled optimization of each mission performance. Payload missions require high thrust at low airspeeds during hand launch, but did not require ability to reach high airspeeds, therefore a relatively large diameter and low pitch propeller was chosen. However, the propeller for the first mission has to have higher pitch in order to provide enough thrust at high airspeeds. In both cases it is necessary to assure that the propeller average current

draw meets the designed conditions for optimal battery usage, and that it does not draw currents beyond the 20 amps restriction under any given flight condition.

Computerized calculations were conducted with wide range of different diameter and pitch propellers in order to find the optimal propeller for each mission in terms of thrust, current draw and efficiency. Based on that analysis, it was decided to use the Aeronaut CAM 13x11 propeller for the first mission and the Aeronaut CAM 14x9 for the second and third missions. Propulsion system performances with the chosen propellers are shown at Fig. 11:

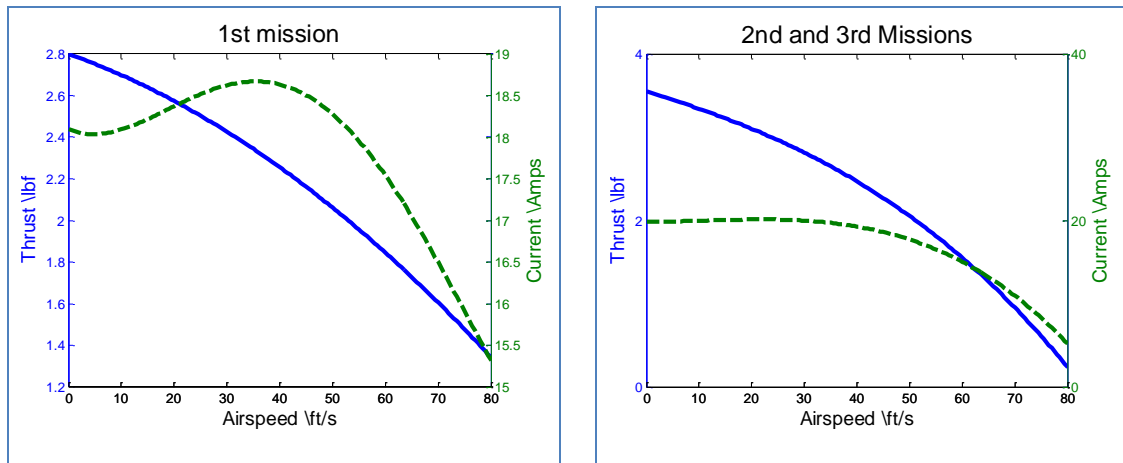


Figure 11: Estimated propulsion system performance.

4.6 Aircraft mission performance

Predictions for one complete lap around the flight path summarized in Table 13:

| Mission Phase | 1'st mission | | 2'nd and 3'rd missions | |
|-----------------------------|--------------|----------------------|------------------------|----------------------|
| | Time [sec] | Battery Capacity [%] | Time [sec] | Battery Capacity [%] |
| Lift-off | 3.3 | 98.4 | 4.6 | 97.7 |
| Straight track | 6.6 | 95.4 | 7.7 | 95.2 |
| 1 st turn – 180° | 2.5 | 94.4 | 0.9 | 94.8 |
| Straight track | 8.2 | 90.0 | 00.3 | 90.4 |
| Loop – 360° | 5.1 | 89.0 | 3.6 | 91.3 |
| Straight track | 5.5 | 86.9 | 7.6 | 88.3 |
| 2 nd turn – 180° | 2.5 | 85.9 | 0.8 | 87.7 |
| Straight track | 6.8 | 83.0 | 9.3 | 84.8 |
| total | 41.5 | 83.1 | 48.1 | 84.8 |

Table 13: Performance summary of the first flight path lap.

In the following rounds, the lift-off phase is replaced with a straight 500 feet pass. Under the assumptions used to calculate the integral performances of the flight, the time needed to complete this part of the section (straight level flight) is approximately 6.8sec. After a quick calculation, rough prediction of maximum amount of laps was determined for the first mission, which the UAV has to complete in a given four minutes time – approximately six full laps.

Special attention had to be given to the amount of power consumed, to assure that the chosen battery contained a sufficient amount of energy to supply four minutes of intense current draw.

In the second and third missions there are no time limitations. The only demand is to successfully complete three full laps around the flight course. Therefore the only calculation required had to confirm whether the battery was capable of sustaining a three lap flight – one lap that includes lift-off and another two laps thereafter.

Again, an accurate calculation showed that not only can the battery last for three laps but it will also allow completion of up to seven laps in an energy saving mode, by reducing the amount of throttle when possible.

5. Detailed Design

At this design stage the airplane was converted from theoretical geometry, to physical structure. Special attention was paid to keeping the design as simple as possible. In order to improve reliability, and reduce the weight, new techniques of manufacturing were explored and considered. The team tried to prevent overdesign, hence the testing process of available materials had to be conducted in parallel, in order to verify their physical properties. A concept of edge design was applied, where the components were designed with a relatively low safety factor. Tests, described in chapter seven, proved the capability and reliability of the designed parts. In a few cases, parts that failed, were redesigned. The described technique allowed the team to ensure keeping structure weight of the airplane to its minimum.

5.1 Main dimensional parameters

| Main wing | | Vertical stabilizer | | Horizontal stabilizer | |
|--------------|----------------------|----------------------|----------------------|------------------------|----------------------|
| Airfoil | S1223 | Airfoil | NACA 0012 | Airfoil | NACA 0012 |
| Span | 6.52 ft | Span | 0.53 ft | Span | 1.18 ft |
| Area | 4.95 ft ² | Area | 0.19 ft ² | Area | 0.43 ft ² |
| Aspect Ratio | 8.7 | Vertical tail volume | 0.3 | Horizontal tail volume | 0.01 |
| flaperons | 20%MAC | Aspect Ratio | 1.4 | Aspect Ratio | 3.2 |
| δ_a | $\pm 20^\circ$ | δ_r | $\pm 15^\circ$ | δ_t | $\pm 25^\circ$ |

| Airplane dimensions | | Electrical system | | Figures of merit | |
|---------------------|---------|-------------------|--------------------------|----------------------|--------------------------|
| Length | 3.9ft | power | 220W | Payload to TOW ratio | 40% |
| Width | 6.2ft | motor | Neu 1107/6D + Maxon Gear | Wing loading | 1.67 lbf/ft ² |
| Height | 1.1ft | Gear ratio | 4.4:1 | Power loading | 42.3 Watt/lb |
| Gross weight | 4.05 lb | batteries | NiMH ELITE 1500 | Load factor | 3 |

Table 14: Dimensional parameters.

5.2 Structural characteristics / capabilities

As described previously, a wide, light weight UAV with high load carrying capabilities was aimed for. However, the fact that the aircraft has to be carried inside a relatively small suitcase forced the team to design a modular structure that will be stowed disassembled.

As the contest rules limit assembly time and personnel, the modular structure has to be easy to assemble. Moreover, the connectors for the modular parts have to be robust enough to not wear out after excessive use. Another aspect of the modularity is the ease of parts replacement

after damaged during flight tests or redesign for better performance, after implementation of flight tests conclusions.

Striving for minimum weight - The materials chosen are of high strength to density ratio and as proof of this concept are prevalently used in the UAV industry. Composite materials such as carbon fiber with epoxy resin, fiberglass and Kevlar fabrics are all utilized to achieve the needed safety factors under the estimated loads in preflight tests and eventually in flight.

The project building time frame of a few months and anticipated supply issues combined with lack of available builders with expertise drew the design closer to the modular concept mentioned earlier for independent parts as well as for assembly building.

5.3 *Systems and sub-systems design, component selection, integration and architecture*

Following is a layout of the principal parts of UAV and their design:

5.3.1 Wing – A rectangular form was preferred over a trapezoid for ease of building, knowing that modeling the laser cut ribs will be time consuming as well as prevent any modifications which might be administered to the wing later on during the building process. Moreover, in terms of wing loading under the assumption of a maximal span of two meters, a rectangular layout was advantageous.

- Main spar – Static preflight loading as well as parabolic lift distribution in a 3g maneuver was mathematically modeled upon the main spar. Modeled as a cantilever beam it was designed to withstand all of the torsional and bending moments. Experiments were conducted to estimate the Young's Modulus as well as the ultimate tensile stress. Driven by commercial availability and price (versus box section or I cross section) a tubular main spar of carbon fiber was chosen for torsional stiffness with a large enough moment of inertia for bending to limit deflection and minimize bending stress. Under the assumption that the spar is the primary element for withstanding the stress within the wing, the trailing edge and leading edge were reduced to the minimal size for maintaining airfoil form. Nonetheless, impact-resistance for unexpected angles of landing was accounted for with fiberglass reinforcement.
- Profiles – These are laser cut for high precision of airfoil form as well as ease of assembly for even the least experienced builder. Ribs are spaced equidistance apart except where servo is installed or in proximity to dihedral-center or center-center connection (increased stress). The distance was determined according to maximal spacing which allowed wing coating to adhere to the airfoil form without sagging.

- Electronics – The servos for the flaperons were to be electrically connected by specially mounted commercial plugs. The idea was to ease the assembly and reduce probability for failure by designing the wing so that the physical contact between parts of the main wing, will automatically close the electrical circuit when assembled, and no further electrical connections will have to be done.

5.3.2 Body – While aiming at a very quick assembly time the design was limited by the geometrical constraints of the suitcase chosen. Thus, a quick connection method was to be implemented allowing future modifications to each of the modular parts of the boom in case of vibrations (aero elastic phenomena, flutter) or even structural failure. Choosing carbon fiber booms with custom made aluminum connectors achieves a very high strength to weight ratio and accords within the design criteria where the boom should withstand the pitch, roll, and yaw moments acting upon the UAV in flight with a sufficient safety coefficient, as well as the wiring to the elevator-rudder unit towards the rear. The team preferred this method over building a single hulled UAV since once flight testing has commenced any alterations in the size or even length of the body are possible without rebuilding any other part. The boom was designed from three parts, in order to extend the arm of the tail, but yet fit into the suitcase. Around the central part the “tower” was designed. The tower has a very light, thin aerodynamical coating, covering all electronics, batteries, and connectors between boom, pod, and main wing.

5.3.3 Pod – This was designed as a separate unit from the rest of the UAV. Its design allowed quick loading of the payload depending on the mission profile. It can be easily and rapidly loaded due to a very large opening to minimize loading time. Once loaded, quick attached to the main boom in previously determined locations depended both on analytical calculations and later, on flight testing sessions.

In order to ease the loading, and reduce CG movement, the pod was designed to have an inner foam core, enabling the loader to slide the payload into special slots as shown at Fig. 12. For the medical supply mission the balls were intended to be loaded one after another in long tubular slots, designed to maintain the CG of the balls within 1/4” accuracy due to uncertainty about each balls weight. The metal bar to be carried in the Ammo re-supply mission fits into a special slot matching its exact dimensions.

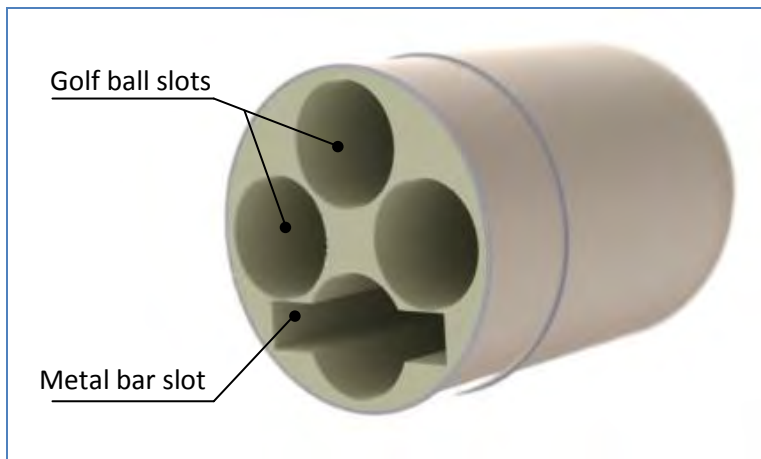


Figure 12: Payload compartment interior design.

Since the UAV is hand launched, the landing gear is relevant only for landing. However, landing may be done in a controlled manner on the belly of the UAV without damaging the aircraft structure or components, saving the weight and reducing the drag of landing gear. Moreover, implementing a retractable landing gear would greatly complicate the building process.

The pod connectors enable CG modification, after flight tests and before fixing them for their final position, via change of the lateral position of the pod to optimize the frontal and the stability margin.

5.3.4 Horizontal stabilizer – In order to reduce the weight as much as possible, a light balsa ribbed structure design was used. Due to the small dimensions of the stabilizer, relatively small aerodynamic forces were anticipated, enabling design of a wooden *I* cross section main spar, and avoiding the use of a heavier carbon fiber structure. In order to simplify on site assembly, the elevator servo was designed to be mounted inside the stabilizer and was automatically electrically connected like the main wing parts, using a commercial male plug. The female plug was mounted in the rudder, accordingly.

5.3.5 Vertical stabilizer – This was designed to be constructed from a carbon fiber box with a 45 degrees fabric layout and a soft balsa skeleton for minimizing torsion deformation while applying δ_r , and ideally transferring the moment to the main boom. The rudder was designed to be part of the rear section of the main boom, running the elevator control servo wiring through it.

5.3.6 Control surfaces – Flaperons, rudder and elevator torsional stamina was achieved through a balsa box based on 45 degrees orientation of the ribs, which enabled precise airfoil curvature, as well as greatly reducing the weight of the ailerons. All control surfaces were already physically connected to their servos inside the suitcase, for ease of on site assembly process.

5.3.7 Power control system – The control subsystems and selection justification are shown in Table 14. The receiver and its battery are located inside the tower, for correct C.G. adjustment. Power control subsystem locations are shown in the Drawing Package.

| Component name | Component description | Selection parameters |
|--------------------------------------|-----------------------|---|
| Savox - SH350 | micro servos | Lightweight, sufficient torque |
| R6106HFC 2.4GHz FASST 6-Channel | Receiver | Long range, low power consumption and lightweight |
| Radical RC 400 mAh NiMh 4.8V | Receiver battery | Lightweight, sufficient power capacity |
| Castle Creations - Phoenix Ice 50 | Speed controller | Low power consumption, lightweight |

Table 15: Power control subsystem components.

5.4 Weight and balance

The designed aircraft weighs about 6.6 lb, of which about 40 percent are the payloads.

The aircraft center of gravity was always kept inside the safety margins to ensure stable flight. The content criteria include a demand for CG location inside the main wing chord. Although the design goal was to keep the center of gravity relatively at the same point, the team decided to make the empty aircraft slightly less stable, in order to ease pilot maneuvers during the first mission, which had to be flown fast.

Due to the uncertainty concerning the golf balls weight, and limited storage compartment physical space, the centrogram shows distribution of the total weight and CG location of the medical supply mission.

| components | weight (oz) | component | weight (lb) | C.G. from LE (in) |
|----------------------------|-------------|-------------------|--------------|-------------------|
| fuselage | 22.9 | system | 3.3 | 4.1 |
| pod | 8.8 | batteries | 0.75 | 0.9 |
| wings | 5.4 | Gross weight | 4.08 | 3.5 |
| motor and speed controller | 7.2 | | Dash mission | Payload missions |
| receiver and Rx battery | 2.1 | Gross weight (lb) | 4.1 | 4.1 |
| servos | 1.3 | payload (lb) | 0.0 | 2.8 |
| propeller | 2.1 | total (lb) | 4.1 | 6.9 |
| wiring | 3.5 | C.G. from LE (in) | 3.2 | 2.9 |
| total | 53.3 | stability margin | 1.8% | 10.1% |

Table 16: Weight build-up.

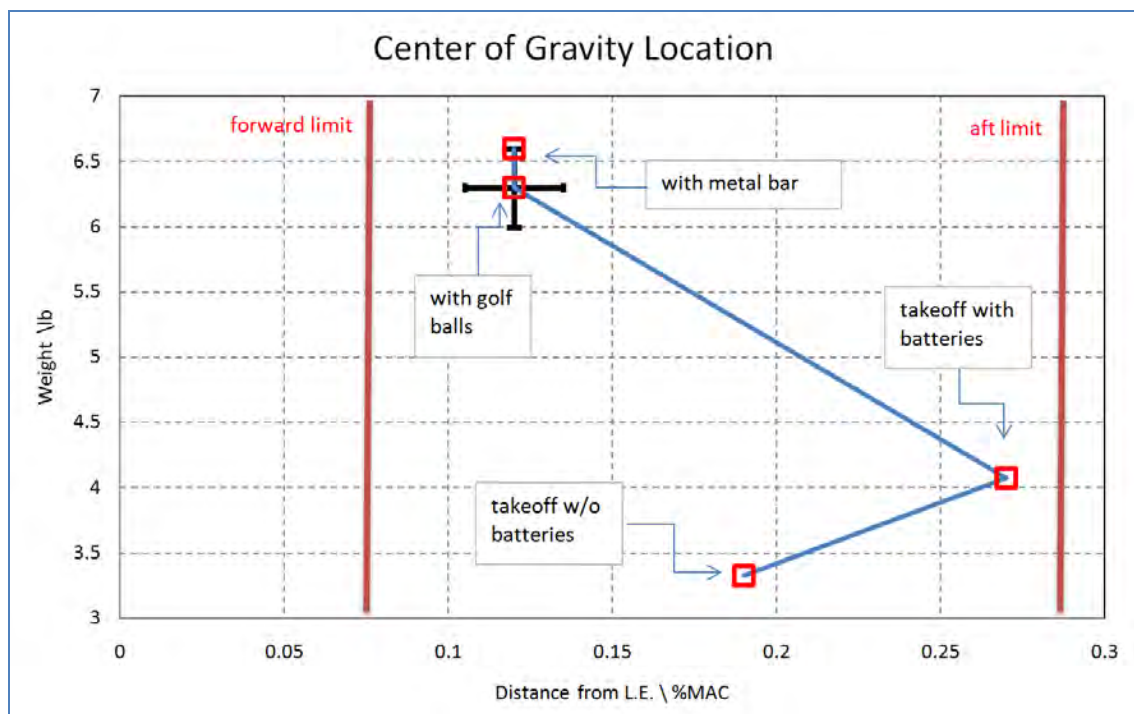


Figure 13: Centrogram.

5.5 Flight performance parameters

The mission parameters for the final airplane configuration are shown in Table 17. Because the payloads, will be carried inside the airplane, the effect of the loading will not change with their kind.

| Performance Parameter | Dash mission | Payload missions |
|--------------------------|--------------|------------------|
| $C_{L,MAX}$ | 2.2 | 2.2 |
| e | 1.827 | 1.827 |
| C_{D0} | 0.0108 | 0.0108 |
| $(L/D)_{MAX}$ | 18 | 18 |
| T/W | 1.667 | 1.485 |
| Takeoff Weight(lbs) | 4.1 | 6.9 |
| Cruise Speed (ft/sec) | 70 | 56 |
| Max. Speed (ft/sec) | 77 | 59 |
| Stall Speed (ft/sec) | 12.4 | 06.6 |
| Max. Turn Rate(deg/sec) | 68 | 68 |
| Max. Climb Rate (ft/min) | 0153 | 601 |

Table 17: Flight performance figures.

5.6 Mission performance

- 5.6.1 After finalizing UAV design, more specific performance predictions were made: Staging box assembly – the aircraft designed to be assembled within 1.5 minutes. Although the aircraft is composed of ten different parts, all joints are designed to click into place with no screws. All the wiring runs inside the joints, and automatically connects when the structural components are fitted together.
- 5.6.2 Dash to critical target mission – The main focus in this mission is on the number of full laps completed within four minutes. The main figures of interest for the simulation made are the distance covered, shown in Fig. 14 and the battery ability to sustain fast flight. The battery discharge chart shown in Fig. 15:

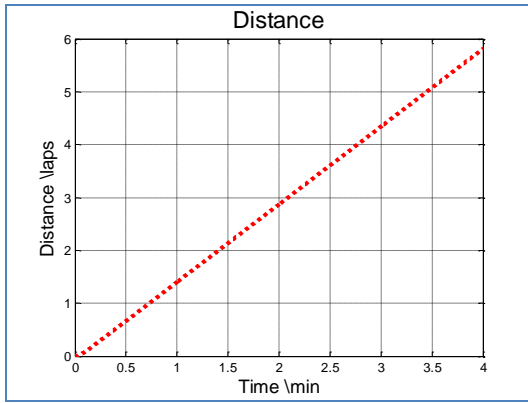


Figure 14: Mission 1 distance coverage.

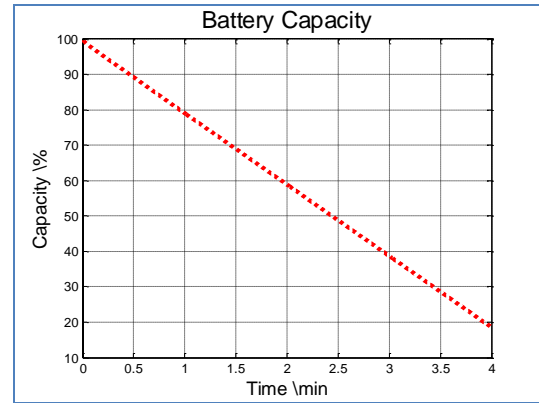


Figure 15: Mission 1 battery discharge.

Moreover, in order to complete the turns as fast as possible, the proper speed with which the pilot had to enter the turn was investigated. Total turn time was calculated, combined from the time to decelerate, time to turn at specific speeds and the time to accelerate back to cruise speed. The simulation revealed that the optimal speed for the pilot to enter the turn was the cruise speed, without any deceleration. During the simulation, special care was taken not to exceed the allowed load factor.

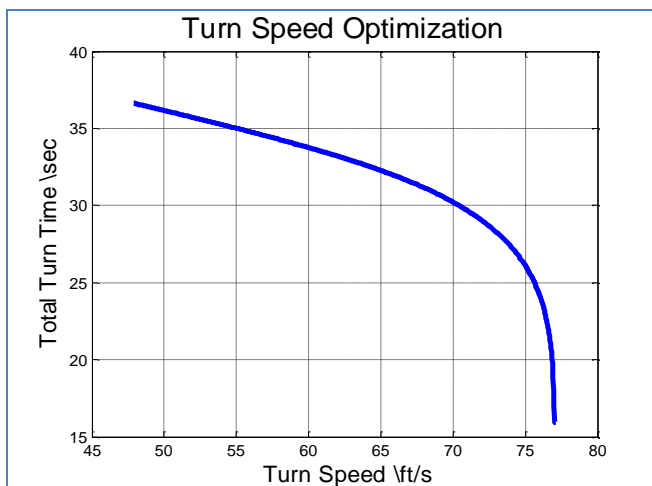


Figure 16: Turning time dependence on UAV speed

5.6.3 The Ammo re-supply and medical supply missions both examine different lift ability aspects of the UAV. The loading of the payload was designed to take no more than 2.5 minutes for the most demanding mission from that aspect – the medical supply mission. However, from the performance point of view the missions were identical, and have been dealt with accordingly. For the fully loaded flight covering only three laps around the course, the main interest was the flight envelope of the plane (Fig. 18), and the structural abilities of the design (Fig. 17).

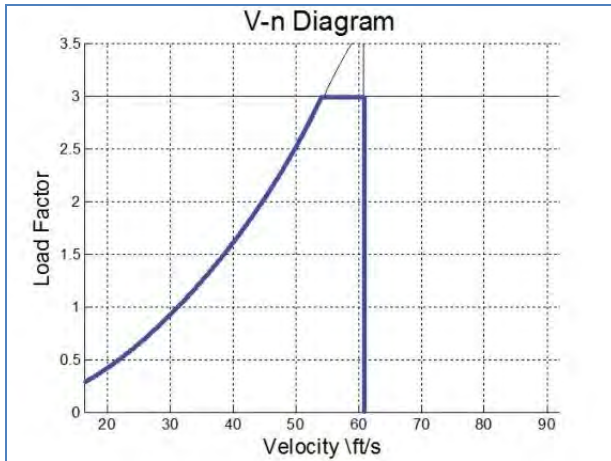


Figure 17: V-n diagram.

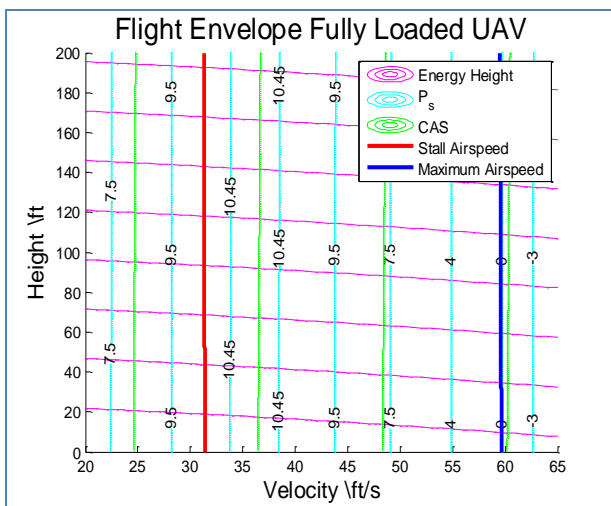
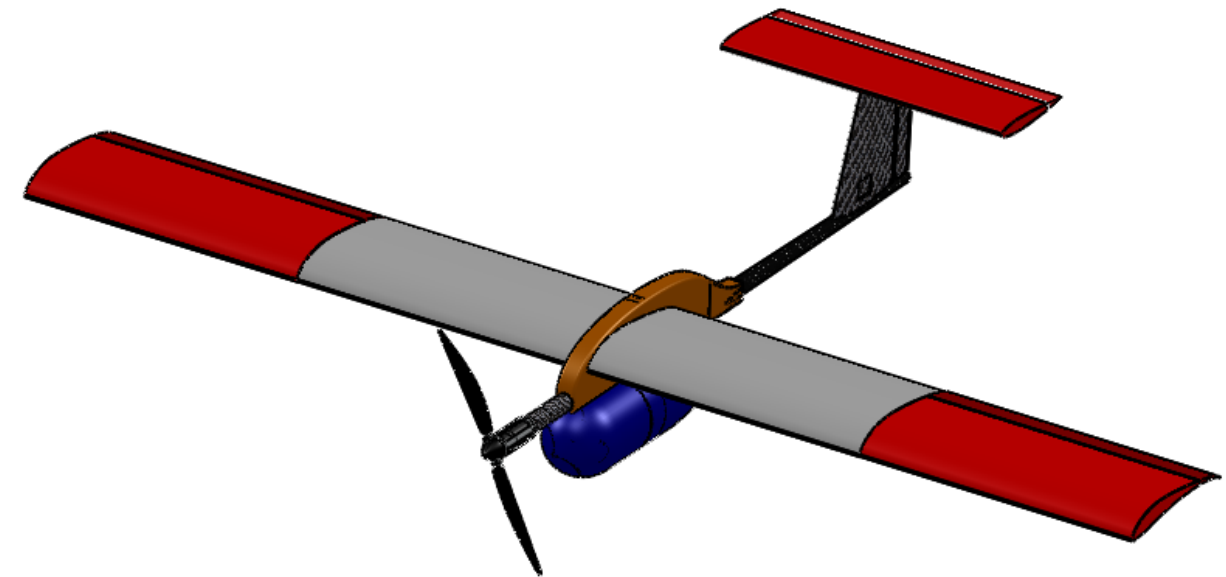
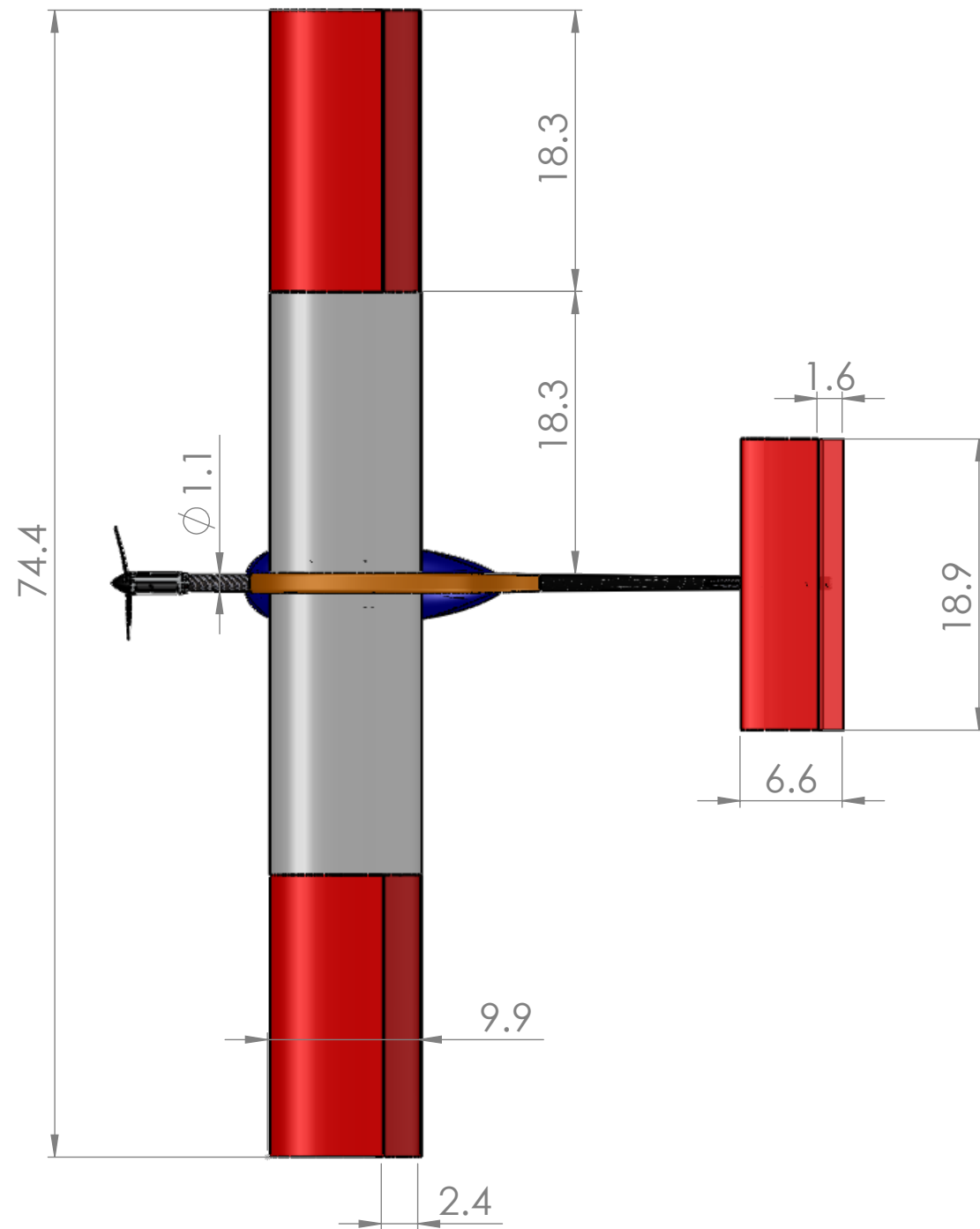
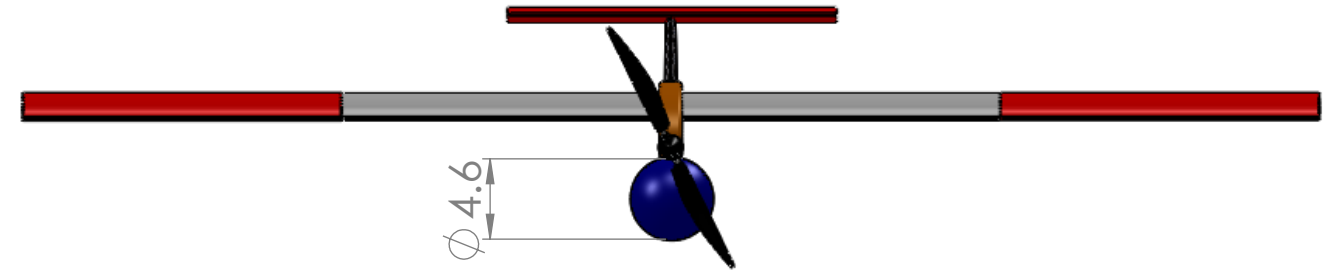
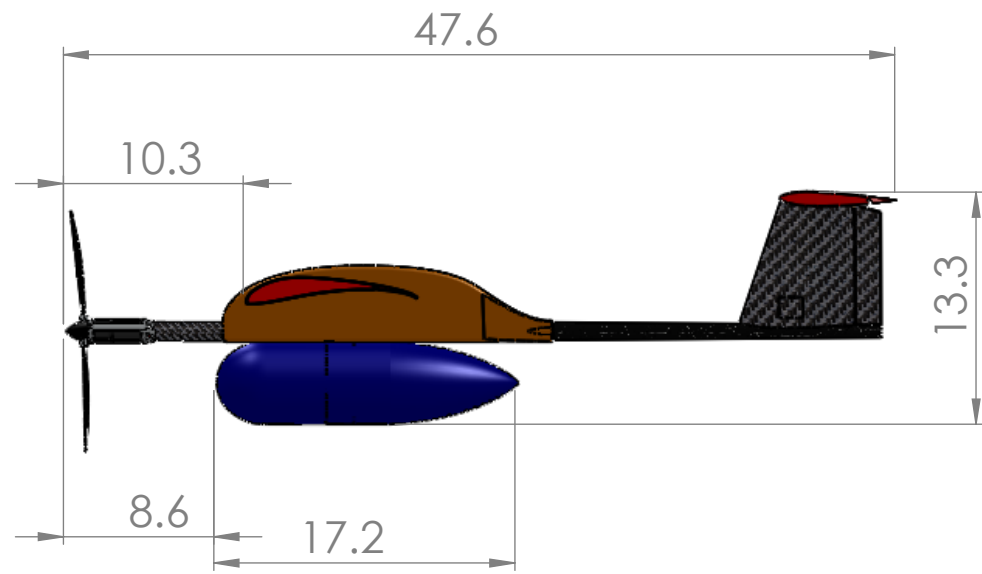


Figure 18: Flight envelope.

It may be observed that there is no height limitation to the flight altitude within the altitude range of the competition (approximately 50ft). Also, flight envelopes confirmed the preliminary analysis feasibility, as earlier calculated velocities appear inside the flight envelope. From the combination of Figs. 16 and 17, the best turn velocity was the highest that the aircraft could withstand, i.e. 60ft/s.

5.7 Drawing Package

The following drawing package presents three main views of the airplane, its structural arrangement, components layout, suitcase layout, and payloads arrangements for the second and the third missions.

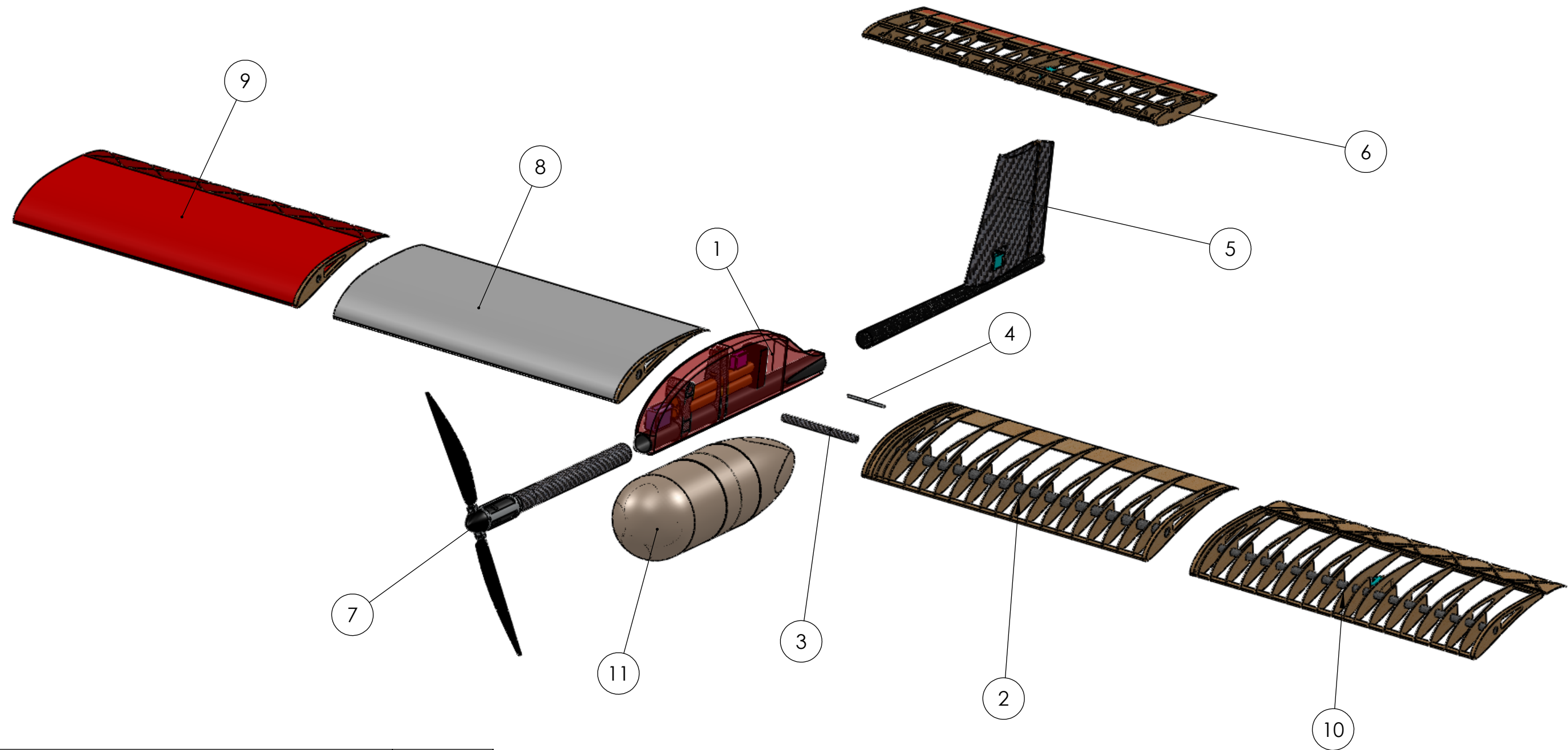


UNLESS OTHERWISE SPECIFIED:
DIMENSIONS ARE IN INCHES
Tolerances: Linear: 0.3";
Angular: 0.2deg



Technion - Israel institute of Technology

| | NAME | DATE | Cessna - Raytheon - AIAA - Design/Build/Fly 2011 | |
|----------|---------------|------------|--|--------------|
| DRAWN | Y. Feigenbaum | 01.02.2011 | TITLE: Standard Views | |
| CHK'D | Y. Lobovikov | 01.02.2011 | | |
| APPV'D | M. Jashinski | 01.10.2011 | DWG NO. 1 | A3 |
| REVISION | Dr S.Tsach | 01.19.2011 | SCALE:1:11 | SHEET 1 OF 5 |



| ITEM NO. | PART NAME | QTY. |
|----------|-------------------------------------|------|
| 1 | Main Body and Tower | 1 |
| 2 | Left Center Section of Main Wing | 1 |
| 3 | Main Wing Bending-rod Connector | 1 |
| 4 | Main Wing torsion-rod Connector | 1 |
| 5 | Rear Boom and Vertical Stabilizer | 1 |
| 6 | Horizontal Stabilizer | 1 |
| 7 | Front Boom and Motor Assembly | 1 |
| 8 | Right Center Section of Main Wing | 1 |
| 9 | Right Dihedral Section of Main Wing | 1 |
| 10 | Left Dihedral Section of Main Wing | 1 |
| 11 | Payloads Compartment | 1 |

UNLESS OTHERWISE SPECIFIED:
DIMENSIONS ARE IN INCHES
Tolerances: Linear: 0.3";
Angular: 0.2deg

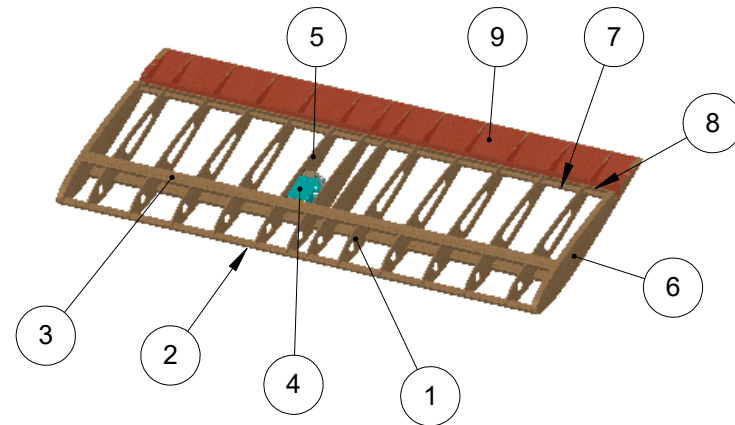


Technion - Israel institute of Technology

| | | NAME | DATE | Cessna - Raytheon - AIAA - Design/Build/Fly 2011 | |
|----------|---------------|------|------------|--|--------------|
| DRAWN | Y. Feigenbaum | | 01.02.2011 | TITLE: Components View | |
| CHK'D | Y. Lobovikov | | 01.02.2011 | | |
| APPV'D | M. Jashinski | | 01.10.2011 | | |
| REVISION | Mr. S.Tsach | | 01.19.2011 | DWG NO. 2 | A3 |
| | | | | SCALE:1:6 | SHEET 2 OF 5 |

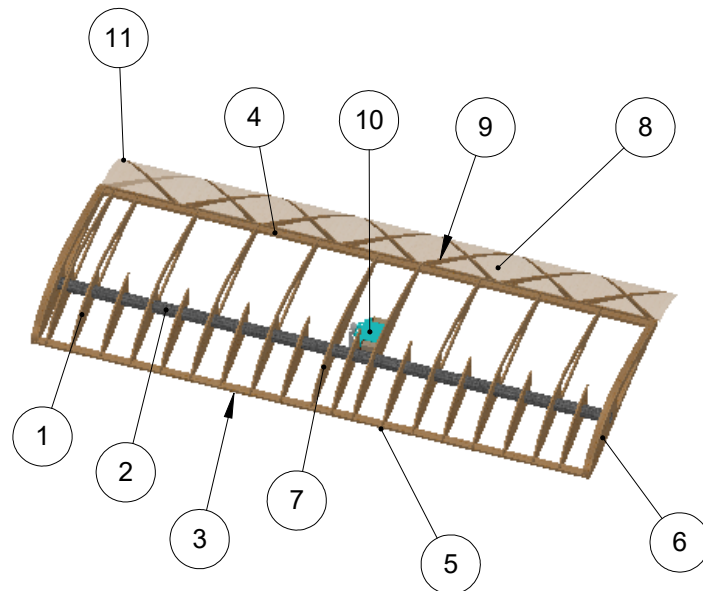
1. Horizontal Stabilizer

| ITEM NO. | PART NAME | QTY. |
|----------|----------------------------|------|
| 1 | Thin NACA 0012 Rib | 10 |
| 2 | Stabilizer L.E. | 1 |
| 3 | Main Beam | 2 |
| 4 | SH350 Servo | 1 |
| 5 | Thin NACA 0012 Central Rib | 3 |
| 6 | Thick NACA 0012 Rib | 2 |
| 7 | Stabilizer T.E. | 1 |
| 8 | Elevator L.E. | 1 |
| 9 | Elevator Balsa Plate | 1 |



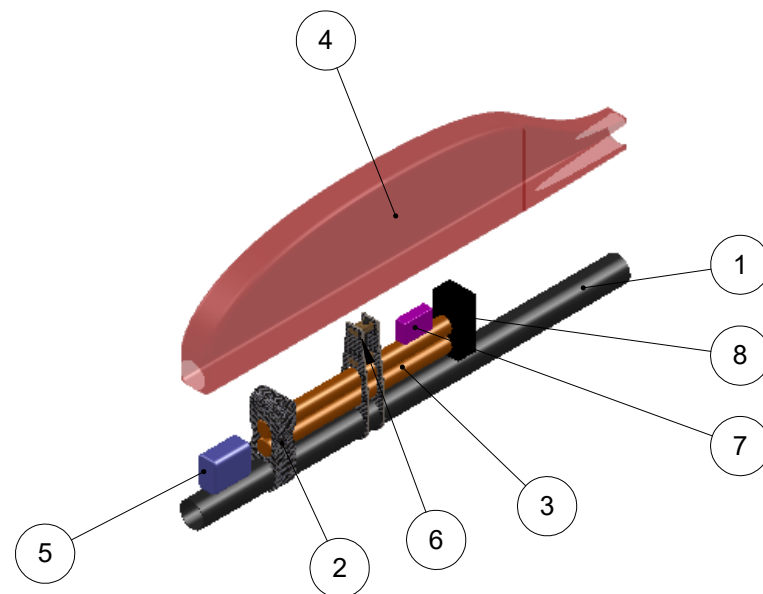
2. Main Wing Section (Dihedral)

| ITEM NO. | PART NAME | QTY. |
|----------|-----------------------------|------|
| 1 | Thin S 1223 Rib | 8 |
| 2 | Main Tubular Spar | 1 |
| 3 | Dihedral L.E. | 1 |
| 4 | Dihedral T.E. | 1 |
| 5 | Frontal Partial S 1223 Rib | 9 |
| 6 | Thick S 1223 Rib | 2 |
| 7 | Dihedral S 1223 Central Rib | 2 |
| 8 | Flaperon Balsa Plate | 1 |
| 9 | Flaperon Reinforcement Rib | 7 |
| 10 | SH350 Servo | 1 |



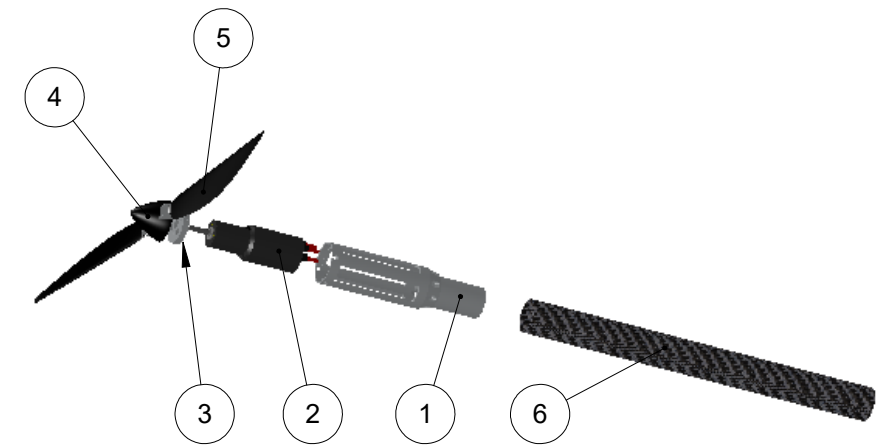
3. Tower

| ITEM NO. | PART NAME | QTY. |
|----------|-----------------------------|------|
| 1 | Main Boom | 1 |
| 2 | Main Wing to Boom Connector | 1 |
| 3 | Elite1500 Batteries | 2 |
| 4 | Aerodynamic Skin | 1 |
| 5 | Speed Controller | 1 |
| 6 | Main Wing Torsion Connector | 2 |
| 7 | Receiver Battery | 1 |
| 8 | Futaba R168DP Receiver | 1 |



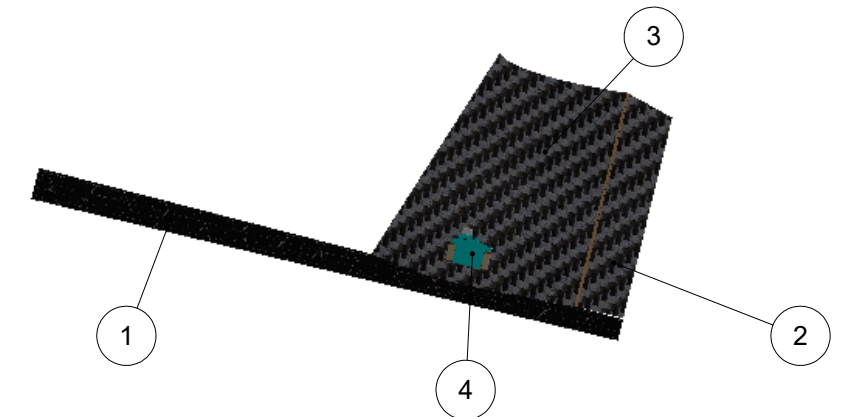
4. Motor Assembly

| ITEM NO. | PART NAME | QTY. |
|----------|--------------------|------|
| 1 | Motor Connector | 1 |
| 2 | Motor | 1 |
| 3 | Propeller Plate | 1 |
| 4 | Spinner | 1 |
| 5 | Propeller | 1 |
| 6 | Front Boom Section | 1 |



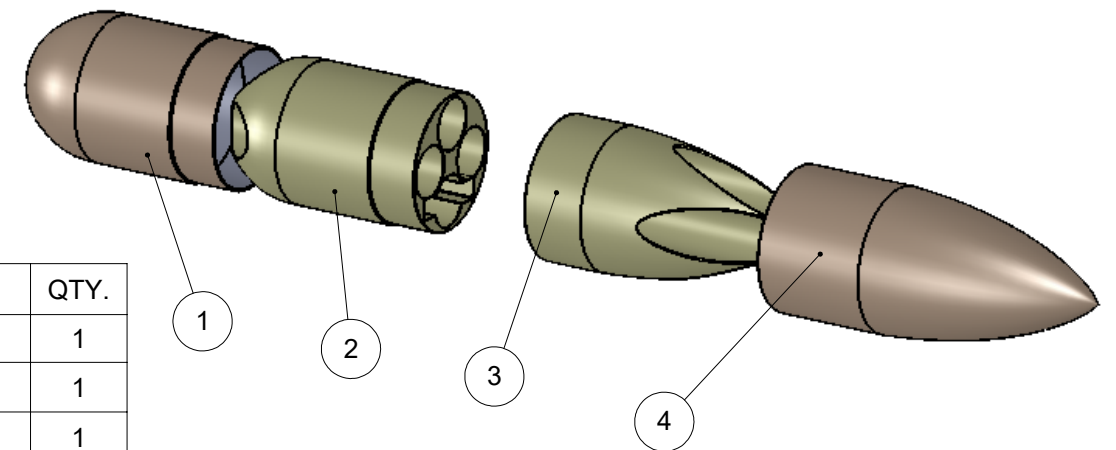
5. Vertical Stabilizer

| ITEM NO. | PART NAME | QTY. |
|----------|---------------------|------|
| 1 | Tail Boom Section | 1 |
| 2 | Rudder | 1 |
| 3 | Vertical Stabilizer | 1 |
| 4 | SH350 Servo | 1 |



6. Pod

| ITEM NO. | PART NAME | QTY. |
|----------|-------------------|------|
| 1 | Front Pod Section | 1 |
| 2 | Front Foam | 1 |
| 3 | Rear Foam | 1 |
| 4 | Rear Pod Section | 1 |



UNLESS OTHERWISE SPECIFIED: DIMENSIONS ARE IN INCHES
Tolerances: Linear: 0.3"; Angular: 0.2deg



Technion - Israel institute of Technology

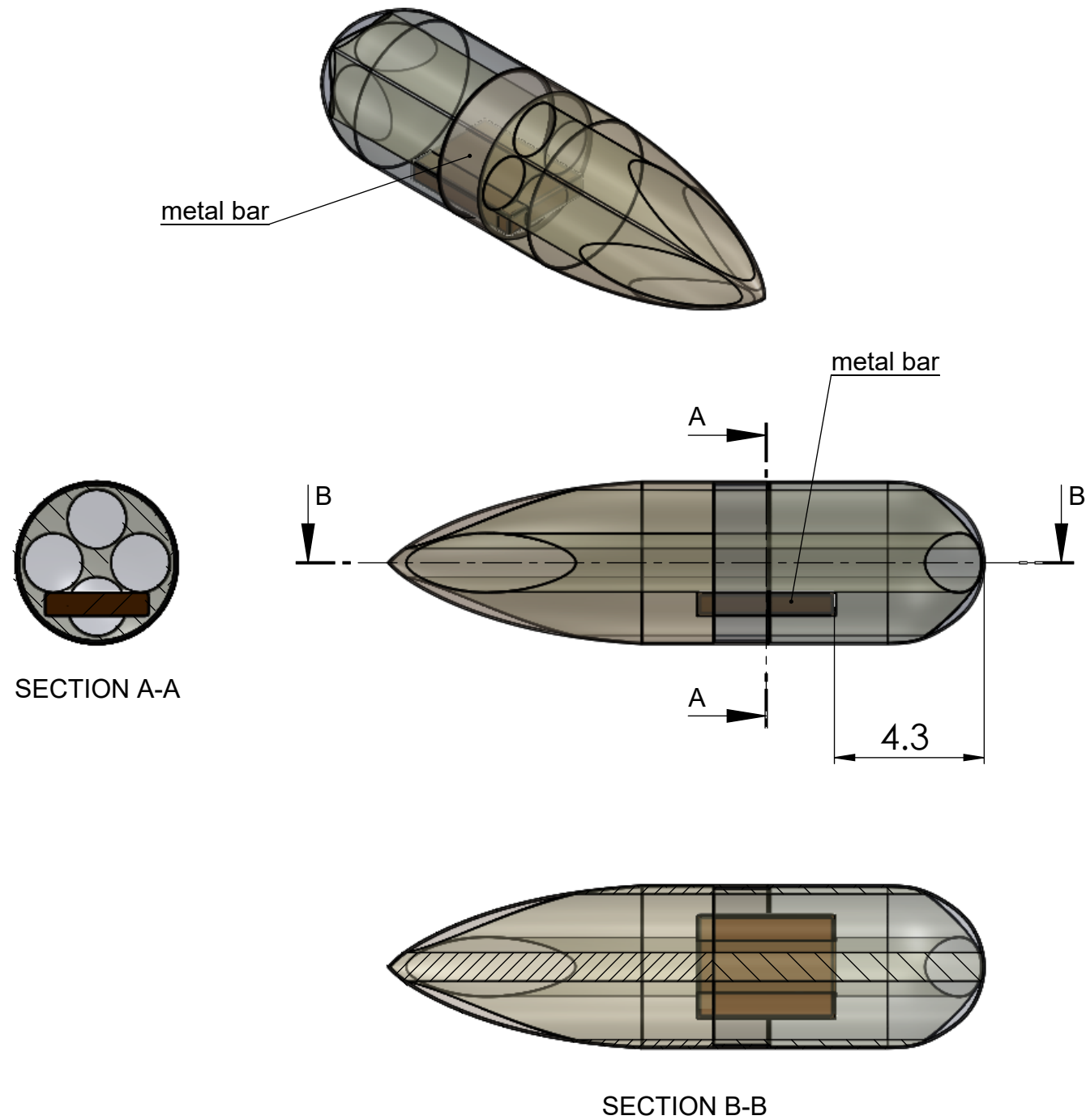
| | NAME | DATE |
|----------|---------------|------------|
| DRAWN | Y. Feigenbaum | 01.02.2011 |
| CHK'D | Y. Lobovikov | 01.02.2011 |
| APPV'D | M. Jashinski | 01.10.2011 |
| REVISION | Mr. S.Tsach | 01.19.2011 |

Cessna - Raytheon - AIAA - Design/Build/Fly 2011

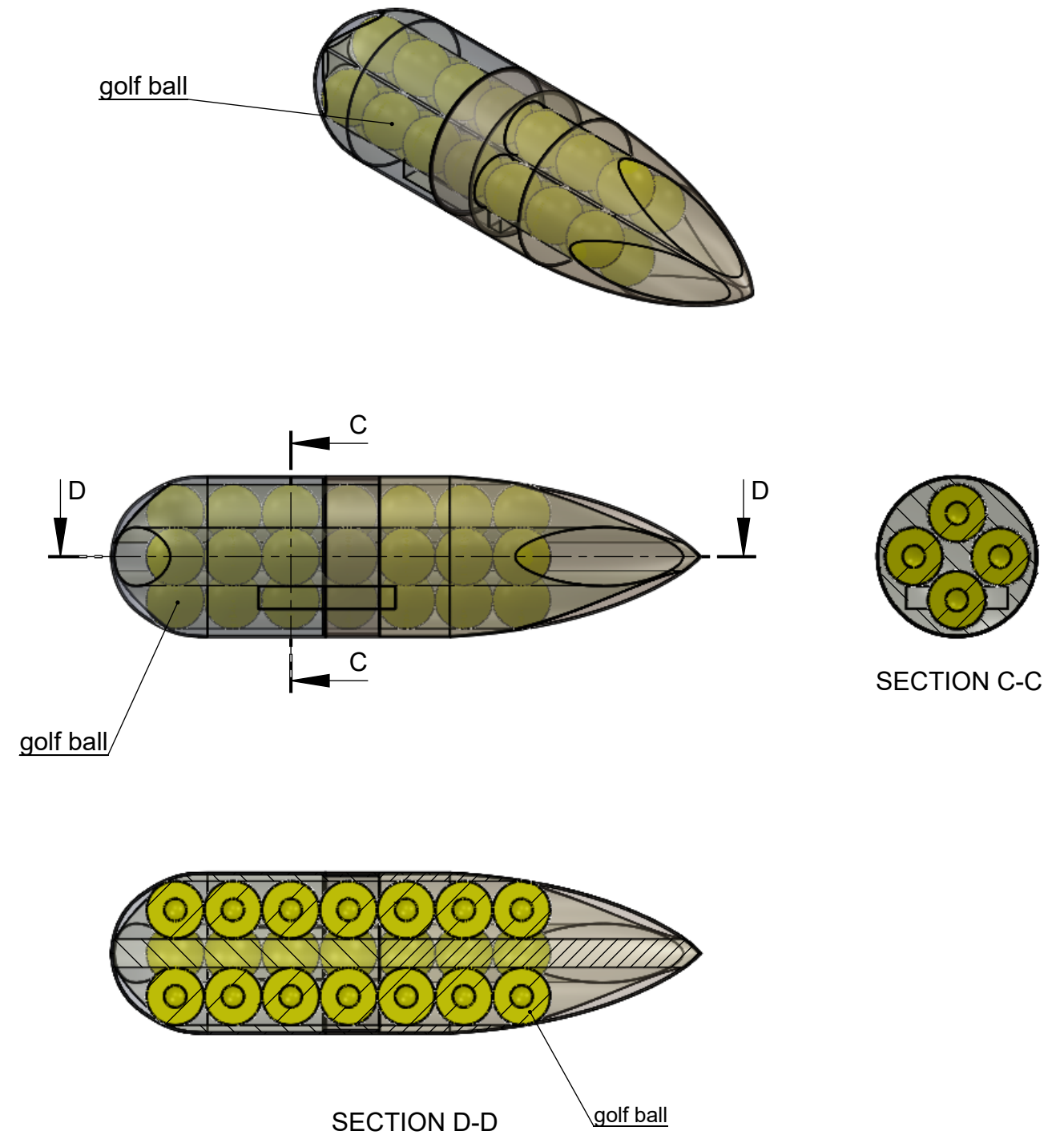
TITLE: **Components Structures**

| | | |
|-----------|--------------|----|
| DWG NO. | 3 | A3 |
| SCALE:1:6 | SHEET 3 OF 5 | |

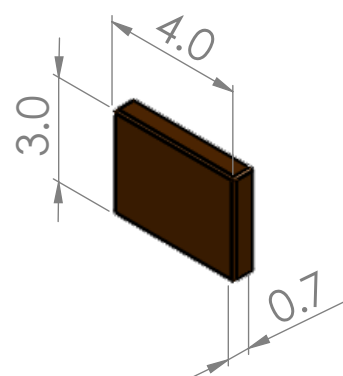
Ammo Re Supply Mission



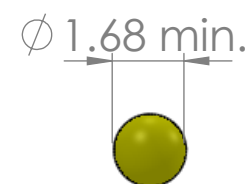
Medical Supply Mission



Metal Bar Payload



Golf Ball Payload



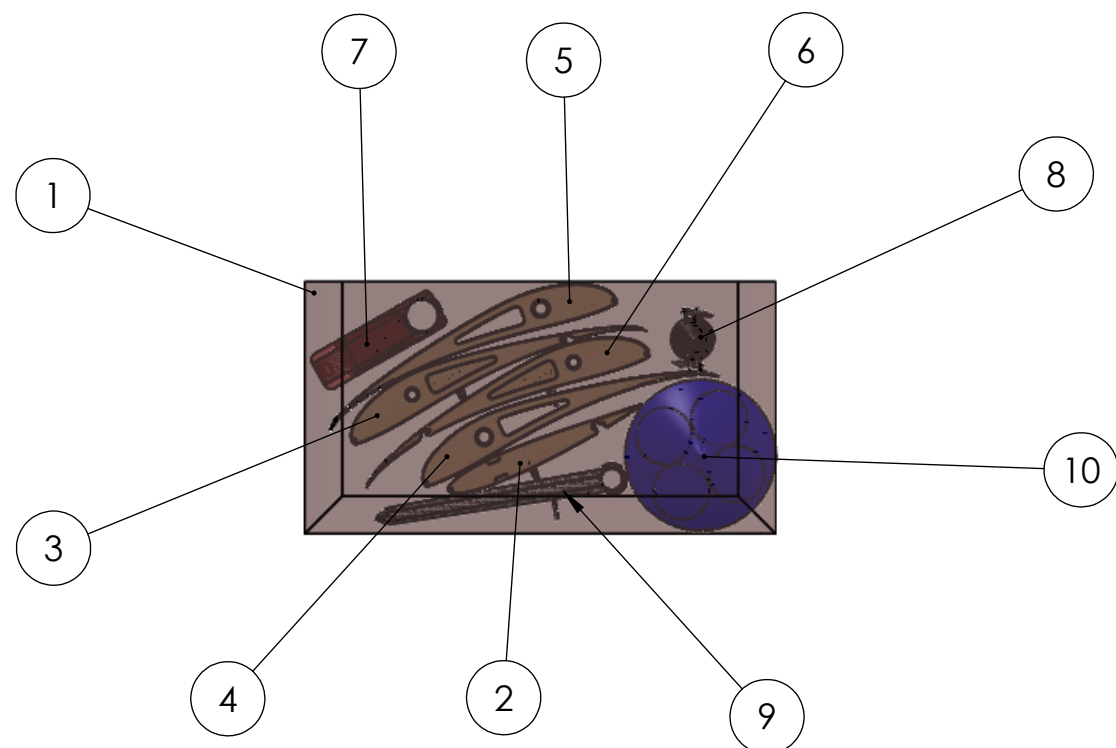
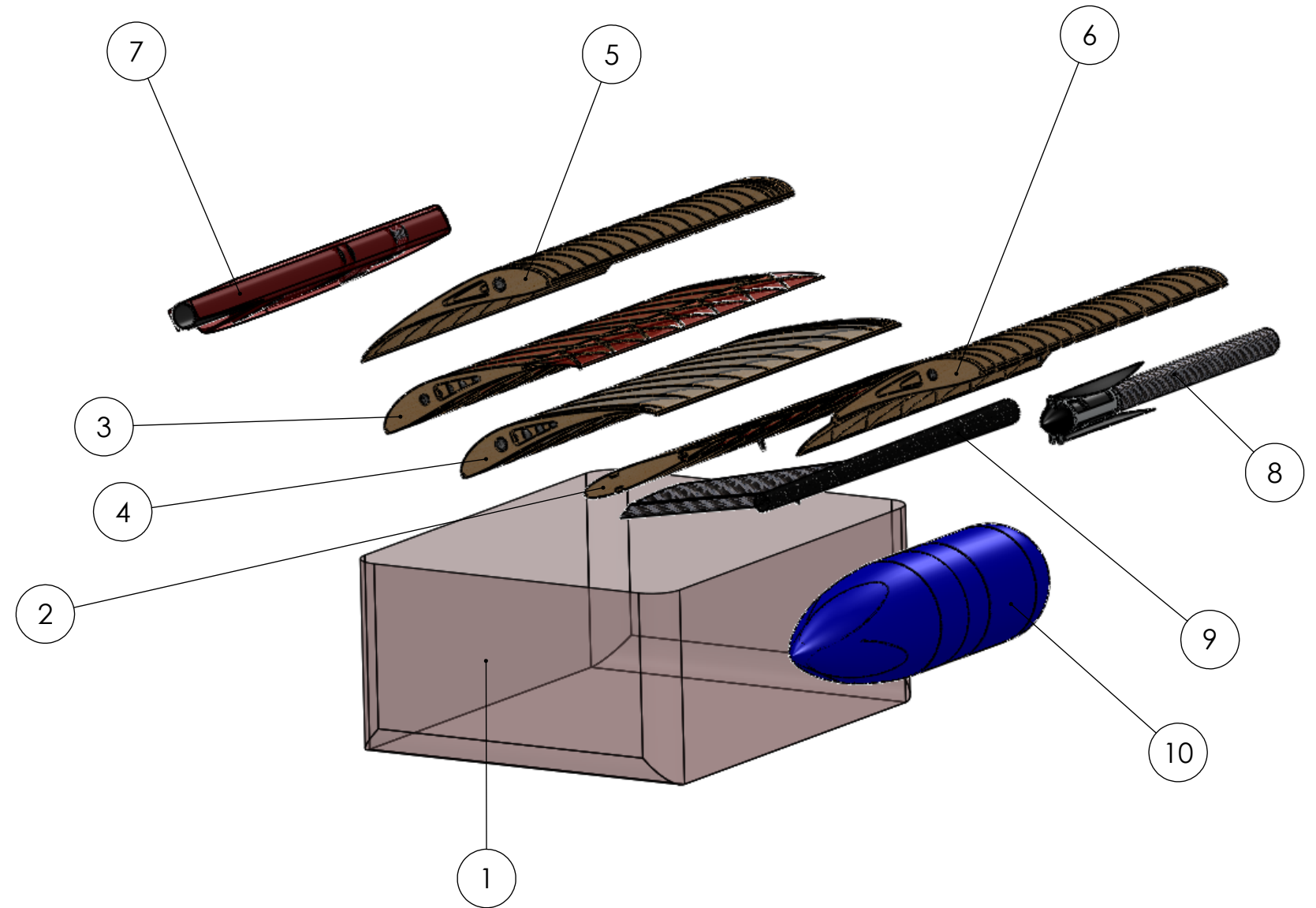
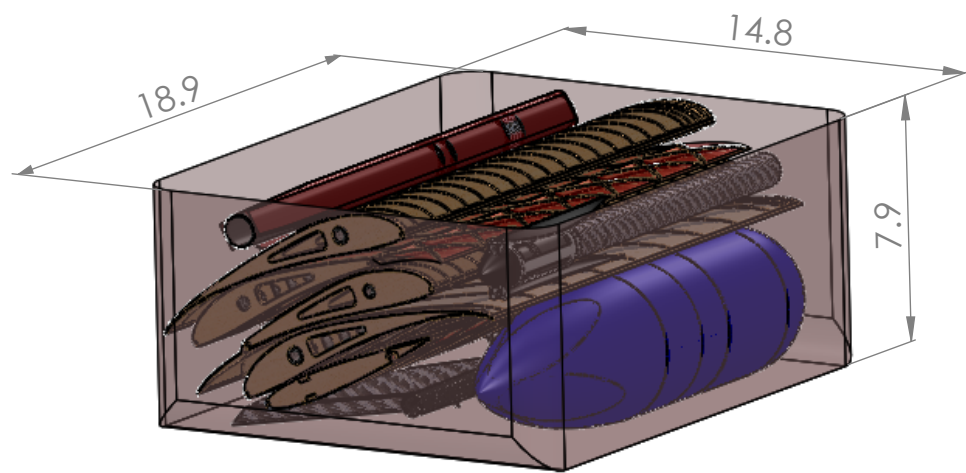
UNLESS OTHERWISE SPECIFIED: DIMENSIONS ARE IN INCHES
Tolerances: Linear: 0.3"; Angular: 0.2deg



Technion - Israel institute of Technology

| | NAME | DATE | Cessna - Raytheon - AIAA - Design/Build/Fly 2011 | |
|----------|---------------|------------|--|--------------|
| DRAWN | Y. Feigenbaum | 01.02.2011 | TITLE: Payload Accomodations | |
| CHK'D | Y. Lobovikov | 01.02.2011 | | |
| APPV'D | M. Jashinski | 01.10.2011 | DWG NO. 4 | A3 |
| REVISION | Dr S.Tsach | 01.19.2011 | SCALE:1:4.5 | SHEET 4 OF 5 |

| ITEM NO. | PART NAME | QTY. |
|----------|----------------------|------|
| 1 | Carry on Suitcase | 1 |
| 2 | Elevator | 1 |
| 3 | Left Dihedral | 1 |
| 4 | Left Center | 1 |
| 5 | Right Center | 1 |
| 6 | Right Dihedral | 1 |
| 7 | Main Body Assembly | 1 |
| 8 | Motor Assembly | 1 |
| 9 | Tail Boom and Rudder | 1 |
| 10 | Pod | 1 |



UNLESS OTHERWISE SPECIFIED:
DIMENSIONS ARE IN INCHES
Tolerances: Linear: 0.3";
Angular: 0.2deg



Technion - Israel institute of Technology

| | NAME | DATE | Cessna - Raytheon - AIAA - Design/Build/Fly 2011 | |
|----------|---------------|------------|--|--------------|
| DRAWN | Y. Feigenbaum | 01.02.2011 | TITLE: Suitcase Layout | |
| CHK'D | Y. Lobovikov | 01.02.2011 | | |
| APPV'D | M. Jashinski | 01.10.2011 | DWG NO. 5 | A3 |
| REVISION | Mr. S.Tsach | 01.19.2011 | SCALE:1:6 | SHEET 5 OF 5 |

6. Manufacturing Plan and Processes

The manufacturing process included construction of both the experimental devices, as well as the contest airplanes.

Right after the preliminary design phase, even before detailed design began, a flight performance demonstrator was built in order to check the aerodynamic feasibility and power system. That prototype was built by rapid building methods. Its fuselage and wings weighed almost twice the final airplane, but it was geometrically identical to the final design, and had the same total weight, as the contest UAV will have in the payload missions.

After the detailed design was completed, the team started to build the first contest airplane. In order to simulate mission performance, this airplane was modular, light, and with a baggage compartment. During flight tests, the airplane's full mission simulation included fast extraction from the suitcase, on site assembly, and payload loading.

After flight tests were completed, conclusions were drawn. Following this the second and third aircraft construction began, optimized for aspects of weight and drag, implementing the design modifications concluded from the test flights.

6.1 Process selected for manufacture of major components and assemblies

- 6.1.1 Performance demonstrator manufacturing – The goal of the performance demonstrator was to simulate real contest flight from aerodynamic and propulsion point of view. However, due to limited time, the construction was completed very quickly. Hence the structures of the airplane were foam based, laminated with fiberglass and epoxy resin to enhance toughness. In order to simulate the chosen geometry exactly, a pod was constructed, also from foam, and laminated with carbon fiber. Inside the pod were placed all the communication and control systems. Moreover, in order to simulate correct flight weight, metal chips were installed into the foam pod, correcting the C.G. location as well.



Figure 19: Prototype at its final stages of assembly.

6.1.2 Manufacturing first aircraft

- Manufacturing main wing– The main wing was manufactured from laser cut profiles mounted on a main tubular spar. At the front third of the chord, more profiles were mounted, to prevent deformation of the wing's thin coating by relatively high curvature and dynamic pressure. The outer sections of the main wing were manufactured exactly the same, except at their back where 20% flaperons were mounted. The flaperons were constructed from balsa ribs, covered with thin balsa panels. In order to achieve better precision, jigs were made, and all the construction process was held on those jigs.



Figure 20: Four sections of the main wing in construction.

- Manufacturing horizontal stabilizer– This was constructed in a very similar manner to the outer parts of the main wing. The only difference was that the elevator main spar was as mentioned at section 5, a wooden *I* section.
- Vertical stabilizer – The vertical stabilizer was made from two layers of very fine carbon fiber fabric with 30% epoxy resin (all carbon fiber parts were constructed with that ratio, as flight standard ration). Figure 21 shows the attention paid to drag reduction in sinking the servo inside the stabilizer's box.



Figure 21: Rudder servo.

- Pod – The pod was designed to be tolerant to impact, but yet be light enough. A fiberglass and Kevlar shell was made, with foam core to support payloads. In order to reduce skin friction drag even more, and in order to easily shape the chosen geometry, a female mold had to be made. A wooden block was hand carved on a lathe. Then female fiberglass mold was manufactured. The pod was made longer than designed, and was cut out to the correct size later.

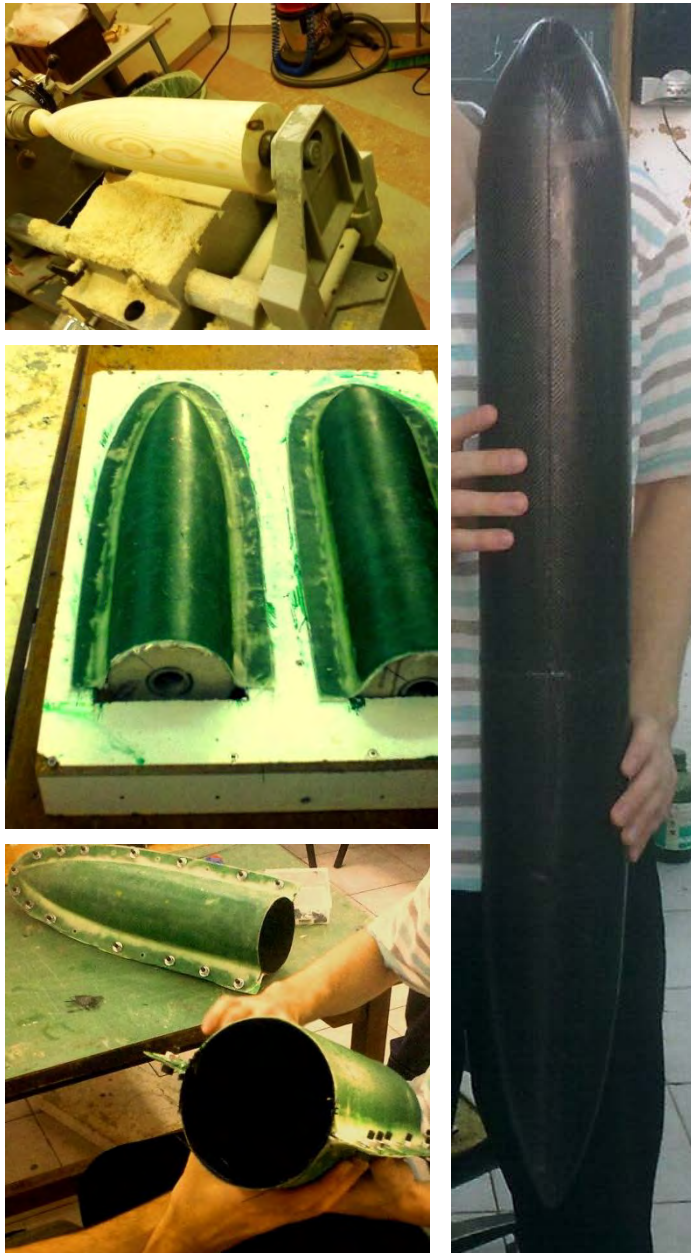


Figure 22: Pod construction process.

6.2 Manufacturing processes selection

The main parameters considered when deciding upon construction of aircraft sub assemblies were:

- Manufacturability – This includes ease of manufacturing by unqualified personnel.
- Precision and Time – Precise construction could improve aircraft performance, however it costs more time. Creative solutions had to be invented in order to save construction time, and maintain high manufacturing precision.
- Drag – Ability to manufacture aerodynamically efficient parts in view of surface friction drag and turbulence reduction.
- Modularity – Construct modular and interchangeable specific parts.
- Commercial availability and price – The commercial availability of parts that the team decided to order like carbon fabrics, carbon tubes, and power sub system components was taken into consideration. The parts delivered had to be bought at a reasonable price, and supplied in proper time.
- Assembly time – The parts constructed, especially connectors, had to be quick to assemble in the field, at the competition.
- Impact energy absorption – Due to belly landing, all aircraft components had to be able to absorb impact energy without damage. However, for some components this quality was less critical than for others.

In order to save later construction time, the tradeoffs investigation, and construction process selection were carried out in almost every major aircraft sub assembly. Process summary and results are shown in Tables 18-24.

| Figure of merit | Weight | Foam Core with Balsa Coating | Foam Core with Carbon Coating | Ribs with Carbon D-box | Ribs with Tubular spar |
|-------------------|--------|------------------------------|-------------------------------|------------------------|------------------------|
| Weight | 0.35 | 3 | 2 | 4 | 5 |
| Strength | 0.35 | 3 | 5 | 4 | 3 |
| Manufacturability | 0.1 | 4 | 3 | 2 | 5 |
| Precision/Time | 0.2 | 4 | 3 | 2 | 4 |
| Total | 1 | 3.3 | 3.35 | 3.4 | 4.1 |

Table 18. Main wing manufacturing tradeoffs.

| Figure of merit | Weight | Body engulfing cargo | Boom |
|-------------------------------|--------|----------------------|------|
| Modularity | 0.2 | 1 | 4 |
| Strength | 0.2 | 4 | 5 |
| Aerodynamic drag | 0.3 | 2 | 4 |
| Commercial Availability/Price | 0.3 | 1 | 4 |
| Total | 1 | 1.9 | 4.2 |

Table 19. Body manufacturing tradeoffs.

| Figure of merit | Weight | Of-The-Shelf cylindrical PVC pipe | Carbon (male mold) | Carbon (female mold) | Kevlar with fiberglass (female mold) |
|-------------------|--------|-----------------------------------|--------------------|----------------------|--------------------------------------|
| Weight | 0.3 | 1 | 3 | 3 | 4 |
| Strength | 0.3 | 4 | 3 | 3 | 2 |
| Durability | 0.2 | 4 | 3 | 3 | 4 |
| Manufacturability | 0.05 | 4 | 4 | 3 | 3 |
| Drag | 0.15 | 3 | 3 | 4 | 4 |
| Total | 1 | 2.95 | 3.05 | 3.15 | 3.35 |

Table 20. Pod manufacturing tradeoffs

| Figure of merit | Weight | Embracers | Bullets | Aluminum connectors (folded to hexagonal shape) |
|--|--------|-----------|---------|---|
| Weight | 0.4 | 1.2 | 1.6 | 1.2 |
| Assembly time | 0.3 | 0.3 | 0.6 | 0.9 |
| Impact Energy Absorption | 0.1 | 0.4 | 0.2 | 0.4 |
| Tolerance of assembly (changes in concentricity on separate occasions) | 0.2 | 0.2 | 0.6 | 0.6 |
| Total | 1 | 2.1 | 3 | 3.1 |

Table 21. Pod connectors manufacturing tradeoffs.

| Figure of merit | Weight | Carbon Drilling with bolts/screws. | Pin Fitting | Aluminum Connectors |
|--|----------|------------------------------------|-------------|---------------------|
| Weight | 0.4 | 3 | 4 | 3 |
| Withstanding Abrasion (repeating usage) | 0.1 | 1 | 2 | 3 |
| Ease of assembly (Time) | 0.3 | 4 | 2 | 4 |
| Tolerance of assembly (changes in concentricity on separate occasions) | 0.2 | 1 | 3 | 3 |
| Total | 1 | 2.8 | 3.5 | 3.7 |

Table 22. Boom Connectors manufacturing tradeoffs

| Figure of merit | Weight | Full Balsa | Ribs | Foam core with balsa coating |
|-------------------|----------|------------|----------|------------------------------|
| Manufacturability | 0.1 | 5 | 3 | 4 |
| Weight | 0.3 | 2 | 5 | 3 |
| Drag | 0.4 | 2 | 4 | 4 |
| Strength | 0.2 | 4 | 3 | 4 |
| Total | 1 | 2.7 | 4 | 3.7 |

Table 23. Elevator manufacturing tradeoffs.

| Figure of merit | Weight | Full Balsa | Ribs | Foam core with balsa coating | Carbon box |
|-------------------|----------|------------|------------|------------------------------|------------|
| Manufacturability | 0.1 | 5 | 4 | 4 | 5 |
| Weight | 0.4 | 1 | 5 | 3 | 4 |
| Strength | 0.5 | 4 | 3 | 4 | 5 |
| Total | 1 | 2.9 | 3.9 | 3.6 | 4.6 |

Table 24. Rudder manufacturing tradeoffs

6.3 Manufacturing work plan

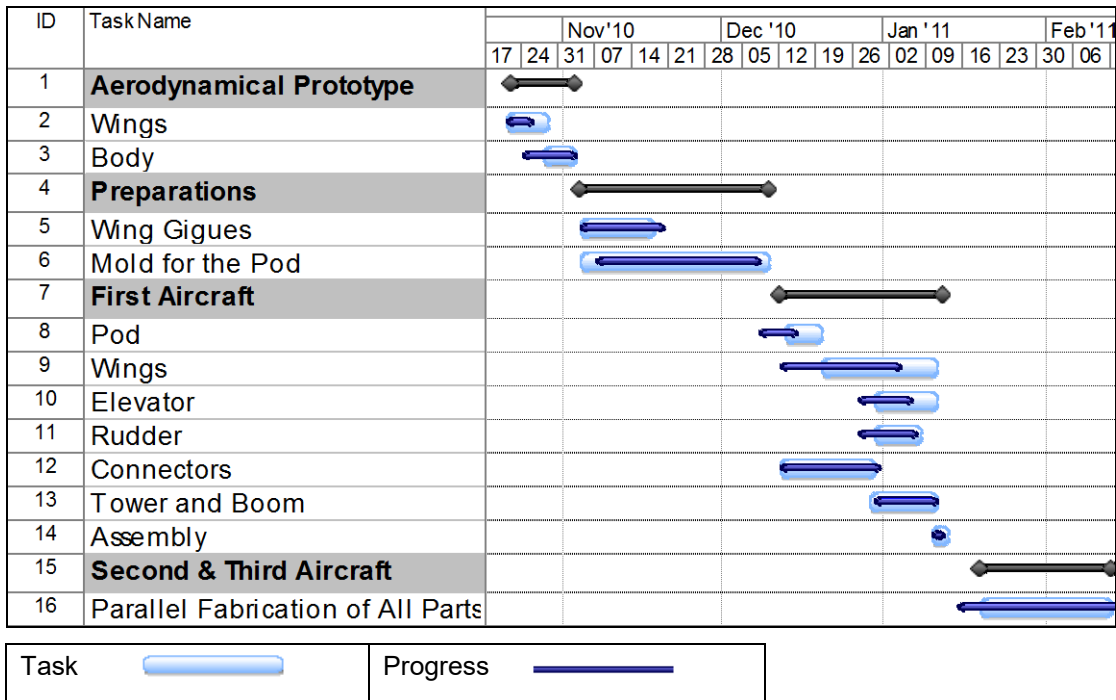


Figure 23: Manufacturing milestone chart.

7. Testing Plan

The testing plan included conceptual testing, preliminary testing and detailed design testing. Conceptual testing focused on revealing design complications in order to change the design at the beginning of the process if necessary. Preliminary design testing focused on validation of the main design features such as airfoil design and performance. Detailed design testing focused on components and their function in the system. Simultaneously, computerized analyses were made in order to validate the design before construction began.

7.1 Objectives

7.1.1 Propulsion System Testing

Propulsion system performance, being a key factor in the aircraft design, was tested prior to the flight testing in order to ensure that the actual system performance matched the predictions made, and to allow for further optimization. The test bed was assembled in the Technion wind tunnel facilities, as shown in Fig. 24.



Figure 24: Wind tunnel test preparations.

- Battery testing – The ELITE 1500 battery packs were tested under load in order to check their performance at expected flight conditions. The main properties checked were the typical voltage drop and actual usable capacity.
- Propulsion system wind tunnel testing – The propulsion system assembly was tested as a complete unit with the components selected in the detail design. The test objective was to see how the components worked together, and to measure the system's actual performance. Parameters such as thrust, torque, RPM, current, and voltage, were measured at various airspeeds.
Additionally, the system was tested with a variety of propellers to create an informative database, enabling verification of the propeller's optimization process, and improving the selection if possible.
- Propeller testing – Propeller testing was performed in the Technion's wind tunnel. A constant power source and motor were used with different values of diameter or pitch angle in order to determine and optimize the thrust and the RPM for each mission. In addition, the temperature of the motor and the current were measured to verify they were within reasonable values.
- Motor testing – Motor testing was performed in the Technion's wind tunnel with the chosen propeller for each mission and using a constant power source, in order to validate the predicted performances so that changes could be made at the beginning of the process.

7.1.2 Structural tests

Structural tests were performed on both the materials prior to assembly and to the finished assemblies. The plan included all recommended tests the team found in the literature, and was vital to this type of aircraft, and its specific mission range.

- Tensile strength testing – The tests were conducted in the Technion structure lab on a tension machine. The main goal of these tests was to determine the properties of the structural components. It was essential to determine whether the structure, made from carbon fiber tubes is feasible and will sustain estimated loads.

Moreover, tests had to establish the specific properties of the selected carbon tube samples to determine the best diameter and thickness. The tension tests permitted establishing Young's modulus and the ultimate tensile strength of the materials.

The selected tubular structure of the plane, enabled a few simple tension tests to ensure the structural capabilities of the ensuing design with very high certainty.



Figure 25: Tension machine in the Structures Laboratory and test samples.

- Assemblies bending tests – Although the materials tests predicted the structural capabilities with high precision, full structure bending tests had to be performed due to high uncertainty in the quality of the connectors and the adhesive bonding between the aluminum connectors and the carbon fiber tubes. Also, despite confidence in early calculations, extra caution was taken in order to see the loads action on the structure in the controlled laboratory environment prior to the outdoor test flights.

The team conducted bending tests on the wing, one simulating static loading on the pre flight check, and one with distributed loading on the whole wing spar, in order to simulate the lift force.

7.1.3 Assembly and loading time simulation

Due to limited time in the competition rules, and despite all efforts made during the design process, the team simulated the on site assembly process in order to improve assembly time and choose the fastest assembler. In addition, the competition ground system was simulated, with the aircraft and all equipment. Timed assembly of the equipment, stores and aircraft was performed. All safety inspections were checked to verify the aircraft can handle the flight properly.

7.1.4 Aerodynamical prototype testing

As earlier mentioned, due to lack of sufficiently wide cross sectioned wind tunnel facility at the Technion able to test a full scale, or even a half scale plane, the team decided to construct a geometrically identical performance demonstrator. The demonstrator goal was to prove the feasibility of the design from the aerodynamical point of view. Also, the team decided to see if the chosen power subsystem components suit the design as expected.

7.1.5 Flight testing

Comprehensive flight testing was performed to confirm if all structural, electrical and flight performances are as planned. All mission requirements were checked. The team collected data about the aircraft and confirmed that all the systems could coexist. The pilot used the flight tests to practice and improve his/her skills and to become familiar with the specific aircraft parameters. Pilot feedback was used to design future improvements of the aircraft such as electrical reliability, weight reduction and controllability.



Figure 26: First aircraft at its fourth flight session.

7.2 Test Schedule and check list

| Test | Objective | Start date | End date |
|-----------------------------------|---|------------|----------|
| Materials | Verify adequate strength needed | 9/25 | 10/20 |
| Propeller | Determine actual performance | 1/1 | 1/7 |
| Motor | Determine actual performance | 1/7 | 1/12 |
| Joint | Verify adequate strength needed | 1/1 | 1/12 |
| Assembling the plane in 5 minutes | Decrease the time to assemble | 1/10 | 1/13 |
| Timed loading of golf balls | Decrease the time of load | 1/10 | 1/13 |
| Flight Tests | <p>Check flight characteristics:</p> <ul style="list-style-type: none"> • Hand launch capabilities • Stall speed • Actual upper limit on carrying capabilities • Flight duration on variable throttle • Light weight mission performance <p>Find parameter to improve:</p> <ul style="list-style-type: none"> • Controllability • Eliminate unnecessary overdesigned parts, thus enabling weight reduction | 1/14 | 1/25 |

Table 25: Testing schedules and checklist.

8. Performance Results

8.1 Performance of key subsystems

- Battery performance - Several discharge tests of the batteries showed a significant voltage drop at high currents. Figure 27 shows an average cell discharge at 20 amps., The actual nominal cell voltage was below early predictions. Nevertheless, discharging over 1450 mAh, the batteries actual capacity under high current draw was beyond predictions, ensuring their ability to sustain mission flight times.

Decrease in battery pack voltage at high loads inevitably lowers the overall power rate of the propulsion system, therefore an attempt was made to add another cell to the battery pack. However the pack was originally designed to maximize its voltage and it was found that an extra cell would slightly exceed the competition battery weight limit.

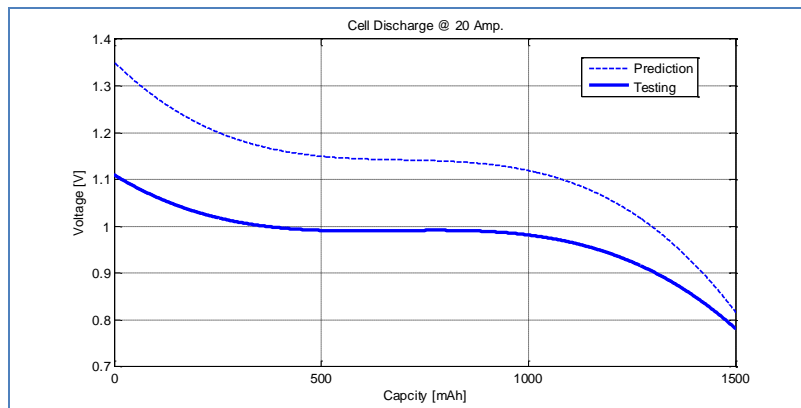


Figure 27: ELITE 1500 cell discharge.

- Propulsion system performance results - The propulsion system wind tunnel testing results are presented in Fig. 28. The results corresponded well with the predictions based on calculations made with MotoCalc software. The 13x11 propeller thrust was lower by 12% to 17% at high airspeeds compared to the prediction, which would subsequently result in lower top speed in mission 1; however, the actual current draw was about 15% lower than expected providing safety margins in terms of battery time. The thrust prediction of the 14x9.5 propeller was pretty accurate. Current draw was lower by about 6% at low-medium airspeeds.

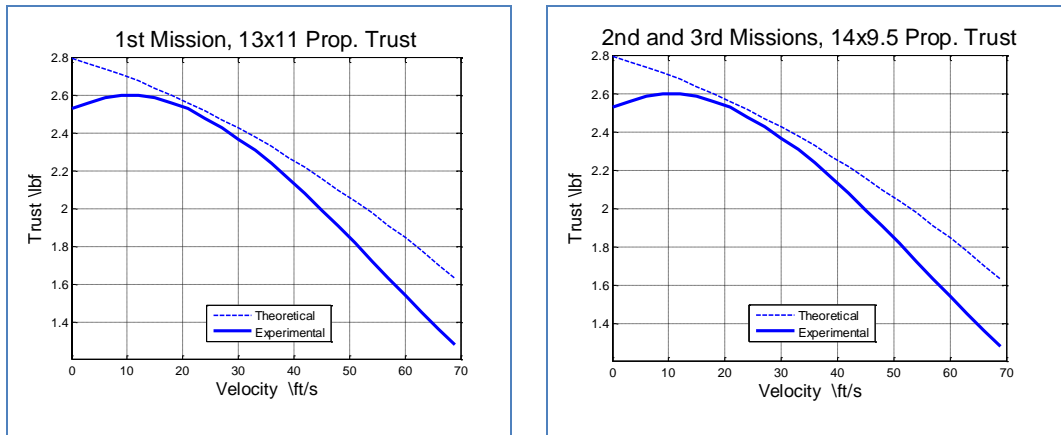


Figure 28: Trust comparison.

The low current draw enabled an improvement of the take off performance in missions two and three by switching to a 15x8 propeller. The larger propeller produced higher thrust by 10% without crossing the maximum allowable current and would enable safer hand-launch of the aircraft with heavier payloads.

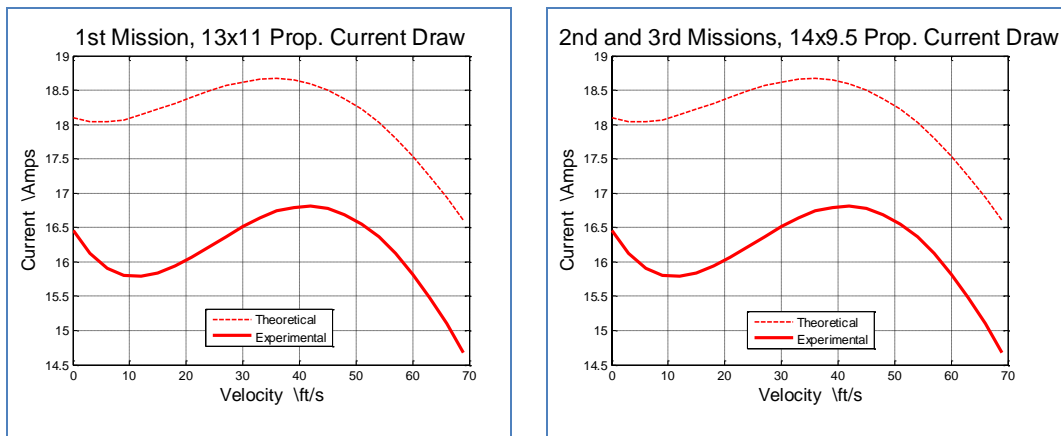


Figure 29: Motor current.

- Tension tests were performed in the Structures Laboratory. The results are shown in Figs. 30-31. Although tests were performed by lab experts, due to the unique structure of the carbon fiber material, and its special clamping technique to the tension machine, the tubes always failed around the clamping point and never reached their theoretical ultimate yield strength. However, the specific Young modulus was obtained for every tube section, enabling precise calculations, tube diameter and thickness selection, and prediction of the deflection.

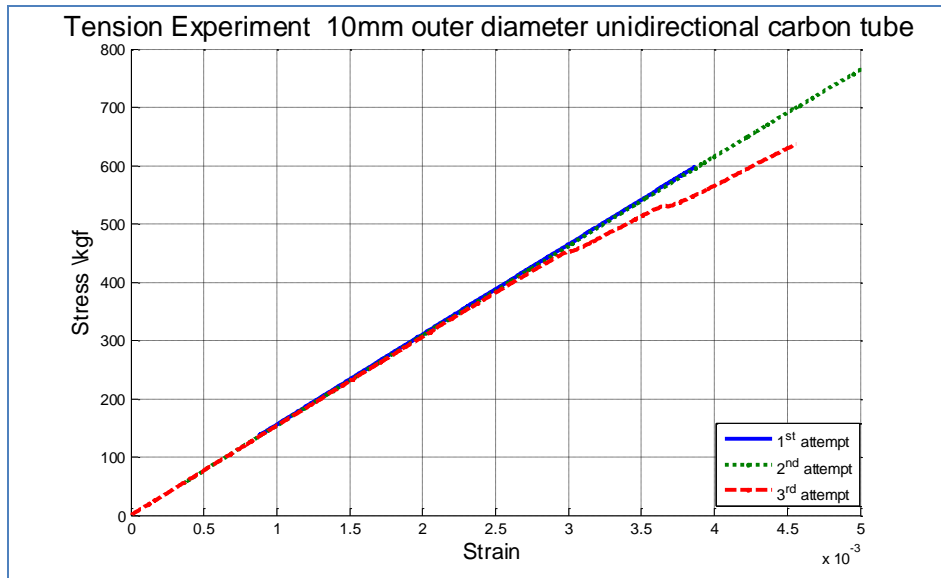


Figure 30: Unidirectional fiber orientation tube tests.

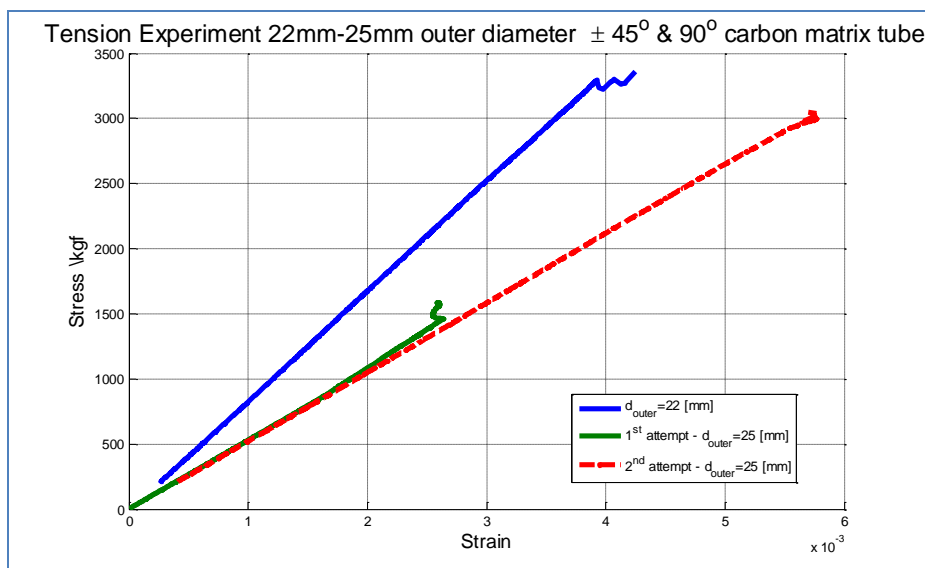


Figure 31: Multi-directional fiber orientation tube tests.

- The bending tests confirmed that the wing could stand a 3-G loading, and passed the preflight static test. Moreover, the team reached 4.5-G load when wing tips deflection crossed the predetermined safe value. The main boom withstands down force of 25 lbf, which is 2.5 times the anticipated tail influence on the lowest radius with the highest airspeed turn.

8.2 Performance of the complete aircraft

The final chapter of this report summarizes flight tests of the complete aircraft as performed at the airfield, and the suggested modifications and improvements that will be made to the aircraft after the submission of this report.

8.2.1 Flight test results of the complete UAV

As previously mentioned, the goals of the flight sessions were both to approve the design and manufacturing techniques, and to spot oversized components, so that future design will improve their functionality and lower their weight.

The first and most critical parameter to monitor was the motor current, as contest limitations prohibited breach of the 20 amps limit. As shown in Fig. 32, the team implemented conclusions from tunnel tests, and prior to the flight a 15" propeller was mounted on the aircraft. Figure 32 clearly reveals that the entire flight was flown close enough to the limit, but without crossing it, increasing payload lifting capabilities of the aircraft.

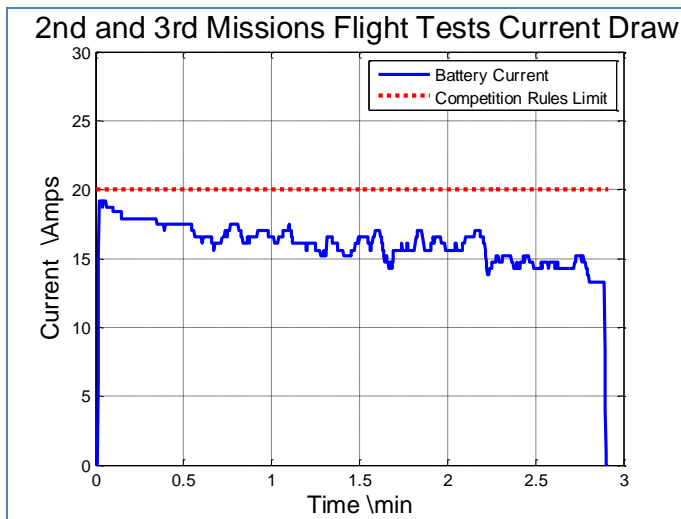


Figure 32: Flight test current draw.

The flight tests also included unpacking, and assembly of the aircraft on the runway. The best measured time was 3.5 minutes, much longer than anticipated. Further investigations will be carried out in order to find the critical components or assembly techniques that have to be modified and improved.

Table 26 summarizes the difference between expectations and demonstrated performance parameters of the whole aircraft:

| Mission | Parameter | Expectation | Test result | Difference |
|--------------------------------|-------------------------|-------------|-------------|------------|
| Dash to critical point mission | Takeoff Weight(lbs) | 4.08 | 4.05 | -1% |
| | Cruise Speed (ft/sec) | 70 | 75 | +6% |
| | Max. Speed (ft/sec) | 77 | 81 | +4% |
| | Stall Speed (ft/sec) | 12.4 | 01 | -19% |
| | Max. Turn Rate(deg/sec) | 68 | 58 | -15% |
| | No of laps completed | 6 | 6.5 | +8% |
| Payload missions | Takeoff Weight(lbs) | 6.9 | 7.2 | +4% |
| | Cruise Speed (ft/sec) | 56 | 56 | 0% |
| | Max. Speed (ft/sec) | 59 | 64 | +8% |
| | Stall Speed (ft/sec) | 06.6 | 05 | -10% |
| | Max. Turn Rate(deg/sec) | 68 | 60 | -12% |

Table 26: Expected and demonstrated performance comparison.

The actual performance of the final design was relatively close to expectations, calculated at earlier stages of the design. However, a few parameters differed by up to 20%, including stall speed, maximum speed and turn rate. A few reasons could explain these differences:

- The main reason for the high difference was probably due to the use of a different diameter propeller. A larger propeller, used as a conclusion from wind tunnel tests was capable of producing more thrust, enabling the airplane to maintain higher cruise speed, and extend its maximum airspeed.
- Different aerodynamics, unpredicted by the relatively simple aerodynamical model may explain the lower stall speed.
- It would appear that the tail of the airplane was less efficient than predicted, and was not able to turn the aircraft at the expected turn rate, especially during the faster flown mission. However, construction of a more massive tail would probably cost more drag, hence it was decided to keep the tail geometry as it is, especially due to the increase in numbers of laps already accomplished.
- The increased number of accomplished laps in the first mission gave an incentive to try and improve aerodynamics with a view to drag reduction. The team decided to try and improve flight performance of the airplane in order to be able to fly seven full laps until competition time.

- Due to the better propeller, the maximum takeoff weight was extended, and after manufacturing was completed, the real airplane weight was 1.2% less than expected according to the computerized model.

All the above parameters, summarized in Table 26, were relayed from a small pitot tube, which was mounted at the front of the main wing, outside the propeller trace. The resulting data fluctuated, and the uncertainty was around 2 ft/sec. Also the turns, and their course, were measured by the team members' eyes; indicating on a possibility for severe uncertainties.

8.2.2 Further improvements summary

The main goal is to enhance all mission parameters in the given time of four weeks. The next aircraft will be constructed to be lighter than the first one. Moreover, the aircraft will be suited to fill more golf balls due to the increase in the payload carrying capability as observed from the test flights. In order to shorten the assembly time on the runway, the connectors will be redesigned, and will all be self locking.



Figure 33: Takeoff by hand launch.



Figure 34: Airborne.

9. Bibliography

- Howe, D., Aircraft Conceptual Design Synthesis, London, 2000.
- Raymer, D.P., Aircraft Design: A Conceptual Approach, AIAA Educational Series, 1999.
- Anderson, J.D., Fundamentals of Aerodynamics, McGraw-Hill, 1991.
- Liepmann, H.W., Roshko, A., Elements of Gasdynamics, NY, 1958.
- Pope, A., Basic Wing and Airfoil Theory, McGraw-Hill, 1951.
- Jones, R.T., Wing Theory, Princeton University Press, 1990.
- Robinson, A., Laurmann, J.A., Wing Theory, Cambridge University Press, 1956.
- Tritton, D.J., Physical Fluid Dynamics, Oxford Science Publications, 1988.
- White, F.M., Viscous Fluid Flow, Mcgraw-Hill, 1991.
- Schlichting, H., Gersten, K., Boundary Layer Theory, Springer, 2003.
- Donaldson, B.K., Analysis of Aircraft Structures: An Introduction, McGraw-Hill, 1993.
- Young, W.C., Roark's Formulas for Stress And Strain, McGraw-Hill, 1989.
- Anderson, J.D., Airplane Performance and Design, McGraw-Hill, 1989.
- McCormic, B.W., Aerodynamics, Aeronautics, and Flight Mechanics, Canada, 1979.
- Holman, J.P., Experimental Methods for Engineers, McGraw-Hill, 1978.
- Doebelin, E.O., Measurement Systems, Mcgraw-Hill, 1975.

Georgia Institute of Technology

There Will Be Buzz

AIAA Design/Build/Fly 2010-2011
Design Report





TABLE OF CONTENTS

| | |
|--|-----------|
| 1. EXECUTIVE SUMMARY | 5 |
| 1.1 DESIGN PROCESS | 5 |
| 1.2 KEY MISSION REQUIREMENTS AND DESIGN FEATURES | 5 |
| 1.3 PERFORMANCE CAPABILITIES OF THE SYSTEM | 6 |
| 2. MANAGEMENT SUMMARY | 7 |
| 2.1 TEAM ORGANIZATION..... | 7 |
| 2.2 MILESTONE CHART..... | 8 |
| 3. CONCEPTUAL DESIGN..... | 9 |
| 3.1 MISSION REQUIREMENTS | 9 |
| 3.2 TRANSLATION INTO DESIGN REQUIREMENTS | 13 |
| 3.3 CONFIGURATIONS CONSIDERED | 14 |
| 3.4 COMPONENT WEIGHTING/SELECTION PROCESS..... | 15 |
| 3.5 FINAL CONCEPTUAL DESIGN CONFIGURATION | 17 |
| 4. PRELIMINARY DESIGN | 18 |
| 4.1 DESIGN METHODOLOGY..... | 18 |
| 4.2 DESIGN TRADES..... | 19 |
| 4.3 MISSION MODEL | 23 |
| 4.4 AERODYNAMIC CHARACTERISTICS..... | 23 |
| 4.5 STABILITY AND CONTROL | 31 |
| 4.6 MISSION PERFORMANCE | 32 |
| 5. DETAIL DESIGN | 33 |
| 5.1 FINAL DESIGN | 33 |
| 5.2 STRUCTURAL CHARACTERISTICS | 34 |
| 5.3 SYSTEM AND SUBSYSTEM DESIGN/COMPONENT SELECTION/INTEGRATION/ARCHITECTURE | 34 |
| 5.4 WEIGHT AND BALANCE | 37 |
| 5.5 FLIGHT AND MISSION PERFORMANCE | 38 |
| 5.6 DRAWING PACKAGE | 40 |
| 6. MANUFACTURING PLAN AND PROCESSES..... | 45 |
| 6.1 MANUFACTURING PROCESSES SELECTED | 45 |



| | |
|--|-----------|
| 6.2 MANUFACTURING PROCESSES INVESTIGATED | 46 |
| 6.3 MANUFACTURING MILESTONES..... | 48 |
| 7. TESTING PLAN | 49 |
| 7.1 OBJECTIVES AND SCHEDULES..... | 49 |
| 7.2 CHECKLISTS..... | 50 |
| 8. PERFORMANCE RESULTS..... | 52 |
| 8.1 COMPONENT AND SUBSYSTEM PERFORMANCE | 52 |
| 8.2. SYSTEM PERFORMANCE | 54 |
| 9. REFERENCES | 58 |



ACRONYMS AND NOMENCLATURE

| | | | |
|---------------|--------------------------------------|------------|----------------------------------|
| C.G. | Center of Gravity | e | Oswald Efficiency |
| M1 | Mission One | G_r | Motor Gear Ratio |
| M2 | Mission Two | K_v | Motor Voltage Constant (V) |
| M3 | Mission Three | n_{pll} | Positive Load Limit |
| FOM | Figures of Merit | \bar{p} | Dimensionless Rolling Rate |
| LT | Loading Time | \bar{q} | Dimensionless Pitching Rate |
| FT | Flight Time | \bar{r} | Dimensionless Yawing Rate |
| NiCd | Nickel-Cadmium | R_A | Aspect Ratio |
| NiMH | Nickel-Metal Hydride | R_e | Reynolds Number |
| NLL | Numerical Lifting Line | R_T | Taper Ratio |
| AVL | Athena Vortex-Lattice | S_w | Wing Area (ft ²) |
| RAC | Rated Aircraft Cost | T_s | Settling Time (s) |
| TFS | Total Flight Score | T_d | Doubling Time (s) |
| EW | Empty Weight | W | Weight, lbs |
| \tilde{C}_L | Airfoil Section Lift Coefficient | α | Angle of Attack (degrees) |
| \tilde{C}_D | Airfoil Section Drag Coefficient | β | Sideslip Angle (degrees) |
| \tilde{C}_m | Airfoil Section Moment Coefficient | μ_r | Rolling Coefficient of Friction |
| C_L | Aircraft Lift Coefficient | ω_d | Damped Natural Frequency |
| C_D | Aircraft Drag Coefficient | ω_n | Natural Frequency of Oscillation |
| C_y | Aircraft Side Force Coefficient | ζ | Damping Ratio |
| C_n | Aircraft Yawing Moment Coefficient | | |
| C_m | Aircraft Pitching Moment Coefficient | | |
| C_l | Aircraft Rolling Moment Coefficient | | |
| $C_{D,i}$ | Aircraft Induced Drag Coefficient | | |
| $C_{D,0}$ | Aircraft Zero-Lift Drag Coefficient | | |



1. EXECUTIVE SUMMARY

This report details the design, testing, and manufacturing of the Georgia Institute of Technology *There Will Be Buzz* entry in the 2010-2011 AIAA Design/Build/Fly (DBF) competition. This aircraft was designed to successfully complete three hand-launched flight missions: a low weight speed mission, and two endurance missions with internally carried payloads, all while minimizing empty weight to maximize the total score.

1.1 Design Process

The primary objective for *There Will Be Buzz* was victory; this would be achieved through the development of a light, compact aircraft that can fit in a carry-on suitcase. Conceptual design was started by translating the key mission requirements and mission scoring equations into design requirements. Next, the team chose a configuration that qualitatively maximized the total score from a wide design space. In the preliminary design phase, the configuration was further defined by evaluating different motors, batteries, propellers, and airfoils. Through this process, weight estimates, drag estimates and aerodynamic coefficients were calculated and introduced into a flight simulation environment that estimated mission performance. To further reduce the design space, a trade study analysis was completed using the flight simulation results. After the trade studies were completed, detailed design finalized all dimensions, airfoils, propulsion system components, and the method for integrating all of these components.

1.2 Key Mission Requirements and Design Features

A successful system design and high score come from the successful balance of key mission requirements. Specific design features were developed for each mission requirement and scoring element to maximize system performance and the overall competition score.

Empty Weight: The aircraft's empty weight is the most significant total score driver, and is composed of the weight of the airframe and propulsion system. To minimize weight and increase the score, the entire aircraft has been designed to be as minimalistic as possible, including structure, sizing, materials, batteries, motors, and propellers, while completing all three missions.

Storage and Assembly Constraints: The aircraft and all of its components are required to fit in an FAA legal-sized carry-on. This constraint complements the empty weight scoring by encouraging the most compact design possible. The largest component of the aircraft is 20" wide, and the total wingspan is only about 30". The small number of components both minimizes weight and drives assembly under the five minute requirement.



Hand Launch Requirement: Instead of the short take off and landing requirements from previous competitions, the aircraft must now be hand-launched, thereby adding a human element to the design. Structure, weight, and propeller thrust had to be adjusted to accommodate the launcher. Aerodynamic performance requirements, including stall velocity, were adjusted due to the lack of a rolling takeoff. The light, compact design required by other constraints helped the team achieve successful, consistent hand launches.

Payload Requirements: Two of the three missions require the storage of an internal payload: golf balls and steel bars. While equivalent in terms of aerodynamic performance, the geometry and structure were designed to safely accommodate either payload. Additionally, the payload requirement has a large influence on the Mission 2 and 3 score. The aircraft was designed to carry its own weight in payload and maximize the mission score.

Flight Time: The first mission requires that the aircraft complete as many laps of the designated flight path as possible in four minutes to maximize score. Accordingly, the propulsion system was designed to sustain near full-throttle flight for the entire duration of the four minutes while completing four to five laps, and still weigh as little as possible.

1.3 Performance Capabilities of the System

All of the specific design features created to maximize the performance of the system can be summarized by the following performance capabilities:

- Empty weight of 0.6 lbs
- 1:1 payload-to-aircraft empty weight
- 4 minute high-speed endurance
- 4-5 lap capability empty
- Simple, safe hand launches
- Successful assembly under 5 minutes
- Securely store the required payloads
- Proven capability through 2 prototypes and 22 test flights to date (as seen in Figure 1.1)



Figure 1.1: Aircraft in flight

Ultimately, the final design is a compact flying-wing design, with the aircraft designed to simultaneously minimize weight, size, and assembly time, while maximizing hand-launch, payload, and range capabilities; the propulsion system is designed to provide enough power to fulfill ambitious performance characteristics but weigh as little as possible; and the aircraft architecture and testing designed to build on previous teams' experience while continuing to push the envelope of practical, minimalistic designs. *There Will Be Buzz* is confident that this design solution has been optimized to best accommodate all performance requirements and maximize the total score.



2. Management Summary

There Will Be Buzz consisted of eleven students: two seniors, three juniors, two sophomores, three freshmen, and a graduate student. Eight of the eleven were returning members from the 2009-2010 Georgia Tech DBF entry, *Down to Buzzness*. *There Will Be Buzz* combines the right amount of manpower with the continued advantage of a core of experienced members returning to build the teams' knowledgebase and pass it down to newer members.

2.1 Team Organization

The team used a hierarchal structure to establish leadership and responsibility amongst its senior members, and have the responsibilities flow down to the team's newer members, as seen in Figure 2.1. This hierarchy served as an outline only, as all team members collaborated extensively to reach deadlines, share ideas, learn the various disciplines, and produce a more successful aircraft. The work was divided during the design phases into aerodynamics, structures, electrical, propulsion, and CAD, while during construction, testing and report writing, all team members participated fully.

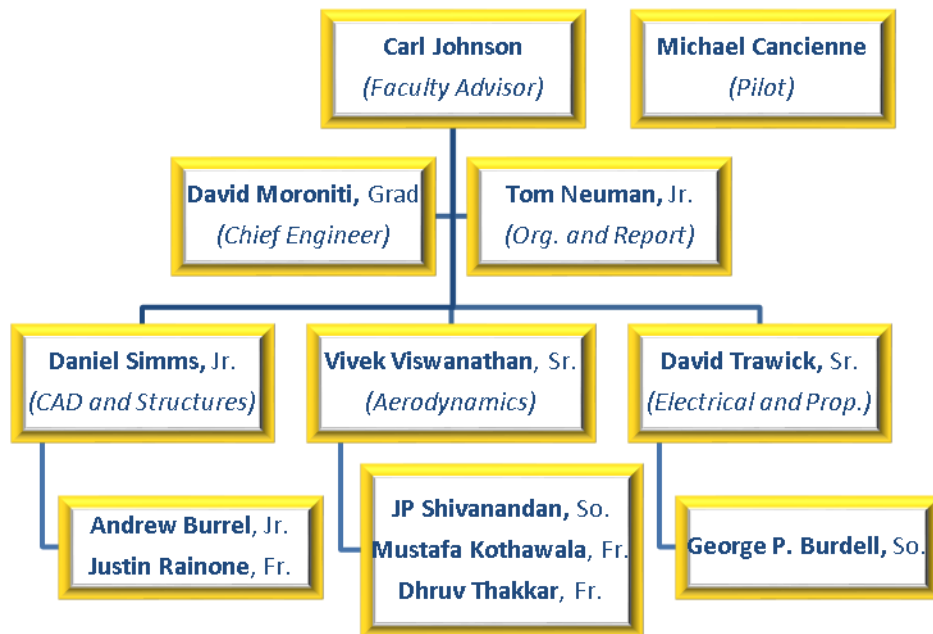


Figure 2.1: Organization chart, with returning members as group leads (italicized)



2.2 Milestone Chart

A milestone chart was established at the beginning of the design process to capture design and manufacturing goals as well as major deadlines. Progress was recorded and monitored by the team leaders to ensure all major milestones were met. The team worked throughout the entire school year, and established stringent deadlines early in order to gain testing and flight experience before the April competition. The team met frequently with faculty advisor Carl Johnson to discuss progress. The milestone chart is shown below in Figure 2.2, capturing planned and actual timing of major events.

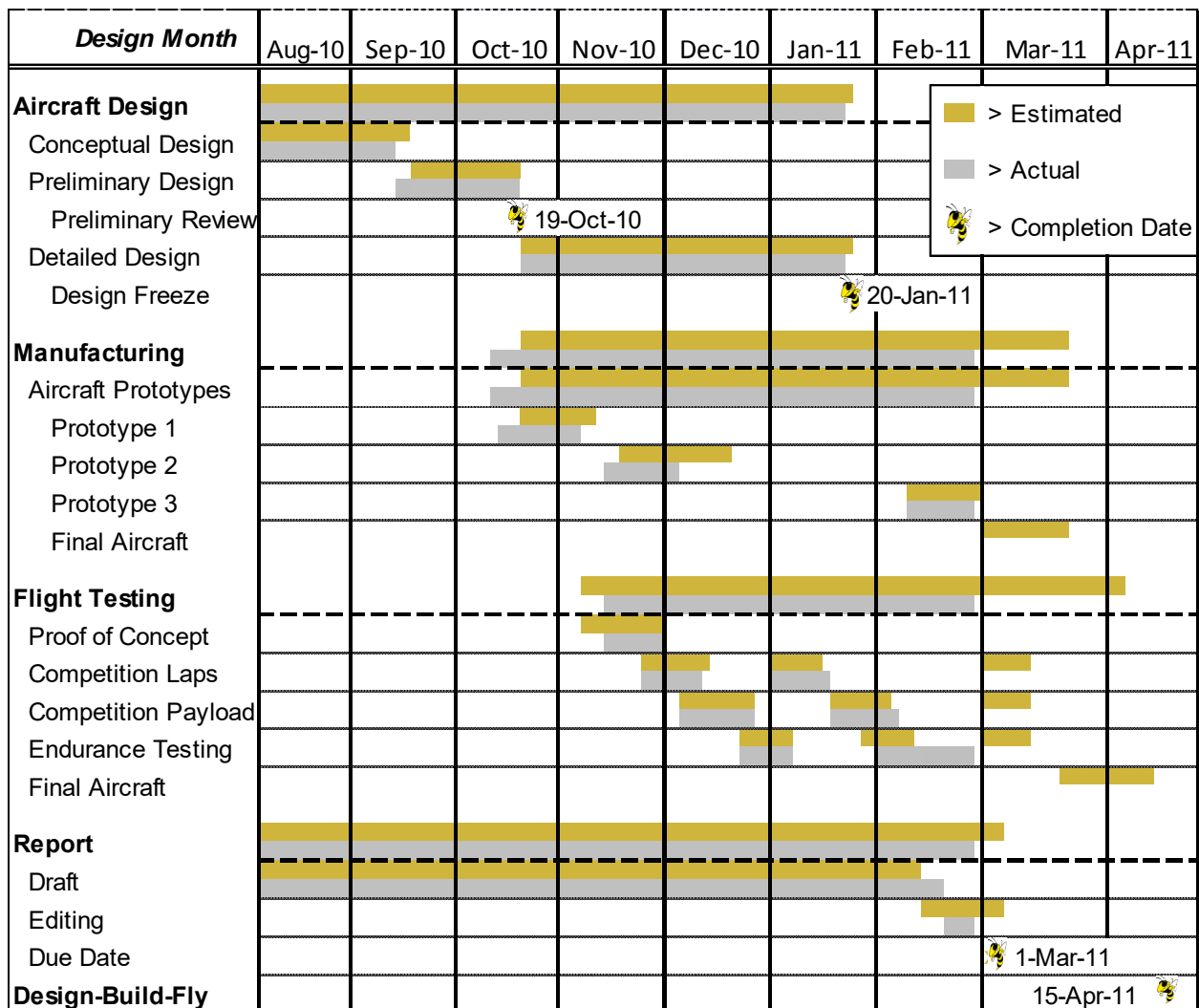


Figure 2.2: Aircraft design milestone chart showing planned and actual timing of objectives – major deadlines are marked by Buzz, Georgia Tech’s mascot.



3. CONCEPTUAL DESIGN

The Conceptual Design phase was used to evaluate the competition rules, translate them into design metrics, and produce a feasible design configuration that maximizes the score. The team performed a quantitative scoring analysis in order to pinpoint scoring drivers, and a qualitative translation of specific mission requirements and rules into characteristics that a successful aircraft must possess. These were combined in Figures of Merit (FOMs), a metric applied to weigh different design choices against each other. The FOMs were applied to a design space of over 55,000 possible aircraft configurations, and yielded a single conceptual design that *There Will Be Buzz* is confident will be the best aircraft. The resulting configuration is a lightweight flying wing with a tractor propeller.

3.1 Mission Requirements

3.1.1 Mission and Score Summary

The AIAA Design/Build/Fly 2011 Competition consists of three flight missions and the design report. The total score for each team is calculated as seen in Equation 3.1:

$$\text{Score} = \text{Report Score} * \text{TFS} / \sqrt{\text{RAC}} \quad (3.1)$$

Where TFS stands for the Total Flight Score from all three missions, calculated using Equation 3.2:

$$\text{TFS} = \text{M1} + \text{M2} + \text{M3} \quad (3.2)$$

Missions 1-3 are each weighed differently, as discussed further below. The last component of the score is RAC, or Rated Aircraft Cost, a term describing the highest empty weight (EW) of the aircraft in any of the missions, as seen in Equation 3.3:

$$\text{RAC} = \text{Max}(\text{EW1}, \text{EW2}, \text{EW3}) \quad (3.3)$$

Therefore empty weight is a direct score driver, whereas various performance factors of the design are lumped into TFS, comprising of Missions 1-3. All missions are flown along the same distance and pattern:

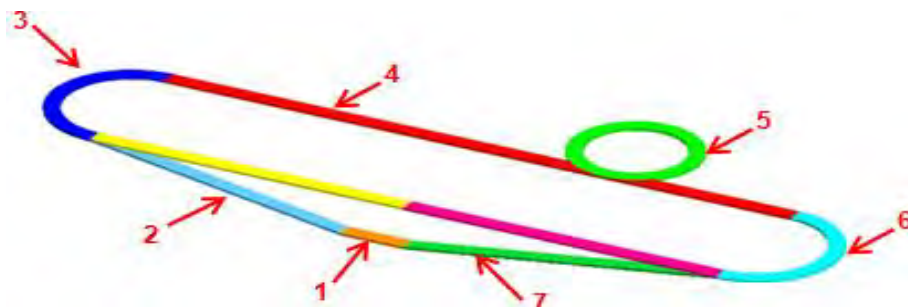


Figure 3.1: Competition flight course split into flight sections



The individual portions of the flight pattern seen in Figure 3.1 are as follows:

1. Successful hand launch
2. Climb to safe altitude
3. 180° U-turn, 500 feet from the start/finish line
4. 1000 feet downwind
5. 360° turn along the backstretch
6. 180° U-turn
7. 500 feet upwind / Successful landing

Each lap is approximately 2000 feet long, or roughly half of a mile when accounting for the turns involved. A complete successful lap is defined as beginning and finishing across the start/finish line while still in the air. The pattern is flown a different number of times for Missions 1-3, and each of the missions is weighed differently.

Mission 1 – Dash to Critical Target – the aircraft must complete as many laps as possible during 4 minutes, with the time beginning when the aircraft leaves the launcher's hand. The number of laps is counted to the last *full lap* completed within the four minute interval. To yield a score, the number of laps is normalized by the maximum number of laps completed by any team flying Mission 1, as seen in Equation 3.4:

$$\text{Mission 1} = 1 \times \frac{\text{Number of Laps}}{\text{Maximum Number of Laps}} \quad (3.4)$$

Mission 2 – Ammo Re-Supply – the aircraft must complete three laps while flying with a team supplied minimum 3"x4" steel bar Payload stored internally. This includes hand-launching with the extra payload. The score is calculated as the weight of the payload divided by the flight weight (gross takeoff weight) of the aircraft, reflecting the aircraft's lift-to-weight ratio. Mission 2 is weighed the most of all three missions, as seen in Equation 3.5:

$$\text{Mission 2} = 3 \times \frac{\text{Payload Weight}}{\text{Flight Weight}} \quad (3.5)$$

Mission 3 – Medical Supply Mission – the aircraft must complete three laps while flying with a team selected number of golf balls stored internally. This includes hand-launching with the extra payload. The number of golf balls carried is normalized by the maximum number of golf balls carried by any team successfully completing Mission 3, as seen in Equation 3.6. This mission is weighed less than M2, but both payload missions are weighed more than M1.

$$\text{Mission 3} = 2 \times \frac{\text{Number of Golf Balls}}{\text{Maximum Number of Golf Balls}} \quad (3.6)$$



3.1.2 Aircraft Constraints

The competition rules stipulate specific constraints on the design's size and storage, propulsion system, and payload:

Size and Storage – the aircraft and all components necessary for its assembly and operation must be stored inside an FAA legal sized soft-case carry-on suitcase. The FAA legal size is a case that does not exceed 45 dimensional inches (height + width + length), with no single dimension exceeding 22". This means that no single solid component of the aircraft may exceed 22", and must actually be even smaller to fit inside the carry-on. There is no requirement that the aircraft be unassembled; however, if the team determines some dimension, for example wingspan, must exceed 22", then tool storage in the case and assembly time must be considered. There is a five-minute assembly limit. The radio transmitter does not need to be stored in the case.

Propulsion System – the aircraft must be propeller driven and electrically powered, with all components of the propulsion system commercially available. These include the motor, propeller, speed controllers, receivers, and batteries. The battery selection is limited to NiCd or NiMH, but may be of any cell count, voltage, or capacity. The entire propulsion battery may weigh no more than 3/4 of a pound, and is limited by a blade style fuse to a 20 amp current draw.

Payload – the aircraft's payloads for Missions 2 and 3 must be stored fully internally to the mold-lines of the airframe. The golf ball payload will be provided by the competition administration. The steel bar payload will be team provided, but the dimensions must be at least 3"x4". Choice of thickness is left up to the team to use in determining payload weight. Both payloads must be securely fastened to the aircraft's structure so that they do not shift or come loose during flight.

3.1.3 Scoring Sensitivity Analysis

The scoring sensitivity analysis of Figure 3.2 visualizes the driving score factors in Missions 2 and 3, both three-lap payload missions, which represent 5/6 (83%) of the possible TFS. Included in the score is the normalization by RAC. The ranges were selected based on the Team's estimate of competitive and realistic aircraft configurations. The term "Payload Factor" is used in order to non-dimensionalize the lifting capability of the aircraft relative to its own empty weight, similar to Mission 2 scoring. For Mission 3, the maximum number of golf balls is defined as the maximum payload, or the highest Empty Weight multiplied by the highest Payload Factor, so the sensitivity analysis reflects its own ranges.

The vertical Score axis is normalized as a percentage of the *best combined M2+M3* Score, not necessarily reflecting the *maximum possible* score of five points, because DBF is an exercise in performing trades to optimize combined performance. The optimum is therefore obtained by minimizing Empty Weight while combining a high Payload Factor. Either an increase of 0.10 lbs. in Empty Weight or a decrease of 0.06 Payload Factor cause a 10% loss of the maximum combined M2+M3 Score.

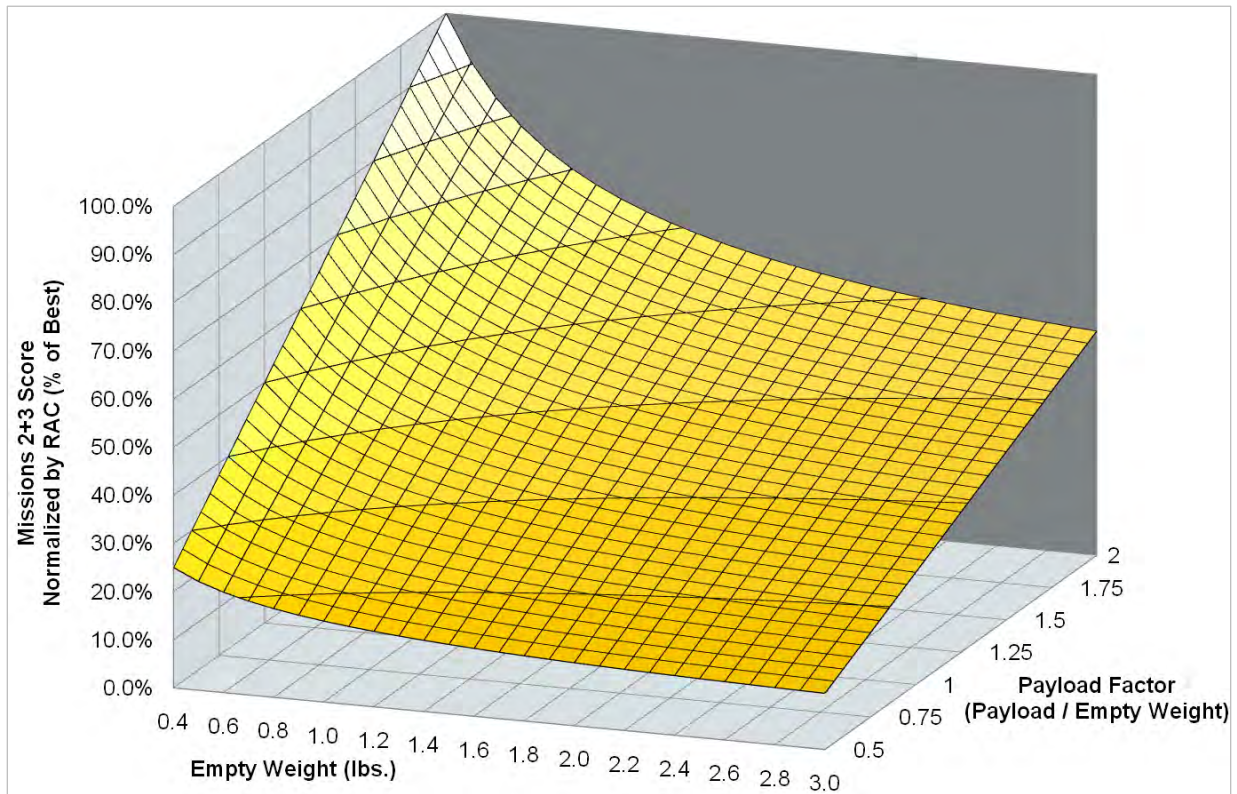


Figure 3.2: Missions 2 and 3 scoring sensitivity analysis

The remaining 17% percent of the score is in Mission 1, the speed ferry mission. Although it only represents a small fraction of the score, in order to compete with the best teams overall, Mission 1 would also have to be competitive. Its scoring sensitivity is seen in Figure 3.3. The maximum realistic number of laps completed by any team was estimated to be 8, reflecting an average flight speed of approximately 90 feet per second for four minutes. Every lap under 8 is a loss of 0.125 points out of the single possible point for M1, or only 2.1% percent of the maximum possible TFS of 6 points. Additionally, every lap under 8 means the propulsive system needs to generate the equivalent of 10 ft/s less thrust, possibly saving weight.

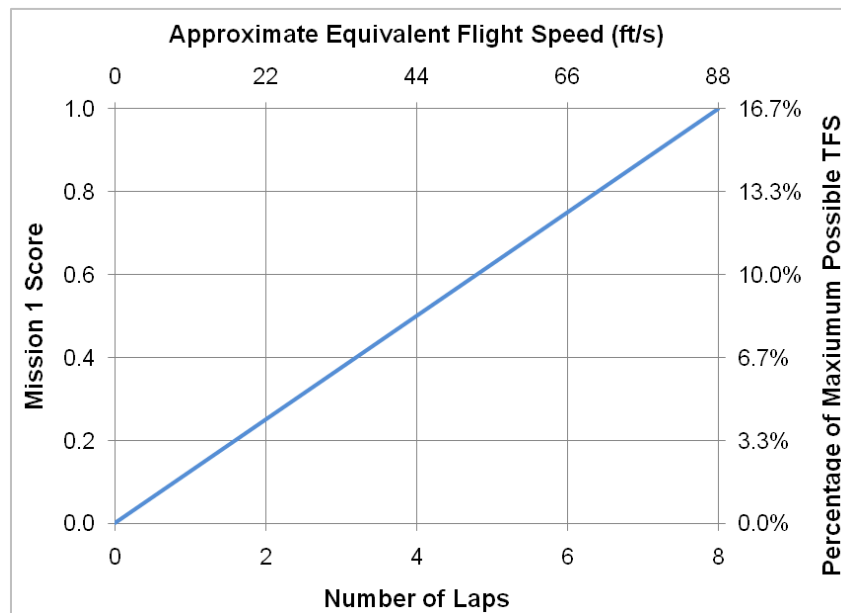


Figure 3.3: Mission 1 score sensitivity analysis

3.1.4. Understanding the Hand Launch Requirement

Since the hand launch requirement adds a human factor to the aircraft's design and takeoff performance, the team sought to gain a firm understanding of the requirement before translating it into design. Using a store-bought glider, various team members practiced a hand-launched takeoff in the style stipulated by the competition rules. The team gained a conceptual grasp of the ergonomics and structural requirements of hand-launching an aircraft.

3.2 Translation into Design Requirements

3.2.1 Qualitative Design Requirements

The competition rules and scoring requirements were translated into qualitative design metrics that could be used to evaluate and choose an aircraft configuration. These are summarized in Table 3.1:

Table 3.1: Translation into Design Requirements

| Mission/Scoring Requirement | Design Requirement |
|-----------------------------|-----------------------------------|
| Hand Launch | Low stall speed, good grip design |
| Low flight times | High thrust, low drag |
| High payload | High lift |
| Internal payloads | Internal bays |
| Low weight | Efficient structure |
| Case storage | Compact structure |



The final configuration needs to fulfill requirements which clearly divide into two components, as follows:

- Performance: high lift-to-drag ratio (L/D), high thrust, and low stall speed
- Structure: a compact, efficient structure with internal payload bays, and a good hand grip

3.2.2. Figures of Merit

From the quantitative scoring sensitivity analysis in Section 3.1.3 and the qualitative translation into design requirements in the section above, *There Will Be Buzz* was able to select and quantify specific metrics that will be used in the down-selection of aircraft configuration, Figures of Merit. These were assigned an importance of 0 through 5, with 5 being the most important factor and 0 being a non-factor in design, as seen in Table 3.2. Weight was determined to be the most critical scoring factor (FOM = 5), and the hand launch a design factor critical to any successful flight (FOM = 3). Both speed and storage were assigned FOMs of 2, because speed does not impact score as significantly, and component storage is a relatively flexible design feature.

Table 3.2: Figures of Merit

| Figure of Merit | 0 | 1 | 2 | 3 | 4 | 5 |
|-----------------|---|---|---|---|---|---|
| Weight | | | | | | 5 |
| Speed | | | 2 | | | |
| Hand Launch | | | | 3 | | |
| Storage | | | 2 | | | |

3.3 Configurations Considered

After determining the FOMs and requirements, the next step of Conceptual Design was establishing a design space that considered all possible aircraft concept configurations. The Matrix of Alternatives contained five major categories: wings, fuselage, empennage, propulsion, and landing gear. With all component alternatives considered, the design space contained over 55,000 different potential configurations, shown in Table 3.3:

Table 3.3: Complete Matrix of Alternatives

| Components | Alternatives | | | |
|---------------------|--------------|--------------|--------------|-------------|
| Wing Layout | Flying Wing | Biplane | Conventional | Tandem Wing |
| Wing Attachment | Low | Middle | High | Blended |
| Fuselage Shape | Blended | Rounded | Circular | Square |
| Number of Fuselages | 0 | 1 | 3 | 4 |
| Tail Type | V-tail | Conventional | H-Tail | T-Tail |
| Tail Attachment | One Boom | Two Booms | On Fuselage | |
| Number of Engines | 1 | 2 | | |
| Engine Location | Pusher | Tractor | Both | |
| Landing Gear | Skids | Tricycle | Tail Dragger | |



3.4 Component Weighting/Selection Process

To downsize the design space from all possible configurations presented in the Matrix of Alternatives, qualities of different options were measured against each other with each Figure of Merit multiplied by a Scoring Value, described in Table 3.4. The alternative with the highest total quality was then selected for further stages of the design.

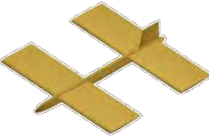
Table 3.4: FOM and alternatives weighting values

| Score | Value |
|-------|----------|
| 1 | Inferior |
| 3 | Average |
| 5 | Superior |

3.4.1 Wing Layout

Four wing configurations were compared to each other based on the FOMs as seen in Table 3.5. The two main FOMs that make a flying wing superior to a conventional wing layout are weight and storage. With Conceptual Design being a qualitative analysis, the team built upon its experience from previous competitions and determined that flying wings are in general a lighter design, due in part to the lack of empennage. The tail-less aircraft would also be simpler to store in the carry-on and assemble, since there would be no need for a removable tail assembly or control lines to be connected to an empennage's control surfaces.

Table 3.5: Weighting for number and style of wings

| | | Wing Layout | | | |
|--------------|--------|---|---|--|---|
| | |  |  |  |  |
| FOM | Weight | Flying Wing | Biplane | Conventional | Tandem Wing |
| Weight | 5 | 5 | 1 | 3 | 3 |
| Speed | 2 | 3 | 3 | 3 | 3 |
| Hand Launch | 3 | 3 | 1 | 3 | 3 |
| Storage | 2 | 5 | 1 | 3 | 1 |
| Total | 12 | 50 | 16 | 36 | 32 |

The design choice of a flying wing automatically excluded the following alternatives: wing attachment, fuselage shape, number of fuselages, tail type, tail attachment, and the tail dragger landing gear option from further consideration. There was therefore no need for qualitative selection in the eliminated categories.



3.4.2 Propulsion

Number of Engines: Two options for the number of engines were compared to each other based on the FOMs as seen in Table 3.6. A single engine proved to be the superior alternative, owing to the weight savings, thereby maximizing score.

Table 3.6: Weighting for number of motors

| | | Number of Engines | |
|--------------|--------|-------------------|-----|
| FOM | Weight | One | Two |
| Weight | 5 | 5 | 1 |
| Speed | 2 | 3 | 5 |
| Hand Launch | 3 | 3 | 5 |
| Storage | 2 | 3 | 1 |
| Total | 12 | 46 | 32 |

Engine Location: With a flying wing design, engine location is an important decision, depicted in Table 3.7. Only one of the selected FOMs was affected by the location of the single motor/propeller combination, hand launching. This is due to the fact that when the aircraft is thrown, a pusher propeller is likely to strike the hand of the thrower unless specific safeguards are made. Moreover, a flying wing design would probably be swept aft, and a Pusher may interfere with that design. The Tractor propeller was therefore the clear choice.

Table 3.7: Weighting for engine location

| | | Engine Location | |
|--------------|--------|---|--|
| | |  |  |
| FOM | Weight | Pusher | Tractor |
| Weight | 5 | 3 | 3 |
| Speed | 2 | 3 | 3 |
| Hand Launch | 3 | 1 | 5 |
| Storage | 2 | 3 | 3 |
| Total | 12 | 30 | 42 |



3.4.3 Landing Gear

Two options for the landing gear configuration were compared to each other based on the FOMs as seen in Table 3.8. A skid proved to be an only slightly better alternative, so the option of using a tricycle gear remained open to later analysis and testing.

Table 3.8: Weighting for landing gear style

| | | Landing Gear | |
|--------------|--------|---|--|
| | |  |  |
| FOM | Weight | Skid | Tricycle |
| Weight | 5 | 3 | 3 |
| Speed | 2 | 3 | 3 |
| Hand Launch | 3 | 3 | 3 |
| Storage | 2 | 3 | 1 |
| Total | 12 | 36 | 32 |

3.5 Final Conceptual Design Configuration

At the conclusion of the Conceptual Design, *There Will Be Buzz* reached a configuration designed to maximize the total score. The design is a compact, lightweight flying wing with a tractor propeller. All of its configuration choices were made on the basis of maximizing score by successfully completing all three missions of the competition and producing a practical airplane that can be hand-launched. Combined with the sensitivity analysis, the configuration's design point was set at 0.6 lbs empty weight, 0.6 lbs of payload for Missions 2 and 3, and 4-5 laps completed for Mission 1. The design point was chosen based on the team's realistic estimate of the configuration's implementation. Figure 3.4 below displays a concept sketch of the proposed design, drawn in Vehicle Sketchpad (VSP).

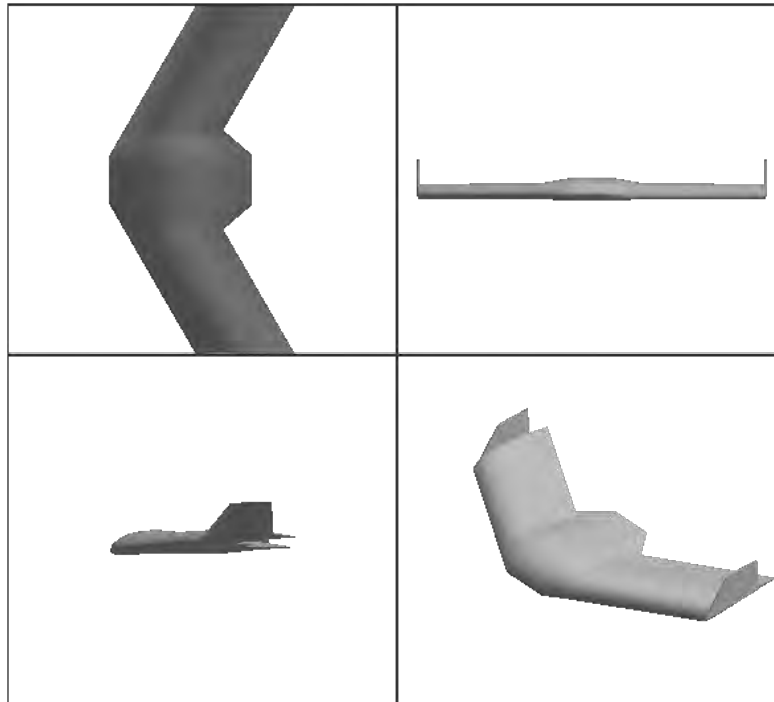


Figure 3.4: Conceptual aircraft design showing major components

4. PRELIMINARY DESIGN

The goal for preliminary design was to further narrow the design space. To do this, design/sizing trades for the system were evaluated. Next, airfoil selections, weight estimates, drag estimates, motor, propeller, and battery data, and aerodynamic coefficients were calculated and introduced into a flight simulation environment that estimated mission performance for all three flight missions. After evaluating the successful configurations that completed each mission, a preliminary propulsion system was selected and preliminary geometry was finalized.

4.1 Design Methodology

4.1.1. Aerodynamic Parameters

Three major propulsion parameters needed to be considered:

Wing Span: The carry-on requirements limit the span of any piece to a maximum of 22 inches, as discussed in Section 3.1.2. If more wing area is required, the wing could be broken into more than one piece, but connections and joints add weight, which reduces the score.

Wing Area: With a fixed wing span, wing area becomes only a function of chord length. Increased wing area decreases wing loading for a fixed weight, resulting in decreased stall speed for hand launch,



but a smaller wing area reduces drag, resulting in increased flight speed, and reduces weight, increasing score.

Airfoil Selection: A flying wing requires special considerations to balance the natural pitching moment produced by the wing. Airfoils with reflex camber lines reduce this moment. A high lift airfoil increases payload capability, but increases drag during flight.

4.1.2 Propulsion Design

Three major propulsion parameters need to be considered:

Motor Selection: A larger motor has increased power, increasing flight speed and payload capabilities, but weighs more, increasing the empty weight and thus the RAC. Since the highest empty weight of any mission is used to calculate RAC, choosing a heavier, more powerful motor in one mission would defeat the purpose of choosing a lighter, less powerful motor in other missions. The single motor selected should therefore be selected to optimize the total mission score.

Propeller Selection: A large diameter propeller spinning at slow speeds produces similar thrust to a small diameter propeller spinning at fast speeds. A large pitch-to-diameter ratio is most efficient at high airspeeds and a small pitch-to-diameter propeller is most efficient at lower airspeeds. Different missions will require different propeller performance, and since propeller selection can vary between missions, the best propeller can be selected for each.

Battery Selection: Lower capacity batteries are lighter and help produce a greater RPM and voltage, but higher capacity batteries can store more energy and are able to endure greater current draws. Also, more batteries have more power, allowing the aircraft to fly faster or with a heavier payload.

4.2 Design Trades

4.2.1 Hand Launch Study

Since the hand launch requirement was a new challenge in aircraft design for the *There Will Be Buzz* team, a study was conducted to determine the possible velocities the aircraft would experience upon leaving a person's hand. To perform this study, a small glider was constructed to better simulate the style of throwing that would be expected on the team's actual aircraft, as opposed to throwing an object such as a baseball. The glider was weighted to the target Mission 2/3 weight of 1.2 lbs. Some members of *There Will Be Buzz* took turns throwing the glider while being video recorded in front of a striped measurement screen, with each stripe separated by 2 inches. By using a High Definition video camera, recording at 30 frames per second, the amount of frames it took the glider to travel the distance of a stripe was used to estimate the glider's velocity. Figure 4.1 shows an example image from this process, and Figure 4.2 shows the plot of each member's attempts and the achieved velocities.



Figure 4.1: Testing hand-launch velocities

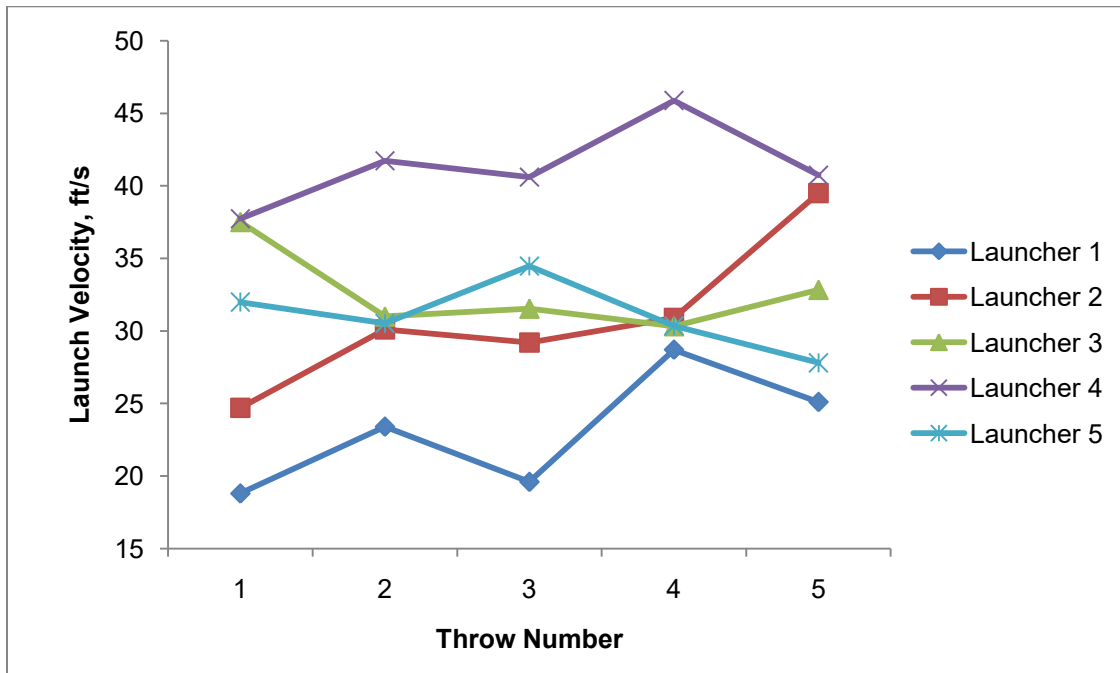


Figure 4.2: Hand-launch velocities for various team members

From this plot it is clear that a speed of 30 ft/sec is achievable from a hand powered launch of a vehicle weighing 1.2 lbs.

4.2.2 Wing Area Study

A critical component of the aircraft's design was the hand launch requirement. The aircraft would have to be sized such that it would not stall immediately after launch. A graph of stall speed versus wing area for a range of full launch weights was plotted in Figure 4.3.

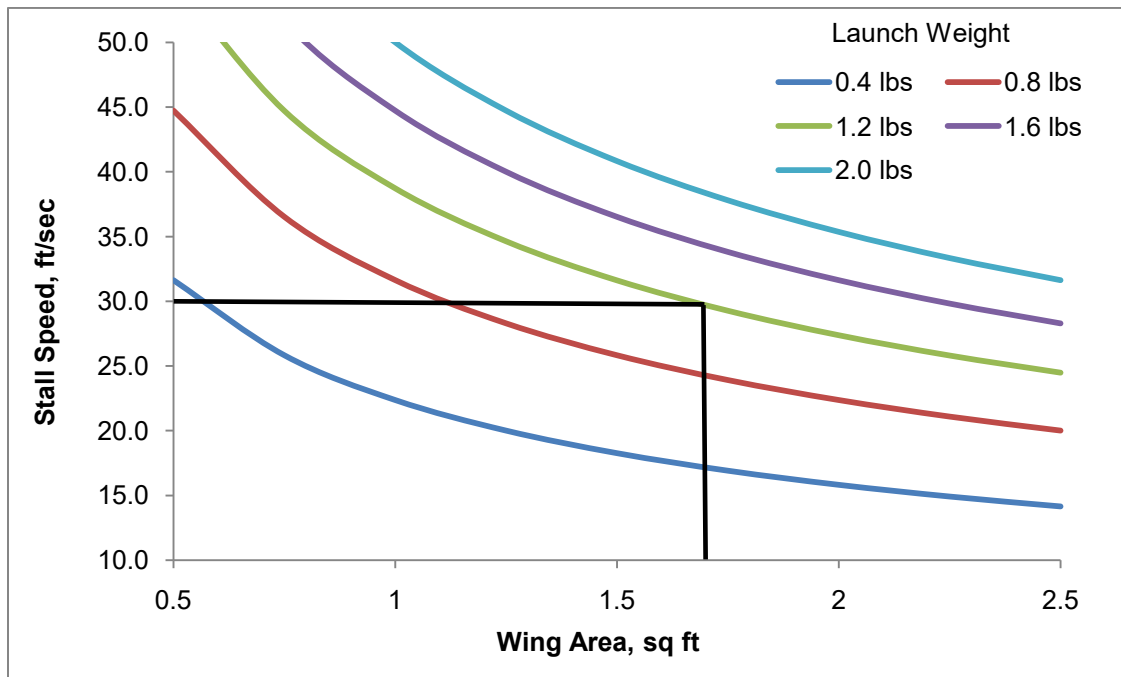


Figure 4.3: Stall speed versus wing area for various launch weights

The stall speed was selected as 30 ft/sec because of the information gathered by the hand-launch trade study discussed previously in Section 4.2.1. With a target launch weight of 1.2 lbs, representing 0.6 lbs of empty weight and six golf balls, the wing area had to be about 1.7 square feet.

4.2.3 Propulsion System Selection

A full factorial simulation was created to evaluate the effectiveness of different propulsion systems. This involved creating a database of a variety of components: 318 motors, 55 electronic speed controllers, 54 propellers, 4 battery capacities, and 11 different battery cell quantities. In total, 41,556,240 system combinations were considered. Using Goldstein's vortex theory from Phillip's *Mechanics of Flight* to evaluate propeller performance and a physics-based electric motor model, a MATLAB simulation was used to determine the full thrust profile for a given propulsion system. Combinations of components that do not work are automatically filtered from the analysis, such as when a speed controller or motor cannot handle the current draw from the batteries. Since there was such a wide range of results and weight was determined to be the most important factor for scoring, only the top performing motors of the lowest weight were kept. The static thrust of each combination was then plotted against the total weight of that propulsion system, shown in Figure 4.4.

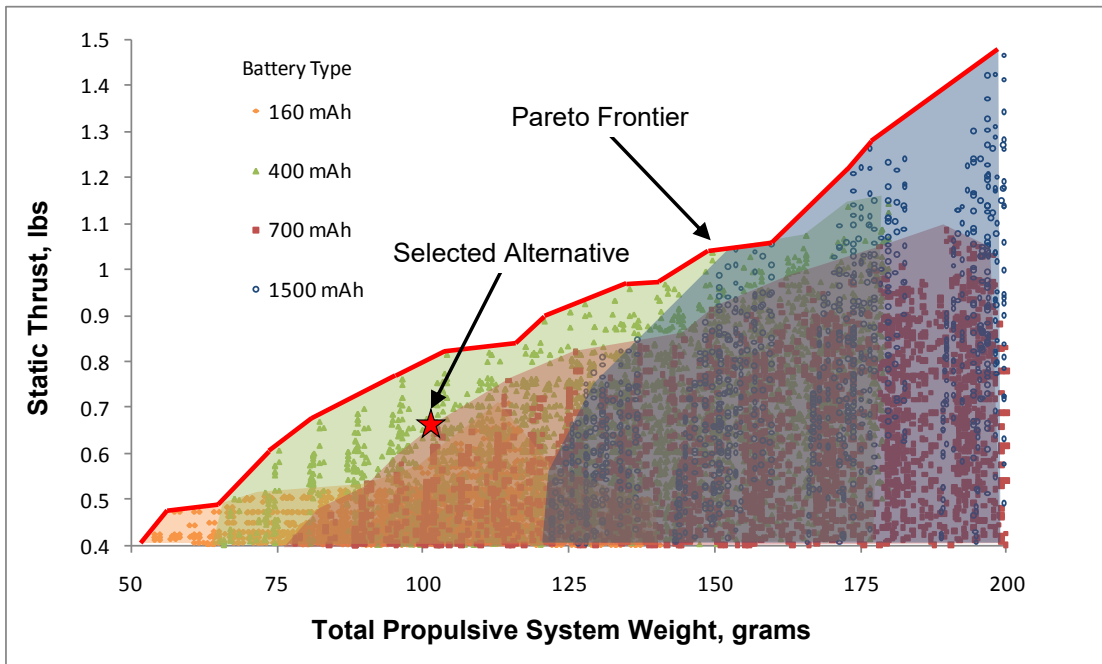


Figure 4.4: Propulsion analysis results with Pareto frontier of static thrust

From this data, it appears that combinations which use 400mAh batteries would be an ideal design point. However, there are more constraints for the propulsion system beyond system weight. The battery capacity needs to last at least 4 minutes to successfully complete Mission 1, and longer to ensure a successful landing. Figure 4.5 shows the remaining systems after those cases that could not last for 4 minutes and 30 seconds were filtered out.

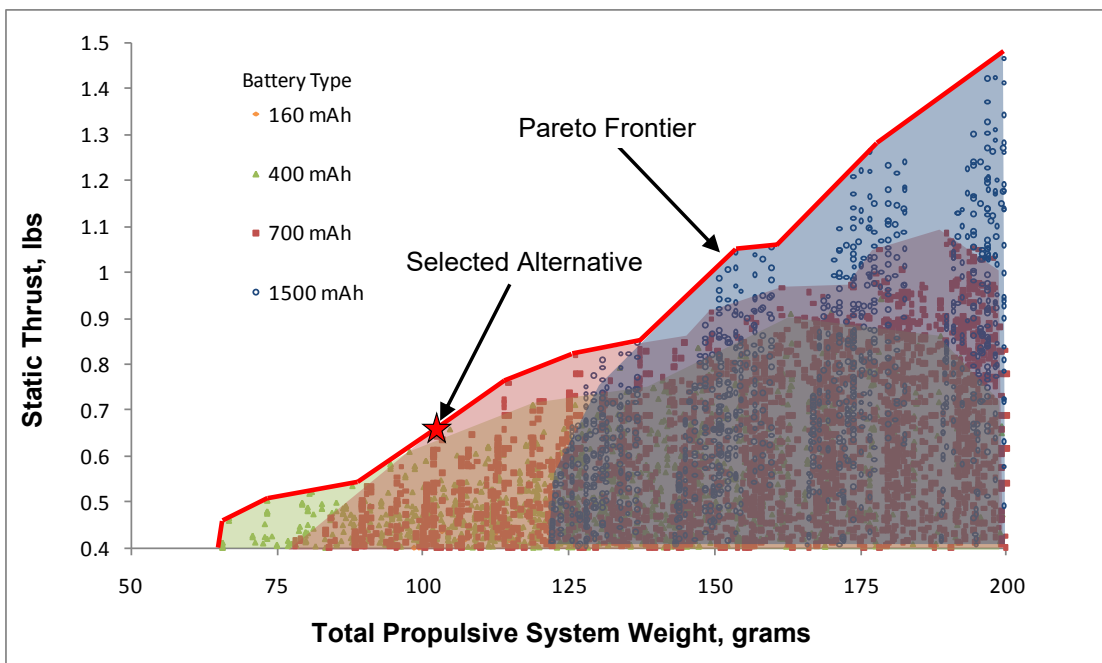


Figure 4.5: Propulsion analysis results after filtering for battery duration



From these results it is clear that many of the 400mAh batteries fall short of being viable options. It was decided to select a propulsion system with an empty thrust to weight ratio of about 1 to minimize weight while ensuring sufficient thrust. The final selection consists of a Hacker A10-9L, 6 cell 700mAh NiMH battery pack, a Phoenix 10 electronic speed controller, and a 9x4.7 propeller. This combination will develop approximately 0.64 lbs of thrust while pulling about 45 Watts from the battery.

4.3 Mission Model

4.3.1 Description and Capabilities

The mission was simulated via a set of first order differential equations (Equations 4.1-4.3) defining the position and orientation of the vehicle throughout the flight. By integrating these equations over time using a 4th Order Runge-Kutta approach in MATLAB with some simple logic defining each of the required mission segments, it is possible to define the position, velocity, and orientation of the vehicle over time. The equations are listed below. The thrust (T) is defined as a function of velocity with the relationship defined by the same propulsion analysis tool used in the propulsion system selection. The drag (D) is represented via a parabolic drag relationship. The load factor is explicitly defined for each turn segment, but if it exceeds the estimated maximum lift coefficient it is limited to that value.

$$\dot{x} = V \quad (4.2)$$

$$\dot{V} = \frac{T - D}{m} \quad (4.1)$$

$$\dot{\psi} = \frac{g\sqrt{n^2 - 1}}{V} \quad (4.3)$$

4.3.2 Uncertainties

The approach described above has specific limitations and uncertainties. The lack of a vertical dimension means that it cannot capture any aerodynamic effect due to altitude changes, or for the energy required or saved due to climbing or diving. The lack of any wind model discounts any additional drag due to sideslip in flight, or changes in velocity depending on traveling with or against the wind. The flight path defined for each lap assumes an idealized flight path, with the pilot turning perfectly after each 500 foot leg and the turns being optimal turns. Finally, there are additional uncertainties in the mission predictions due to any errors or inaccuracies in the thrust and drag predictions.

4.4 Aerodynamic Characteristics

4.4.1 Airfoil Selection

As a flying wing design, selection of an airfoil to fulfill unique requirements is critical. These requirements are explained in Table 4.1:



Table 4.1: Flying wing constraints on airfoil selection

| Parameter | Requirement | Rationale |
|-----------|-------------|---|
| C_{m0} | ~ 0 | Reduce elevon workload |
| C_{ma} | ~ 0 | Increase elevon effectiveness Minimize servo force |
| L/D | High | Maximum performance |

Using an estimated Reynolds number of 200,000 in cruise conditions for *There Will Be Buzz*, candidate airfoils were analyzed and plotted for sectional lift coefficient, lift to drag ratio, neutral pitching moment coefficient and manufacturability using XFOIL. Drag, lift, and pitching moment coefficient curves for top performing airfoils were constructed. To achieve the low pitching moment requirement, only reflex airfoils were considered. A reflex airfoil is defined as having a camber line that follows a shallow S-curve, with the trailing edge turned upwards. The airfoil coordinates were obtained from the UIUC Airfoil Coordinates Database. The lift curves and moment polars are compared in Figure 4.6 and Figure 4.7, respectively. The small amount of waviness in the graphs is due to numerical instabilities in XFOIL at low Reynolds numbers.

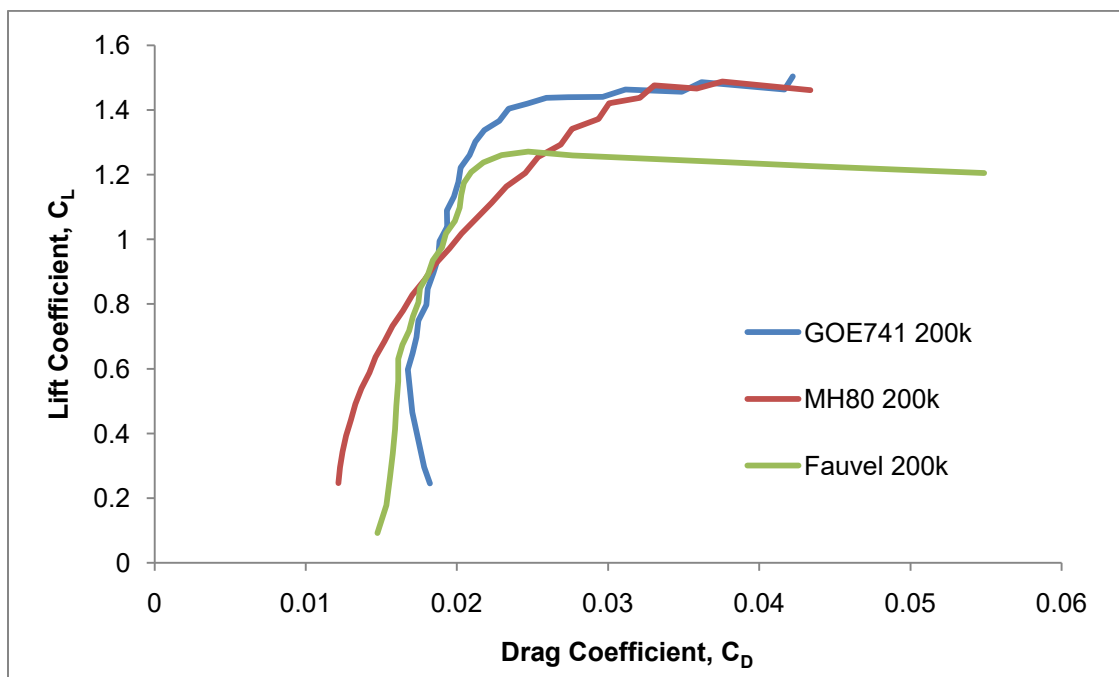


Figure 4.6: Drag polars for several reflex airfoils

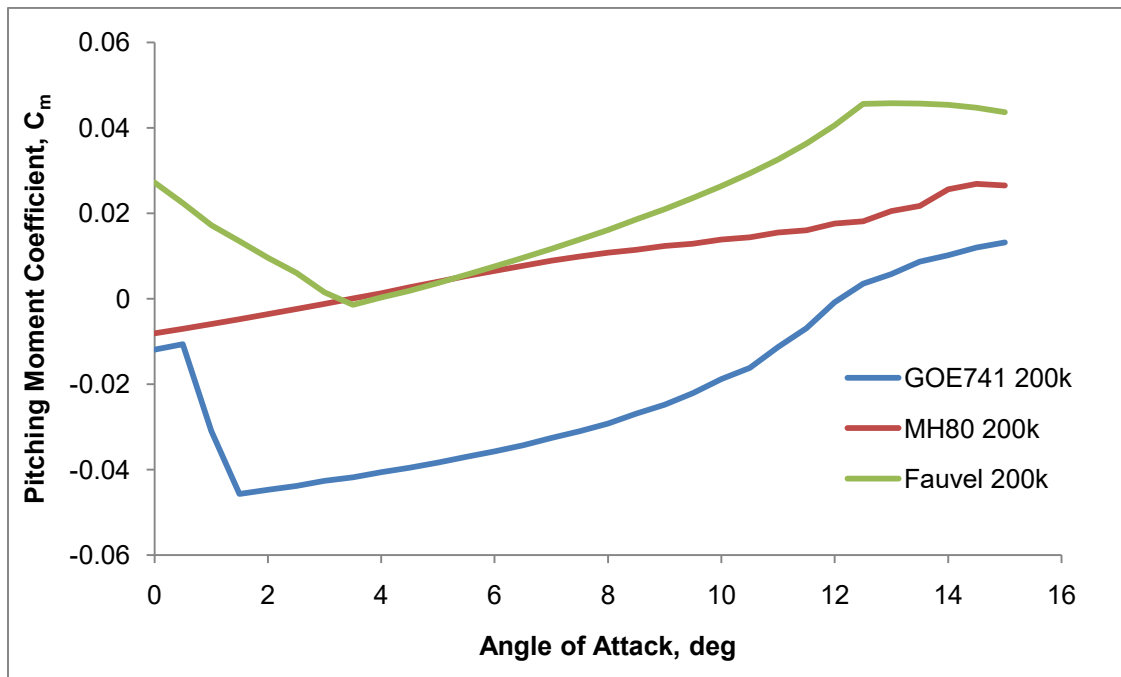


Figure 4.7: Pitching moment curves for several reflex airfoils

The examination of the drag polar show that the GOE741 airfoil has a slightly better lift coefficient but the lower pitching moment of the Fauvel lends itself favorably for a flying wing design.

Airfoil Manufacturability: Complex airfoil geometry, as shown in Figure 4.8, can result in manufacturing error and any imperfections will negatively affect vehicle performance. On reflex airfoils especially, this means ensuring the manufactured trailing edge holds the curve as designed. To reduce manufacturing difficulty and get the desired performance out of an airfoil, that airfoil must not have high camber or a sharp trailing edge. The airfoil must also be of sufficient thickness to make the internal structure lighter and/or stronger, as the geometric stiffness of the structure is increased with thickness. An airfoil that would be easier to manufacture correctly is shown in Figure 4.8:

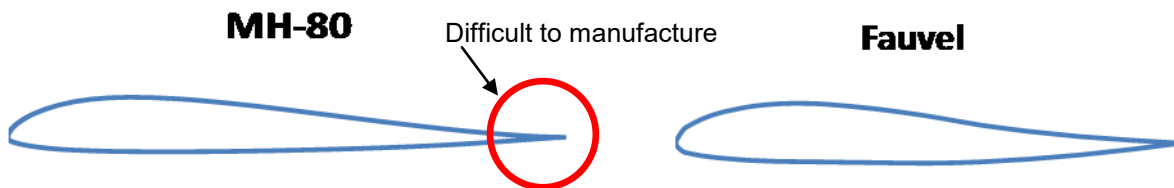


Figure 4.8: Geometry of airfoils and manufacturing properties

Wing Airfoil Thickness: In addition to manufacturing difficulty, an airfoil with a low thickness will suffer stall effects at a smaller angle of attack, reducing the effectiveness of the elevons. For such an



airfoil, there would be little to no buffer between flying at the maximum section lift coefficient and stalling. The Fauvel airfoil was selected because of its combination of high maximum C_L , low pitching moments, manufacturability, and a high thickness to chord ratio of ~14%.

Centerbody Airfoil Thickness: The Fauvel airfoil was also selected for the centerbody. However, the airfoil had to internally store two golf balls chord-wise and maintain enough thickness to still allow for structure. To accommodate this, and because the airfoil chord was limited by storage constraints, the airfoil thickness was increased to 20%.

4.4.2 Aerodynamics

Athena Vortex Lattice (AVL) was used to model the lifting surfaces of the aircraft to compute the induced aerodynamic characteristics of the entire aircraft. AVL models lifting surfaces as an infinitely thin sheet of discrete vortices to compute the aerodynamic characteristics of the aircraft. The geometry of the aircraft was developed inside AVL to provide stability while matching the predetermined wing area. The centerbody size was constrained by the internal payload requirements, so the wing span and chord were adjusted. During the design process, the addition of winglets was also considered to improve the aerodynamic and stability characteristics of the aircraft. The airfoil selection, stability and geometric constraints resulted in a wing planform with a span of 28 inches, sweep of 30 degrees and a wing chord of 8 inches. A visualization of the lifting surfaces as discretized in the AVL model for the final aircraft configuration with winglets is shown in Figure 4.9. The AVL-calculated lift coefficient distribution of the final configuration aircraft is shown in Figure 4.10.

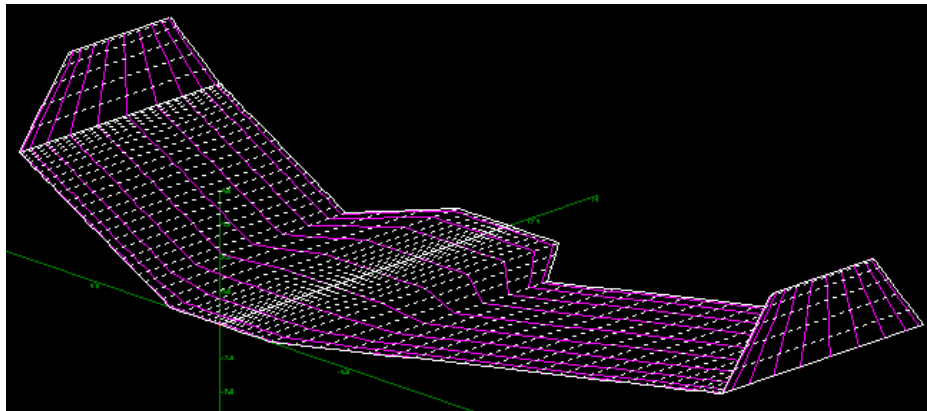


Figure 4.9: Aircraft AVL Virtual Model (with winglets)

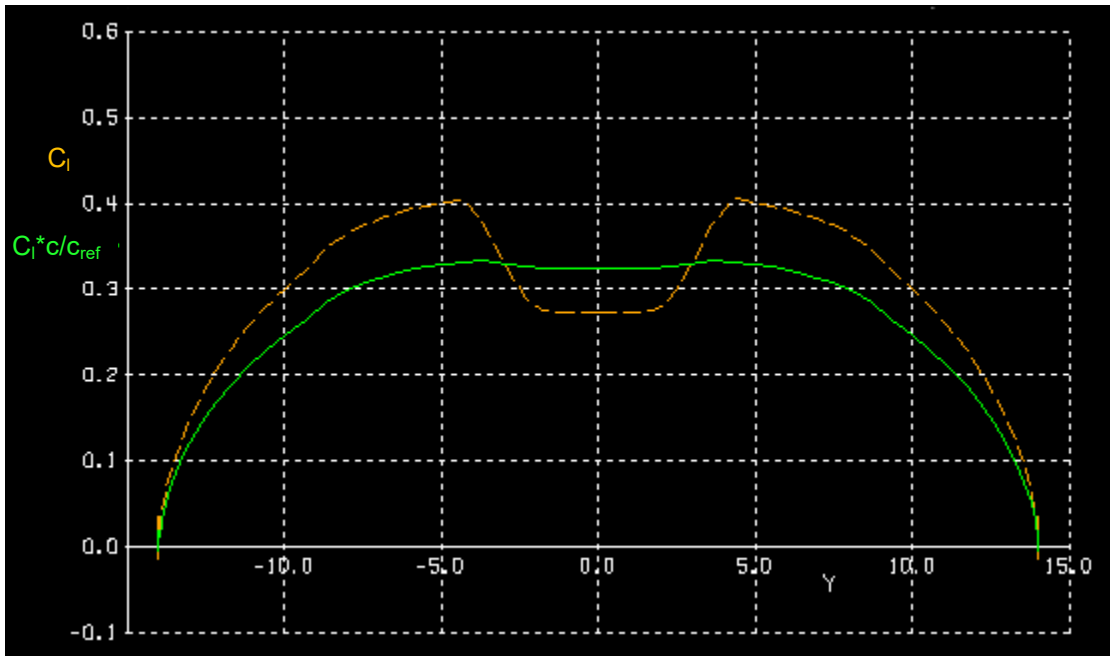


Figure 4.10: AVL predicted lift distribution of the aircraft (with winglets)

Once the sizing was complete, the AVL model was used to calculate elevon-balanced aerodynamic parameters. The lift curve and induced drag polar are shown below in Figure 4.11.

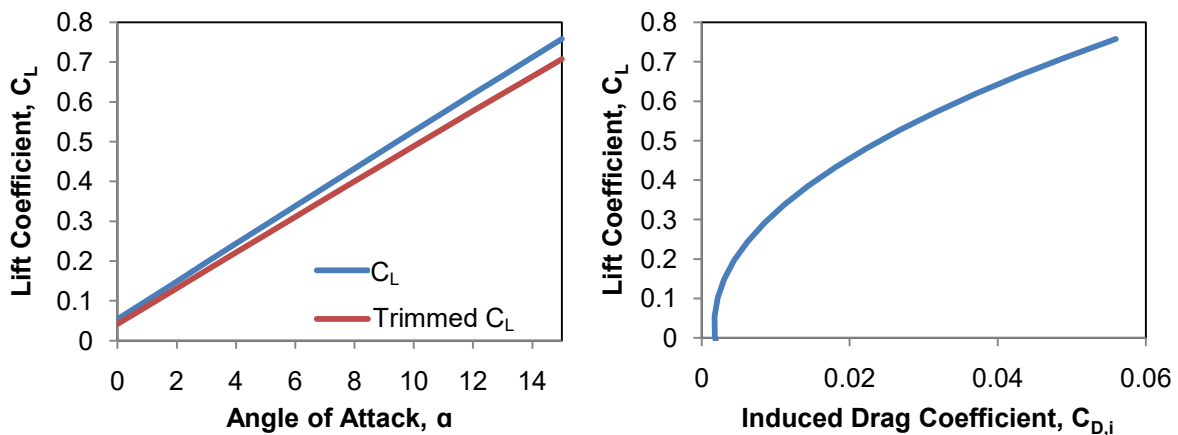


Figure 4.11: Drag polar and trimmed and non-trimmed lift curves

The lift curve is shown for both trimmed and untrimmed conditions. The lift coefficient at 15 degrees is ~ 0.7 , near the vehicle max lift coefficient. Because the flying wing configuration has no tail or vertical surfaces, the addition of winglets was necessary to improve the yaw stability derivative ($C_{n,\beta}$) for a minimum level of directional stability. The final configuration of the aircraft has a yaw stability derivative of 0.0469.



4.4.3 Drag

A preliminary parasitic drag estimate was computed by summing each component's drag contributions, approximated using Hoerner's experimental data in *Fluid Dynamic Drag*, and then normalizing each component according to the wing reference area. Table 4.2 shows the contributions of the main aircraft components, with Figure 4.12 displaying the same data as a percentage breakdown.

Table 4.2: Summary of drag estimates

| Component | $C_{D,0}$ |
|---------------------------|-----------|
| Wing | 0.019 |
| Wing Tip Skids | 0.018 |
| Landing Gear (Mono Wheel) | 0.015 |
| Winglets | 0.01 |
| Total | 0.062 |

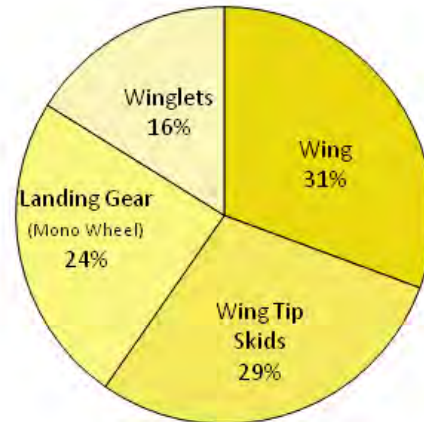


Figure 4.12: Graphical representation of drag estimates

Wing: Due to its flying wing configuration, the largest single component of *There Will Be Buzz* is the wing, so it was the largest contributor of drag. The drag coefficient for the wing was calculated using Hoerner's method as seen in Equation 4.4:

$$C_{D,0} = R_{wf} R_{LS} C_{f_w} \left\{ 1 + L' \left(\frac{t}{c} \right) + 10 \left(\frac{t}{c} \right)^4 \right\} \frac{S_{wet_w}}{S} \quad (4.4)$$

where R_{wf} is the wing fuselage interference factor (assumed to be equal to 1, since the wing is the fuselage), R_{LS} is the lifting surface correction, which is a function of the sweep angle of the wing, C_{f_w} is the turbulent plate friction coefficient of the wing, which is a function of Mach number and Reynolds number, L' is the airfoil thickness location factor, t/c is the thickness-to-chord ratio, S_{wet_w} is the wetted area of the wing and S is the wing reference area. The total $C_{D,0}$ contribution by the wing was calculated to be 0.019.

Winglets: The winglets were modeled as flat plates and their drag contributions were calculated based on Reynolds number. Since the maximum speed of the aircraft is very low, Schlichting's formula for skin friction drag was used directly to calculate the skin friction drag coefficient without any correction for compressibility effects, as seen in Equation 4.5:

$$C_f = \frac{0.455}{(\log_{10} R_N)^{2.58}} \quad (4.5)$$



Where R_N is the cruise Reynolds number of the aircraft which was estimated to be 200,000. The $C_{D,0}$ contributions of both the winglets combined was 0.010.

Landing Gear and Wing Tip Skids: The landing gear and wing tip skids are significant contributors to the overall drag of the aircraft. Continuing with the two landing gear alternatives considered in Section 3.4.3, $C_{D,0}$ was calculated for a dual wheel gear and a mono wheel gear, both depicted in Figure 4.13. The dual wheel was modeled as a pair of cylinders with wheels at the ends; the mono wheel was modeled as a wheel, a cylinder, and two flat plates; while the wing tip skids (common to both configurations) were modeled as cylinders.



Figure 4.13: Comparison of prototype aircraft with different styles of landing gear

The result of applying Hoerner's methods to the dual wheel landing gear configuration is a $C_{D,0}$ of approximately 0.037, even larger than the wing. In contrast, the mono wheel resulted in a $C_{D,0}$ of approximately 0.015. Therefore, an aircraft configured with the mono wheel has 30% less drag than an aircraft with the dual wheel gear. This is further conveyed in Figure 4.14, which shows a comparison in drag break down between the two landing gear configurations. Note that drag contributions due to the wing and the winglets remain constant, while there is a significant reduction in the drag contribution due to the landing gear and the wing tip skids when using the mono wheel.

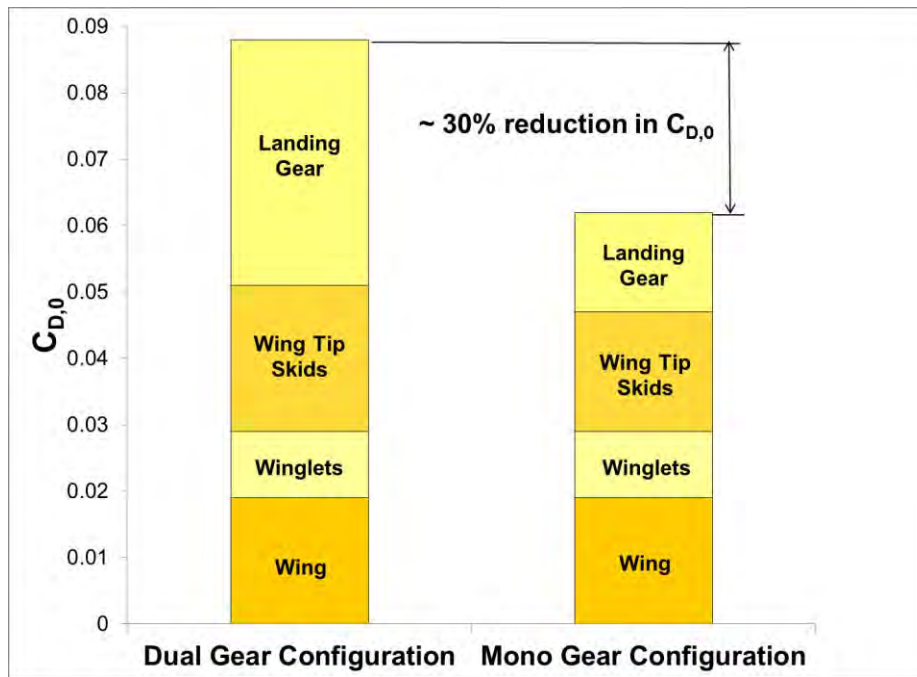


Figure 4.14: Graphical comparison of drag contributions from different styles of landing gear

AVL was used to model the lifting surfaces of the aircraft to compute the induced drag. The estimated Oswald's efficiency was 0.87 for the full configuration. The full drag polar is displayed in Figure 4.15, and was calculated using the induced drag from AVL and the parasitic drag from above.

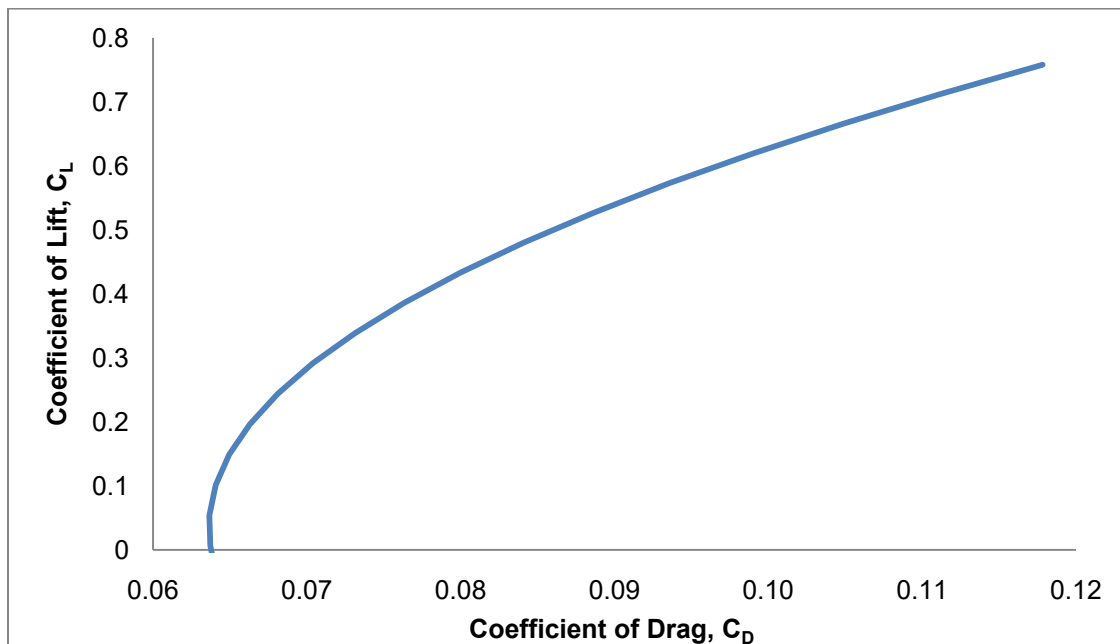


Figure 4.15: Full drag polar



4.5 Stability and Control

To ensure that the aircraft would be able to successfully complete the missions in the air, both static and dynamic stability were analyzed. The fastest speeds, slowest speeds, heaviest weights, lightest weights, cruise, climbs, and turns were all considered.

4.5.1 Static Stability Analysis

Static stability was evaluated using the vortex lattice method as implemented in AVL. The most important stability derivatives are given for the scenario shortly after launch in Table 4.3. After launch for M3 is the most demanding flight condition for stability. Static stability analysis for all cases showed that the aircraft is statically stable. Since the flying wing design is controlled through the use of a control surface acting as both aileron and elevator, elevator deflection is referring to a symmetric control deflection, and aileron deflection refers to an asymmetric deflection. No extreme deflections are required for any control surface and all coefficients are within a normal range.

Table 4.3: Relevant stability coefficients and derivatives for elevator-balanced trim conditions

| Parameter | AVL Results | |
|------------------------|-----------------------------|--------|
| Inputs | W_{total} (lbs) | 1.2 |
| | V (ft/s) | 24 |
| Deflections | $\delta_{elevator}$ (deg) | -1.58 |
| | $\delta_{aileron}$ (deg) | 0.0 |
| Aerodynamic Parameters | C_L | 0.522 |
| | α (deg) | 9.9 |
| | β (deg) | 0.0 |
| Stability Derivatives | $C_{l,\beta}$ (1/rad) | -0.176 |
| | $C_{L,\alpha}$ (1/rad) | 3.068 |
| | $C_{m,\alpha}$ (1/rad) | -0.225 |
| | $C_{n,\beta}$ (1/rad) | 0.057 |
| Damping Derivatives | $C_{l,p}$ (1/rad) | -0.287 |
| | $C_{m,q}$ (1/rad) | -0.875 |
| | $C_{n,r}$ (1/rad) | -0.026 |
| Control Derivatives | $C_{l,\delta a}$ (1/degree) | 0.002 |
| | $C_{m,\delta e}$ (1/degree) | -0.004 |
| Static Margin | % Chord | 7.3 |

4.5.2 Dynamic Stability Analysis

Having found the trim conditions as a part of the static stability analysis, the next step was to take the aerodynamic derivatives about the trim conditions described earlier and investigate the dynamic behavior of the airplane. The stability and control derivatives were obtained from the AVL, the mass properties from the CAD file, and the stability characteristics calculated from the full twelve by twelve 6 DOF



linearized differential equations found in Phillips' *Mechanics of Flight* section 9.8. The eigenvalues and eigenvectors of the matrix showed the stability of each of the five dynamic modes, revealing that the aircraft is stable in the Short Period, Dutch Roll and Roll modes, while unstable in Phugoid and Spiral modes. The doubling time for the Phugoid and Spiral modes are long enough to be easily handled by the pilot, and the stability was therefore deemed acceptable. The flight conditions used were the same as used in the static stability section, listed in Table 4.3. The dynamic stability characteristics are tabulated below in Table 4.4.

Table 4.4: Dynamic stability analysis for least stable case

| Mode | Longitudinal Modes | | Lateral Modes | | |
|----------------------------------|--------------------|---------|---------------|-------|--------|
| | Short Period | Phugoid | Dutch Roll | Roll | Spiral |
| Damping Rate (1/s) | 12.91 | -0.0204 | 1.768 | 24.49 | -0.189 |
| Time to double/half (s) | 0.053 | 33.9 | 0.392 | 0.028 | 3.67 |
| Damping Ratio | 0.647 | -0.0124 | 0.127 | | |
| Damped Natural Frequency (1/s) | 15.23 | 1.642 | 13.79 | | |
| Undamped Natural Frequency (1/s) | 19.96 | 1.642 | 13.9 | | |

4.6 Mission Performance

The lap trajectory was calculated using the mission simulation described in Section 4.3 using the propulsion and aerodynamic characteristics of the airplane. The velocity profile for the first two laps using a 9x4.7 propeller is shown in Figure 4.16 for Mission 1 and Figure 4.17 for Mission 2/3. The velocity deficits correspond to the required turns over the course of each lap. The maximum velocity estimated for the Mission 1 is 28.2 mph (41.6 ft/s), and the maximum velocity for Mission 2/3 is 27.8 mph (40.8 ft/s). The estimated lap times using the initial propeller is shown in Table 4.5 for both mission configurations.

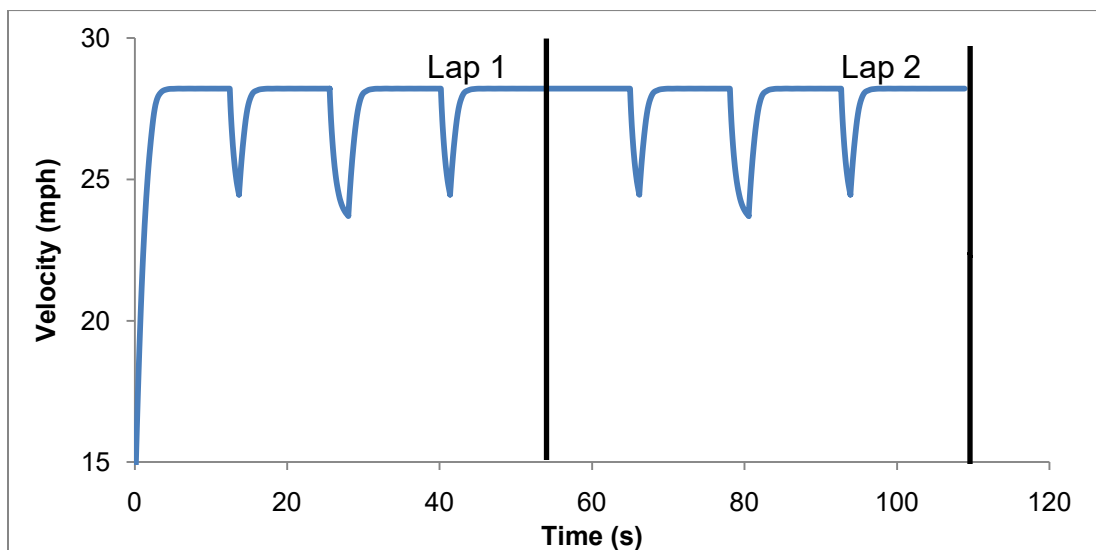


Figure 4.16: Simulation of Mission 1 lap trajectory

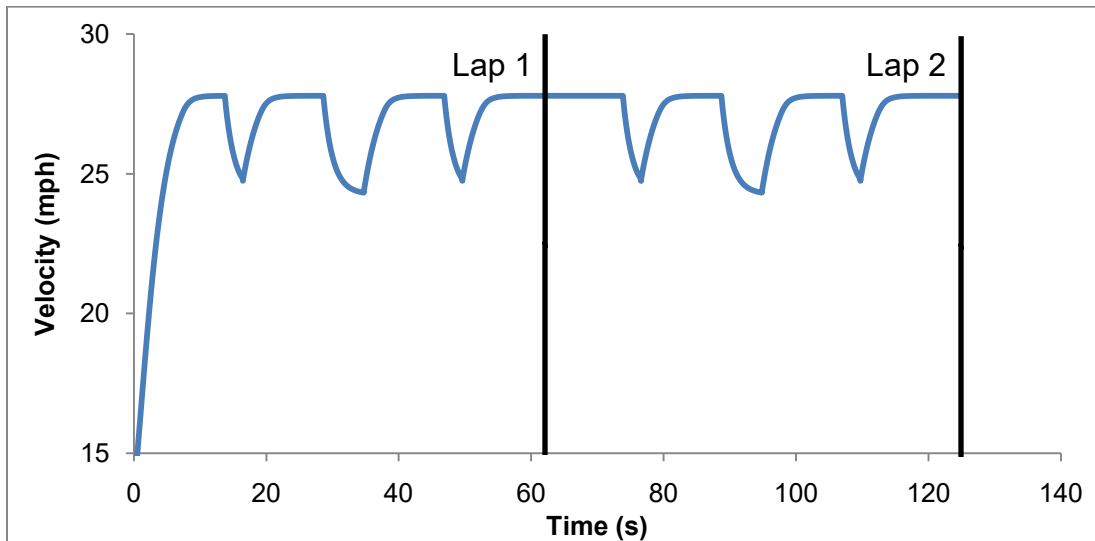


Figure 4.17: Simulation of Mission 2 lap trajectory

Table 4.5: Simulated mission times

| Mission | Propeller | Lap Time(s) |
|---------|-----------|-------------|
| M1 | 9x4.7 | 52.8 |
| M2/3 | 9x4.7 | 61.7 |

5. DETAIL DESIGN

5.1 Final Design

After all optimization was completed, the final dimensional parameters are listed in Table 5.1. The dimensions of the aircraft did not vary between the preliminary design and detailed design stages. The final aircraft was designed for flight stability, simplicity, and to fit inside the carry-on by detaching the outer 5 inches of each wing from the centerbody.

Table 5.1: Final aircraft dimensional parameters

| Wing | | | Elevon | | |
|---------------|--------|---------------------|--------------------|------------|---------------------|
| Span | 28 | inches | Span | 5 | inches |
| Wing Chord | 8 | inches | Chord | 2.4 | inches |
| Root Chord | 11.5 | inches | $\delta_{e, \max}$ | 35 | degrees |
| Sweep | 30 | degrees | Reference area | 22.8 | inches ² |
| Aspect Ratio | 3.2 | | Winglet | | |
| Wing Area | 245 | inches ² | Reference area | 25 | inches ² |
| Airfoil | Fauvel | | Airfoil | Flat Plate | |
| Static Margin | 8% | chord | | | |



5.2 Structural Characteristics

The structure of the airplane was designed to withstand a 2.5 g loading in the maximum payload configuration of 1.2 lbs. This translates into a maximum load limit of 5 g in the empty configuration of 0.6 lbs. It was also assumed that negative loading was a maximum of 1 g fully loaded and therefore 2 g when empty. Using these loadings and the maximum lifting capability of the airplane the operational flight envelope was defined as shown in the V-n diagram in Figure 5.1. The maximum velocities were calculated using the method explained in section 5.6.1.

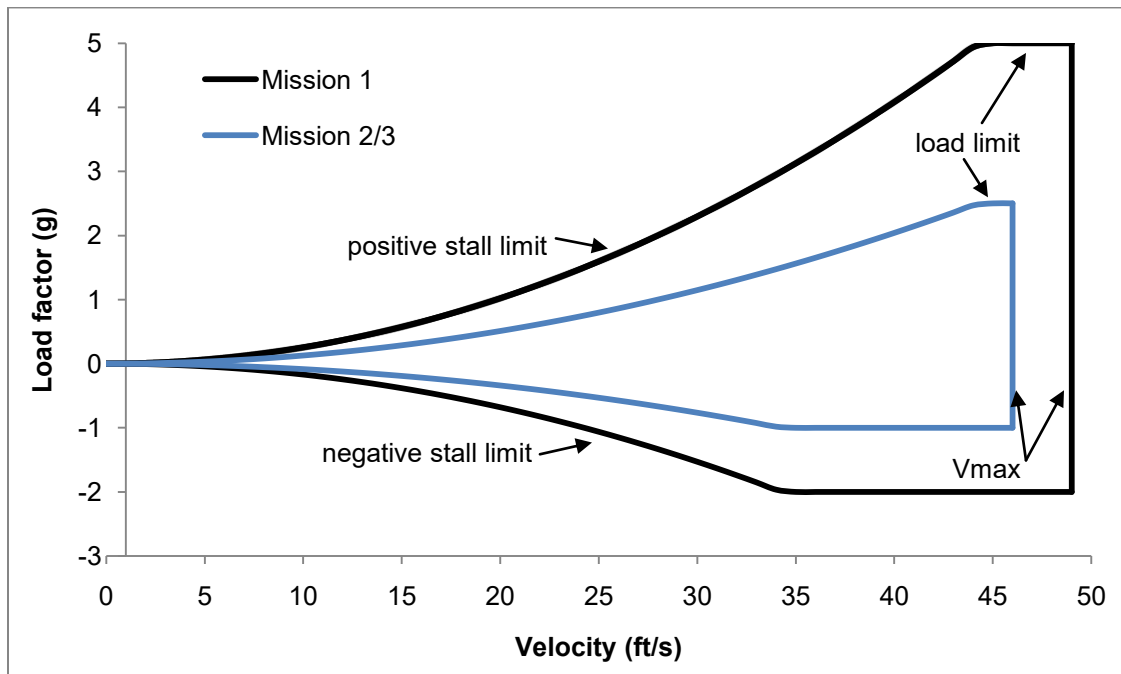


Figure 5.1: V-n Diagram for all missions

5.3 System and Subsystem Design/Component Selection/Integration/Architecture

To finalize the aircraft design, the following subsystems were analyzed with greater detail: radio controller, servos, main wing, centerbody, propulsion system, landing gear, and the structural architecture/assembly of each of these components.

5.3.1 Receiver/Controller Selection

The receiver selected is the Spektrum 6255, as it provides the required failsafe mechanism with minimum weight. *There Will Be Buzz* will use a JR PCM10X radio controller to communicate with the Spektrum receiver.



5.3.2 Propulsion System

The propulsion system was selected using the analysis from section 4.2.2. The final selection consists of a Hacker A10-9L, 6 cell 700mAh NiMH battery pack, a Phoenix 10 electronic speed controller, and a 9x4.7 propeller.

5.3.3 Centerbody Structure/Payload Bay

The aircraft centerbody is constructed from a combination of spanwise and chordwise balsa wood ribs that connect together in interlocking slots. The CAD model was used to design the ribs such that they fit together like a jigsaw. This interlocking method allows for distribution of loads across the entire structure, as well as more efficient manufacturing. The interior of the centerbody is open, allowing for the payloads of steel bars or golf balls to fit internally. The joints between the spanwise and chordwise ribs have hemispherical cutouts to provide constraints for the payloads, and eliminate motion in flight without additional structure.

5.3.4 Wing Structure

The inner wing sections are connected to the centerbody via spars and stringers. The outer wing sections are constructed in a similar manner, with ribs connected by stringers. The outer wing sections connect to the inner sections by wood pins, the servo casing, and are held together by tape. Although the joint is very small, it is sufficient to transfer the load from the relatively small outboard wing area. The location of the joint allows the aircraft to easily fit into the carry-on. A picture of this joint is shown in Figure 5.2.

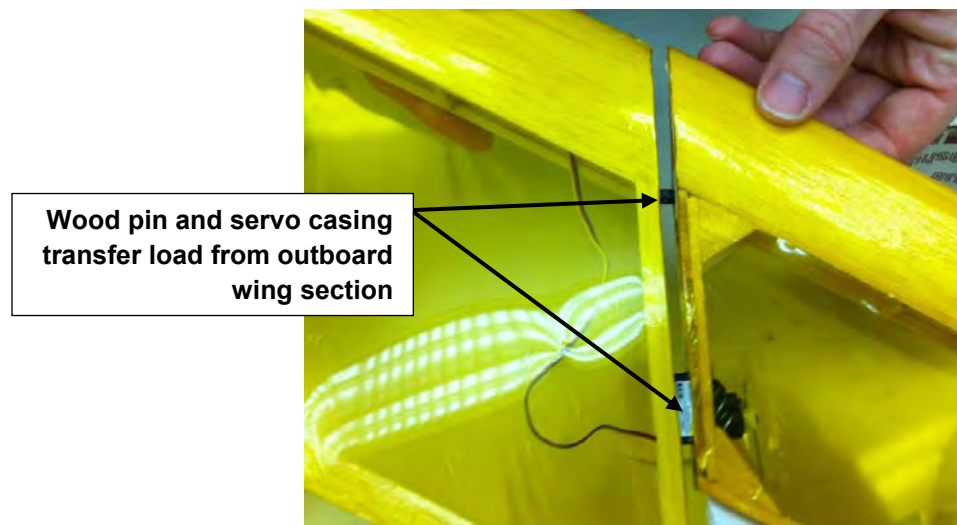


Figure 5.2: The joint between outboard and inboard wing sections

5.3.5 Control Surfaces

Elevons are attached to the wing using conventional CA hinges. These control surfaces are controlled with pushrods that are attached to servos located in the wings.



5.3.6 Servo Selection/Integration

The servos selected for the elevons were Futaba S3114. These servos were selected by analyzing hinge-moments for each control surface using AVL and then finding servos that had sufficient control power to handle the calculated moments, with the lightest weight possible.

5.3.7 Motor Mount

In keeping with the team design goal of minimizing system weight to maximize overall score at the competition, an integrated solution that combined the leading edge of the centerbody airfoil with the motor mount was implemented. Experimental results indicated that a 1/8th inch piece of birch plywood was sufficient to withstand the torque and static thrust of the motor.

5.3.8 Landing Skid/Launch Grip

The landing skid is made from two pieces of birch plywood attached to the centerbody via the two main ribs. The spacing enables the skid to double as the grip when hand-launching the aircraft. A wheel is attached on an axle spanning the two parts of the grip to enable ground roll upon landing.

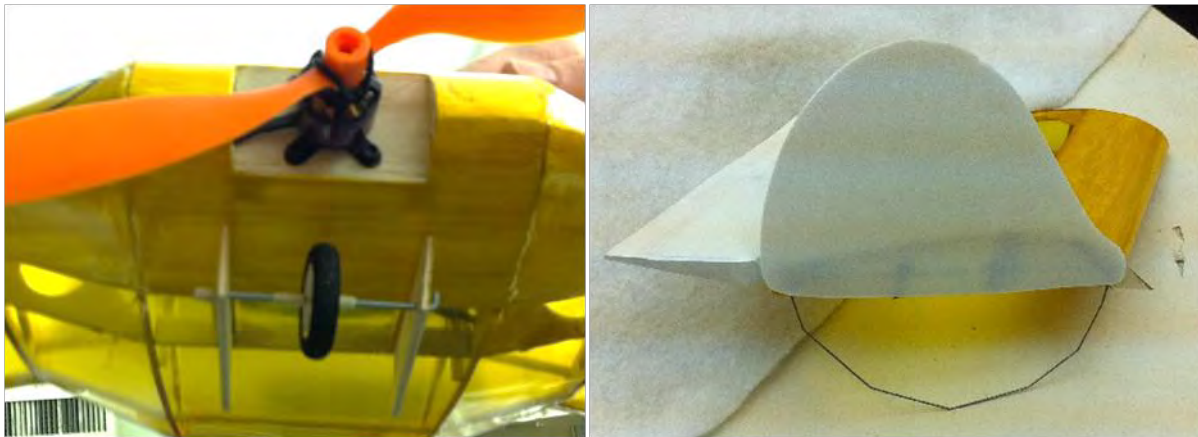


Figure 5.3: Detail views of the landing gear and winglet

5.3.9 Winglets/Wingtip Skids

The winglets are made of Depron, a low density foam, cut to the shape seen in Figure 5.3. The wingtip skids are bent metal wires that are attached directly to the winglets. This structure is then attached to the ribs on the outboard sections with epoxy glue.

5.3.10 Suitcase

The suitcase selected is a standard commercially available carry-on suitcase. The external dimensions of the suitcase are 21 by 8.25 by 14 inches. The internal dimensions are 20.5 by 8 by 13. The sum of the external dimensions is 43.25, within the 45 inch limit. The rules require that the aircraft must fit inside this suitcase, as shown in Figure 5.4.



Figure 5.4: The aircraft unassembled to fit in the suitcase

5.3.11 Component Summary

The full list of selected components for *There Will Be Buzz* is tabulated below in Table 5.2.

Table 5.2: Selected components

| Components | Description |
|------------------|---------------|
| Motor | Hacker A10-9L |
| Battery | 6 cell 700mAh |
| Speed Controller | Phoenix 10 |
| Receiver | Spektrum 6255 |
| Transmitter | JR PCM10X |
| Servos | Futaba S3114 |

5.4 Weight and Balance

An important aspect of stability is correct C.G. measurements. To measure the C.G., a simple calculator was created that consisted of a list of all components, the weights of all components, and the locations of the components along the various axes. The weight and balance was first estimated using the CAD model and then confirmed with the prototype. The moments of inertia were calculated in similar fashion. The results for empty and loaded scenarios are given in Table 5.3. The x-axis was measured positive aft of the nose of the aircraft. The predicted C.G. location from the CAD is shown in Figure 5.5.



Table 5.3: Weight and balance chart

| Empty Weight | | | |
|-----------------------|---------------|---------------------------------|------------------|
| Component | Weight (lbs.) | CG location (in.) (x-direction) | Moment (in.-lbs) |
| Center Section | 0.230 | 3.681 | 0.847 |
| Wing Sections | 0.012 | 8.076 | 0.097 |
| Ailerons | 0.001 | 11.987 | 0.012 |
| Servos | 0.010 | 8.753 | 0.088 |
| Motor | 0.051 | 0.336 | 0.017 |
| Batteries | 0.167 | 2.065 | 0.345 |
| Receiver | 0.012 | 1.138 | 0.014 |
| Receiver Battery | 0.053 | 1.330 | 0.071 |
| Speed Controller | 0.015 | 1.388 | 0.021 |
| Landing Gear | 0.022 | 2.553 | 0.056 |
| Propeller | 0.009 | -0.268 | -0.002 |
| Winglets | 0.022 | 10.393 | 0.229 |
| Aircraft Total | 0.604 | 2.593 | 1.566 |

| Steel Bar Payload | | | |
|-------------------|---------------|---------------------------------|------------------|
| Component | Weight (lbs.) | CG location (in.) (x-direction) | Moment (in.-lbs) |
| Aircraft | 0.604 | 2.593 | 1.566 |
| Steel Bar Payload | 0.600 | 3.725 | 2.235 |
| Total | 1.204 | 3.157 | 3.801 |

| Golf Ball Payload | | | |
|-------------------|---------------|---------------------------------|------------------|
| Component | Weight (lbs.) | CG location (in.) (x-direction) | Moment (in.-lbs) |
| Aircraft | 0.604 | 2.593 | 1.566 |
| Golf Balls | 0.600 | 3.452 | 2.071 |
| Total | 1.204 | 3.021 | 3.637 |

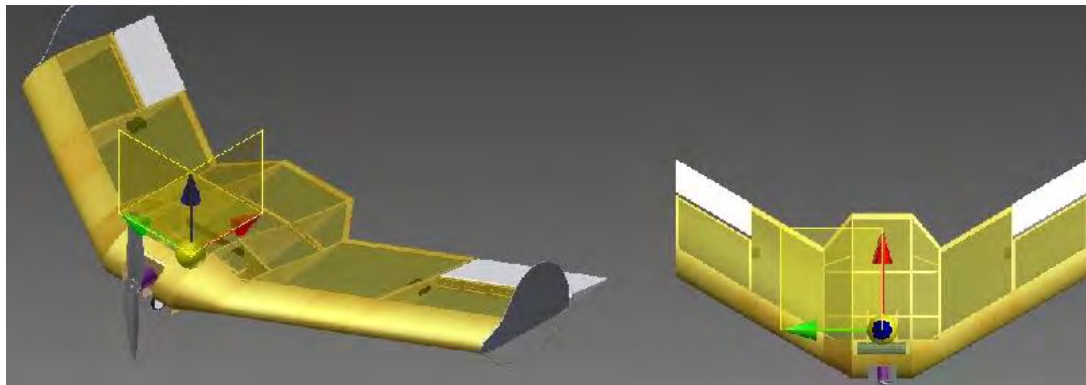


Figure 5.5: C.G. Location on CAD model

5.5 Flight and Mission Performance

5.5.1 Flight Performance

The flight performance of the aircraft is described by point performance of the vehicle. The maximum velocity of the aircraft occurs at the point when the thrust required is equal to the thrust available. The thrust available was calculated from the MATLAB simulation and propulsive system selected earlier in Section 4.2.2. Multiple propellers were selected to evaluate their effectiveness at higher velocities. The thrust required curve was calculated from Equation 5.1, where $C_{D,0}$ and k were calculated in Section 4.4.3.

$$T_R = \frac{1}{2} \rho v^2 S C_{D,0} + k \frac{2W^2}{\rho v^2 S} \quad (5.1)$$

The graph of the thrust available/required versus velocity is shown below in Figure 5.6.

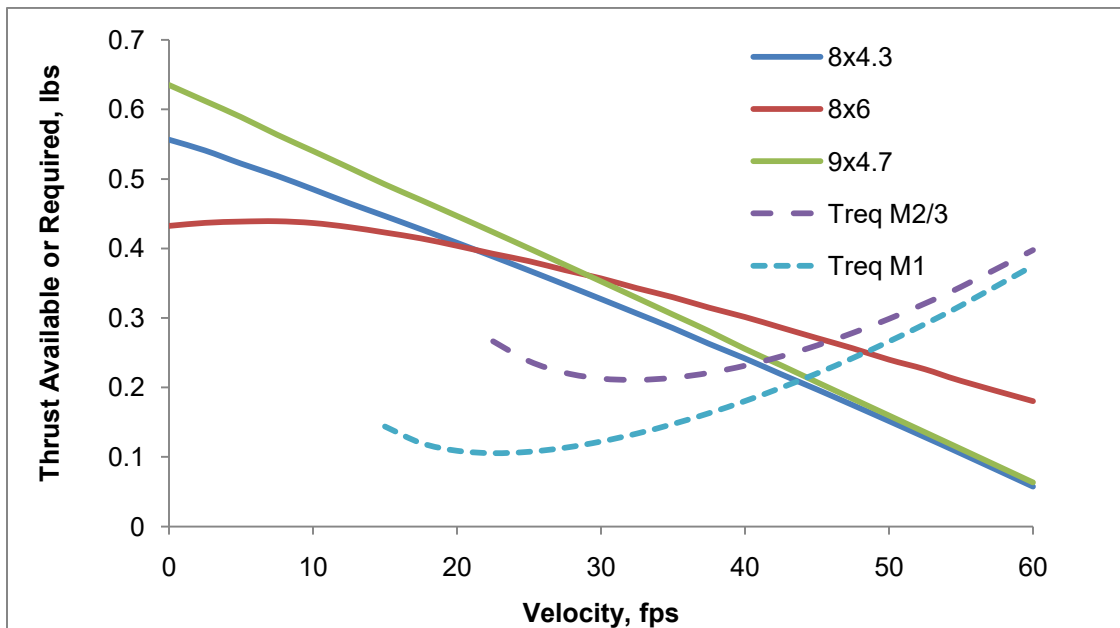


Figure 5.6: Thrust available and thrust required vs. velocity

This data was used to find the maximum velocity for each mission. Stall speed was calculated from the value of C_{Lmax} along with the maximum load factors determined in Section 5.2. Using maximum velocity, the turn radius and time for a 360° could be calculated for each mission. The values are tabulated in Table 5.4.

Table 5.4: Aircraft mission performance parameters

| | Mission 1 | Mission 2/3 |
|----------------------|-----------|-------------|
| V_{stall} (ft/sec) | 21 | 29.7 |
| V_{max} (ft/sec) | 48 | 46 |
| Load Factor | 5.0 | 2.5 |
| Turn Radius (ft) | 14.6 | 28.6 |
| Time for 360° (s) | 1.91 | 3.9 |

5.5.2 Mission Performance

The lap trajectory was calculated using the mission simulation described in the previous section using the final propulsion system and aerodynamic characteristics of the airplane. The velocity profile for the first two laps of Mission 1 using an 8x6 propeller is shown in Figure 5.7. The velocity deficits correspond to the required turns over the course of each lap.

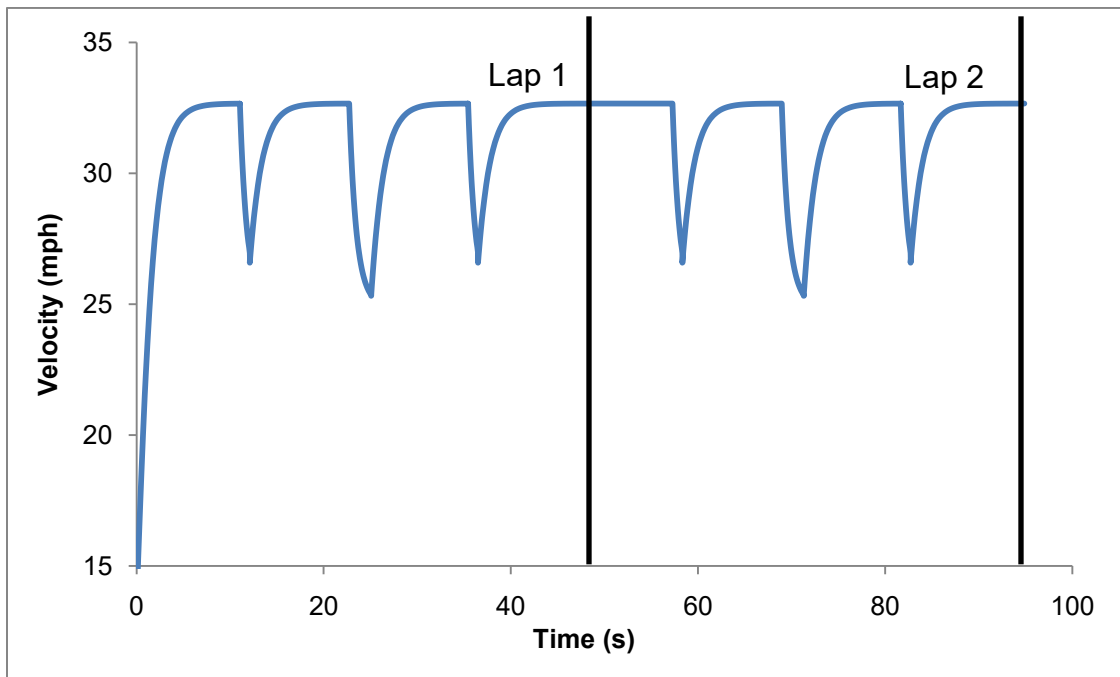


Figure 5.7: Velocity profile prediction for Mission 1 with an 8x6 propeller

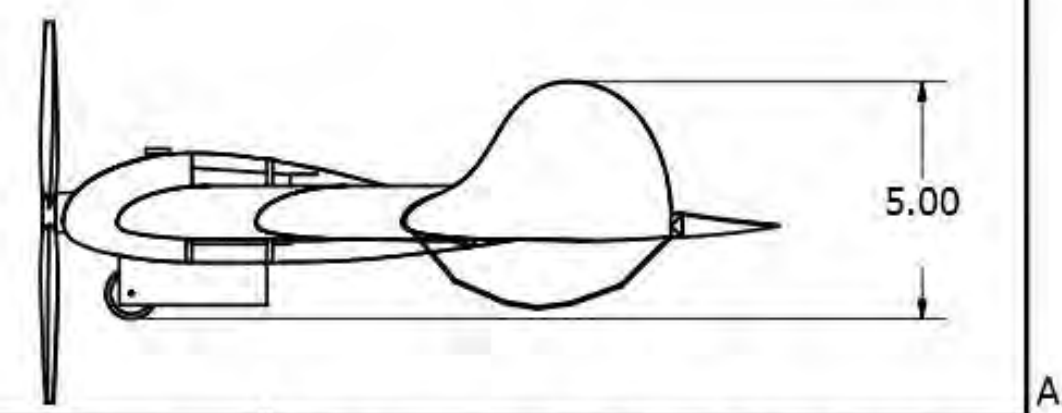
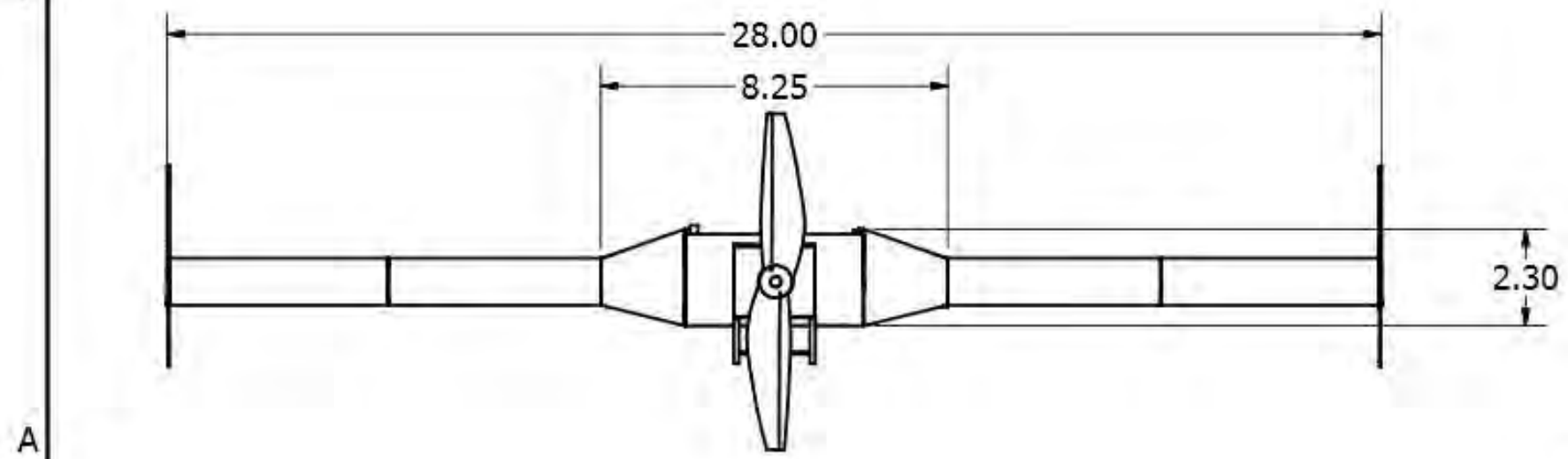
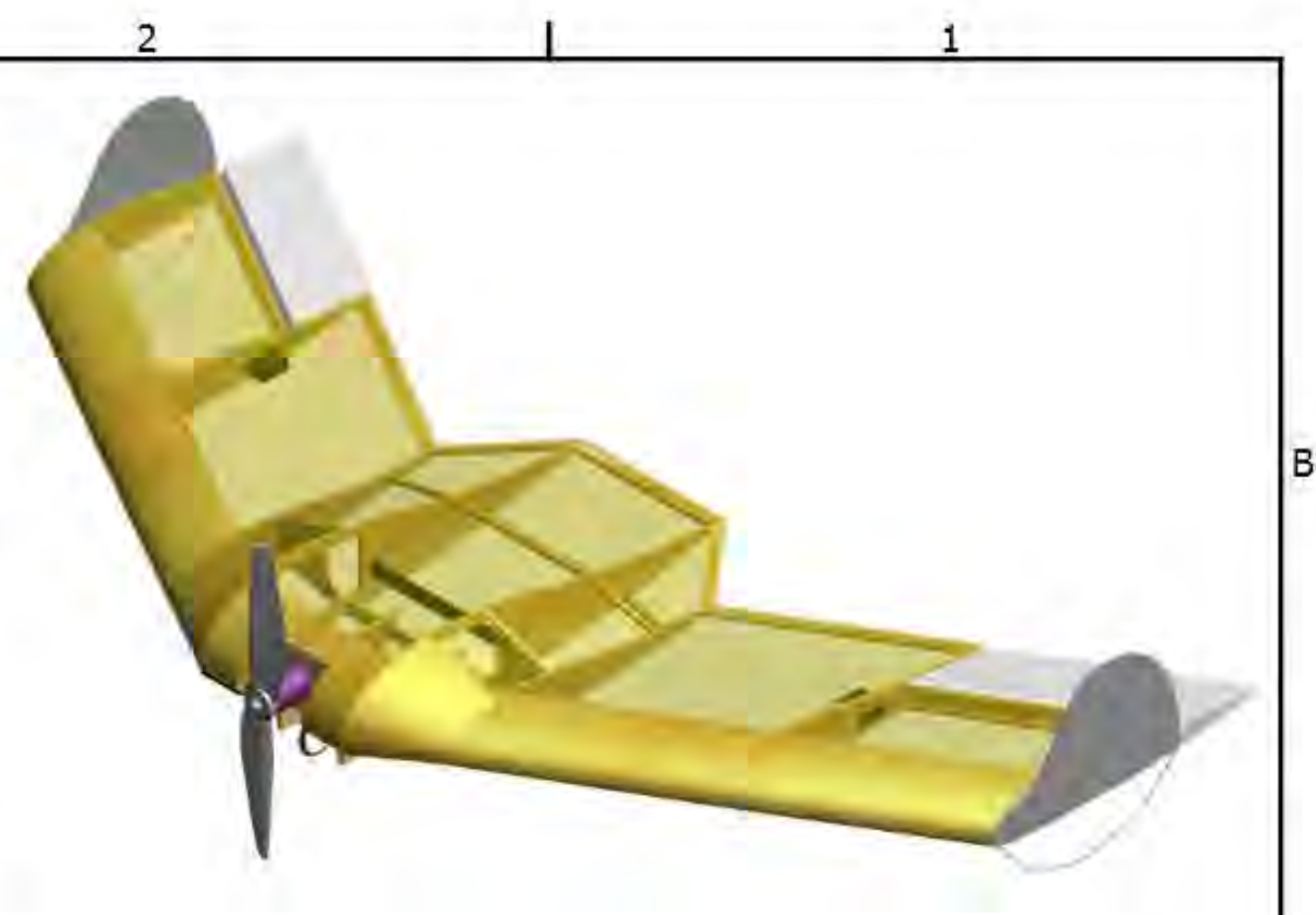
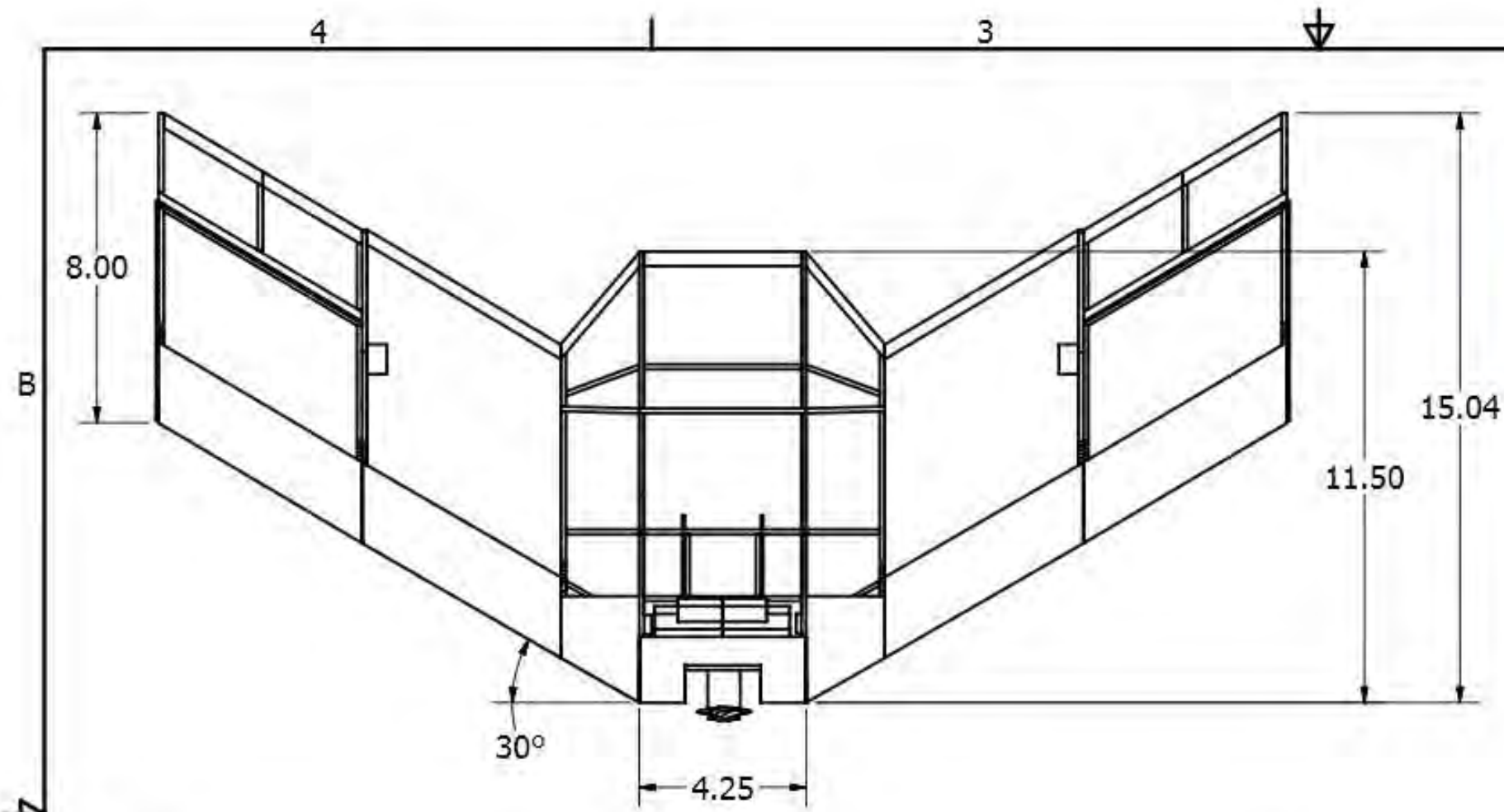
The estimated average lap time for each mission configuration using each different propeller option is displayed in Table 5.5. From the table it is clear that using the 8x6 propeller is best for minimizing lap time in the first mission and maximizing scoring potential.

Table 5.5: Predicted mission performance for various aircraft-propeller combinations

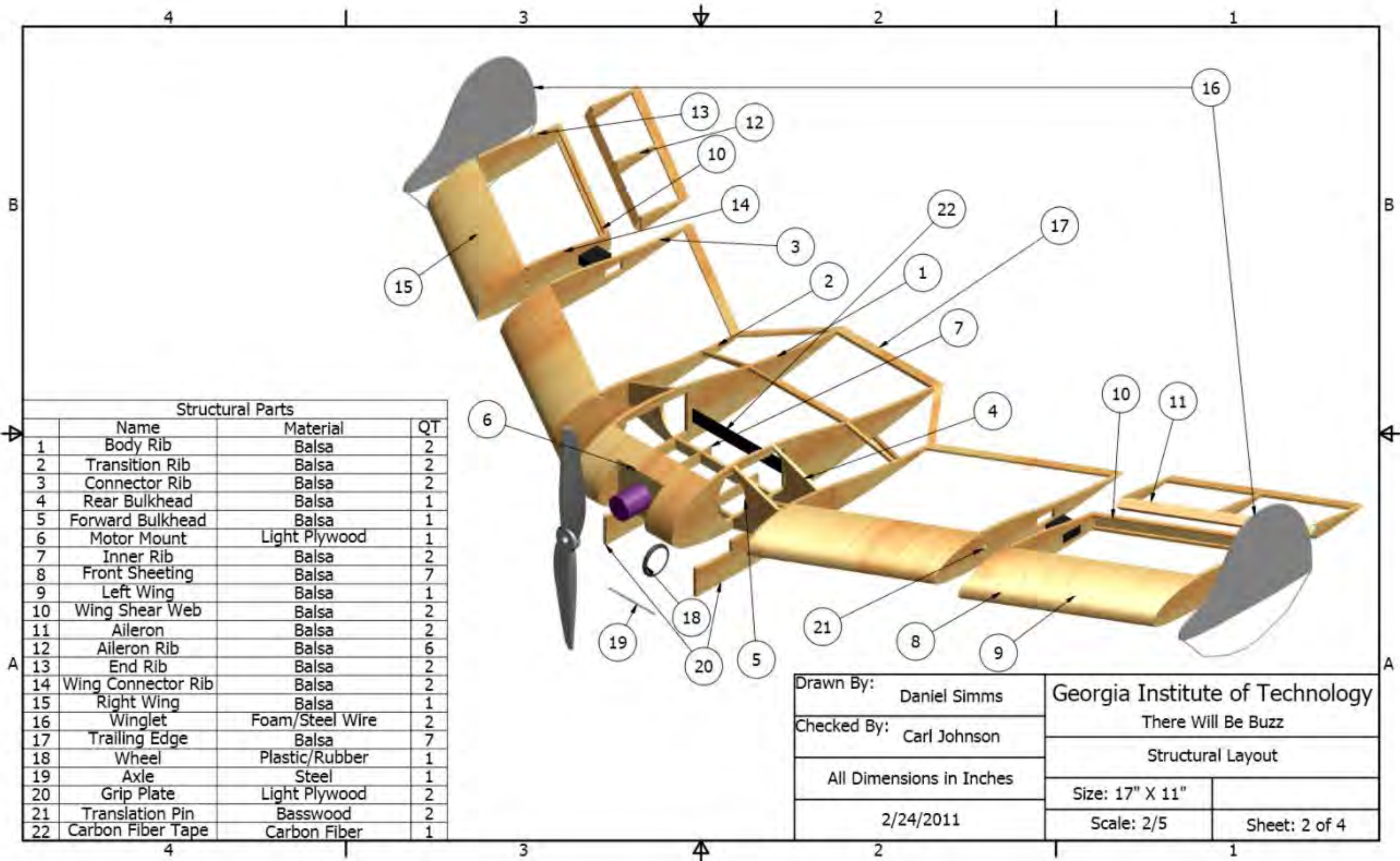
| Mission | Propeller | Lap Time(s) |
|---------|-----------|-------------|
| M1 | 8x4.3 | 53.6 |
| M1 | 8x6 | 47.4 |
| M1 | 9x4.7 | 52.8 |
| M2/3 | 8x4.3 | 63.6 |
| M2/3 | 8x6 | 55.9 |
| M2/3 | 9x4.7 | 61.7 |

5.6 Drawing Package

The following four pages illustrate the detailed CAD of *There Will Be Buzz*. A three-view diagram and payload configuration with relevant dimensions of the aircraft is shown. Exploded views are also included to show the internal structure of the aircraft.



| | | |
|--------------------------|---|---------------|
| Drawn By: Daniel Simms | Georgia Institute of Technology | |
| Checked By: Carl Johnson | There Will Be Buzz | |
| All Dimensions in Inches | Multi-view of Airplane and General Dimensions | |
| 2/24/2011 | Size: 17" X 11" | |
| | Scale: 1/4 | Sheet: 1 of 4 |



4 | 3 | 2 | 1

B

B

A

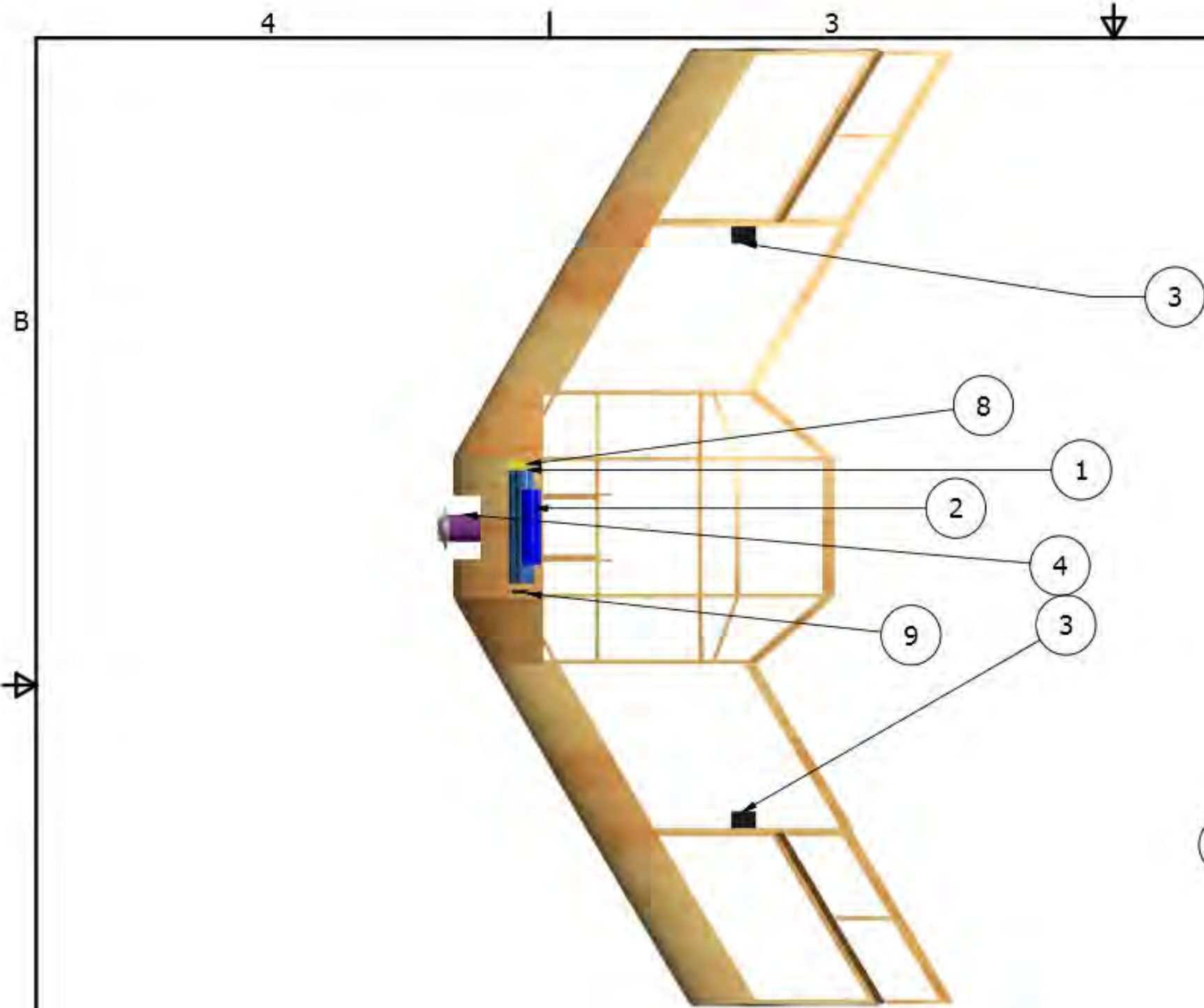
A

4 | 3 | 2 | 1

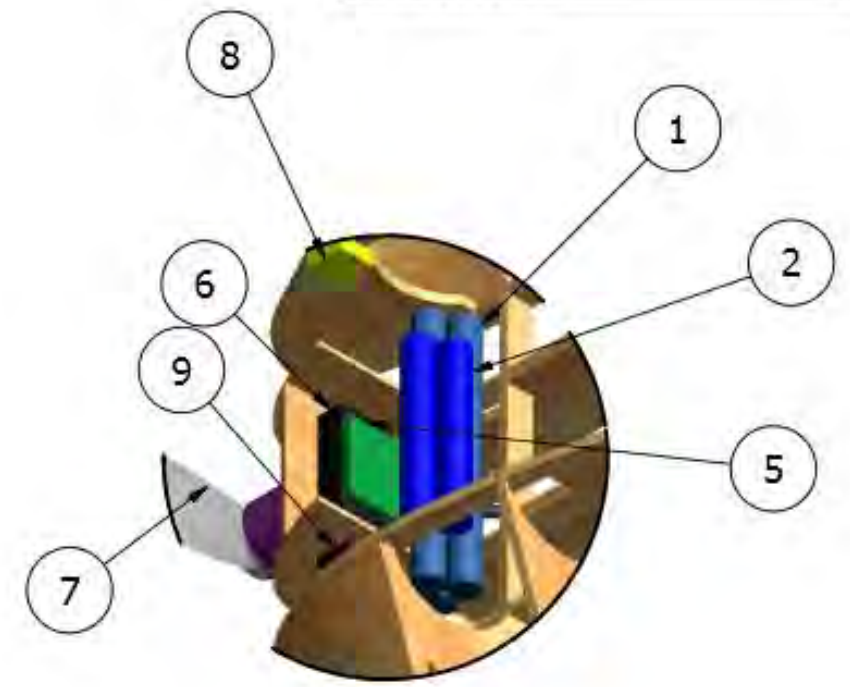
Structural Parts

| | Name | Material | QT |
|----|--------------------|-----------------|----|
| 1 | Body Rib | Balsa | 2 |
| 2 | Transition Rib | Balsa | 2 |
| 3 | Connector Rib | Balsa | 2 |
| 4 | Rear Bulkhead | Balsa | 1 |
| 5 | Forward Bulkhead | Balsa | 1 |
| 6 | Motor Mount | Light Plywood | 1 |
| 7 | Inner Rib | Balsa | 2 |
| 8 | Front Sheeting | Balsa | 7 |
| 9 | Left Wing | Balsa | 1 |
| 10 | Wing Shear Web | Balsa | 2 |
| 11 | Aileron | Balsa | 2 |
| 12 | Aileron Rib | Balsa | 6 |
| 13 | End Rib | Balsa | 2 |
| 14 | Wing Connector Rib | Balsa | 2 |
| 15 | Right Wing | Balsa | 1 |
| 16 | Winglet | Foam/Steel Wire | 2 |
| 17 | Trailing Edge | Balsa | 7 |
| 18 | Wheel | Plastic/Rubber | 1 |
| 19 | Axle | Steel | 1 |
| 20 | Grip Plate | Light Plywood | 2 |
| 21 | Translation Pin | Basswood | 2 |
| 22 | Carbon Fiber Tape | Carbon Fiber | 1 |

| | | | |
|--------------------------|--------------|---------------------------------|---------------|
| Drawn By: | Daniel Simms | Georgia Institute of Technology | |
| Checked By: | Carl Johnson | There Will Be Buzz | |
| All Dimensions in Inches | | Structural Layout | |
| 2/24/2011 | | Size: 17" X 11" | |
| | | Scale: 2/5 | Sheet: 2 of 4 |



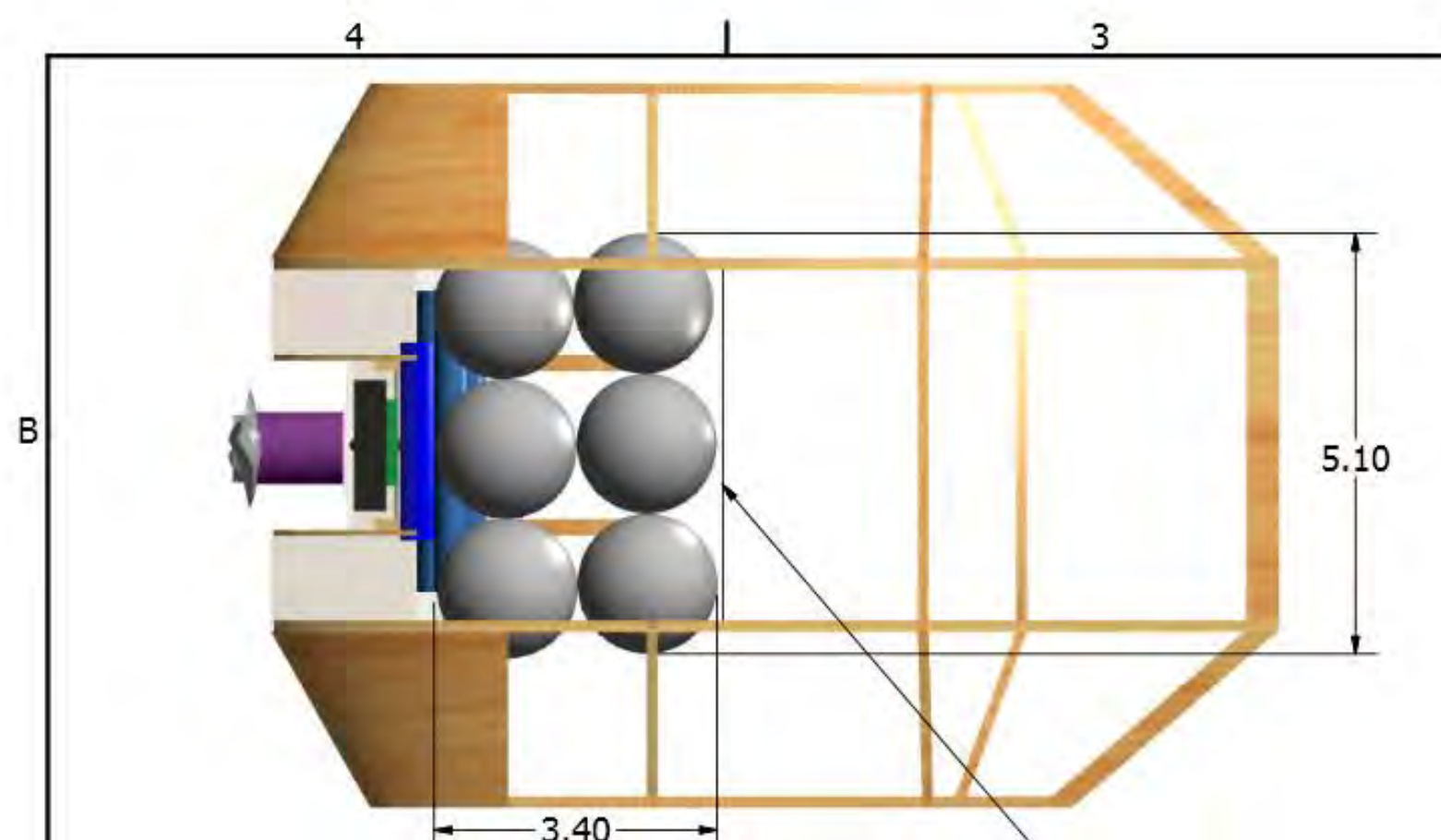
| SUBSYSTEMS LIST | | | | |
|-----------------|--------------------|----------|------------|---|
| | PART | MANUF. | MODEL | Q |
| 1 | MAIN BATTERIES | KAN | 700mAh | 1 |
| 2 | RECEIVER BATTERIES | KAN | 400mAh | 1 |
| 3 | AILERON SERVO | FUTABA | S3114 | 2 |
| 4 | MOTOR | HACKER | A10-9L | 1 |
| 5 | SPEED CONTROLLER | CASTLE | PHOENIX 10 | 1 |
| 6 | RECEIVER | SPEKTRUM | 6255 | 1 |
| 7 | PROPELLOR | GWS | EP-0947 | 1 |
| 8 | FUSE | | 20 AMP | 1 |
| 9 | SWITCH | | | 1 |



DETAIL A
SCALE 1 / 2

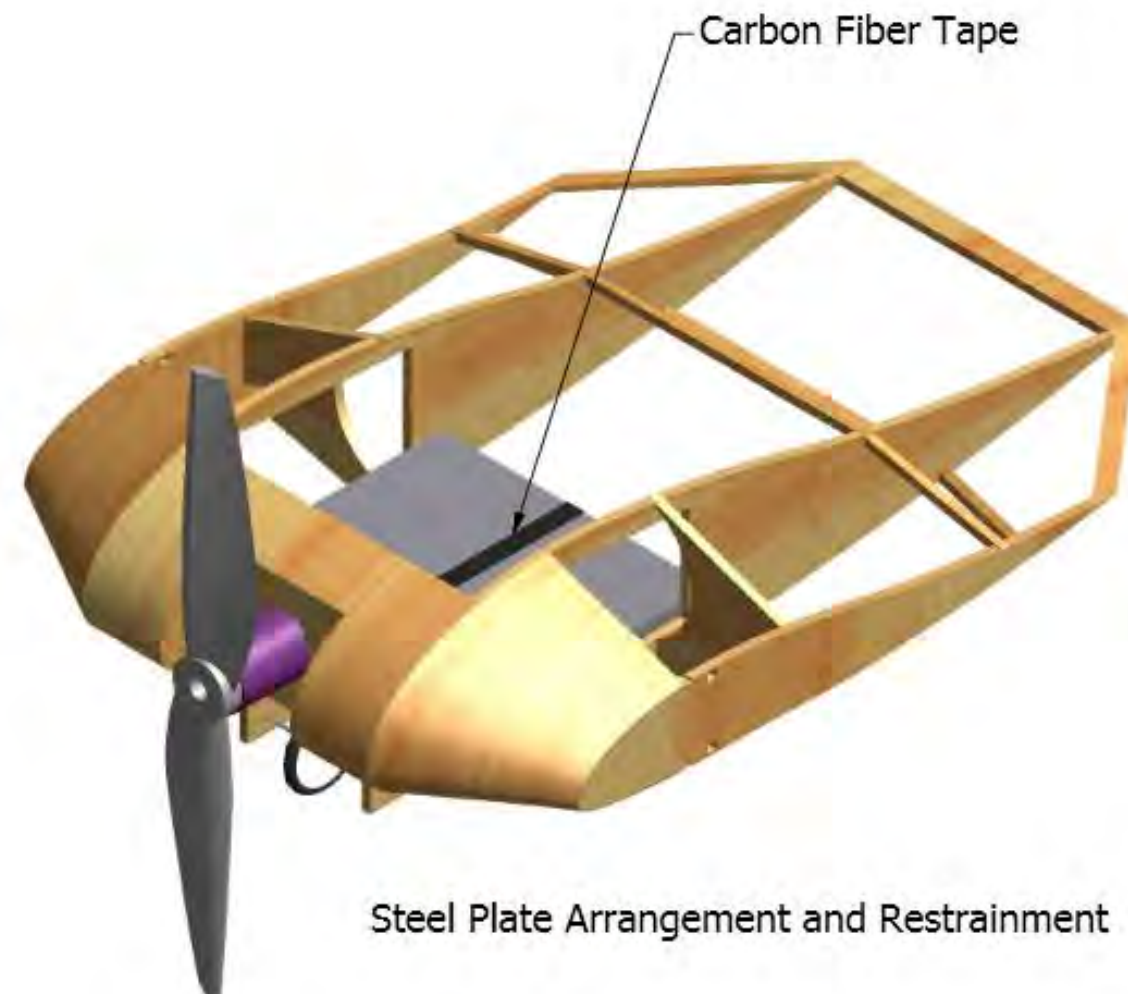


| | | |
|--------------------------|---------------------------------|---------------|
| Drawn By: Daniel Simms | Georgia Institute of Technology | |
| Checked By: Carl Johnson | There Will Be Buzz | |
| All Dimensions in Inches | Subsystems Layout | |
| 2/24/2011 | Size: 17" X 11" | |
| | Scale: 1/4 | Sheet: 3 of 4 |

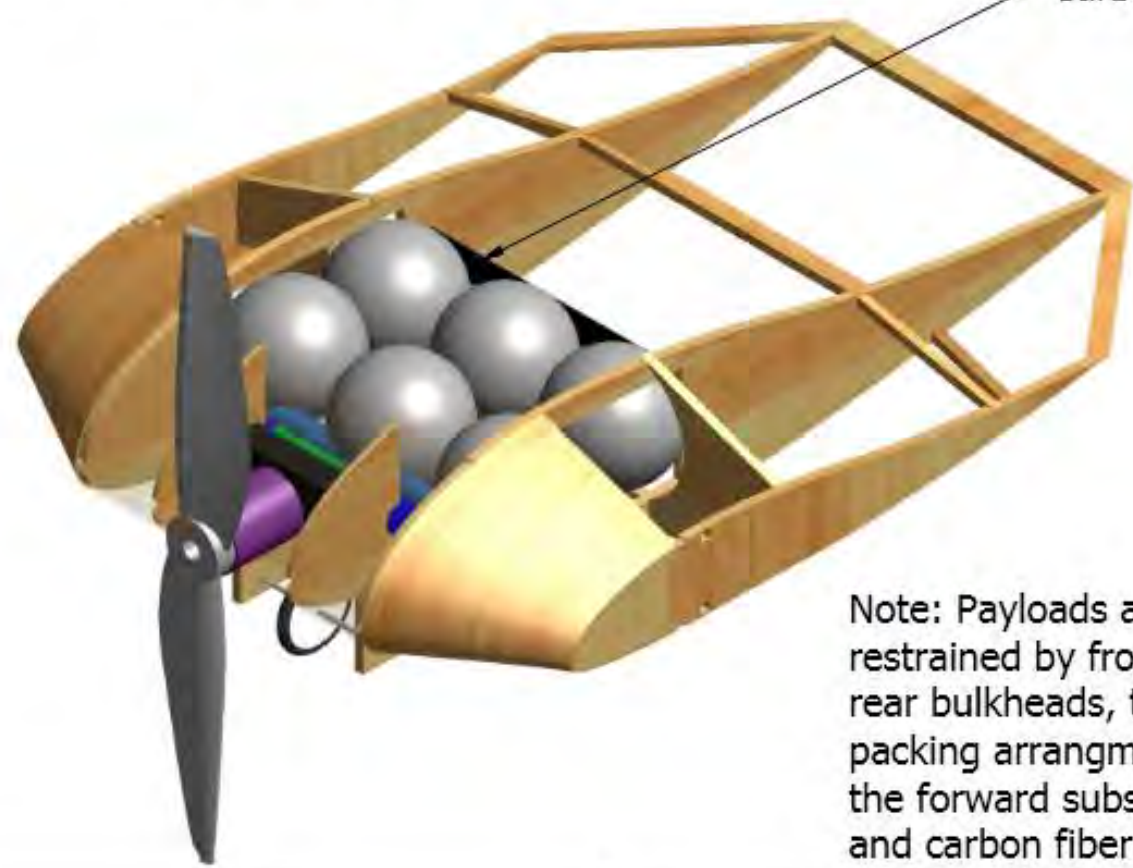


Golf Ball Arrangement and Restraint

Carbon Fiber Tape



Steel Plate Arrangement and Restraint



Note: Payloads are restrained by front and rear bulkheads, the packing arrangement of the forward subsystems, and carbon fiber tape

| | | |
|--------------------------|---------------------------------|---------------|
| Drawn By: Daniel Simms | Georgia Institute of Technology | |
| Checked By: Carl Johnson | There Will Be Buzz | |
| All Dimensions in Inches | Payload Arrangement | |
| 2/24/2011 | Size: 17" X 11" | |
| | Scale: 1/2 | Sheet: 4 of 4 |



6. MANUFACTURING PLAN AND PROCESSES

Correct materials and manufacturing techniques, alongside appropriate build planning, are the essential steps between design and fly. Following a qualitative investigation, the team selected manufacturing processes that would accurately translate the design discussed above into a successful aircraft.

6.1 Manufacturing Processes Selected

There Will Be Buzz sought to further refine and push the envelope of the manufacturing techniques developed in previous years, and to transfer construction knowledge to newer team members. Built-up balsa was selected as the manufacturing process, detailed in Table 6.1:

Table 6.1: Built-up balsa manufacturing technique

| Manufacturing Component | Material / Technique |
|-------------------------|-------------------------------|
| Principal material | Competition Grade balsa wood |
| Other materials | Local fiber reinforcements |
| Adhesive | CA, or epoxy if needed |
| Coating | Ultracote |
| Part manufacture | CAD-guided laser cutting |
| Part assembly | Designed-to-fit jigsaw pieces |

The manufacturing process in Table 6.1 was selected because of the team's confidence and proven capability to not only produce the aircraft to specification, but also to build a very light structure, which the team outlined as one of the design requirements. Further reasons for choosing built-up balsa over other techniques are detailed in the next section.

Of the many different ways to apply built-up balsa, the team chose specific techniques and materials that would minimize the aircraft structure's weight without compromising its strength. These strategies are:

Selective material use: since balsa wood can vary significantly in density and strength, the team sorted its entire stock of balsa by weight. The lightest pieces were selected for construction and were sent to the team's in-house laser cutter, with lightest of those being reserved for the final competition aircraft.

Local reinforcements: because very low density balsa was used, the structure lacked strength in several key locations. Rather than over-building the entire aircraft to compensate, these locations were reinforced with composites or additional balsa, adding strength at minimal penalty in weight.

Light sheeting: the leading edge of the airfoil must be sheeted in order to maintain its shape while being coated. Since this process covers a large area with balsa wood, adding weight, the team used



1/16" sheeting instead of thicker sheets, as seen in Figure 6.1. The thinner sheeting offered sufficient leading-edge definition and structural torsional stiffness with little weight penalty.



Figure 6.1: The team fitting balsa sheeting to the aircraft

Lightening holes: because the team uses a very concentrated, localized structure, most other members do not experience significant loading. Where possible, the team laser-cut lightening holes into ribs and bulkheads to reduce weight with little losses in the overall stiffness of the aircraft.

Coating: most balsa aircraft are coated with Monokote, which is durable and easy to handle. However, the team chose to use the more delicate Ultracote because it is much lighter.

6.2 Manufacturing Processes Investigated

Although the team had a well-established technique in built-up balsa, other manufacturing processes were investigated as well. That is because every new set of rules requires team members to re-think conventional designs and materials to produce a winning design. The candidate aircraft manufacturing processes were qualitatively compared using Figures of Merit, detailed below and summarized in Table 6.2.

Weight: similarly to conceptual design, weight is still the most important factor for any design decision, and is assigned a FOM of 5.

Reparability: with the new hand launch requirement, and ever-present unknown factors, the reparability of the aircraft in case of an accident or a crash had to be accounted for, and was assigned a FOM of 2.



Ease of Manufacture: the ability to produce the aircraft to specification is critical to it performing according to predictions, and is directly related to Ease of Manufacture; it was therefore assigned a FOM of 3.

Experience: the team's knowledge was given some weighting because it relates to the ability to produce good results effectively and quickly, as well as to refine existing techniques. However, since the team is always willing to learn new techniques, Experience was only assigned a FOM of 2.

Cost: keeping in mind that the team has limited resources, Cost was inevitably added as a FOM. However, since the team emphasizes winning above all, Cost was assigned a FOM of only 1.

Table 6.2: Manufacturing FOM weighting

| Figure of Merit | 0 | 1 | 2 | 3 | 4 | 5 |
|---------------------|---|---|---|---|---|---|
| Weight | | | | | | 5 |
| Reparability | | | 2 | | | |
| Ease of Manufacture | | | | 3 | | |
| Experience | | | 2 | | | |
| Cost | | 1 | | | | |

The manufacturing processes and materials common to remote control aircraft construction that were investigated are:

Built-up Balsa: stocks of competition grade balsa wood are laser cut from CAD parts and are glued together using cyanoacrylate (CA) adhesive to form the skeleton of the aircraft. It is then locally reinforced with fiberglass or carbon fiber if necessary, and coated with Ultracote heat shrink film.

Foam Core Composite: large blocks of foam are cut with a hot-wire or CNC router to form the basic shape of the aircraft. Structural reinforcements are locally added if needed, and the entire foam-core is coated in fiberglass or carbon fiber, adding strength as a monocoque.

Molded Composite: this process is similar in principle to a foam core; however, the foam parts are only used to mold the composites and are then removed, with the fiberglass or carbon fiber also acting as a monocoque structure.

The processes were evaluated against each other by assigning each FOM a score, with 5 indicating a superior choice, 3 an average choice, and 1 an inferior choice. All methods were assumed to result in an aircraft designed for an identical load. The results of the comparison are summarized in Table 6.3:



Table 6.3: Weighting for various manufacturing techniques

| FOM | Weight | Manufacturing Process | | |
|---------------------|--------|-----------------------|----------------------|-------------------|
| | | Built-up Balsa | Foam Core Composites | Molded Composites |
| Weight | 5 | 5 | 3 | 5 |
| Reparability | 2 | 3 | 1 | 1 |
| Ease of Manufacture | 3 | 3 | 3 | 1 |
| Experience | 2 | 5 | 3 | 3 |
| Cost | 1 | 5 | 3 | 1 |
| Total | 13 | 55 | 35 | 37 |

This table shows that built-up balsa is the clear choice for the construction of the compact flying wing design. Moreover, the wide margin of superiority of balsa over other processes indicates that personal experience was not the only differentiating factor in the choice of manufacturing process.

6.3 Manufacturing Milestones

A milestone chart was established at the beginning of aircraft manufacture to ensure a logical, consistent order was followed during construction. Progress was recorded and monitored by the team leader to ensure all major milestones were met. The milestone chart is shown below in Figure 6.2, capturing planned and actual timing of major events.

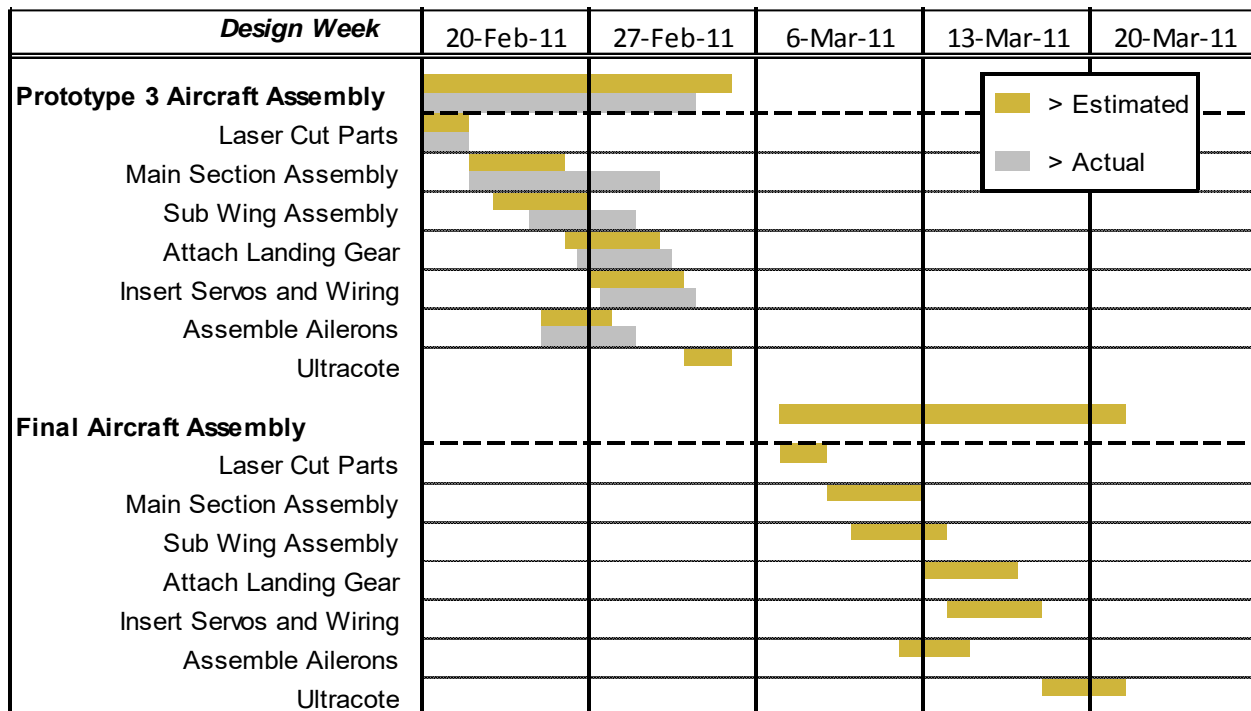


Figure 6.2: Aircraft manufacturing milestone chart showing planned and actual timing of objectives



7. TESTING PLAN

The goal of testing is to determine whether the aircraft and its various subsystems are capable and operable in line with the theory that guided the various design phases. Moreover, this section details the planning and main objectives of the various tests performed, with methods and results discussed in Section 8.

7.1 Objectives and Schedules

The testing was broken up into three main categories: propulsion, structures, and performance. The propulsion and structures subsystems were tested before flying the whole aircraft if possible; this was in order to gain knowledge and set realistic and useful objectives at each test flight. The testing breakdown with objectives and dates is detailed in Table 7.1:

Table 7.1: Testing objective and schedules

| Category | Component | Objectives | Dates |
|------------------------------|----------------|--|---------------------|
| Propulsion | Batteries | Determine discharge curves Find battery resistance | 10/6 – 11/4 |
| | Propeller | Determine static thrust Validate propeller theory model | 11/5 – 11/22 |
| Structures | Wings | Satisfy 2.5g wingtip test | 11/7 – 12/10 |
| | Landing Gear | Achieve successful landing | 11/8 |
| Performance (Flight Test) | Whole Aircraft | Verify mission capability Record flight data to validate mission models Gain pilot 'stick-time' | 11/8 – 4/15/2011 |

The testing schedule is better visualized in the following Gantt chart, shown in Figure 7.1:

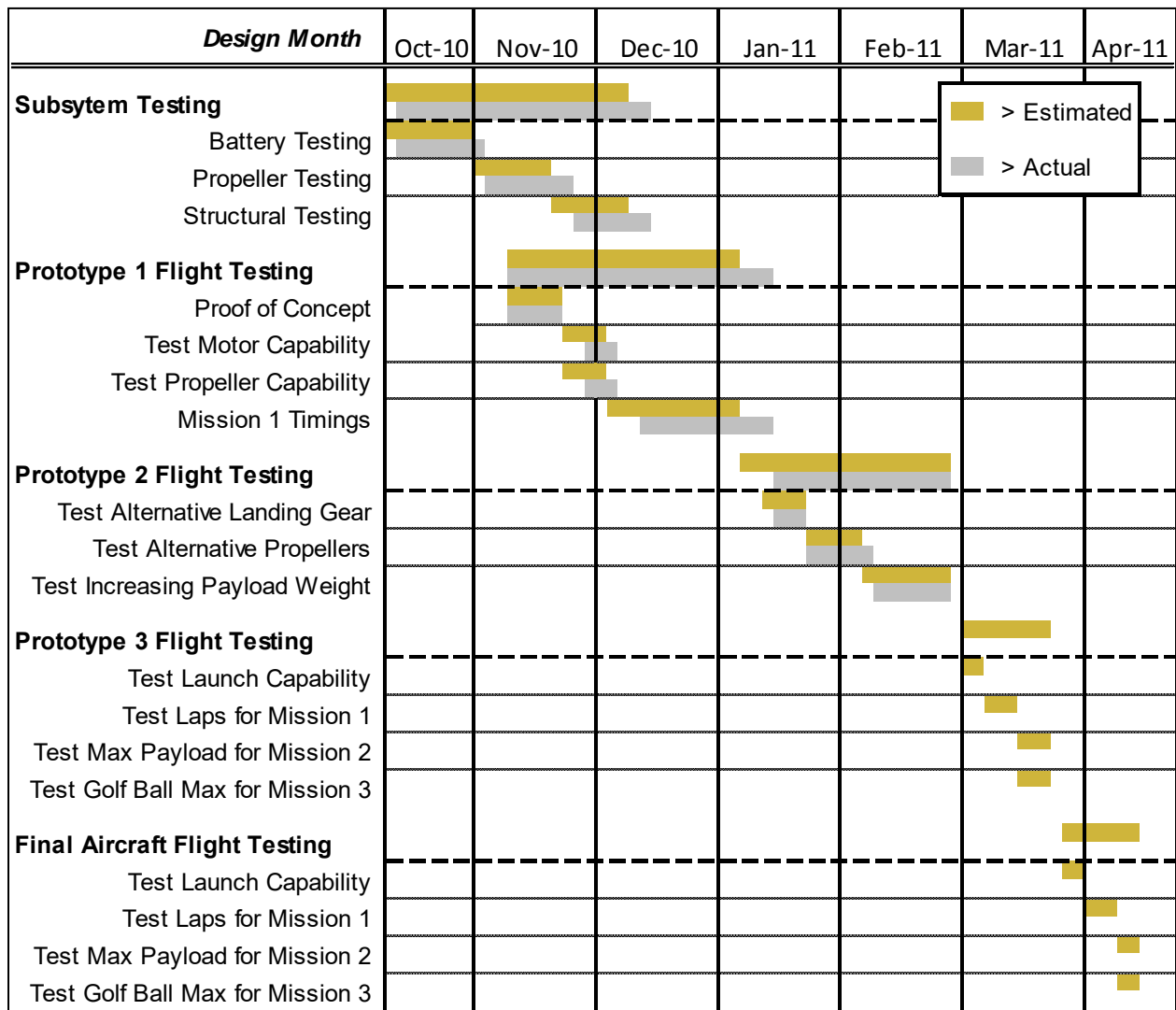


Figure 7.1: Aircraft and subsystem testing milestone chart showing planned and actual timing of objectives

7.2 Checklists

Various tests have specific procedures which must be followed accurately down to the last step in order to produce the desired objectives and ensure safety. This section lists the checklists utilized by *There Will Be Buzz* while conducting tests that required a significant amount of steps, such as propulsion and flight tests.

7.2.1 Propulsion Test Checklist

The checklist in Figure 7.2 was created to ensure safety while dealing with propellers and electrical equipment, and to make sure the test is not wasted due to some mistake in preparation. It applies to both battery and propeller tests, since both utilize an identical setup.



| Propulsion Test Checklist | |
|----------------------------------|--------------------------|
| 1. Batteries peaked? | <input type="checkbox"/> |
| 2. Receiver off? | <input type="checkbox"/> |
| 3. All plugs secured? | <input type="checkbox"/> |
| 4. Propeller secured? | <input type="checkbox"/> |
| 5. Motor mount secured? | <input type="checkbox"/> |
| 6. Data system on? | <input type="checkbox"/> |
| 7. Receiver on, throttle down? | <input type="checkbox"/> |
| 8. All clear of propeller plane? | <input type="checkbox"/> |

Figure 7.2: Propulsion test checklist

7.2.2 Flight Test Checklist

The checklist in Figure 7.3 was created with the extremely important goal of preventing any system from malfunctioning in mid-air, which could lead to the aircraft crashing; its thorough execution is paramount to the team's success, and it will be used in the DBF event as well.

| Pre-Flight Checklist | | | |
|----------------------------|--------------------------|---|--------------------------|
| Electrical | | Payload | |
| <u>Main Batteries:</u> | | | |
| Charged? | <input type="checkbox"/> | Hot? | <input type="checkbox"/> |
| <u>Receiver Batteries:</u> | | | |
| Charged? | <input type="checkbox"/> | Hot? | <input type="checkbox"/> |
| <u>Secure connections:</u> | | | |
| All receiver slots? | <input type="checkbox"/> | All power plugs? | <input type="checkbox"/> |
| Data systems? | <input type="checkbox"/> | | |
| Final Checks | | Aircraft | |
| CG correct? | <input type="checkbox"/> | Propeller secure? | <input type="checkbox"/> |
| Wing sections secure? | <input type="checkbox"/> | | |
| Final Checks | | Signatures | |
| Receiver On? | <input type="checkbox"/> | Control surfaces work? | <input type="checkbox"/> |
| Lid secure? | <input type="checkbox"/> | CG re-verified? | <input type="checkbox"/> |
| Hand grip functional? | <input type="checkbox"/> | Visual inspection OK? | <input type="checkbox"/> |
| | | Chief Engineer _____ Pilot _____ Faculty Advisor _____ | |

Figure 7.3: Pre-flight checklist



8. PERFORMANCE RESULTS

8.1 Component and Subsystem Performance

8.1.1 Propulsion

Batteries: Two different battery packs were tested on the propulsion test stand with the data for each run recorded using a data acquisition system. Both battery packs were run at full throttle using the Hacker motor with an 8x4.3 propeller until they were exhausted. The resulting data for power and RPM is plotted in Figure 8.1. It is clear from the graph that the 400mAh pack provides grossly insufficient capacity to complete the 4 minutes of flight time at full throttle required to maximize the number of laps for Mission 1. This testing data supports the MATLAB simulation performed in Section 4.2.2 and validates the propulsion system selected.

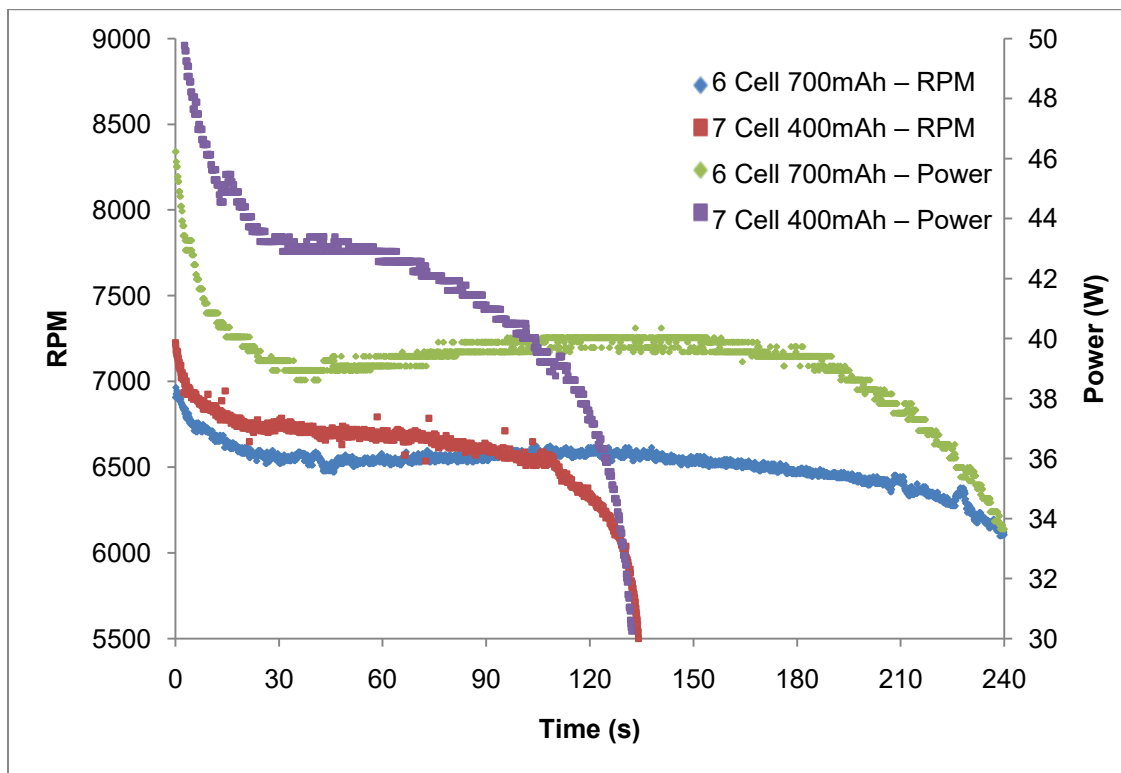


Figure 8.1: Power discharge curves and RPM data for various battery packs

Propeller: A range of propellers were also tested on the propulsion test stand to verify the static thrust predictions made in Section 5.5.2 of the report. For each test the 6 cell 700mAh battery pack was used with the Hacker motor. The results of this testing are compared to the previous predictions in Figure 8.2 and Table 8.1. The analytical results are quite good, except that the thrust is slightly under predicted for the 8x6 propeller. This underprediction could be due to the higher pitch-to-diameter ratio for the 8x6 resulting in decreased accuracy in the analytical tool.

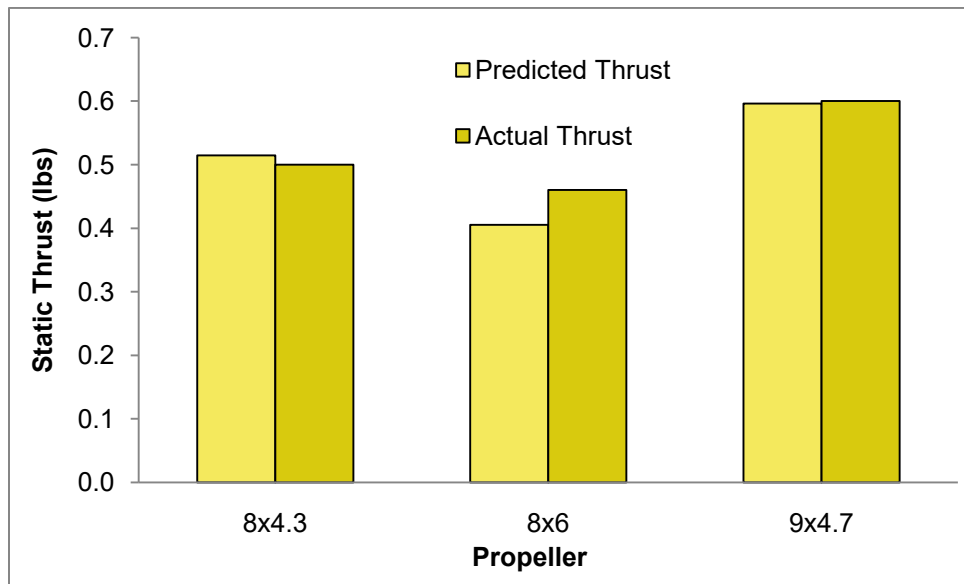


Figure 8.2: Comparison of predicted to actual thrust for various propellers

Table 8.1: Numerical comparison of thrust for various propellers

| Propeller | Measured Thrust (lbs) | Predicted Thrust (lbs) | % Difference |
|-----------|-----------------------|------------------------|--------------|
| 8x4.3 | 0.50 | 0.51 | -3% |
| 8x6 | 0.46 | 0.41 | 13% |
| 9x4.7 | 0.60 | 0.60 | 1% |

8.1.2 Structural Tests

Wing Testing Results: The full size airplane was subjected to the required wing tip testing specified in the rules as part of the technical inspection process. This was done by loading the payload bay with the maximum expected payload of 0.6 lbs, corresponding to 6 golf balls, and lifting the airplane by the wing tips. The successful test is shown in Figure 8.3.



Figure 8.3: Wingtip structural test with full payload



Landing Gear Testing Results: The two landing gear options were tested via full flight test. Both the dual and single wheel options were successful in landing without payload. Under full payload conditions the dual wheel landing gear suffered plastic deformation in the wires, which in combination with the substantial drag penalty involved in the dual wheel design led the team to select the single wheel option for the final design.

8.2. System Performance

As of the time of this report, twenty-two flight tests have been performed on two different airplanes. On a number of these flights a data acquisition system taking ten measurements each second was added to the airplane to record data on the propulsion system and trajectory. An example of a full lap trajectory is displayed in Figure 8.4 superimposed on satellite imagery using Google Earth.

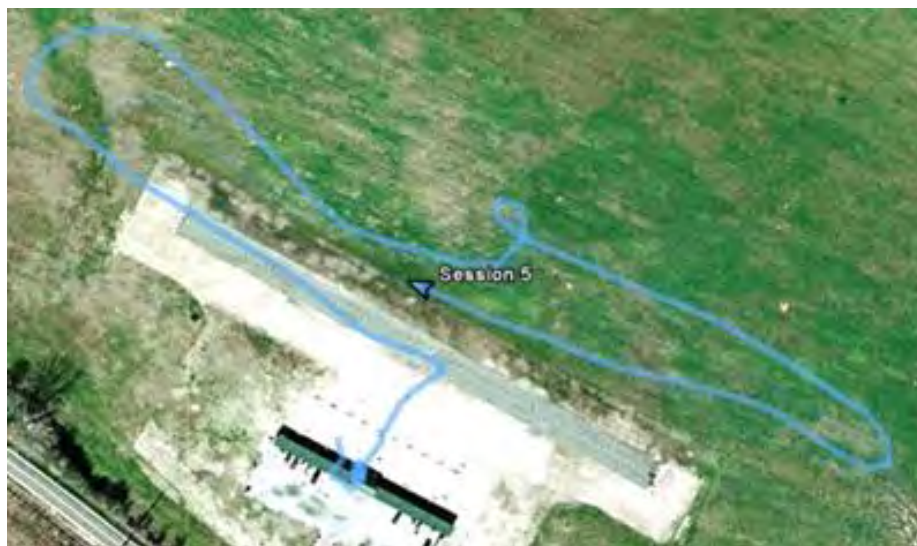


Figure 8.4: Trajectory of aircraft during competition laps from GPS data

The velocity profile for a Mission 1 flight is shown in Figure 8.5. The GPS speed corresponds to ground speed, such that there is a significant difference depending on if the airplane is flying with or against the wind. From this graph it can be estimated that the approximate wind speed during that flight was ~7-8 mph, assuming the airplane was flying at approximately its top airspeed for each straight line mission segment. Another note to make is that the GPS speed is artificially low during turns, as the data refresh rate is not high enough to characterize the tight turns of the airplane. The figure also shows the airplane completing five laps in four minutes and twenty seconds. The airplane should therefore have no difficulty finishing four laps, but will most likely be unable to complete a fifth.

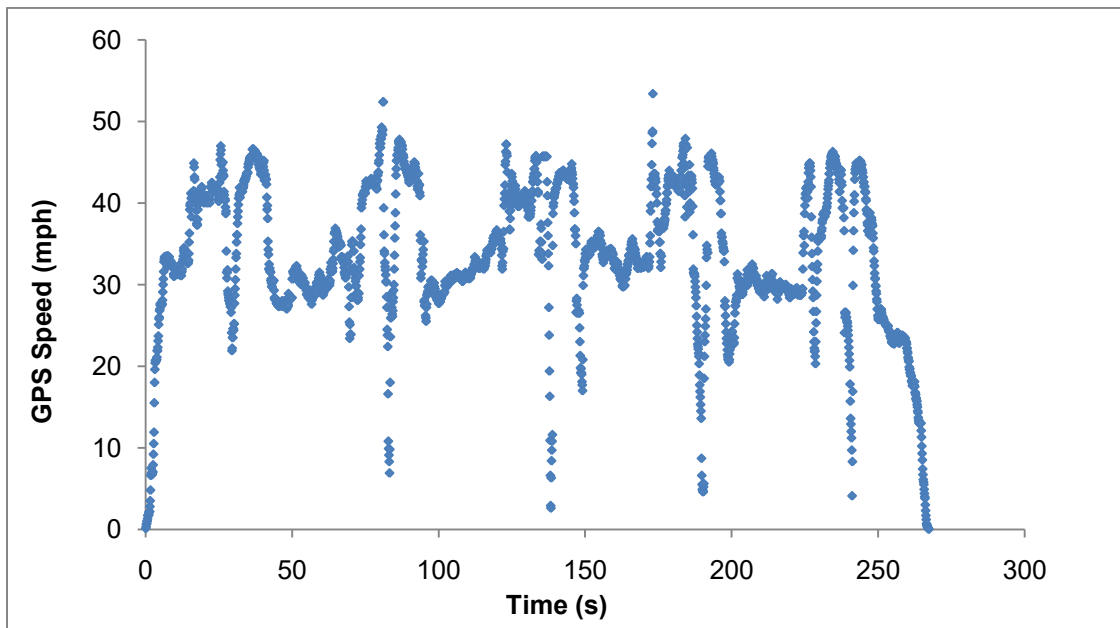


Figure 8.5: Velocity profile for Mission 1 flight test

The power output of the electrical motor throughout the flight was also recorded, as shown in Figure 8.6. The pilot maintained full throttle throughout the flight, excepting a small period near the end, and this is borne out by the results shown in the graph. The average power output of approximately 39 Watts is fairly close to the predicted power output of ~45 Watts.

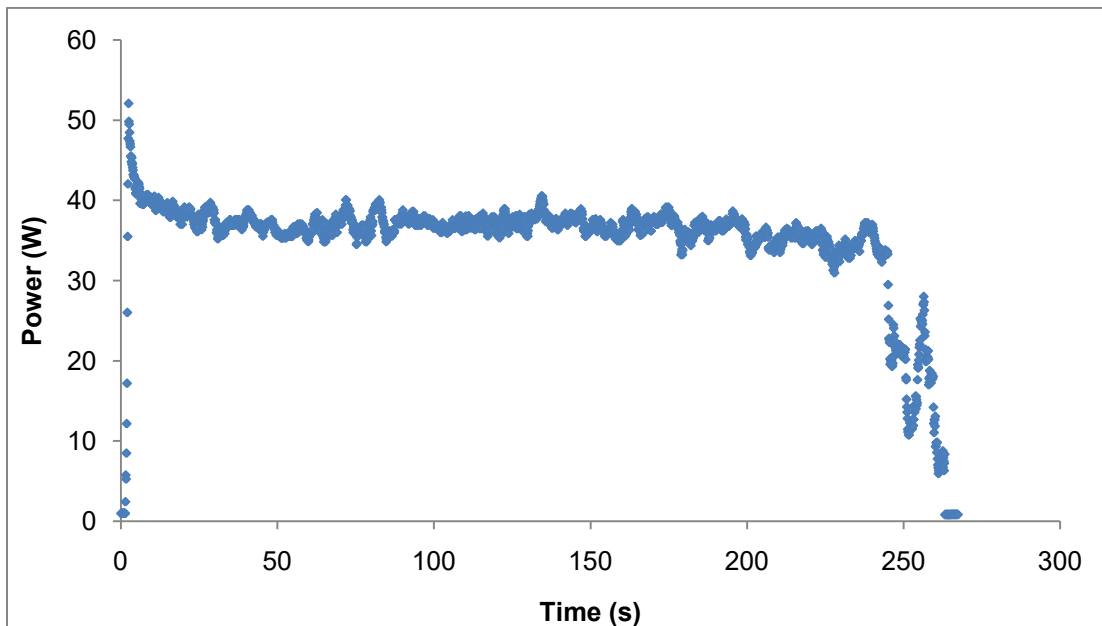


Figure 8.6: Power output of propulsion system during Mission 1 flight test



A comparison of the velocity profile for just the first lap is compared with the predicted trajectory in the detailed design section of the report in Figure 8.7. They are similar, but the predicted lap time is approximately 8 seconds shorter than the actual. This can be explained by the theory ignoring the effect of wind, any imperfections in the pilot trajectory relative to an ideal path, and any uncertainties in the predictions for the aerodynamic or propulsion estimates used to develop the predictions.

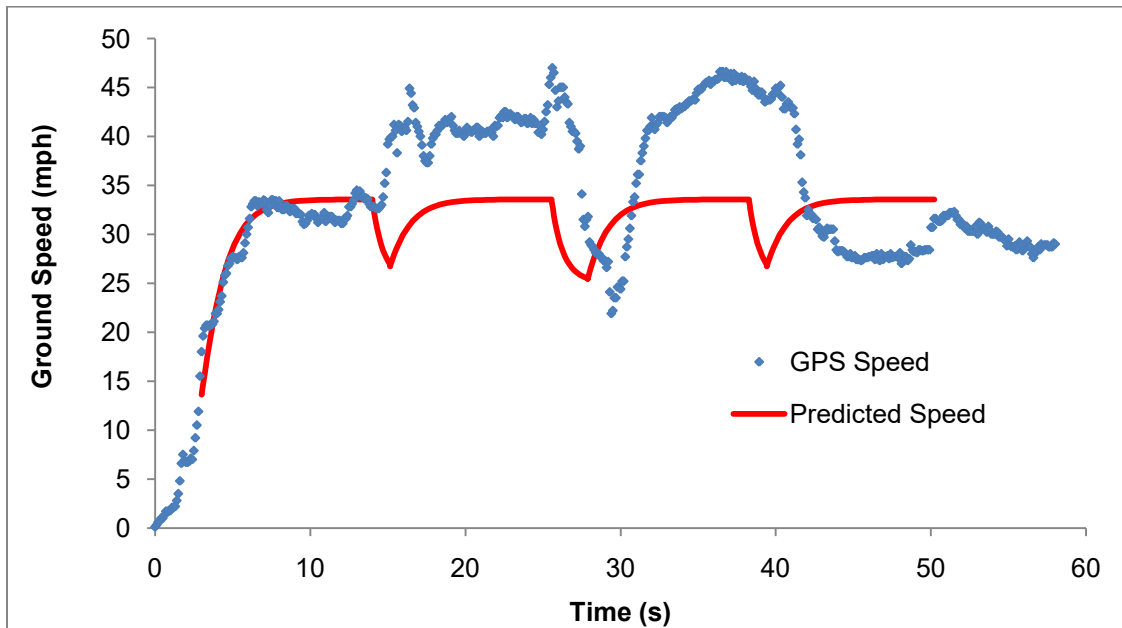


Figure 8.7: Graphical comparison of predicted Mission 1 flight profile to actual

The average lap times for a range of propellers for different missions is shown in Table 8.2 from both flight test results and the performance predictions. The predicted lap times are uniformly shorter than the actual, due to the reasons mentioned above.

Table 8.2: Numerical comparison of predicted mission lap times to actual

| | Propeller | Actual Lap Times (s) | Predicted Lap Time (s) |
|-------------|-----------|----------------------|------------------------|
| Mission 1 | 8x4.3 | 63.8 | 53.6 |
| | 8x6 | 52.5 | 47.4 |
| | 9x4.7 | 61.3 | 53.8 |
| Mission 2/3 | 8x4.3 | 73.5 | 63.6 |



Figure 8.8: Example of hand-launched flight test



9. REFERENCES

Anderson, J. D. *Fundamentals of Aerodynamics*, 4th edition, McGraw Hill.

Bauchau, O. A., & Craig, J. I. (January 7, 2009). *Aerospace Structural Analysis*. Springer.

Drela, M., & Youngren, H. (2008, 08 04). *AVL*. Retrieved 01 10, 2009, from [<http://web.mit.edu/drela/Public/web/avl/>].

Drela, M., & Youngren, H. (2008, 04 07). *XFOIL*. Retrieved 10 01 2008, from Subsonic Airfoil Development System: [<http://web.mit.edu/drela/Public/web/xfoil/>].

Hoerner, Sighard F. *Fluid Dynamic Drag*. 2nd. Published by author, 1965.

Katz, Joseph and Maskew, Brian. "Unsteady low-speed aerodynamic model for complete aircraft configurations," *Journal of Aircraft*. Vol. 25, pp. 302-310. Apr. 1988.

McDaniel, Katie et al. (2008). *Georgia Institute of Technology Team Buzzed*. Editor: Johnson, Carl.

Phillips, Warren F. *Mechanics of Flight*. 1st. Hoboken, NJ: Wiley, 2004.

Roskam, Jan. *Airplane Flight Dynamics and Automatic Flight Controls Part I*. Darcorp, 2007.

Roskam, Jan. *Airplane Design Part VI*. Darcorp, 2000.

Selig, M. (2008, 02 19). *UIUC Airfoil Data Site*. Retrieved 10 01, 2008, from [www.ae.uiuc.edu/m-selig/ads.html].

AIAA/Cessna/Raytheon DBF 2010 -11

The RFB



University of Southern California
AeroDesign Team



Table of Contents

| | |
|--|----|
| Acronyms, Abbreviations, and Symbols | 2 |
| 1. Executive Summary | 3 |
| 2. Management Summary | 4 |
| 2.1 Team Organization | 4 |
| 2.2 Subgroups | 5 |
| 2.3 Scheduling and Budget Control | 6 |
| 3. Conceptual Design | 6 |
| 3.1 Evolution of Design | 7 |
| 3.2 Mission Requirements | 8 |
| 3.3 Design Requirements | 9 |
| 3.4 Score Analysis | 9 |
| 3.5 Conceptual Design Selection Process | 12 |
| 3.6 Systems Downselects | 15 |
| 3.7 Conclusion | 17 |
| 4. Preliminary Design | 17 |
| 4.1 Critical Design Parameters | 17 |
| 4.2 Design and Analysis Methodology | 19 |
| 4.3 Performance Trade Studies & Optimization | 21 |
| 4.4 Aerodynamics | 22 |
| 4.5 Stability and Control | 26 |
| 4.6 Propulsion | 27 |
| 4.7 Structures | 31 |
| 4.8 Dimensional Parameters & Weight | 33 |
| 4.9 Payloads | 33 |
| 4.10 Flight Testing | 35 |
| 4.11 Preliminary Design Summary | 36 |
| 5. Detailed Design | 36 |
| 5.1 Dimensional Parameters | 36 |
| 5.2 Structural Characteristics and Capabilities | 37 |
| 5.3 System Design, Component Selection and Integration | 38 |
| 5.4 Aircraft Component Weight and CG Buildup | 41 |
| 5.5 Flight Performance Parameters | 41 |
| 5.6 Mission Performance | 42 |
| 6. Manufacturing Plan and Processes | 47 |
| 6.1 Manufacturing Techniques | 47 |
| 6.2 Figures of Merit | 48 |
| 6.3 Manufacturing Downselects | 49 |
| 6.4 Manufacturing Schedule | 52 |
| 7. Testing Plan | 52 |
| 7.1 Schedule | 52 |
| 7.2 Subsystems Testing | 53 |
| 7.3 Flight Testing | 53 |
| 8. Performance Results | 54 |
| 8.1 Subsystems | 54 |
| 8.2 Flight Testing | 57 |
| 9. References | 59 |



Acronyms, Abbreviations, and Symbols

| | | | |
|---------------------------|--|---------------------------|------------------------------------|
| Δ | Change in variable | Kt | Torque Constant |
| δ_a | Aileron deflection | Kv | Speed Rating |
| δ_e | Elevator deflection | LE | Leading Edge |
| δ_r | Rudder deflection | MAC | Mean Aerodynamic Chord |
| AIAA | American Institute of Aeronautics and Astronautics | MDO | Multi-Disciplinary Optimization |
| AoA | Angle of Attack (also α) | N | Number of laps flown by USC |
| AVL | Avena Vortex Lattice | NiCad | Nickel Cadmium |
| b | span | NiMH | Nickel Metal Hydride |
| B | Number of balls carried by USC | N_{max} | Maximum number of laps by any team |
| B_{max} | Maximum number of balls carried by any team | OD | Outer Diameter |
| BWB | Blended Wing Body | OML | Outer Mold Line |
| c/4 | Quarter Wing Chord | RAC | Rated Aircraft Cost |
| C_D | 3-Dimensional Drag Coefficient | R/C | Rate of Climb |
| c_d | 2-Dimensional Drag Coefficient | Re | Reynolds Number |
| C_{Dmin} | 3-Dimensional Minimum Drag Coefficient | RFB | Dr. Ron F. Blackwelder ☺ |
| c_{dmin} | 2-Dimensional Minimum Drag Coefficient | R₀ | Resistance |
| C_{DO} | Parasite Drag Coefficient | S | Planform Area |
| CG | Center of Gravity | S&C | Stability and Control |
| C_L | 3-Dimensional Lift Coefficient | SM | Static Margin |
| c_l | 2-Dimensional Lift Coefficient | S_{wet} | Wetted Surface Area |
| C_{Lmax} | Wing Maximum Lift Coefficient | USC | University of Southern California |
| c_{lmax} | 2-Dimensional Maximum Lift Coefficient | V_{cruise} | Cruise Velocity |
| DBF | Design Build Fly | | |
| FOM | Figure of Merit | | |
| I_{cruise} | Cruise Current | | |
| ID | Inner Diameter | | |
| I₀ | Idle Current | | |



1. Executive Summary

This design report describes the design, testing, and manufacturing efforts of the University of Southern California's team, The RFB, in preparation for the 2010-2011 AIAA Design/Build/Fly Competition. The team's aim is to produce an airplane that maximizes the total score according to the rules provided by the contest organizers. A comprehensive management plan was developed and executed to ensure efficient use of the team's resources.

The scoring for this year's competition is dependent upon three elements: a written report score, the mission scores, and a cost score (Rated Aircraft Cost, RAC). The RAC is the maximum empty weight of the aircraft for any of the three flight missions. The first mission requires the aircraft to fly as many laps as possible in a time limit of four minutes, simulating a dash to a critical target. The second mission consists of flying three untimed circuits of the course while carrying an internal payload of a steel bar, which simulates ammunition. The third mission consists of flying three untimed laps while carrying an internal payload of golf balls, which simulates medical supplies. The aircraft must fit in a commercially available carry-on suitcase with a total dimension not to exceed 45 linear inches, where one single dimension may not exceed 22 in. For all missions, the aircraft is to be hand launched. Early score analysis and trade studies show that the most significant design parameter is RAC, as it has the strongest sensitivity on the Total Flight Score. Analysis shows that the team with the lowest RAC that could successfully complete all three missions would be the likely winner of the competition. Therefore, an aggressive integrated configuration, sizing, propulsion, and aerodynamic program is used to minimize the aircraft's RAC while still making it possible to successfully complete all missions.

The preliminary design phase involves selecting the optimum general aircraft and subsystem configurations using Figure of Merit (FOM) analyses, yielding the choice of a monoplane with a conventional tail and single tractor propeller. Each component is selected to provide sufficient aircraft performance while minimizing the RAC. Further into the detailed design phase, iterations for aerodynamic and structural performance result in an aircraft with a balsa-sheeted foam wing with a span of 13.3 in, a wing surface area of 50 in² and a custom low drag airfoil. The small wing size and material selection ensures a low weight yet aerodynamically excellent wing that will allow the aircraft to fly the high-speed mission (Mission 1) as well as withstand a large wing loading resulting from carrying a steel bar that is one half of the total flight weight (Mission 2). The chosen wing sizing also allows for the aircraft to successfully carrying a single golf ball in Mission 3. Propulsion package optimization and testing results in a propulsion package selection for all three missions to be a Tmotor T1805 spinning an APC 6x5.5 propeller, powered by 8 KAN 400mAh 2/3 AAA batteries. This propulsion package selection ensures a low weight contribution to the RAC while providing adequate power for the aircraft to fly for at least four minutes in Mission 1 as well as to fly with a large wing loading in Missions 2 and 3. The empennage surfaces solid balsa surfaces. The aircraft is sized with ailerons and elevators only, providing adequate stability and control in flight tests, confirming the estimated computational design. To further



ensure a rigid light-weight aircraft, a carbon fiber tube runs the full length of the aircraft, encompassed by a fuselage made of two plies of 1.7 oz/yd² Kevlar; this light-weight material provides wear resistance upon landing and rigidity during in-flight loads. The competition aircraft and some of its important features are depicted in Figure 1.

The predicted capabilities of the final competition aircraft are as follows: cruise speeds of approximately 104 ft/s for all three missions, wing loadings (lbs/ft²) are 1.29, 2.51, 1.63, and thrust-to-weight ratios are 0.281, 0.146, 0.222 for Missions 1, 2, and 3 respectively. The predicted RAC is 0.4 lbs. These predicted performance and scoring parameters couple to result in a highly competitive mission-oriented vehicle.

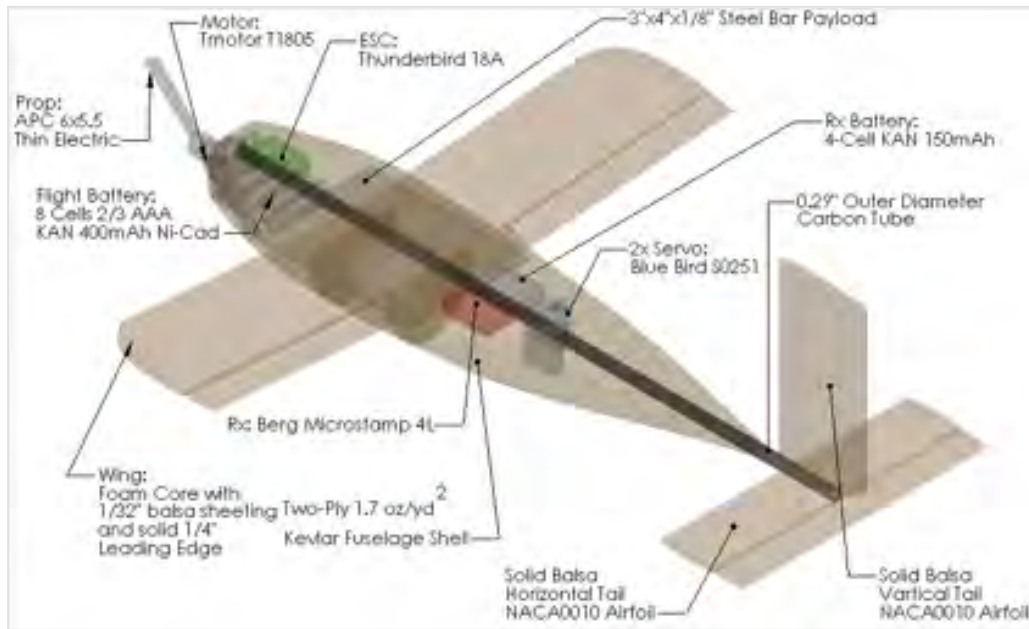


Figure 1: The competition aircraft and important features.

2. Management Summary

The AeroDesign Team consists of about 40 members ranging from freshmen to graduate students. The team operates as an extracurricular activity. Input and guidance from industry advisors and USC faculty aided the direction of the team.

2.1 Team Organization

The team used a hierarchical structure to facilitate active collaboration amongst all its members. The structure is shown in Figure 2. The team was led by the Program Manager and Chief Engineer. The Program Manager oversaw all logistic aspects of the team and was responsible for overall team productivity and progression. The Program Manager's tasks included overseeing the master schedule, organizing design reviews, and running team meetings. The Chief Engineer worked closely with the manufacturing and design groups to confirm effective collaboration, ensuring that all subgroups integrated in terms of design cohesively, fabrication, and testing.



Figure 2: USC AeroDesign team architecture.

2.2 Subgroups

Figure 2 shows the subgroup division of the team. The individual subgroups and corresponding responsibilities are as follows:

- **Aerodynamics and Stability & Control:** Carries out all analyses related to the flight performance of the aircraft. Analysis is conducted using software and traditional wind tunnel methods. Software used includes Athena Vortex Lattice (AVL) code, XFOIL, and XFLR5.
- **Configuration:** Maintains the virtual construction of the airplane using SolidWorks as the primary program to create a 3D model of the airplane and all corresponding components.
- **Flight Test Coordinator:** Plans and executes all tests that involve the complete airframe. Responsibilities include the use of RCATS, a data collection program, to collect test flight data.
- **Fuselage & Landing Apparatus:** Sizes and constructs the landing surface and skids of the aircraft.
- **Manufacturing/Build:** Works closely with the Chief Engineer to oversee the manufacturing process. The Build Captain acts as lab manager and directs the construction of the aircraft.
- **Payloads:** Develops and integrates payload restraints and loading methods. The choice of the system suitcase is also this subgroup's responsibility.
- **Performance:** Is responsible for sizing the aircraft using the team's multidisciplinary optimization (MDO) tool, PlaneSizer. This subgroup is the focal point of the iterative design process and incorporated designs from all other subgroups.
- **Propulsion:** Conducts the sizing, prediction, optimization, and analysis of the electric motors and batteries.
- **Structures:** Sizes, optimizes, and analyzes all critical load bearing members of the airframe.

2.3 Scheduling and Budget Control

The Program Manager is responsible for maintaining and updating the master schedule for the project. The master schedule portrays planned and actual execution of all team functions throughout the school year, as shown in Figure 3. The team enjoys substantial financial and leadership support from the Viterbi School of Engineering Office of Student Affairs as well as donations from corporate sponsors. Their combined generosity ensures that the team has sufficient resources to participate in the DBF competition.

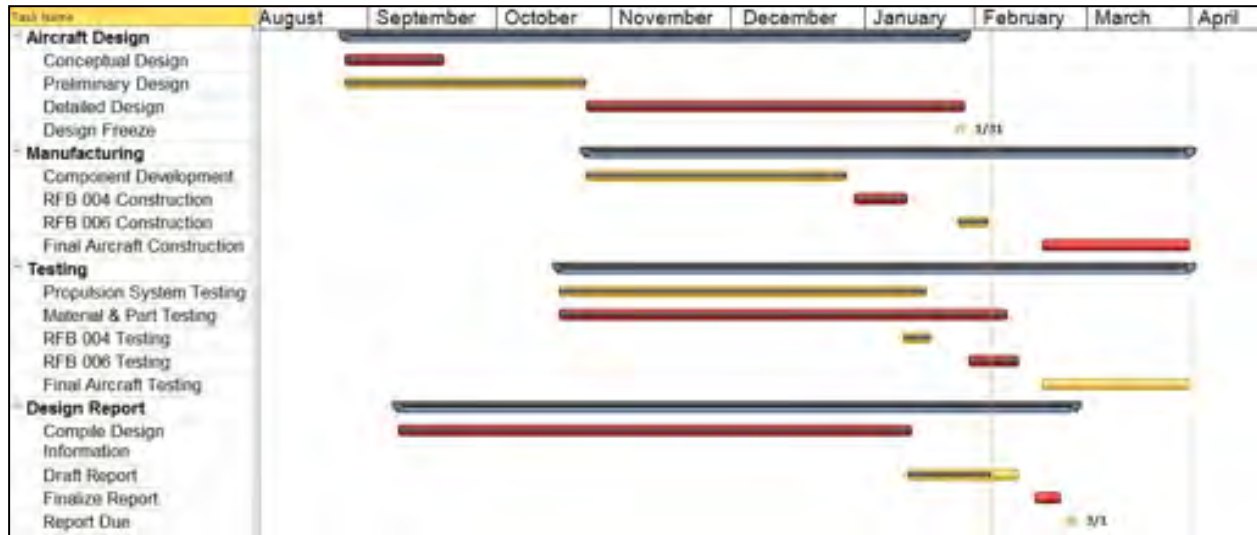


Figure 3: Master schedule for the USC AeroDesign Team.

3. Conceptual Design

The mission requirements and design constraints were taken as the beginning point of conceptual design for the team. The conceptual design process selected a configuration that provided the best total score of all missions. The initial configuration was selected through figure of merit analysis; this was followed by subsequent selection of subsystems. The downselect methodology is shown in Figure 4.

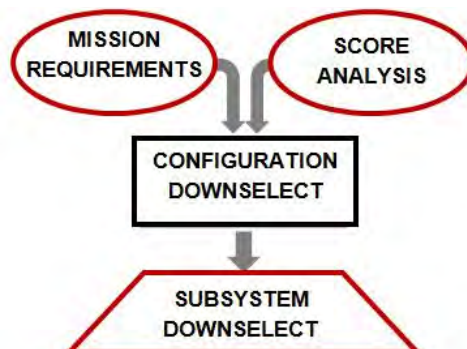


Figure 4: Methodology for conceptual aircraft selection

3.1 Evolution of Design

This year the competition rules underwent a few changes, which inevitably resulted in evolution of design of the team's conceptual aircraft. The initial set of rules did not include any dependence on aircraft weight; thus the initial score analysis produced a primitive plane that was designed, built, and tested in the second week of the school semester. Then, a first set of rule changes incorporated a factor of aircraft empty weight, which brought forth a new score analysis and induced changes to the original conceptual design. Then, a second set of rule changes altered the effect of the empty aircraft weight on the score, calling for another score analysis and subsequent evolutionary changes. The morphology of the conceptual aircraft is shown in Figure 5 below with indications of rule change occurrences. The Preliminary Design and Detailed Design Phase aircraft in following sections are RFB 004 and RFB 006, respectively. Iterations RFB 001, 003, 004, and 006 are pictured below in Figure 6.

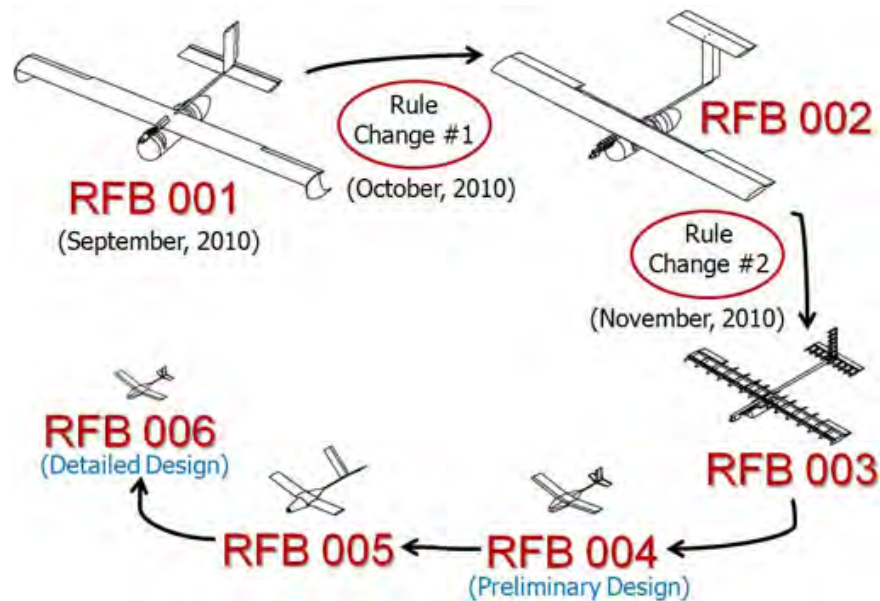


Figure 5: Morphological chart of aircraft iterations. All images are to scale.



Figure 6: RFB iterations (right to left): RFB 001, 003, 004, and 006.

3.2 Mission Requirements

The 2011 DBF Competition is comprised of three flying missions, including one speed mission and two payload-carrying missions. Each mission requires the aircraft to be hand launched and capable of flying the laps illustrated in Figure 7.

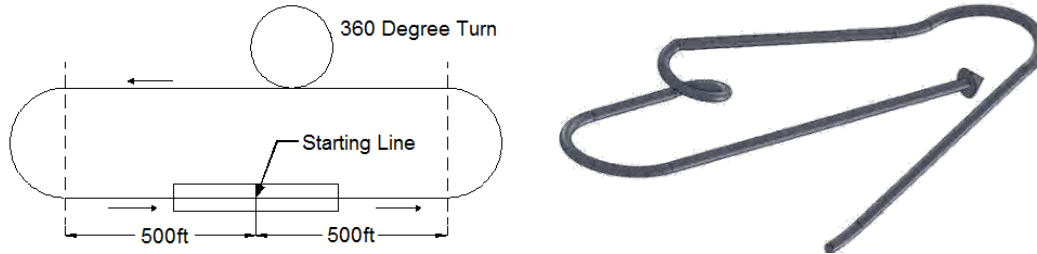


Figure 7: AIAA Design Build Fly competition laps in their 2-dimensional layout (left) and simulated 3-dimensional path (right).

Additionally, contest-specified mission and vehicle requirements are as follows¹:

- Maximum ¾ lb. battery weight, using only nickel cadmium (NiCad) or nickel metal hydride (NiMH).
- 20 Amp (slow-blow fuse) current limit.
- The complete flight system must fit inside a commercially available carry-on suitcase, the size of which cannot exceed 45 linear inches (the sum of length, width, height of the suitcase cannot exceed 45 in). No single dimension can exceed 22 in.
- A steel bar with minimum dimensions of 3 in by 4 in serves as the simulated ammunition in Mission 2 and must be carried inside of the aircraft outer mold lines; the steel bar must be supplied by the team.
- Standard golf balls serve as the simulated medical supplies in Mission 3 and must be carried inside of the aircraft outer mold lines; the golf balls will be provided at the contest.

3.2.1 Mission 1: Dash to Critical Target

This mission is purely a speed mission and does not include a payload. The aircraft has a time constraint of 4 minutes to complete as many competition laps as possible. The flight time begins when the aircraft leaves the launcher's hand; only complete laps, not partial laps, will be counted in the total lap count. The Mission 1 score, $M1$, is based on the number of laps flown by USC, N , and the maximum number of laps flown by any team in this mission, N_{max} , as shown in Equation 1:

$$M1 = \frac{N}{N_{max}} \quad (1)$$

3.2.2 Mission 2: Ammo Re-Supply

This mission requires the aircraft to complete three competition laps while internally carrying the steel bar. There is no time constraint for this mission. The Mission 2 score, $M2$, is determined by the fraction between the payload weight, W_{pay} , and flight weight, W_{flight} (where $W_{flight} = W_{pay} + RAC$); $M2$ is given by Equation 2:



$$M2 = 3 \cdot \frac{W_{pay}}{W_{flight}} \quad (2)$$

3.2.3 Mission 3: Medical Supply

This mission also requires the airplane to fly three competition laps without time constraint. The airplane must carry an internal payload of golf balls; the number of golf balls carried is chosen by the individual teams. The Mission 3 score, $M3$, depends on the number of golf balls carried by USC, B , and the maximum number of golf balls carried by any team in this mission, B_{max} , as shown in Equation 3:

$$M3 = 2 \cdot \frac{B}{B_{max}} \quad (3)$$

3.2.4 Total Score

The three mission flight scores, $M1$, $M2$, and $M3$, make up the Total Flight Score (TFS), as show in Equation 4:

$$TotalFlightScore = M1 + M2 + M3, \quad (4)$$

The 2011 DBF Competition score takes into account the Written Report Score, Total Flight Score and RAC, given by Equation 5:

$$SCORE = \frac{(WrittenReportScore) \cdot (TotalFlightScore)}{\sqrt{RAC}} \quad (5)$$

3.3 Design Requirements

The requirements for the different missions are determined by the most sensitive scoring parameters which are the following:

- Mission 1: Dash to Critical Target – Maximize the number of laps flown
- Mission 2: Ammo Re-Supply – Maximize steel bar weight while minimizing RAC
- Mission 3: Medical Supply – Maximize the number of golf balls carried
- Overall Competition – Minimize RAC

3.4 Score Analysis

3.4.1 Rules Interpretations

To maximize the individual mission scores, the first three design requirements stated in § 3.2 demands an aircraft design that is fast with powerful propulsion, able to withstand large loading, and large in volume, respectively. However, simultaneously fulfilling the fourth requirement of minimizing RAC becomes difficult as all of the aforementioned design characteristics adversely affect RAC. An aircraft able to obtain a maximum score for each *individual* mission is possible to design, but such an aircraft will most likely obtain a low Total Flight Score. Therefore, sacrifices to individual mission scores are necessary to achieve the best possible Total Flight Score.



3.4.2 Sensitivity Analysis

To determine which of the mission and system parameters most influential to score, a score sensitivity analysis is conducted to compare them to one another as well as the overall score. The equation for flight score that incorporates all key parameters of the aircraft is shown in Equation 6 below:

$$\tau = \frac{\left(\frac{N}{N_{\max}}\right) + 3\left(\frac{W_{\text{pay}}}{W_{\text{pay}} + RAC}\right) + 2\left(\frac{B}{B_{\max}}\right)}{\sqrt{RAC}} \quad (6)$$

Since USC's Total Score, τ , is affected by competing team's parameters, the maximum numbers of laps and carried golf balls are assumed to be following:

- Competitor N_{\max} : 9 laps
- Competitor B_{\max} : 42 golf balls

The USC parameter values for score sensitivity were initially assumed to be the following:

- $N = 6$ laps
- $W_{\text{pay}} = 1.2$ lbs (Payload Fraction, $W_{\text{pay}} / (W_{\text{pay}} + RAC) = 0.7$)
- $B = 10$ balls
- $RAC = 0.5$ lbs

The sensitivity analysis was determined by taking the partial derivative of τ in the Eq. (6) with respect to each of the four independent variables N , W_{pay} , B , and RAC , and plotting the percentage change on Total Score. Thus the sensitivity of each parameter is determined while the remaining three are held constant, and the Total Score is plotted against the corresponding varying parameter. The initial score sensitivity

results are shown in Figure 8.

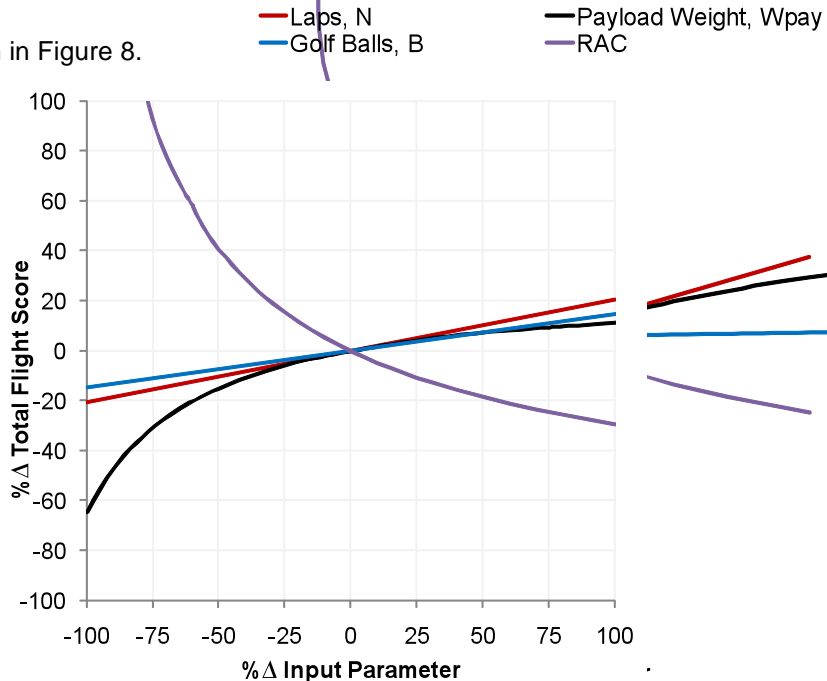


Figure 8: Preliminary score sensitivity.



The results of the sensitivity study indicate that RAC is the most dominant of the four tested parameters. Increasing the TFS is strongly dependent on reducing RAC. A 50% reduction in RAC increases the TFS by 40%, while a 50% increase of N , B , or W_{pay} increases TFS by less than 10%. A similar plot was obtained for other values of the assumed competitors' parameters N_{max} and B_{max} . Upon examining the remaining three parameters N , W_{pay} , and B , it can be determined that aiming for a high number of golf balls would inherently entail a large internal volume and added fuselage structure, which hurts the RAC and Total Score. Therefore the number of golf balls carried is first to be sacrificed for the gain of a smaller RAC. The secondary score analysis assumes that the team would carry one golf ball in order to minimize the overall geometry and weight of the aircraft. This secondary score analysis keeps N at 6 laps and RAC at 0.5lb and compares different nominal values of W_{pay} and payload fraction. The secondary score sensitivity is shown below in Figure 9:

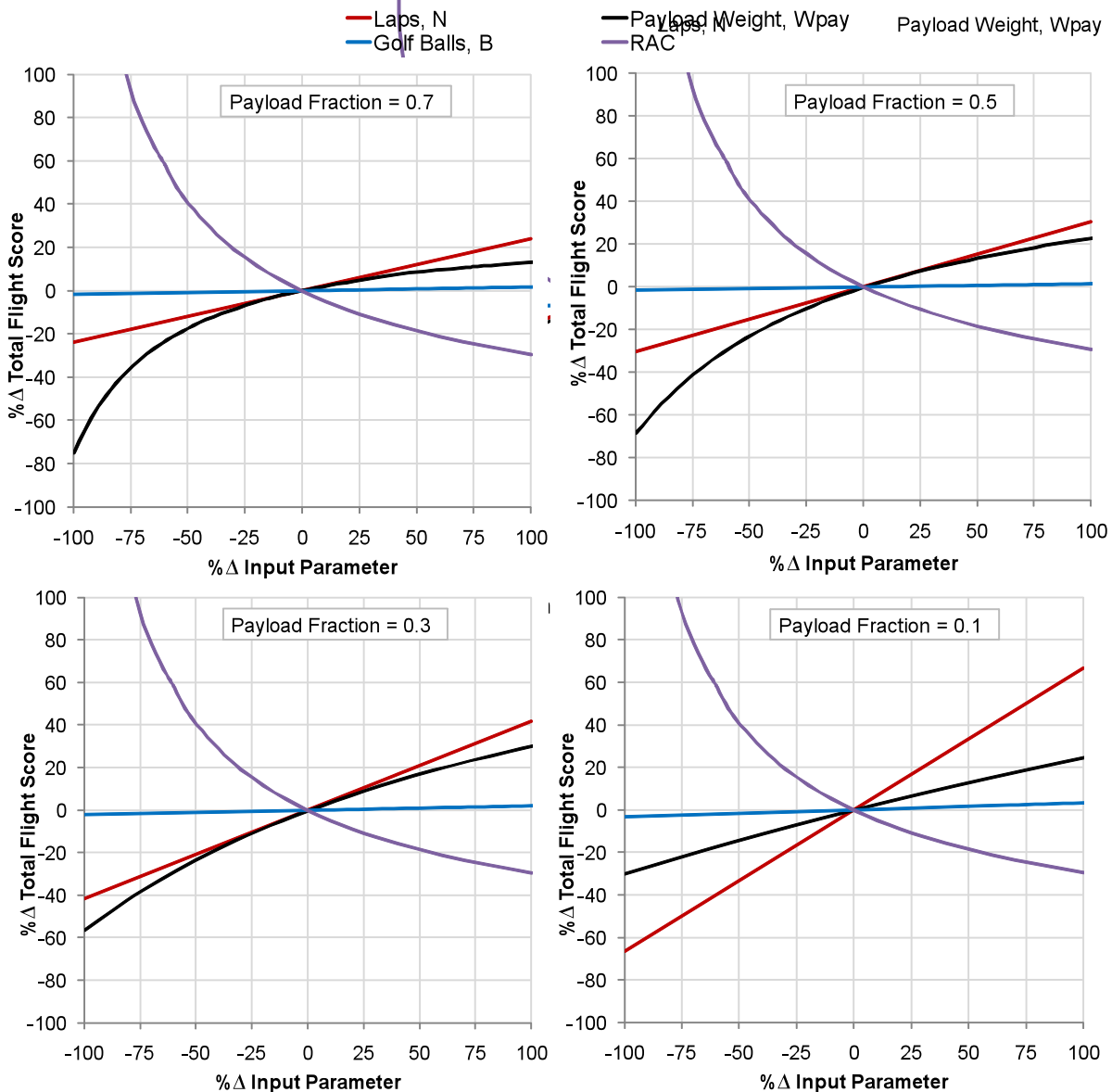


Figure 9: Secondary score sensitivity analysis: W_{pay} and payload fraction evaluation.



This score analysis depicts that decreasing the nominal value of the payload fraction (decreasing W_{pay}) results in an increased slope for N (the number of laps flown), creating an increased sensitivity on flight score due to number of laps flown in Mission 1. Therefore an adequate payload fraction is still needed to maintain a competitive score. A payload fraction of 0.5 was chosen as a design target and deemed appropriate since USC has successfully built and flown planes with similar payload fractions in past competitions.

3.4.3 Score Analysis Conclusions

The sensitivity analysis provides the following conclusions:

- The most important design criterion is building the lowest empty aircraft weight possible (smallest possible RAC).
- Mission 3 is the least important of the three missions; the aircraft does not necessarily need to carry as many balls as possible. The competition aircraft will be therefore be designed to carry one golf ball.
- Mission 1 has more effect on Total Flight Score than Mission 2 has, but it is important to still carry an adequate payload weight. The competition aircraft will hence be designed to fly as many laps as possible and carry a payload fraction of 0.5.

Sensitivity analysis examines only *ideal* situations in which no other parameter varies. In reality, varying one parameter will affect others. For example, flying a substantially higher number of laps in Mission 1 will inherently require a correspondingly larger propulsion system, increasing RAC. Likewise, carrying a higher W_{pay} will result in an increased wing area to maintain a sustainable wing loading that would inherently require added material and structure, also increasing RAC. Therefore, the score sensitivities lay out a simplified baseline – a starting point – that can then be optimized. However idealized the study may be, the RAC parameter stands out as the dominant factor in the total score and the airplane's main design parameter.

3.5 Conceptual Design Selection Process

3.5.1 Figures of Merit

The downselect used Figures of Merit (FOM) that were based upon the team's past experience and current manufacturing capabilities as well as adjusted for the 2011 competition rules. The FOM's are the following:

- **Weight (RAC)** – The aircraft's empty weight is the most crucial component to the total score.
- **Drag** – The drag of the aircraft heavily affects both endurance and speed.
 - **Aerodynamic Efficiency, L/D** – The aircraft must fly for 4 minutes in Mission 1 in addition to carrying as much payload weight in Mission 2, thereby requiring adequate endurance.
 - **Wetted Area, S_{wet}** – Minimizing wetted area will result in less drag, and therefore higher top speed to maximize number of laps in Mission 1.



- **Wing Loading** – The aircraft should have a wing loading that allows for both endurance and speed in Mission 1 and pure endurance for Missions 2 and 3.
- **C_{D0}** – The aircraft should have as small of parasite drag as possible to reduce the overall drag of the aircraft, which affects endurance and speed.
- **Stability and Control** – The aircraft must be stable and easily controllable so the pilot can effectively navigate the course and respond to flight disturbances.
- **Design and Manufacturability** – The design should be realistically manufacturable given internal structure requirements, estimated size, type of fabrication, and the team's experience in the required construction processes.
- **Assembly** – The aircraft must be assembled by one operator within five minutes.

3.5.2 Configurations

The team considered several aircraft configuration choices. Each configuration was analyzed based on the FOMs in § 3.4.1. The configuration candidates and respective consideration reasons were the following:

- **Monoplane** – The concept is conventional and has experienced several successful competition results from past years. The monoplane was chosen as the baseline configuration against which all the other designs were compared.
- **Biplane** – This configuration allows for a reduced wing span for a given wing area, which affects the wing loading. This configuration is also more complex to design and manufacture, and it has more joints, which adds weight.
- **Canard** – This configuration's horizontal stabilizer contributes to the overall lift of the aircraft, but the associated high trim drag does not make it ideal for a speed-based mission.
- **Blended Wing Body** – This configuration combines the fuselage with the lifting surfaces. It eliminates the tail and reduces the overall S_{wet} , giving a high L/D .
- **Joined Wing** – This configuration sweeps the main wing aft, joining it to a forward-swept aft-located wing. Control surfaces placed on the aft wing eliminates the need for a tail to stabilize and control the plane. This configuration is more complicated to design and manufacture, and requires more joints, which adds weight.
- **Lifting Body** – This configuration has a large fuselage volume that contributes to the overall aircraft lift, giving it high L/D and larger internal volume.
- **Tandem Wing** – This configuration consists of two wings aligned in a staggered arrangement. With appropriate wing separation from the CG location, a horizontal tail can be eliminated; however, this configuration is inherently heavier than the baseline.
- **Tandem Body** – This configuration consists of two fuselages joined by a wing and horizontal stabilizer. This configuration is more complex to design and manufacture and inherently much heavier than the baseline.



3.5.3 Configuration Downselect

Traditionally, the team uses Pugh's Method² for the configuration downselect, in which the Figures of Merit (FOM's) are given respective weightings according to their importance in the score, and each configuration is assigned a value -1, 0, or 1, signifying worse than baseline, same as baseline, or better than baseline. The baseline is a monoplane, which has the value of 0 for all FOMs. Pugh's Method is shown below in Table 1.

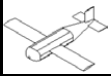
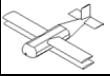
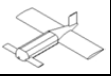
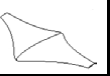
| | |  |  |  |  |  |  |  |  |
|-----------------------|-----------|---|---|---|---|--|---|---|---|
| Figures of Merit | Weight | Monoplane | Biplane | Canard | BWB | Joined Wing | Lifting Body | Tandem Wing | Tandem Body |
| Weight (RAC) | 10 | 0 | -1 | 0 | 0 | -1 | 0 | -1 | -1 |
| Drag | 8 | | | | | | | | |
| L/D (Endurance) | 3 | 0 | 0 | 0 | 1 | -1 | 1 | -1 | 0 |
| Swet (Speed) | 2 | 0 | -1 | 0 | 1 | -1 | -1 | -1 | -1 |
| Wing Loading | 2 | 0 | -1 | 0 | 1 | 0 | 0 | -1 | -1 |
| C_{D0} | 1 | 0 | -1 | -1 | -1 | -1 | -1 | -1 | -1 |
| Stability and Control | 4 | 0 | -1 | -1 | -1 | -1 | 0 | -1 | -1 |
| Design & Manufacture | 2 | 0 | 0 | -1 | -1 | 0 | 0 | 0 | 0 |
| Assembly | 1 | 0 | 0 | 0 | -1 | -1 | 0 | 0 | 0 |
| Total | 13 | 0 | -19 | -7 | -1 | -21 | 0 | -22 | -19 |

Table 1: Initial configuration downselect.

This initial downselect produced three winners: monoplane, BWB, and lifting body. This initial result suggested that the ultimate design would most likely be a blend of the three. However, to better extract a starting configuration, a secondary downselect was done using the Pair Wise Comparison Method. In this method, the FOM's as stated in § 3.4.2 are first scored against each other in a square Figures of Merit Matrix, as shown in Table 2. The FOMs along the left column are compared to those along the top row; each FOM is delegated a number out of 5 in terms of its importance to its competitor, with a score of 5 being the most important. If the FOM is compared to itself, the entry receives a 0. The entries reflected across the main diagonal must add up to 5. Then the total weighting of calculated by normalizing each FOM's total importance score out of 1.

| Figures of Merit | Weight | Drag | Stability & Control | Design / Manufacture | Assembly | Total | Score Factor |
|---------------------|--------|------|---------------------|----------------------|----------|-----------|--------------|
| Weight | 0 | 3 | 4 | 4 | 4 | 15 | 0.30 |
| Drag | 2 | 0 | 3 | 4 | 4 | 13 | 0.26 |
| Stability & Control | 1 | 2 | 0 | 4 | 4 | 11 | 0.22 |
| Design/Manufact. | 1 | 1 | 1 | 0 | 4 | 7 | 0.14 |
| Assembly | 1 | 1 | 1 | 1 | 0 | 4 | 0.08 |
| | | | | | | 50 | 1.00 |

Table 2: Figures of Merit matrix.

Next, in the Evaluation Matrix, each configuration is given a score 1 – 5 for each FOM. A score of 3 is average performance, a score of 5 is extremely high performance, and a score of 1 is extremely low performance. The Evaluation Matrix is shown in Table 3:

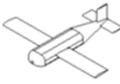
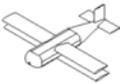
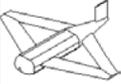
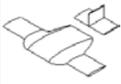
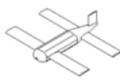
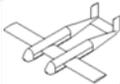
| Aircraft Configuration |  |  |  |  |  |  |  |  |
|---------------------------|---|---|---|---|--|---|---|---|
| Evaluation | Monoplane | Biplane | Canard | BWB | Joined Wing | Lifting Body | Tandem Wing | Tandem Body |
| Weight | 3 | 2 | 3 | 4 | 1 | 3 | 1 | 1 |
| Drag | 3 | 2 | 3 | 4 | 2 | 3 | 2 | 1 |
| Stability & Control | 4 | 3 | 2 | 2 | 1 | 3 | 2 | 2 |
| Design/Manufact. Assembly | 5 | 4 | 2 | 1 | 1 | 4 | 2 | 2 |
| Assembly | 3 | 2 | 3 | 3 | 1 | 3 | 2 | 1 |

Table 3: Evaluation matrix.

Finally, in the Weighted Scores matrix, the individual entries in the Evaluation matrix are multiplied by their corresponding Score Factors from the first Figures of Merit Matrix (Table 2), and the total score is calculated. The Weighted Scores matrix is shown below in Table 4. The Pair Wise Comparison Matrix Method extracted the monoplane as the winner and therefore starting configuration.

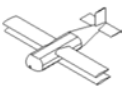
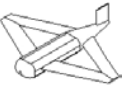
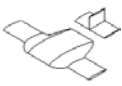
| Aircraft Configuration |  |  |  |  |  |  |  |  |
|---------------------------|--|--|--|--|---|--|--|--|
| Weighted Scores | Monoplane | Biplane | Canard | BWB | Joined Wing | Lifting Body | Tandem Wing | Tandem Body |
| Weight | 0.90 | 0.60 | 0.90 | 1.20 | 0.30 | 0.90 | 0.30 | 0.30 |
| Drag | 0.78 | 0.52 | 0.78 | 1.04 | 0.52 | 0.78 | 0.52 | 0.26 |
| Stability & Control | 0.88 | 0.66 | 0.44 | 0.44 | 0.22 | 0.66 | 0.44 | 0.44 |
| Design/Manufact. Assembly | 0.70 | 0.56 | 0.28 | 0.14 | 0.14 | 0.56 | 0.28 | 0.28 |
| Assembly | 0.24 | 0.16 | 0.24 | 0.24 | 0.08 | 0.24 | 0.16 | 0.08 |
| Total | 3.50 | 2.50 | 2.64 | 3.06 | 1.26 | 3.14 | 1.70 | 1.36 |

Table 4: Weighted Scores Matrix.

3.6 Systems Downselects

Following the decision to pursue a monoplane, analyses and selections for each major subcomponent of the airplane were performed. As with the aircraft configuration, downselects were used to select optimum system designs. While the ternary rating system of the Pair Wise Comparison Method still applied, there was no baseline configuration against which to rate each option. Instead, Pugh's Method for advanced decision matrices was used, where the sum of the weights is one.

3.6.1 Propulsion

Various motor placements and configurations were studied to identify the most efficient and least obstructive setup to drive the system payloads. While the competition permits multi-motor configurations, practicality, RAC, and past experience led to considerations of only single and twin motor configurations.

- **Tractor:** The propulsion system is located near the front of the airplane where the propeller sees undisturbed air, resulting in higher efficiency.
- **Pusher:** Mounted aft of the fuselage, the motor and propeller push the airplane with less efficiency than the tractor configuration. Propeller ground clearance may be a concern for upon landing. In addition, a pusher propeller impairs the person hand launching the aircraft.
- **Twin:** Two motors are used to produce the same thrust as one larger motor at the expense of additional weight.

Table 5 shows the propulsion configuration downselect for these three propulsion configurations. The tractor is seen to be the best for weight and efficiency.

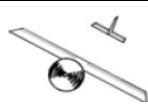
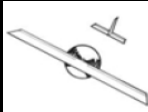
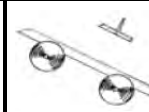
| | |  |  |  |
|----------------------|-------------|---|--|---|
| Figures of Merit | Weight | Tractor | Pusher | Twin-Prop |
| Weight (RAC) | 0.45 | 1 | 0 | -1 |
| Efficiency | 0.35 | 1 | -1 | 0 |
| Payload Interference | 0.20 | -1 | 0 | 1 |
| Total | 1.00 | 0.60 | -0.35 | -0.25 |

Table 5: Propulsion configuration downselect.

3.6.2 Empennage

The empennage provides stability and control for the aircraft throughout the entire flight. Key factors for empennage selection included minimizing RAC and drag while providing necessary stability and control at lower Reynolds numbers (below 200,000). The estimated Reynolds number for the competition plane, which is particularly discussed in § 4.4.1, is around 100,000. The tail designs that were considered were the following:

- **Conventional** – This configuration is simple to design and implement, allowing for a minimized RAC while providing necessary stability and control requirements. The interference of the fuselage with the tail surfaces can increase the conventional tail's effective aspect ratio³.
- **T-Tail** – This configuration is similar to the conventional tail except that the horizontal stabilizer is placed on top of the vertical stabilizer. This type of tail is effective at high angles of attack. Potential issues with this design include higher vertical fin loads, potential flutter difficulties, and deep-stall problems³. The required additional structure gives rise to weight concerns.
- **V-Tail** – Two surfaces form a “V” provide both elevator and rudder controls as well as assist in decreasing wetted area with the elimination of one tail surface. This configuration has increased ground clearance and reduced number of surface intersections, which helps in weight savings. However, the mixed controls sometimes exhibit reduced control authority in yaw and pitch maneuvers³.
- **Inverted V-Tail** – This design is similar to the V-Tail but inverted. While effective at high angles of attack, this configuration faces ground rotation issues when used with a single tail boom.

- **U-Tail** – This configuration consists of two vertical stabilizers mounted on either end of a horizontal. This configuration provides vertical clearance benefits but adds extra weight complexity.

Table 6 shows the empennage configuration downselect and illustrates the optimum configuration of the conventional tail. This choice is simple to design and build, and has minimum weight and drag penalties.

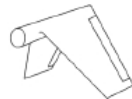
| | |  |  |  |  |  |
|-----------------------|-------------|---|---|--|---|---|
| Figures of Merit | Weight | Conventional | T-Tail | V-Tail | Inverted V | U-Tail |
| Weight (RAC) | 0.35 | 1 | 0 | 1 | -1 | -1 |
| Stability and Control | 0.25 | 1 | 1 | -1 | -1 | 1 |
| Drag | 0.20 | 0 | 0 | 1 | 0 | 0 |
| Design & Manufacture | 0.10 | 1 | 0 | 0 | -1 | 0 |
| Assembly | 0.10 | 0 | -1 | 0 | 0 | 1 |
| Total | 1.00 | 0.70 | 0.15 | 0.30 | -0.70 | 0.00 |

Table 6: Empennage configuration downselect.

3.7 Conclusion

A series of configuration downselects and FOM decision matrices analyzed several configurations and subsystems. A wing-body configuration was chosen from a list of configurations analyzed in two different FOM-based downselects that placed heavy emphasis on weight (RAC). A monoplane was chosen as the optimum wing-body configuration over several other non-conventional choices. A tractor motor setup was chosen for the optimum propulsion configuration, and a conventional tail was chosen as the optimum tail configuration to meet stability and control requirements.

4. Preliminary Design

The preliminary design phase optimized the configuration selected in the conceptual design phase (see § 3.4 and § 3.5). From the score sensitivity, designing and building the lightest possible aircraft was the main focus. The preliminary design phase aircraft is henceforth referred to as RFB 004.

4.1 Critical Design Parameters

4.1.1 Aerodynamic Critical Parameters

- **Airfoil:** Careful selection of the airfoil is critical for aerodynamic performance, especially at a low Reynolds number range. The airfoil should be designed with low drag and with safe stall characteristics, with no hysteresis or sharp drop near stall conditions. The airfoil should also lend itself to manufacturing at a small scale by having a large thickness-to-chord ratio (t/c) and a generous leading edge radius.



- **Wing Chord:** The wing chord sets the wings' Reynolds number in flight. Low Reynolds number can lead to laminar separation. Larger wing chords were selected to maintain a higher Reynolds number (higher than the critical Reynolds number of 100,000).
- **Wing Span:** Wing span is vital to both aerodynamic performance in terms of an adequate aspect ratio (AR), and also in terms of RAC, as a decrease in wing span and number of joints greatly decreases RAC, which in turn, increases the score.

4.1.2 *Stability and Control Critical Parameters*

- **Static Margin:** The static margin (SM) is important in preliminary design since it determines tail area. To minimize pitch sensitivity SM may not be less than 5% of the Mean Aerodynamic Chord (MAC). To ensure the elevator does not saturate, SM should be less than 40% MAC and require no more than 20° of elevator deflection to stall the wing.
- **Control Surface Location and Sizing:** Control surface deflections should not exceed 20° to avoid separation drag and preserve linear control⁵. Hinge chord fraction should be selected to minimize torque, thus reducing servo weight. Control surface area must be adequate for longitudinal and lateral control.

4.1.3 *Propulsion Critical Parameters*

- **Motor:** Aircraft weight and required power affect motor selection. AIAA DBF contest rules state that only off-the-shelf, unmodified brushless or brushed electric motors are allowed and motors cannot be changed between missions¹. The motor selected must be light to minimize RAC while still having enough power to complete speed and heavy lift missions.
- **Batteries:** DBF rules limit battery chemistry to nickel cadmium (NiCad) or nickel metal hydride (NiMH)¹. Batteries can be changed for different missions, but RAC is based on the heaviest pack used for any mission¹. The most demanding propulsion requirements are the four-minute speed mission (Mission 1) and the heavy lift mission (Mission 2). For small batteries, it's especially important to test the batteries and audit the manufacturers' specifications.
- **Propeller:** The choice of propeller affects current draw and power available. While robust propellers are ideal, more lightweight propellers will benefit RAC. Propeller performance characteristics (thrust, torque, power coefficients) are obtained from previous USC test results and ongoing static and wind tunnel testing.

4.1.4 *Structures Critical Parameters*

- **Material Selection:** The key characteristic for wing, tail and fuselage material selection is specific strength. It's important to acknowledge the gauge limit based on available materials.
- **Construction Techniques:** The construction techniques must provide adequate and durable support, while reducing weight. Dimensional accuracy, repeatability, and team experience are also important considerations, especially at the small scale of the RFB 004.

4.2 Design and Analysis Methodology

4.2.1 Multidisciplinary Optimization

This year, a multidisciplinary optimization (MDO) code with a new mission simulation package was developed from the ground up using MATLAB. This package tests an arbitrary design in the three competition missions with score as the final output. Using this mission simulation tool, trade studies have been developed to output the score as a function of different design parameters. For an individual trade study, typically a single parameter is perturbed from the current baseline configuration. The results of each trade study are then fed back into the baseline configuration for further analysis. A diagram of this process is shown as Figure 10.

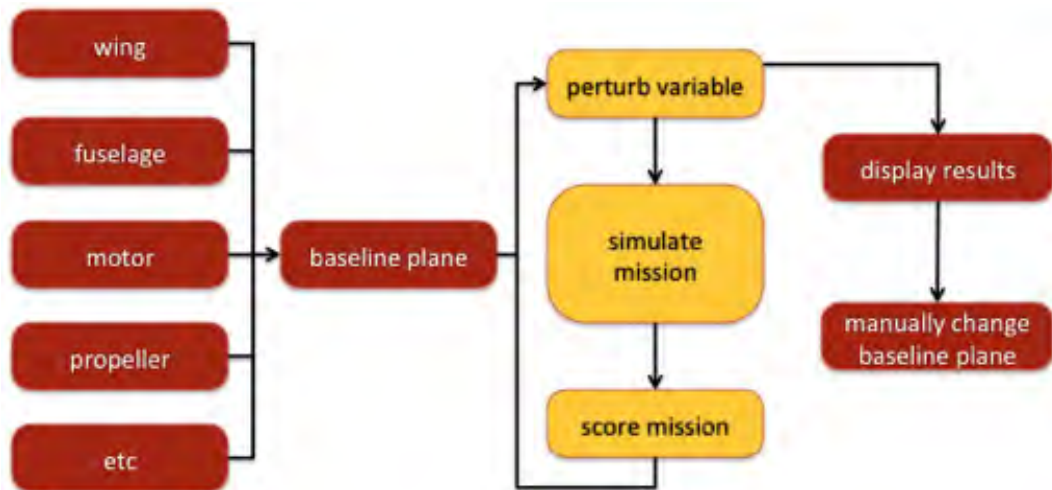


Figure 10: Flowchart for a single iteration in the global MDO process.

4.2.2 Mission Model

The most important part of the optimization process is mission simulation. The mission simulation assumes a constant throttle and defines a maximum load factor for turns. Altitude is reckoned relative to the “Red deck” which is the minimum safe flying height above the ground, and Δh is the altitude loss during turns. Starting from the bottom, reference planes are shown for the red deck, Δh , and $2\Delta h$. Other mission inputs include maximum elapsed time (pertaining to Mission 1), launch (throw) velocity, and red deck. With these inputs and the average wind conditions for this year’s competition flying field, a mission is simulated as best as possible with the given plane configuration.

A rough outline of the mission simulation code is shown in Figure 11. Assertion statements are used throughout the program to ensure conditions for viable flight are met. When an assertion fails, the mission simulation is aborted, and the offending assert-statement is reported to the user.

The first parameter that is calculated is the launch velocity followed by the corresponding maximum lift coefficient, C_{Lmax} , for that velocity. This lift coefficient, C_L , is calculated from the assumed airplane geometry, selected airfoil and launch Reynolds number. The program then asserts that the C_L required for launch is less than C_{Lmax} . Next, the parasite drag coefficient, C_{D0} , of the entire airplane is calculated via a drag build up that includes each component of the plane. The C_{D0} of the airfoil is again calculated

from the airfoil's drag polar for the specific C_L required at cruise. Next, the program iterates to find the most likely cruise velocity, V_{cruise} . Propulsion and drag calculations occur until the drag is equal to the thrust at the set cruise throttle. Within this step, the program iterates again to find the current, I_{cruise} , and the power required in the electrical system for a given velocity. Once I_{cruise} and V_{cruise} are calculated, the turn is simulated. First the drag is calculated and the altitude loss is then found from the rate of sink. Combined with the red deck input, this gives the altitude increase required from the point of launch. The climb angle can then be calculated from this altitude increase and the length of half of a lap (500 ft). From the drag and thrust available at takeoff, the program can assert that the required rate of climb, $R/C_{required}$, is less than or equal to the available rate of climb, $R/C_{available}$. Next, the distance and elapsed time per lap is calculated, including the extra distance due to the change in altitude drop around the course. Multiplying the electrical power required (from earlier) with the elapsed time gives the energy required per lap. Finally, the number of laps and total elapsed time can be calculated by completing as many laps as possible before the batteries are depleted. The program then outputs either an error or the number of laps and elapsed time.

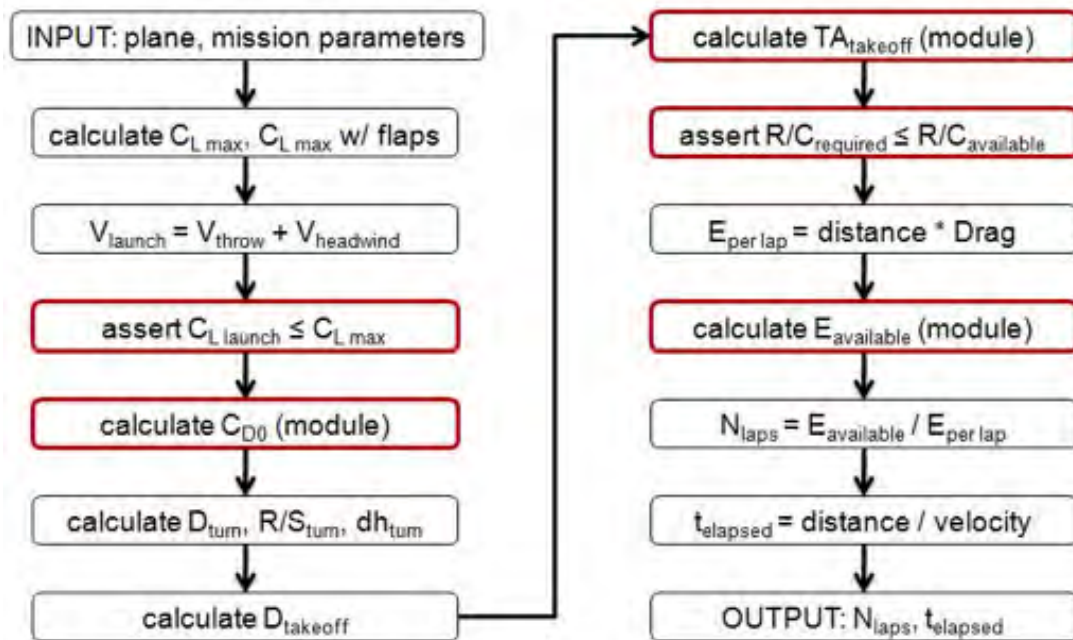


Figure 11: MDO mission simulation flowchart.

4.2.3 Other Analytical Tools

Athena Vortex Lattice (AVL) provides an aerodynamic analysis of inviscid aircraft of arbitrary configuration⁶. The program simulates steady flight and uses an extend vortex lattice model for lifting surfaces in conjunction with a slender-body model for fuselages. The team uses a variety of AVL's features to perform three-dimensional aircraft configuration analysis.

XFOIL is a program which allows for the design and analysis of subsonic, two-dimensional airfoils⁷. The program can calculate the lift and drag characteristics of an airfoil by analyzing the pressure



distribution. XFOIL also allows the modification of airfoil parameters, such as camber, to achieve a more desirable result.

XFLR5 is an additional analysis tool for airfoils, wings, and planes that combines XFOIL's direct and inverse analysis powers with theoretically-based wing design capabilities⁸. Additionally, XFLR5 can hybridize airfoils operating at low Reynolds Numbers to create enhanced airfoils.

4.3 Performance Trade Studies & Optimization

4.3.1 Site Analysis

Weather conditions for April 15-17 in Tucson, AZ were analyzed using historical data from 2008-2010⁹. The wind data suggests a 10 mph minimum headwind can be claimed in the mission model. The Tucson temperature data provided altitude and density estimates for the MDO. Historical data are shown in Figure 12.

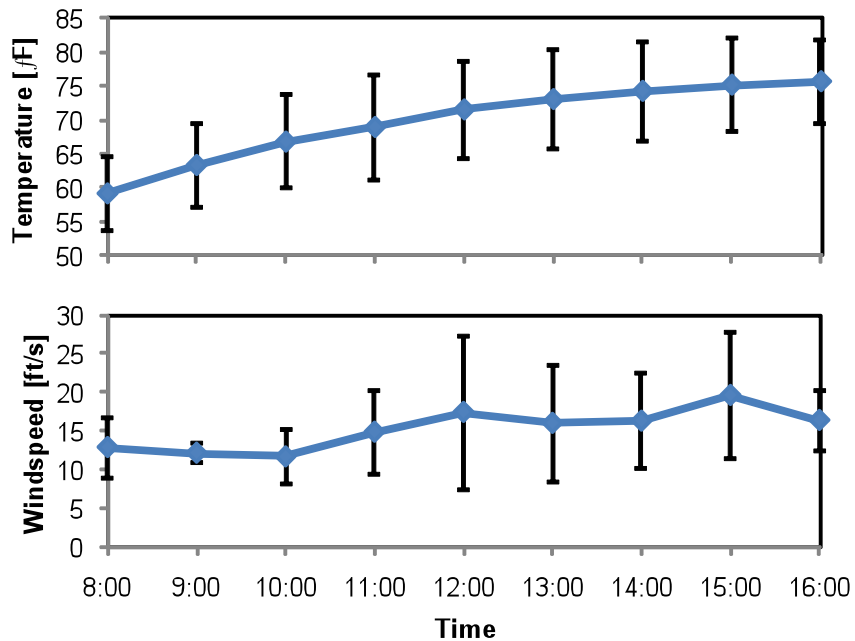


Figure 12: Weather trends for Tucson, AZ averaged over April 15-17, 2008-2010.

4.3.2 Trade Studies

One of the more important trade studies is shown as a carpet plot of score vs. wing geometry in Figure 13. A cliff occurs on the left boundary of the plot, where the wing is unable to fly the heavy payload of Mission 2 due to insufficient wing area. This trade study concludes that the highest scoring aircraft is one with a 20 in span, b , with a 50 in² surface area, S .

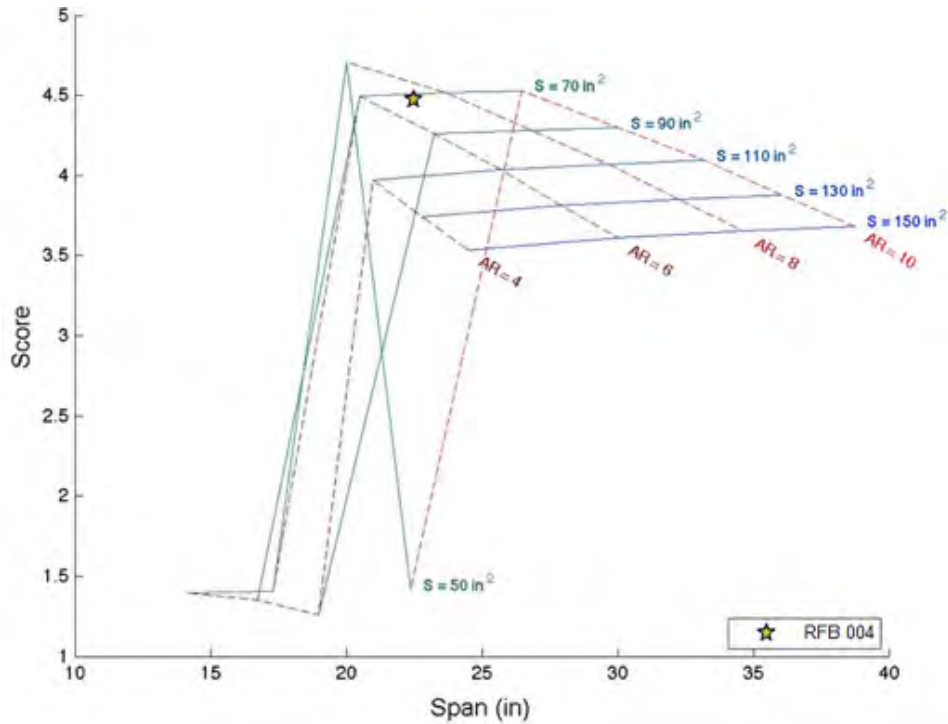


Figure 13: Carpet plot of wing geometry vs. score. Lines of constant AR and span are shown. The preliminary design phase, RFB 004, is indicated by the star.

4.4 Aerodynamics

4.4.1 Low Reynolds Number Aerodynamics

The score analysis detailed in § 3.3 led the team to design a substantially smaller aircraft than in previous years. The small aircraft size challenged the aerodynamics team to examine and design many different airfoils using XFOIL and XFLR5. The largest concern for the aerodynamics team was that the estimated Reynolds number of the preliminary aircraft was approximately 100,000. At this Reynolds number, viscous effects have a greater influence and can lead to laminar separation around the airfoil¹⁰. If an airfoil with an entirely laminar boundary layer separates it causes the wing to stall. This is likely to start at one wing tip and progress inboard, which leads to an uncontrollable roll.

Numerous measures can be implemented to prevent stall, such as leading edge cuffs on the wing tips, tripping the boundary layer to turbulent flow at a specific location on the chord or specifically designing an airfoil with favorable stall characteristics. The first two options forcibly transition the boundary layer from laminar to turbulent on the airfoil, which prevents the wing from stalling abruptly; however, those methods increase drag and are therefore considered as backup options if tip stall becomes a major problem. The third method—specifically designing an airfoil with favorable stall characteristics—was determined to be the ideal method by the aerodynamics team, as the lift and drag characteristics of the airfoil can be controlled in the design process.

4.4.2 Airfoil Optimization

The aerodynamics team designed airfoils specifically to have low drag and favorable stall characteristics using the direct and inverse airfoil design tools of XFOIL and XFLR5. After multiple design iterations of separate airfoils, three airfoils were selected for their superior performance parameters, such as c_{lmax} , low drag, and stall characteristics. These three airfoils were further compared to a flat plate and the LA203KB at the flight Reynolds number of 100,000. The flat plate was considered briefly because the low Reynolds numbers of the aircraft could dictate no advantage for a cambered airfoil, but was discarded quickly after determining it could not fly all the required missions. The LA203KB is a baseline airfoil used by the team in previous years, which is useful for comparison, but was not designed to fly at Reynolds numbers this low. The drag polars and lift curves for the five airfoils are shown in Figure 14 along with the required C_L values for each mission. The BA572LS was chosen as the optimum airfoil because of its low and consistent drag over a wide range of 2-dimensional (airfoil) lift coefficient, c_l , values and its favorable stall characteristics near its maximum 2-dimensional lift coefficient, c_{lmax} .

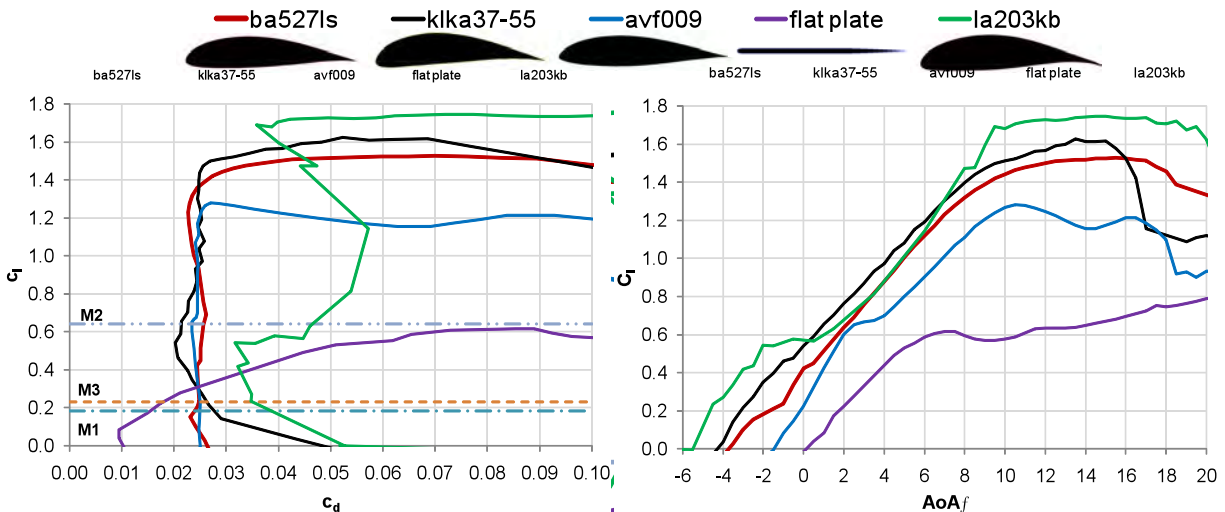
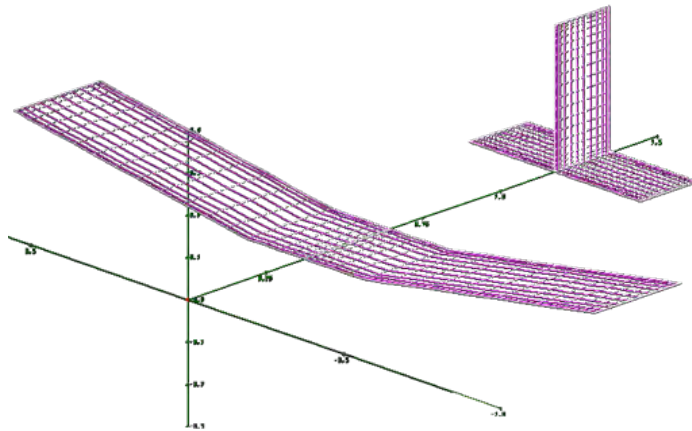


Figure 14: Drag polars and alpha lift curves for candidate airfoils.

4.4.3 Computational Flow Analysis

Athena Vortex Lattice (AVL), an inviscid flow solver program, was used for the flow analysis of the initial design. In AVL, the aircraft is modeled as a series of panels along the wing and tail surfaces, on which flow characteristics at each panel is calculated and compiled together to obtain a three-dimensional solution. Figure 15 shows the AVL geometry of the preliminary RFB 004 airplane without the fuselage and accompanying dimensions.



| Aircraft Geometry: RFB 004 | |
|------------------------------|-----------|
| Wing | |
| Span (in) | 22 |
| Chord (in) | 3.3 |
| Airfoil | BA527LS |
| Horizontal Stabilizer | |
| Span (in) | 6.6 |
| Chord (in) | 2.2 |
| Airfoil | NACA 0010 |
| Elevator | 30% |
| Vertical Stabilizer | |
| Span (in) | 4.2 |
| Chord (in) | 2.1 |
| Airfoil | NACA 0010 |
| Rudder | 30% |

Figure 15: AVL model of the RFB004 plane geometry (left) and geometric dimensions (right).

Using the AVL model, flight performance was evaluated at the different required values of C_L for each mission. Analysis was performed for Missions 1 and 2, as those missions had the greatest difference in flight conditions. Trefftz plots were used to examine the span wise load distribution to evaluate efficiency and trim deflections of the control surfaces. Figure 16 show the Trefftz plots for Missions 1 and 2, respectively.

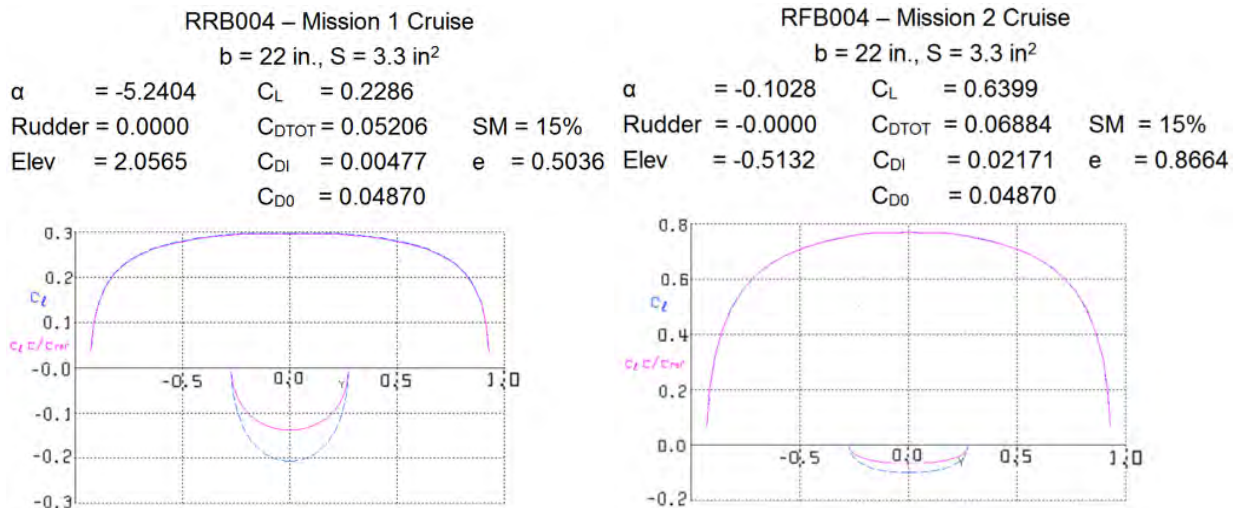


Figure 16: Mission 1 (left) and 2 (right) Trefftz plots showing the span wise load distribution along the wing and tail. Span wise units are feet.

Figure 16 displays that the wing is relatively lightly loaded. Lightly-loaded wings are not considered aerodynamically efficient, giving over to a low L/D (aerodynamic efficiency), as their span wise load distribution is not elliptical, as seen by the estimated Oswald efficiency factor of 0.504 for Mission 1. However, the low C_L required for Mission 1 makes the low efficiency factor negligible. Mission 2 has a much greater span wise loading, and in turn is more elliptical, which increases the efficiency factor of the wing to 0.866.

4.4.4 Lift and Drag Estimates

Initial lift and drag estimates for RFB 004 were calculated after selection of the airfoil and geometric dimensions. AVL was used to estimate the vortex drag on the wing and tail surfaces. The viscous drag buildup consisted of estimating the viscous drag on the wings, tails, fuselage, joints, etc. using the drag estimates from Hoerner and Page^{11, 12}. These two drag components were combined for the different missions and are shown in Figure 17. Notice that at the expected Reynolds number of approximately 100,000, friction forces dominate the drag buildup relative to the induced vortex drag.

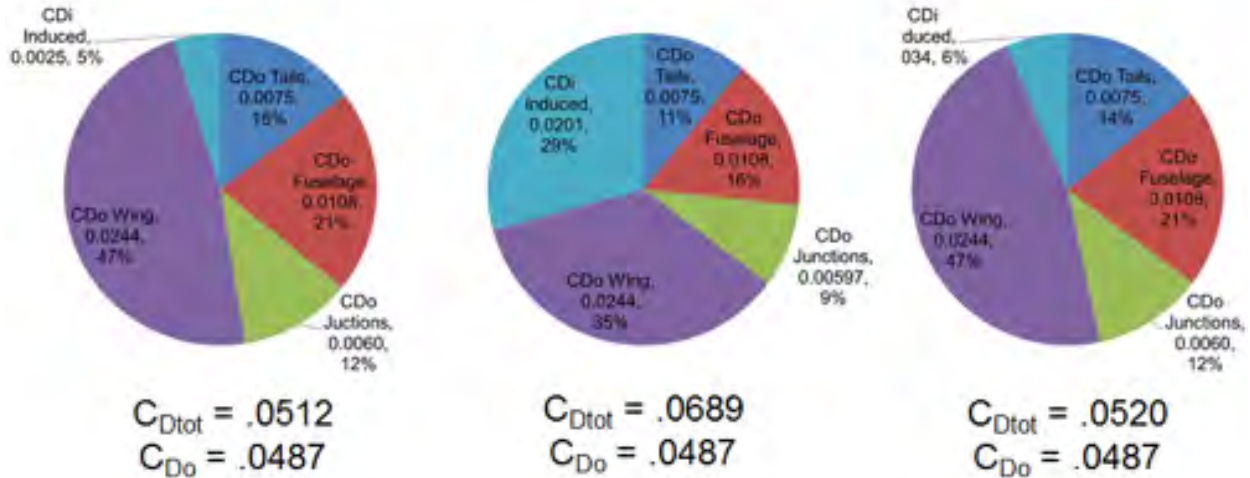


Figure 17: Drag buildups of Missions 1, 2 and 3 from left to right.

The drag buildup verifies the interesting phenomenon of low Reynolds number flight. Usually, approximately 50% of the total drag is due to vortex drag near maximum aerodynamic efficiency, L/D_{max} . However, most of the missions are at C_L 's well below the C_L for L/D_{max} , so parasite drag is more important than the team has seen in past years.

Using the total aircraft drag buildup, an approximation of flight performance was evaluated by examining the aerodynamic efficiency, L/D , of the aircraft over a range of C_L 's. The three required C_L 's for each mission was then plotted, as shown in Figure 18. This shows that for Mission 2, the aircraft is expected to fly close to L/D_{max} to maximize the efficiency of the aircraft during cruise. Missions 1 and 3 are cruising on the lower end of the L/D curve since their cruise C_L 's are low, and at these C_L 's induced drag is minimal as shown from the drag buildup in Figure 18.

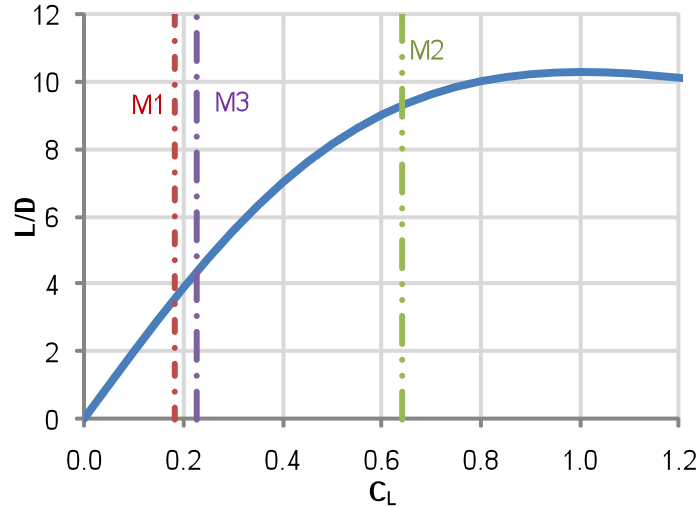


Figure 18: 3-Dimensional L/D curve over a range of C_L values.

4.5 Stability and Control

In the preliminary design phase, only rudder and elevator control surfaces are used to minimize the overall weight of the aircraft. A control analysis was done using AVL by inputting standard roll, pitch and yaw rates along with the flight conditions. It was verified that the required control surface deflections for the rudder or elevator were below 20° , which is the maximum deflection to provide an adequate safety margin from stalling the surface¹³. In addition, the hinge moments on the surfaces were calculated to verify that the servos could provide the required torque.

Since only a rudder and elevator surfaces were to be used to control the plane, it was desired to design in some extra spiral stability, especially since the plane is so small that the pilot could lose sight of it momentarily. Hence some dihedral was added to enhance its spiral stability. Polyhedral was used to provide a flat surface for the interface between the wing and fuselage of the aircraft to accommodate the 3 in x 4 in payload in Mission 2. The angle of polyhedral was determined to be 7.5° , which produced a stable spiral mode. A more in-depth analysis is explained in § 4.5.1.

4.5.1 Stability Parameters

Aircraft have five modes of motion that need to be accounted for during stability analyses – roll, spiral, phugoid, short period, and Dutch roll. When analyzing stability, special care must be taken to prevent Dutch roll due to the wing polyhedral. AVL was used to obtain stability derivatives, shown in Table 7. From these derivatives, the stability parameters were calculated and a root locus plot is shown in Figure 19 that illustrates that each mode is statically stable. Each mode has individual requirements that need to be satisfied in order to have acceptable stability characteristics. The acceptable stability characteristics were obtained from the Military Specification (MIL-F-8785C)¹⁴. Table 8 summarizes the natural frequency, damping coefficient, and time constant of each mode that was shown in Figure 19.

| | | | | | | | | | | | | | |
|------------------|-------|------------------|--------|--------------|--------|-----------------|---|-----------------|---------|-----------|--------|-----------|-------|
| $C_{L\alpha}$ | 4.500 | $C_{M\alpha}$ | -0.658 | $C_{Y\beta}$ | -0.414 | $C_{Y\delta_a}$ | 0 | $C_{Y\delta_r}$ | -0.0005 | C_{Y_p} | -0.022 | C_{Y_r} | 0.446 |
| C_{L,δ_e} | 0.001 | C_{M,δ_e} | -0.021 | $C_{l\beta}$ | -0.208 | $C_{l\delta_a}$ | 0 | $C_{l\delta_r}$ | 0.0005 | C_{l_p} | -0.425 | C_{l_r} | 0.245 |
| C_{Lq} | 7.150 | C_{Mq} | -9.631 | $C_{n\beta}$ | 0.412 | $C_{n\delta_a}$ | 0 | $C_{n\delta_r}$ | 0.0002 | C_{n_p} | -0.045 | C_{n_r} | 0.169 |

Table 7: Stability derivatives for Mission 2 cruise.

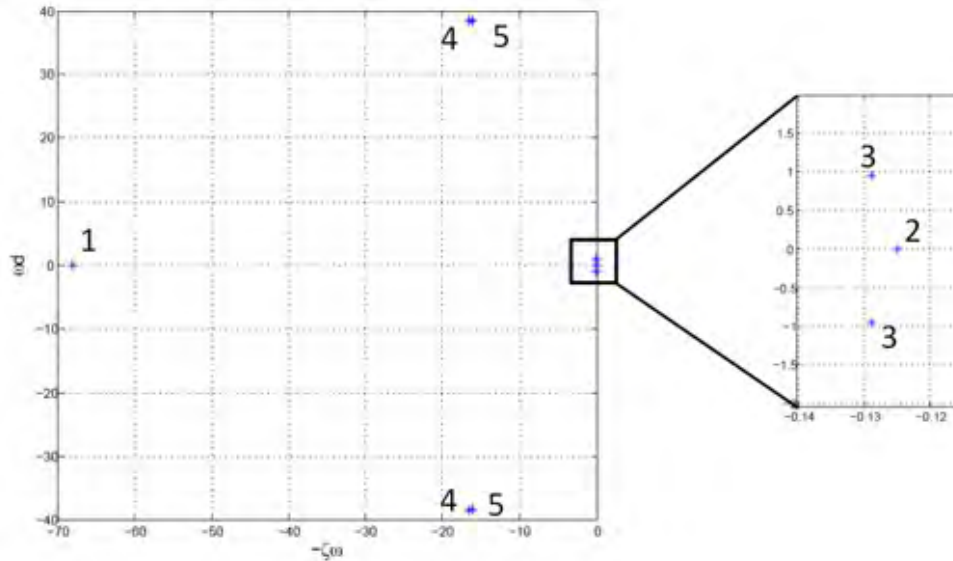


Figure 19: Stability root locus plot of the 5 modes of motion. Corresponding numbers to the mode can be found in Table 8.

| | Mode | ζ | ω_n (rad/s) | $\zeta\omega$ (rad/s) | τ (s) |
|---|--------------|--------------------|--------------------|-----------------------|--------------|
| 1 | Roll | - | - | - | .015 (< 1.4) |
| 2 | Spiral | - | - | - | 8 (> 0) |
| 3 | Phugoid | .1337 (> 0) | 0.9638 | 0.1289 | 7.76 |
| 4 | Short Period | .3956 (.35 to 1.3) | 41.9 (> 1.0) | 16.6 | 0.06 |
| 5 | Dutch Roll | 0.3882 | 41.6 | 16.1 (> 15.8) | 0.06 |

Table 8: Frequency, damping and time constants of the 5 modes of motion of the aircraft corresponding to the root locus plot in Figure 19. Values in parentheses are the requirements of the stability characteristics according to MIL-F-8785C.

Satisfying the spiral mode requirements verified that the polyhedral design was effective and would allow for stable turns with minimal pilot input. However, polyhedral would require a large vertical tail for increased yaw stability necessary to prevent Dutch roll. The vertical tail was iteratively sized until the conditions for Dutch roll stability were satisfied according to Table 8. The roll, phugoid, and short period were also shown to provide adequate damping and rates.

4.6 Propulsion

4.6.1 Power Loading & Flight Performance Classification

A common way to characterize the flight performance of model aircraft is through power loading, or the propulsion package's instantaneous power output divided by the total weight of the aircraft. A table of power loading for several different types of aircraft's flight performance is shown in Table 9. Higher



power loading corresponds to better flight performance. The goal of the propulsion system, therefore, is to provide the highest power loading possible for sufficient duration to complete all missions.

| Power Loading | Flight Performance |
|----------------|--|
| 50-70 W / lb | Trainer / Powered Glider |
| 70-100 W / lb | Sport / Aerobatic |
| 100-150 W / lb | Hotliner / High-Performance Aerobatic |
| 150 + W / lb | Extreme Unlimited Vertical Climb |
| 120 W / lb | Approximate Limit of NiCd and NiMH Chemistries |

Table 9: Power loading and flight performance classification.

In order to center the initial search for power components, a target power loading of 120 Watts/pound (W/lb) was chosen. The highest power loading possible is desirable; however, 120 W/lb was used as an initial assumption based on previous experience with NiMH and NiCd batteries until further trade studies could fully optimize the propulsion package. Since the RFB 004 airframe was expected to weigh 0.5 lb, the initial power package selection was expected to output approximately 60 W. Additional assumptions for propulsion system weight were based on previous experience with DBF aircraft and other model airplanes, namely that the propulsion system would be 50% of RAC, or 0.25 lb, and that the battery pack would be 75% of the propulsion package weight, or 0.188 lb.

4.6.2 Motors

The most important parameter in characterizing a motor is its Kv value, also called Speed Constant or Speed Rating, which represents the rotational velocity per unit of electrical potential supplied to the motor. Typical model aircraft motors often have Kv values in the range of 1000-4000 rpm/V. Kv is coupled with a similar parameter, Kt, the Torque Constant. Kt is 1/Kv, times a fixed constant to account for units, with dimensions of torque (moment) per unit of current. Kv and Kt values provide a complete representation for an ideal motor, since these values determine exactly how the electrical power of the battery will be converted into mechanical power at the propeller.

In the real world, motors will suffer power losses due to electrical resistance and mechanical bearing friction, which will scale inversely with motor size and hence weight. It is the goal of the motor selection process to choose a motor with the optimal Kv and Kt value for the expected power loading and velocity of the aircraft, while also choosing a motor with the least weight that still has acceptable armature resistance and bearing friction. Manufacturers generally supply a maximum power capacity for each motor, which is the most electrical power the motor can handle before overheating. As mentioned before, the assumed power output of the propulsion system was 60 W; leading to an exhaustive search through motor manufacturers' catalogs to generate a database of all motors advertised to operate with a peak power capacity around 60 W, spanning a wide range of Kv values. Grossly smaller motors risk overheating and grossly larger motors are excessively heavy, so motors with a rated power capacity outside $\pm 40\%$ of the 60 W assumption were excluded from the search. Manufacturer-provided

parameters of K_v , Resistance (R_o), Idle Current (I_o) and W for the motor candidates were then added to the MDO library in preparation for a detailed trade study to select the top motor choice.

4.6.3 Propellers

Propeller performance is dependent on many variables, including flight speed, rotations per minute (RPM), propeller pitch and diameter, and is closely tied to the motor and battery performance. For the initial propulsion sizing search, the propeller used was simply the size recommended for each motor by the manufacturer in order to ensure the combination is operating in an efficient range without going through the complex iterative analysis required to fully optimize the propeller. When multiple propellers were recommended, the higher pitch, lower diameter propeller was used in accordance with the relatively high speed of this airplane compared to similarly sized model aircraft. A complete propeller analysis was done using the MDO once the other propulsion components had been selected.

The MDO uses an iterative method to determine power package performance for a given airplane design, which was described in § 4.2.2. The propeller parameters are obtained from prop maps that were generated from dynamic wind tunnel testing. The MDO library contains a database of multi-dimensional prop maps, which allow parameters of thrust, current, and RPM to be obtained with inputs of velocity, torque, and current from the previous iteration. The propeller maps exist as multi-dimensional arrays in MATLAB, but representative samples of this data are provided below for reference in Figure 20, which show power coefficient, C_p , and thrust coefficient, C_T , curves for different propeller sizes, as denoted by J Design (pitch / diameter).

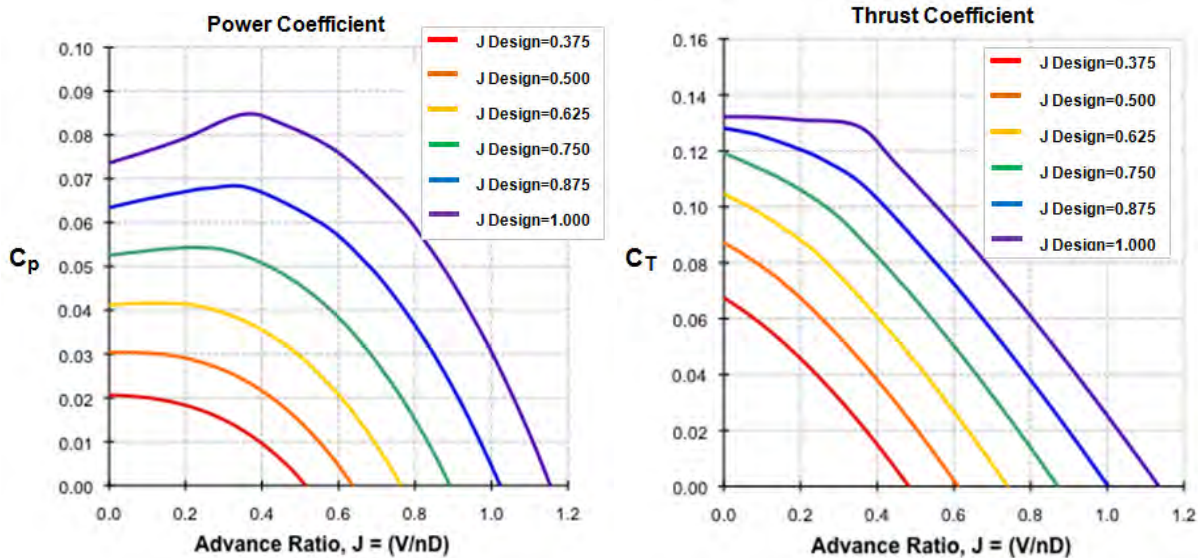


Figure 20: Propeller maps: power and thrust coefficients for varying J designs.

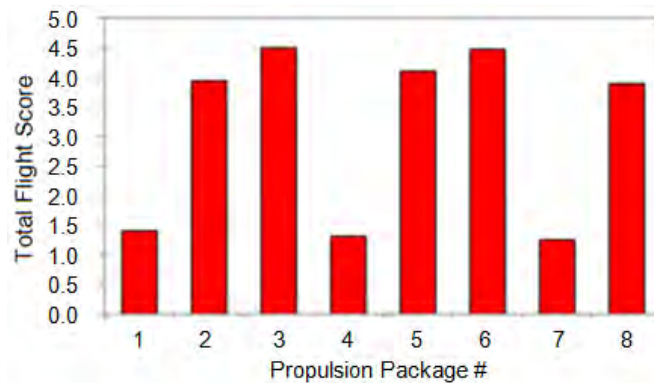
4.6.4 Batteries

The battery selection process was initiated using the 60 W initial power assumption, and began with an extensive search of manufacturer and vendor catalogs. A spreadsheet was generated to organize available battery cells by weight, using the maximum cell count possible for each pack without exceeding

three ounces of weight. The cell count determined the voltage of each pack, and a value for current was obtained for each pack by dividing the 60 W power assumption by the pack voltage, which had been adjusted to account for advertised internal resistance of the cell. No limitation was enforced on high cell count, as none of the available battery types allowed an extraordinarily high cell count due to the low weight assumption. However, low cell count combinations require a higher current in order to attain the 60 W assumption. Therefore, any packs requiring a current far exceeding the manufacturer's maximum discharge rating were discarded. Duration was calculated using current and cell capacity, and packs falling far short of the four-minute requirement of mission one were discarded. As a result of these parameters, the cell types selected for further trade studies were all sub-AA and AAA NiMH cells. The feasible cell types were all from the manufacturer KAN, due to their advertised relative high discharge ratings and many small sizes available.

4.6.5 Propulsion Package Comparison

Once the baseline search for propulsion components was completed, the highest-scoring propulsion package was determined using the MDO. An array of 30 different motor/battery combinations was tested in the MDO, where each of the six battery types was tested with five motors, with each motor using a manufacturer-recommended propeller. The airframe geometry was held constant by using the previously optimized span and airfoil, with the only changing contributor to RAC being the masses of the varying propulsion components. Total scores were calculated for each package, with the highest eight displayed below in Figure 21. Of the 30 packages tested, numbers 3, 5, and 6 were the highest scoring, and were therefore selected for further detailed optimization.



| Propulsion Package # | Battery | Motor | Motor Kv (RPM/V) | Propeller |
|----------------------|-----------------------|--------------------|------------------|-----------|
| 1 | 6S KAN 700mAh AAA | Hacker A10-12S | 2900 | APC 6x5.5 |
| 2 | 8S KAN 500mAh 4/5AAA | Hacker A10-12S | 2900 | APC 6x5.5 |
| 3 | 8S KAN 500mAh 4/5AAA | Tmotor T1804 | 2250 | APC 6x5.5 |
| 4 | 8S KAN 500mAh 4/5AAA | Tmotor T1805 | 2000 | APC 7x4 |
| 5 | 11S KAN 400mAh 2/3AAA | Tmotor T1805 | 2000 | APC 7x4 |
| 6 | 11S KAN 400mAh 2/3AAA | Scorpion 2503-1610 | 1610 | APC 7x4 |
| 7 | 11S KAN 400mAh 2/3AAA | BPA2204-19 | 1400 | APC 7x4 |
| 8 | 16S KAN 220mAh 1/2AAA | BPA2204-19 | 1400 | APC 7x4 |

Figure 21: Propulsion package trade study.



4.6.6 Propulsion Performance Predictions

Each of the high-scoring propulsion packages then underwent a further trade study to fully optimize each combination and determine the optimal performer. For each package, cell count was varied up and down to attain the peak scoring cell count, free from the restrictive 0.188 lb battery weight assumption. The propeller was also varied through all available pitches and diameters, and the resultant high-scoring propeller was selected. These two trade studies were done concurrently so that the ultimate peak combo could be attained. The output of these component studies is displayed in Figure 22 and shows that at least 8 cells are required to complete Mission 2 and that the optimum propeller size is 6 x 5.5.

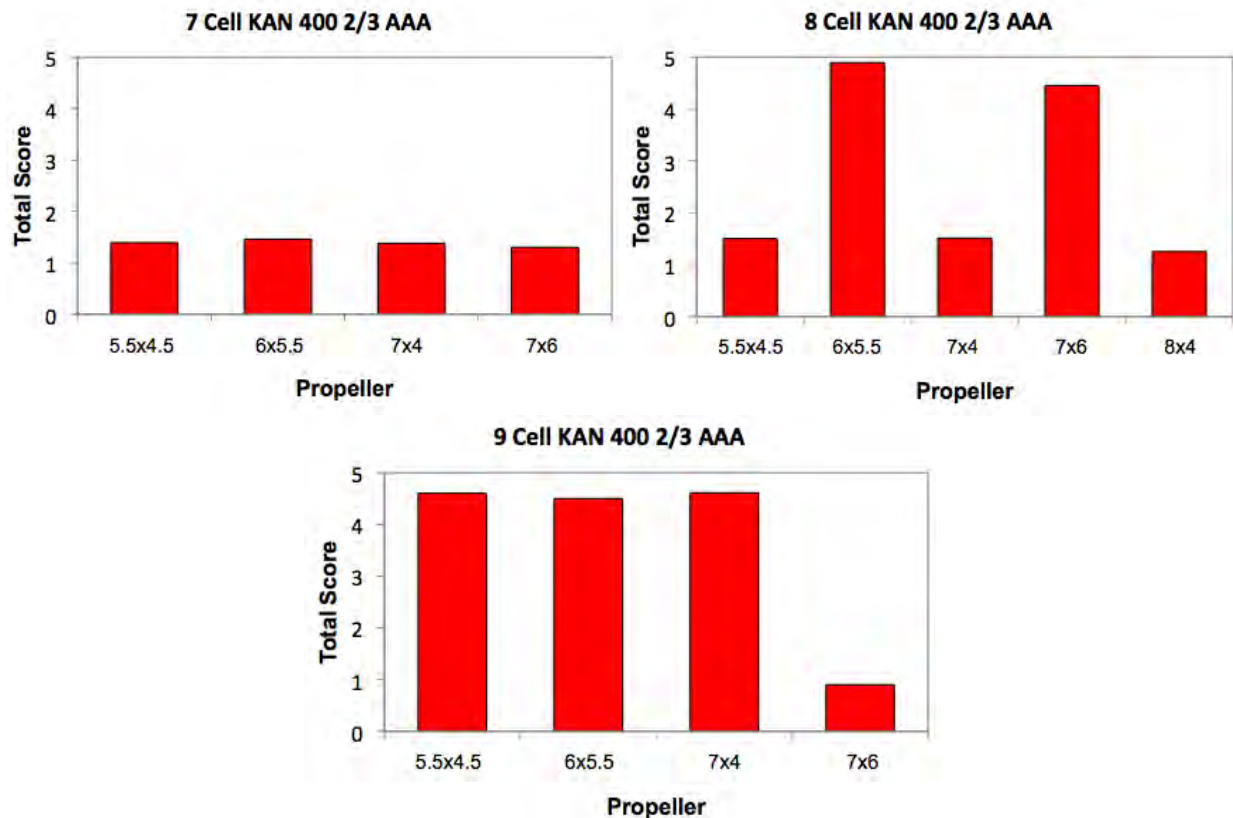


Figure 22: Propulsion package trade study and optimization.

4.7 Structures

The key focus of the structural design group was to develop the most weight effective structure for the aircraft due to the significant effect of RAC on the total score. While designing low-weight structural components, it was necessary to also design components that were high in strength to accommodate high loadings. Thus, it was extremely necessary to decide on the optimum manufacturing techniques used during the preliminary design of the aircraft.

4.7.1 Structural Components

An initial numerical study was done to determine the worst case flying and landing loads each main component would encounter. The load conditions considered were 5g flight maneuvers and 5g landing.



The most stringent case for the aircraft carrying its heaviest payload in Mission 2 in a 5g turn. A conservative rectangular loading in the fuselage was assumed, and numerical results, shown in Figure 23, indicate the wing structure never exceeds material limits.

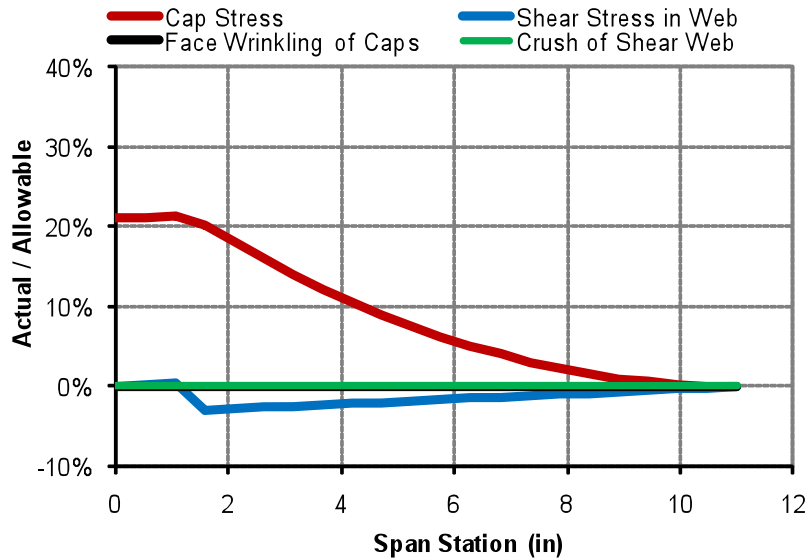


Figure 23: Normalized stresses of a semi-span wing in a 5g maneuver.

4.7.2 Wing and Empennage Structures

Initially, both the wing and empennage were constructed out of solid balsa wood. This method was chosen primarily for its manufacturing simplicity and aerodynamic smoothness. Blocks of solid balsa were sanded with the desired wing and empennage airfoil profiles. The strength of this fabrication technique was sufficient to sustain the maneuvering loads on the wing and loads required to stabilize the aircraft on the tail, as shown by Figure 23: **Normalized stresses of a semi-span wing in a 5g maneuver.**

4.7.3 Fuselage Structure

The fuselage was constructed from a composite underbelly with balsa bulkheads, a foam top covering, and a carbon fiber tube tail boom. This type of fuselage was chosen for its low weight, durability upon landing, and ease of access to payloads. Low density, bi-directional composite fabrics were considered for the underbelly skin, including one and two layers of 1.7 oz/yd² Kevlar and 2.3 oz/yd² carbon fiber, and one layer of 5.6 oz/yd² fiberglass. Each material was rated by RAC, conformation to complex molds, and durability; more details on the material comparison can be found in § 6.3.1.2. Using those FOMs, the skin was constructed from two layers of 1.7 oz/yd² Kevlar, since it is lightweight, durable, and easy to shape.



4.8 Dimensional Parameters & Weight

The dimensional parameters and weight buildup of the preliminary design phase aircraft, RFB 004, is shown below in and Figure 24. Note the substantial contribution from fixed weight items, such as the propulsion package (54%) and control systems (20%).

| Component | Weight (lbs) | Percent of Total |
|---------------------------|--------------|------------------|
| <i>Wing</i> | 0.06 | 11.1 |
| <i>Tail Section</i> | 0.03 | 4.8 |
| <i>Fuselage</i> | 0.05 | 9.8 |
| Fuselage Skin | 0.02 | 3.3 |
| Bulkheads | 0.01 | 1.2 |
| Foam Caps | 0.01 | 1.0 |
| Others | 0.02 | 4.3 |
| <i>Propulsion Package</i> | 0.08 | 14.8 |
| Propeller & Saver | 0.01 | 2.2 |
| Motor | 0.03 | 6.0 |
| ESC | 0.04 | 6.6 |
| <i>Control Package</i> | 0.11 | 20.5 |
| Servos (x2) | 0.04 | 6.6 |
| Receiver | 0.04 | 6.6 |
| Receiver Battery | 0.04 | 7.2 |
| <i>Flight Battery</i> | 0.21 | 39.1 |
| TOTAL | 0.53 | 100.0 |

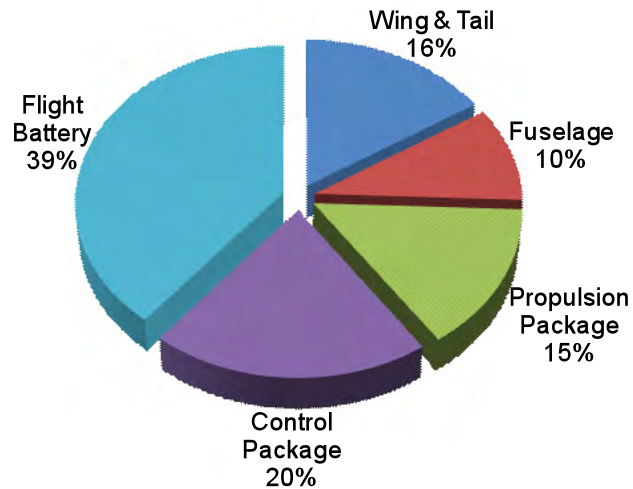


Figure 24: Dimensional parameters and weight buildup for preliminary design: RFB 004.

4.9 Payloads

4.9.1 Mission 2 Payload Analysis

Two steel bar payload configurations with minimum (3 in x 4 in) dimensions, were considered. In the first configuration, the steel bar would be placed horizontally directly below the wing, with the 4 in dimension running longitudinally along the plane. Placing the 4 in dimension (as opposed to the 3 in dimension) longitudinally would allow for a narrower fuselage, thereby saving surface area and drag. The other configuration considered would place the steel bar vertically, with the longitudinal 4 in dimension touching the flat part of the wing. This vertical configuration would require an aerodynamic fairing around the steel bar, similar to adding another vertical stabilizer. The two configurations are shown in Table 10. For the vertical configuration, the volume of the ball as well as internal components such as batteries needed to be taken into account, resulting in the bulbous structure near the wing. As indicated by Table 10, the vertical bar configuration uses more surface area to hold the same payload; because of this and the increased complexity of building the fairing enclosure, the horizontal bar configuration was chosen.

| | Horizontal | Vertical |
|-----------------------|-----------------------|-----------------------|
| Front View | | |
| Side View | | |
| Bottom View | | |
| Fuselage Surface Area | 260.2 in ² | 280.4 in ² |

Table 10: Steel bar configuration analysis.

4.9.2 Mission 3 Payload Analysis

From the conceptual phase design, the target payload for Mission 3 was set to one golf ball. However, a study was performed to examine the effect of golf ball count on the fuselage surface area, which was done by modeling approximate fuselages to carry a varying number of golf balls in SolidWorks. As Figure 25 indicates, the required surface area and the number of golf balls carried are directly proportional, indicating a need to carry as few balls as possible. The decision to carry only one golf ball was confirmed, as decreasing the surface area of the fuselage reduces both C_{D0} and RAC.

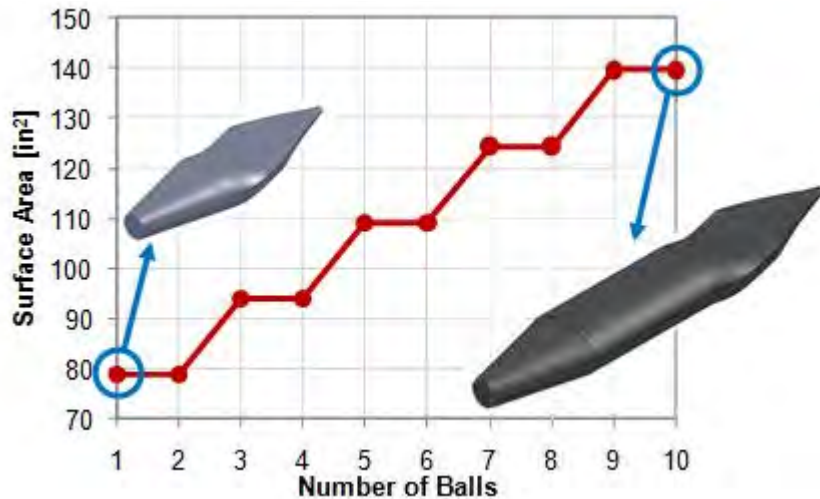


Figure 25: Fuselage surface area variation with number of golf balls.

4.10 Flight Testing

The team constructed a prototype, RFB 004, at the end of the preliminary design stage to verify the MDO estimates. RFB 004 suffered from stability and control issues that led to several crashes before completing an entire lap. Changes were made in the field to improve performance, as detailed in the following subsections.

4.10.1 Aerodynamic Lessons Learned

The main problem encountered during the test flight was tip stall. The selected manufacturing process prevented accurate reproduction of the BA527LS and NACA 0010 airfoils. The resulting airfoil was closer to a flat plate with a blunt leading edge. Computational analysis of the as-built airfoil confirmed it was the cause of the tip stall. This led to a re-examination of the selected wing materials and fabrication method. Subsequent wings achieved much better airfoil fidelity.

4.10.2 Stability and Control Lessons Learned

RFB 004's center of gravity (CG) was designed to be at 35% of the wing chord. However, in flight test it was necessary to move the CG to 5% MAC for adequate pitch stability possibly due to improper placement of internal systems. RFB 004 also exhibited Dutch roll due to an undersized vertical stabilizer and extreme pitch sensitivity due to the flat plate airfoil on the tails. The initial Dutch roll issues were solved in the field by extending the vertical stabilizer; however, since new tail surfaces with the proper airfoil could not be constructed during the test flight, the pitch sensitivity persisted throughout the flight testing. Overall, RFB 004 flew worse at higher speeds, and had difficulties making tight turns. The most likely reason for the discrepancy between the pre-flight analysis and flight is due to poor airfoil fidelity.



Figure 26: Images of preliminary design flight tests of RFB 004.



4.11 Preliminary Design Summary

Using the iterative technique of the MDO, in addition to the team's other analysis tools, the team decided on an optimum configuration for the preliminary design, named RFB 004, as illustrated in Table 11. This design was presented in a formal preliminary design review delivered to a panel of industry experts. At the time of the review, a subsequent iteration, RFB 005, was under consideration; however, upon receiving the reviewers' feedback and advice, a new iteration that also incorporated flight test lessons learned was developed as the detailed design phase, RFB 006, described in § 5.

| Performance Parameter | Mission 1 (Empty) | Mission 2 (Steel Bar) | Mission 3 (Golf Ball) |
|-----------------------------|----------------------|--------------------------|--------------------------|
| $C_{L_{cruise}}$ | 0.11 | 0.21 | 0.15 |
| $C_{L_{max}}$ | 1.5 | 1.5 | 1.5 |
| e | 0.8 | 0.8 | 0.8 |
| C_{D0} | 0.049 | 0.049 | 0.049 |
| L/D_{cruise} | 4 | 7.8 | 5.6 |
| L/D_{max} | 12 | 12 | 12 |
| Climb Rate (ft/s) | 59 | 28 | 54 |
| W/S (lb/ft ²) | 1.1 | 2.2 | 1.3 |
| Cruise Speed (ft/s) | 97 | 96 | 90 |
| Stall Speed (ft/s) | 26 | 36 | 28 |
| Total Flight Time (sec) | 240 | 505 | 486 |
| Empty Aircraft Weight (lbs) | 0.45 | 0.45 | 0.45 |
| Gross Weight (lbs) | 0.45 | 0.89 | 0.55 |
| Total Flight Score | 3.532 | | |

Table 11: Characteristics of preliminary design aircraft, RFB 004.

5. Detailed Design

RFB 004 test flights provided a great starting point for the detailed design phase, in which RFB 006 was built and tested. The overall size of RFB 006 was smaller than its predecessor, with a decreased wing span and AR. The wing material and build-up methodology were also changed from solid balsa to a solid foam wing in order to manufacture the exact airfoil shape.

5.1 Dimensional Parameters

Table 12 shows the finalized dimensional parameters for the general structural, propulsion, and electrical systems.

| Wing | | Horizontal Stabilizer | | Vertical Stabilizer | |
|--------------------|----------------------|-----------------------|----------------------|---------------------|----------------------|
| Span | 13.3 in | Span | 6.2 in | Span | 4.5 in |
| Chord | 3.2in | Chord | 2.1 in | Chord | 2.3 in |
| Aspect Ratio | 4 | Area | 13.0 in ² | Area | 10.4 in ² |
| Wing Area | 42.5 in ² | Airfoil | NACA0010 | Airfoil | NACA0010 |
| Airfoil | BA-527-LS | Incidence | 3.5° | | |
| Static Margin | 38% | Elevator | | | |
| Incidence | 3.5° | Span | 6.2 in | | |
| Aileron | | % of Chord | 30% | | |
| Span | 3.1 in | Max δ _e | 15° | Fuselage | |
| % of Chord | 25% | | | Length | 17.0 in |
| Max δ _a | 7° | | | Width | 3.3 in |
| | | | | Height | 2.5 in |

Table 12: General aircraft dimensions and parameters.

5.2 Structural Characteristics and Capabilities

The core structural element of the aircraft is the wrapped carbon fiber tube (0.197 in OD, 0.157 in ID) ‘spine’ that runs the full length of the aircraft. The motor is fixed coaxially to the tube with a 1/16in plywood plate, which also serves as the forward bulkhead for the fuselage. There are two other bulkheads, 1/16 balsa wood, that serve as fixture points for the fuselage and retain both the golf ball and steel bar payload. The steel bar is also retained in the fore-aft direction by a Kevlar net in front and wire clips aft. The bulkhead arrangement and motor mount is shown in Figure 27 (left).

The fuselage skin is comprised of two plies of 1.7oz/yd² Kevlar (Aramid 195) to provide wear resistance during landing to provide rigidity and transfer impulse loads from landing to the aircraft spine. The fuselage has one hatch running full length of the fuselage providing access to all internal systems. The hatch is hinged with a forward latch and locked by magnets and balsa tongues, as indicated in Figure 27 (right).

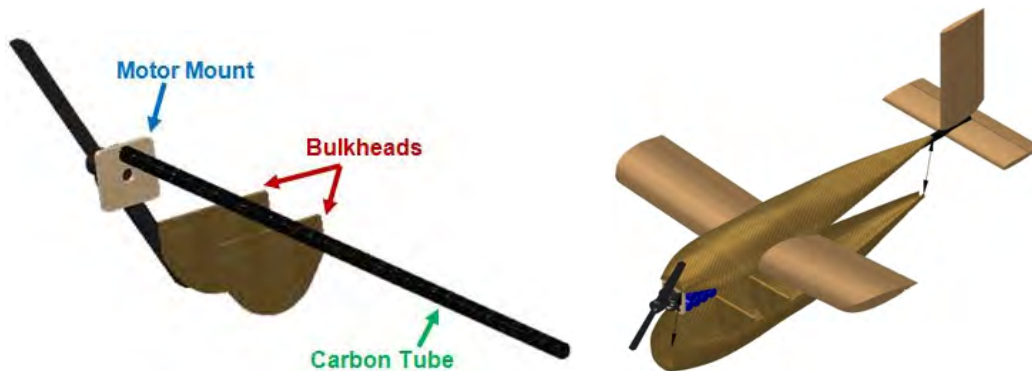


Figure 27: Bulkhead arrangement and motor mount on aircraft spine (left) and hatch arrangement (right).

The wing consists of 2.2 lb/ft³ blue foam cores that have been partially cut away to reduce weight, giving the foam cores approximately 60% solidity. The leading edges and trailing edges have been replaced with balsa to facilitate sheeting, improve the geometric accuracy of the leading edges and allow for the use of cyanoacrylate hinges in the control surfaces. This manufacturing technique represents a change from earlier iterations. The balsa over foam technique had not been considered by the team until

it was suggested as a means of saving weight during one of the team's design reviews. The empennage surfaces are solid balsa. The control surfaces are constructed from solid balsa that has been sanded to the correct shape. Both ailerons and elevators are actuated by torque rods connected to Blue Bird S0251 servos. The wing is permanently fixed to the aircraft spine; this is achieved by sinking the spine into the wing and gluing the two together using thickened epoxy and a small amount of carbon cloth to transfer forces to the lower surface of the wing.

RFB 006 is small enough to fit inside the suitcase without disassembly. However, the loading procedure will include arming the aircraft, done by attaching the batteries and fuse, and loading the necessary payloads

5.3 System Design, Component Selection and Integration

5.3.1 Aerodynamics

The overall shape of the RFB 004 fuselage presented some aerodynamic concerns in that the front half of the fuselage was found to have too much of a step structure and was not blended well enough to the rest of the aircraft. Furthermore, the horizontal stabilizer was questionably in the turbulent wake coming off of the fuselage. Hence, the detailed design phase aircraft, RFB 006, was designed with a more faired and blended fuselage to reduce any turbulence affecting the horizontal stabilizer's performance. The change in fuselage shape can be seen in Figure 28; the fuselage of RFB 006 (right image) is better faired than that of RFB 004 (left image) and has a shallower separation angle between the sides of the fuselage and the free stream flow.

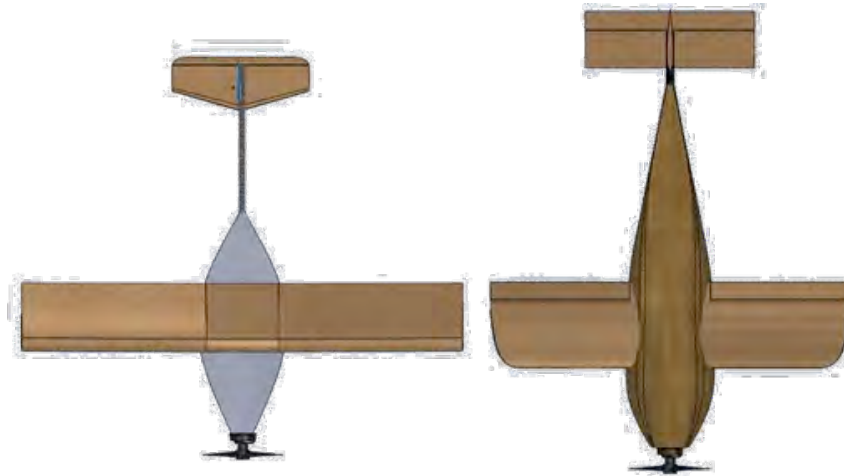


Figure 28: Fuselage shape design change from RFB 004 (left) to RFB 006 (right).

5.3.2 Stability and Control

The preliminary design plane, RFB 004, had elevators and a rudder but no ailerons and saw stability and control issues during its flight tests, as mentioned in § 4.10.2. For the detailed design phase, RFB 006 was designed with ailerons and elevators but no rudder. The ailerons were controlled by a single servo mounted in the aft portion of the fuselage, as seen in Figure 29. The elevators were in turn

controlled by the second servo that also mounted in the aft portion of the fuselage, also shown in Figure 29. The stability derivatives for RFB 006 are shown in Table 13.

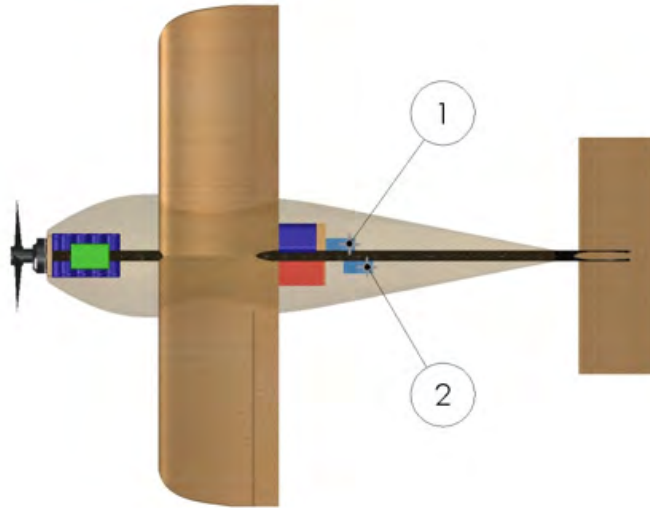


Figure 29: Servo configuration. 1 indicates aileron servo; 2 indicates elevator servo.

| | | | | | | | | | | | | | |
|------------------|-------|------------------|--------|--------------|--------|-----------------|---------|-----------------|---|-----------|--------|-----------|--------|
| $C_{L\alpha}$ | 4.208 | $C_{M\alpha}$ | -1.456 | $C_{y\beta}$ | -0.677 | $C_{y\delta_a}$ | 0 | $C_{y\delta_r}$ | 0 | C_{y_p} | -0.008 | C_{y_r} | 1.094 |
| C_{L,δ_e} | 0.002 | C_{M,δ_e} | -0.004 | $C_{l\beta}$ | -0.222 | $C_{l\delta_a}$ | 0.0060 | $C_{l\delta_r}$ | 0 | C_{l_p} | -0.376 | C_{l_r} | 0.330 |
| C_{Lq} | 10.09 | C_{Mq} | -22 | $C_{n\beta}$ | 0.460 | $C_{n\delta_a}$ | -0.0006 | $C_{n\delta_r}$ | 0 | C_{n_p} | 0.036 | C_{n_r} | -0.833 |

Table 13: Stability derivatives for RFB 006.

5.3.3 Propulsion

The propulsion system consists of a T-Motor T1805 motor, spinning an APC 6x5.5 propeller, powered by 8 KAN 400mAh 2/3 AAA battery cells. The propulsion components are shown in Table 14.

| Component | All Missions |
|------------------|--------------------------------------|
| Battery Pack | 8 cells KAN 400mAh 2/3 AAA batteries |
| Propeller | APC 6 x 5.5 |
| Motor | T-Motor T1805 |
| Speed Controller | Castle Creations Thunderbird 9 |
| Receiver | Berg Microstamp 4L |
| Elevator Servo | Blue Bird S0251 |
| Aileron Servo | Blue Bird S0251 |

Table 14: Propulsion and electrical system components.

5.3.4 Structures

The wing of RFB 006, instead of solid balsa like that of RFB 004, is solid foam with balsa sheeting in order to more accurately fabricate the actual optimized airfoil design. With this change, appropriate numerical simulations were done to examine the loads, shear forces, and bending moments that the wing would undergo. Figure 30 shows normalized stresses experienced by different structural components in

the RFB 006 wing in a 5g turn. These numerical simulations depict that the maximum stress seen by any structural component of the wing is less than 20% of its respective maximum allowable stress. Later testing, which is described in § 8, verified that the wing would sustain these values without failure.

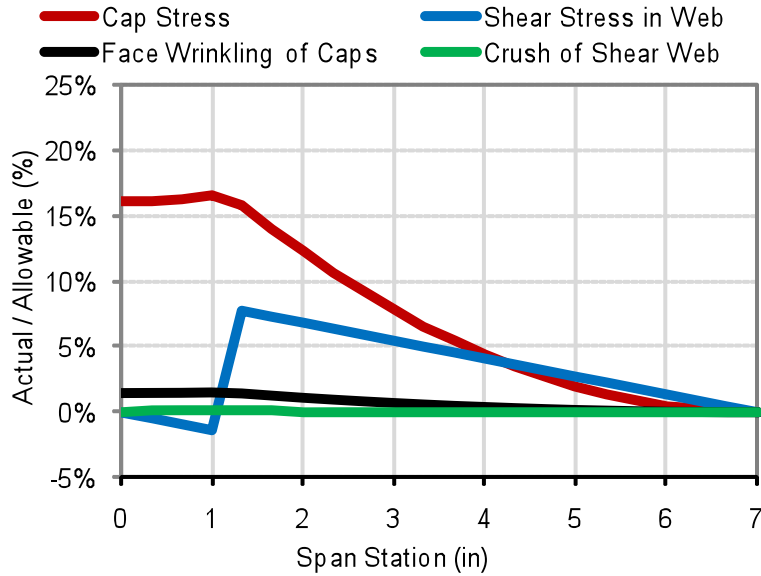


Figure 30: Normalized stresses for a half-span wing for a 5g loading on the RFB 006 wing.

5.3.5 Payloads

For Mission 2, the steel bar would be placed in the fuselage directly below the wing. Likewise, for Mission 3, the golf ball would be placed in the fuselage also directly below the wing. Mission 2 and 3 payload configurations are shown in Figure 31.

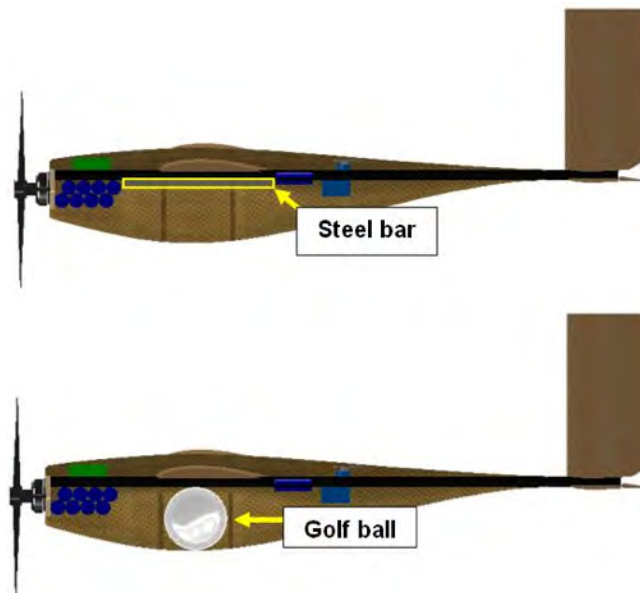


Figure 31: Steel bar (top) golf ball (bottom) mounting method.



5.4 Aircraft Component Weight and CG Buildup

The total empty weight of the airplane (RAC) was estimated to be 0.4 lbs. Accurate weights and CG locations are presented for each mission in Table 15.

| Empty | Weight (lbs) | CG Location (in) | | |
|----------------|--------------|------------------|--------------|--------------|
| | | x | y | z |
| Airframe | 0.325 | 4.95 | 0.00 | 0.00 |
| Motor | 0.038 | 0.80 | 0.00 | 0.00 |
| Propeller | 0.011 | 0.17 | 0.00 | 0.00 |
| Servos | 0.019 | 9.10 | 0.00 | -0.15 |
| Radio Receiver | 0.007 | 7.64 | -0.40 | 0.00 |
| Total | 0.400 | 22.66 | -0.40 | -0.15 |

| Mission 1 | Weight (lbs) | CG Location (in) | | |
|--------------|--------------|------------------|--------------|--------------|
| | | x | y | z |
| Batteries | 0.143 | 1.90 | 0.00 | -0.20 |
| Total | 0.543 | 24.56 | -0.40 | -0.35 |

| Mission 2 | Weight (lbs) | CG Location (in) | | |
|--------------|--------------|------------------|--------------|--------------|
| | | x | y | z |
| Batteries | 0.143 | 1.90 | 0.00 | -0.20 |
| Steel Bar | 0.400 | 4.95 | 0.00 | 0.10 |
| Total | 0.943 | 29.51 | -0.40 | -0.25 |

| Mission 3 | Weight (lbs) | CG Location (in) | | |
|--------------|--------------|------------------|--------------|--------------|
| | | x | y | z |
| Batteries | 0.143 | 1.00 | 0.00 | -0.20 |
| Golf Ball | 0.101 | 4.95 | 0.00 | -0.50 |
| Total | 0.644 | 28.61 | -0.40 | -0.85 |

Table 15: Component weight and CG buildup.

5.5 Flight Performance Parameters

Table 16 details the flight performance parameters for the three missions obtained through the MDO. Figure 32 displays the predicted L/D curve and drag polar for RFB 006, obtained through AVL. Both MDO and AVL results indicate low cruise C_L and L/D values for Missions 1 and 3, and a L/D value close to L/D_{max} (approximately 8.5) for Mission 2. As Table 16 indicates, V_{cruise} is approximately 104 ft/s for all three missions.

| Performance Parameter | Mission 1 (Empty) | Mission 2 (Steel Bar) | Mission 3 (Golf Ball) |
|-----------------------------|-------------------|-----------------------|-----------------------|
| $C_{Lcruise}$ | 0.11 | 0.21 | 0.13 |
| C_{Lmax} | 1.5 | 1.5 | 1.5 |
| e | 0.8 | 0.8 | 0.8 |
| C_{D0} | 0.058 | 0.058 | 0.058 |
| L/D_{cruise} | 3.6 | 6.7 | 4.5 |
| L/D_{max} | 9.6 | 9.8 | 9.7 |
| Climb Rate (ft/s) | 53 | 24 | 41 |
| W/S (lb/ft ²) | 1.3 | 2.6 | 1.6 |
| Cruise Speed (ft/s) | 105 | 104 | 104 |
| Stall Speed (ft/s) | 28 | 39 | 31 |
| Total Flight Time (sec) | 240 | 463 | 475 |
| Empty Aircraft Weight (lbs) | 0.38 | 0.38 | 0.38 |
| Gross Weight (lbs) | 0.38 | 0.75 | 0.48 |
| Total Flight Score | 3.892 | | |

Table 16: Flight performance parameters for RFB 006 from MDO.

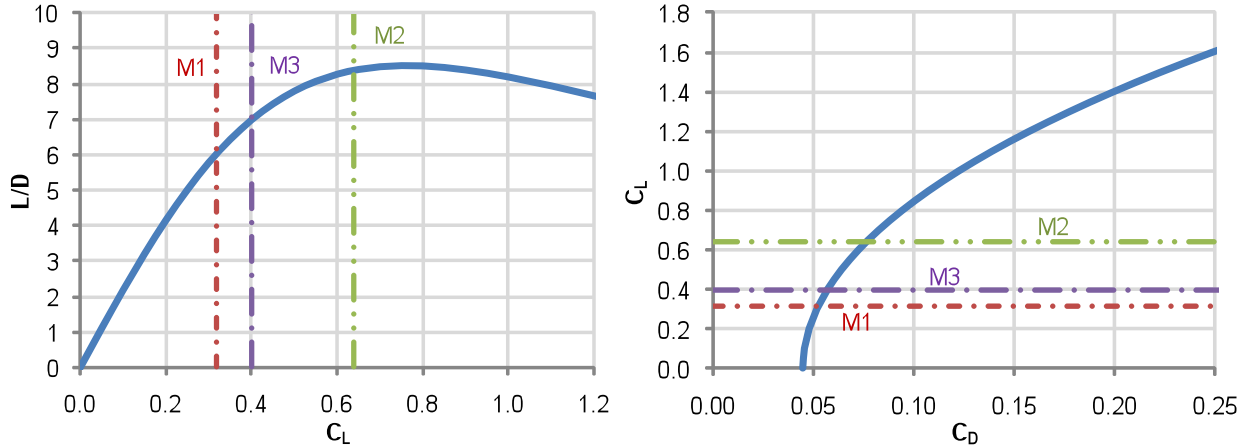


Figure 32: 3-dimensional L/D curve (left) and drag polar (right) for RFB 006 from AVL.

5.6 Mission Performance

Table 17 displays battery capacity, current draw, and time expenditures for the three missions. In all cases, the plane uses about 67% of the available energy, which leaves adequate excess in case of unforeseen occurrences.

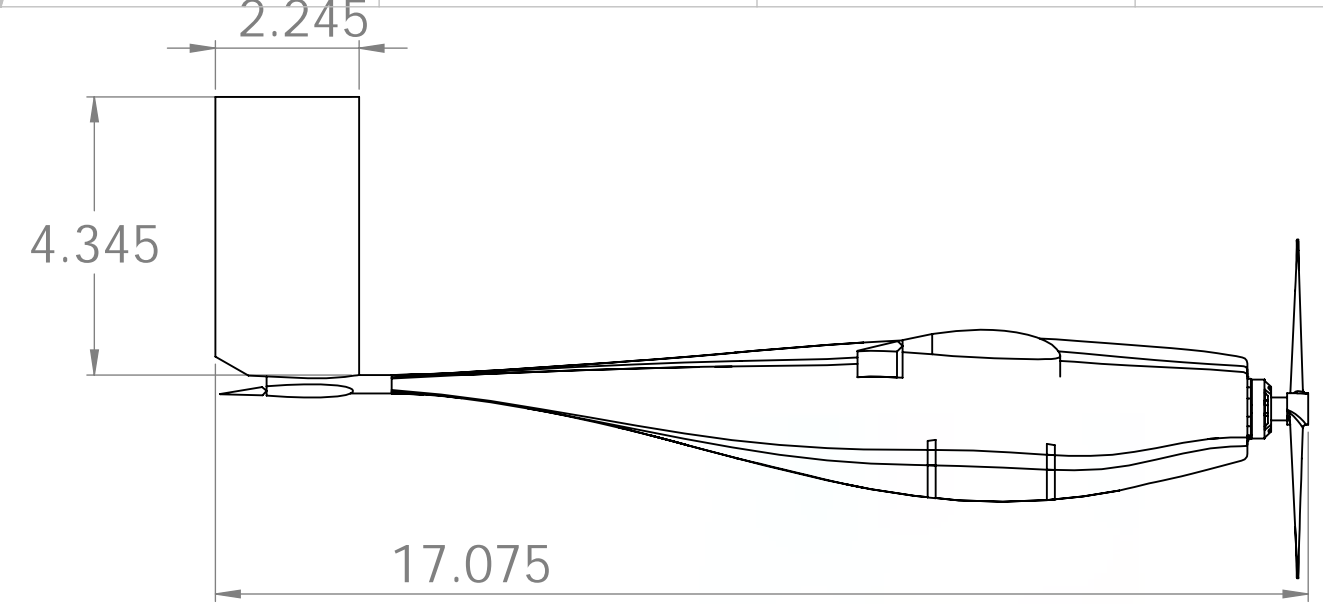
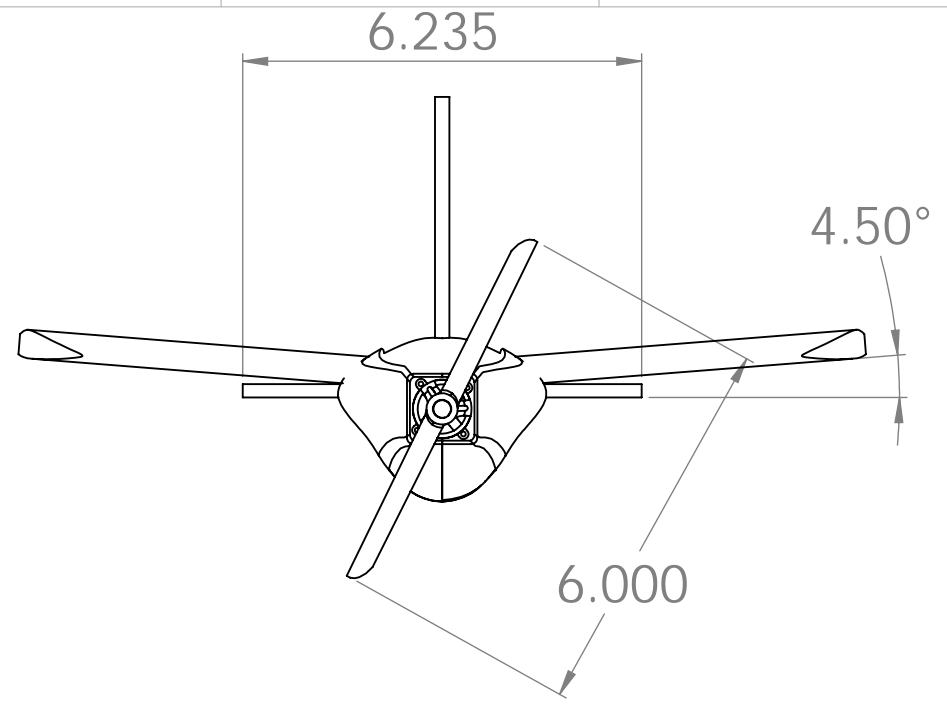
| Mission 1 | | | | Mission 2 | | | |
|----------------------------|----------------|--------------|---------------|----------------------------|----------------|--------------|---------------|
| | Current (Amps) | Time (sec) | Energy (J) | | Current (Amps) | Time (sec) | Energy (J) |
| Launch / Climb | 8.3 | 6.3 | 262 | Launch / Climb | 8.3 | 6.2 | 259 |
| Cruise (2000 ft/lap) | 3.4 | 21.0 | 417 | Cruise (2000 ft/lap) | 3.4 | 21.0 | 427 |
| 180° Turn (x2) | 3.4 | 5.3 | 219 | 180° Turn (x2) | 3.4 | 17.0 | 703 |
| 360° Turn | 3.4 | 5.3 | 219 | 360° Turn | 3.4 | 17.0 | 703 |
| Descent | 0 | 5.3 | 0 | Descent | 0 | 5.3 | 0 |
| Sub Total (per lap) | - | 31.6 | 855 | Sub Total (per lap) | - | 55.0 | 1833 |
| Total (7 laps) | - | 227.5 | 6142.8 | Total (3 laps) | - | 171.2 | 5651.3 |
| Available Energy | - | - | 9502 | Available Energy | - | - | 9502 |
| Excess | - | - | 3359.3 | Excess | - | - | 3850.8 |

| Mission 3 | | | |
|----------------------------|----------------|--------------|---------------|
| | Current (Amps) | Time (sec) | Energy (J) |
| Launch / Climb | 8.3 | 6.4 | 265 |
| Cruise (2000 ft/lap) | 3.4 | 21.0 | 420 |
| 180° Turn (x2) | 3.4 | 5.4 | 224 |
| 360° Turn | 3.4 | 5.4 | 224 |
| Descent | 0 | 5.3 | 0 |
| Sub Total (per lap) | - | 31.8 | 868 |
| Total (3 laps) | - | 101.8 | 2764.0 |
| Available Energy | - | - | 9502 |
| Excess | - | - | 6738 |

Table 17: Mission performance predictions.

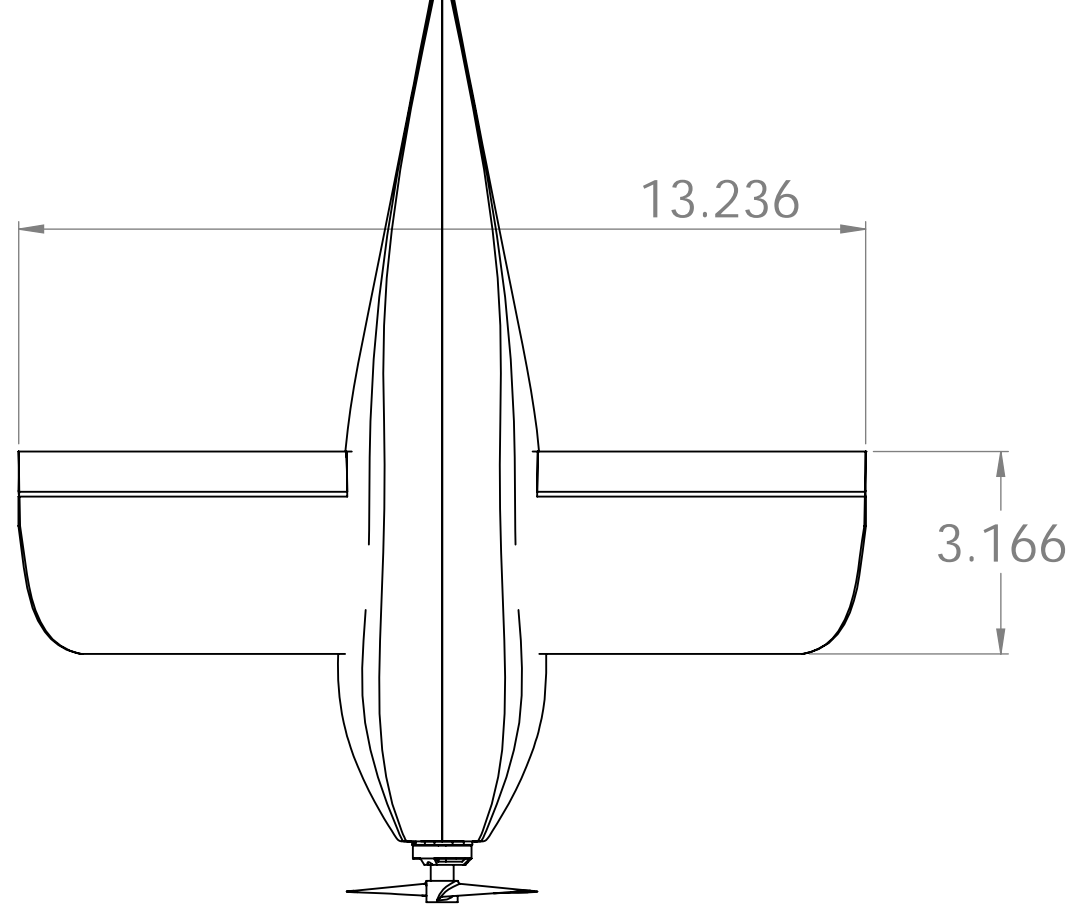
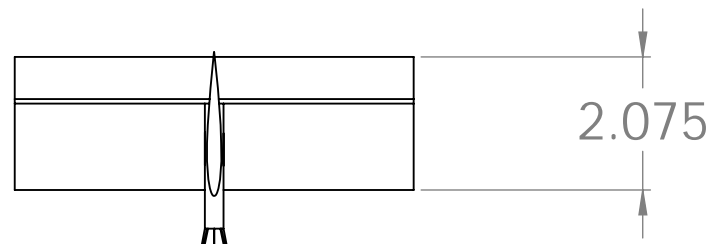
8 7 6 5 4 3 2 1

D



D

C



C

B



B

A

8 7 6 5 4 3 2 1

| | | |
|-------------------|----------------|--------------|
| 2010-2011 USC ADT | | |
| TITLE: | | |
| Three-View | | |
| SIZE | Entry | REV |
| B | The RFB | 006 |
| SCALE: 1:2 | Units: Inches | SHEET 1 OF 4 |

A

8 7 6 5 4 3 2 1

D

D

C

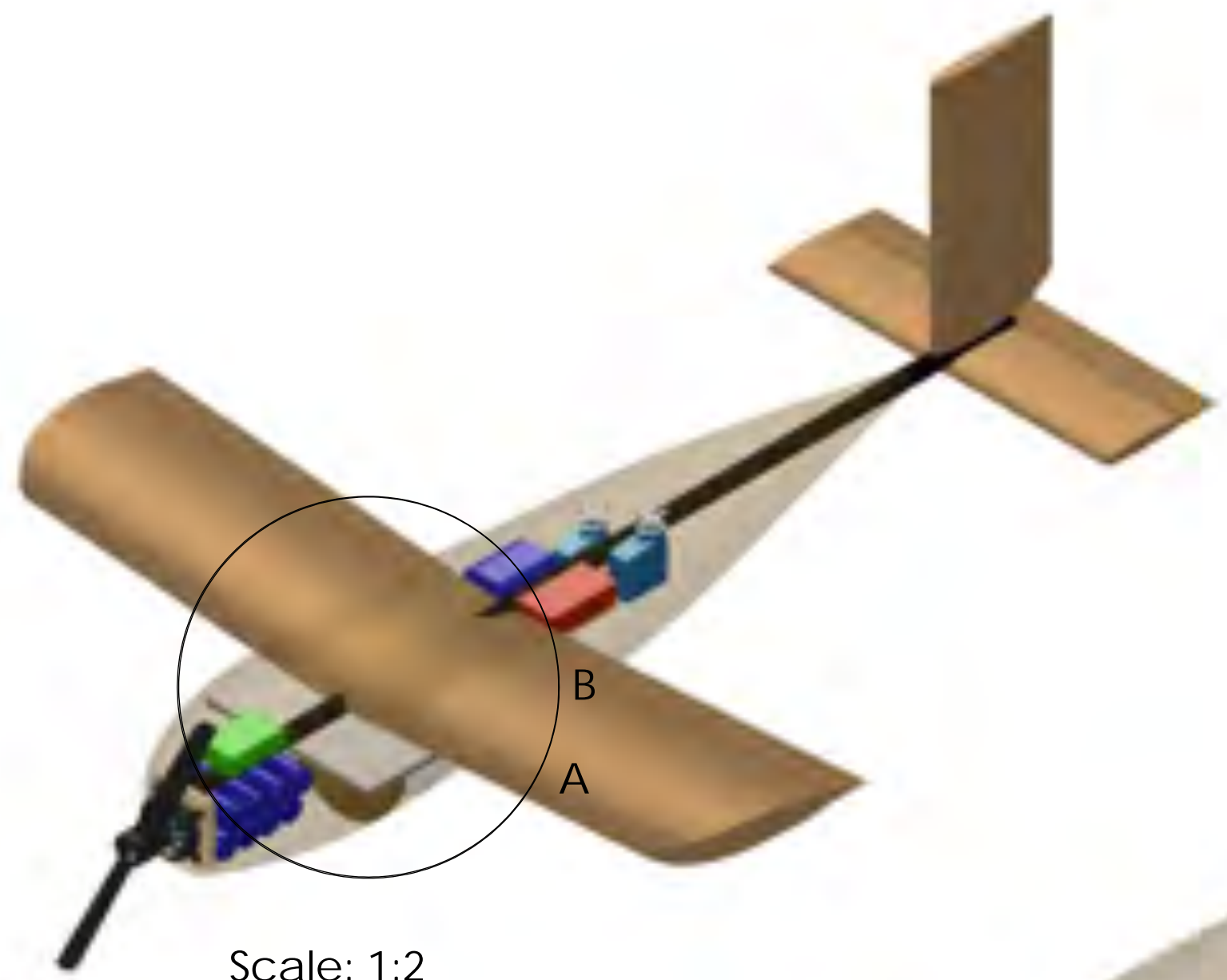
C

B

B

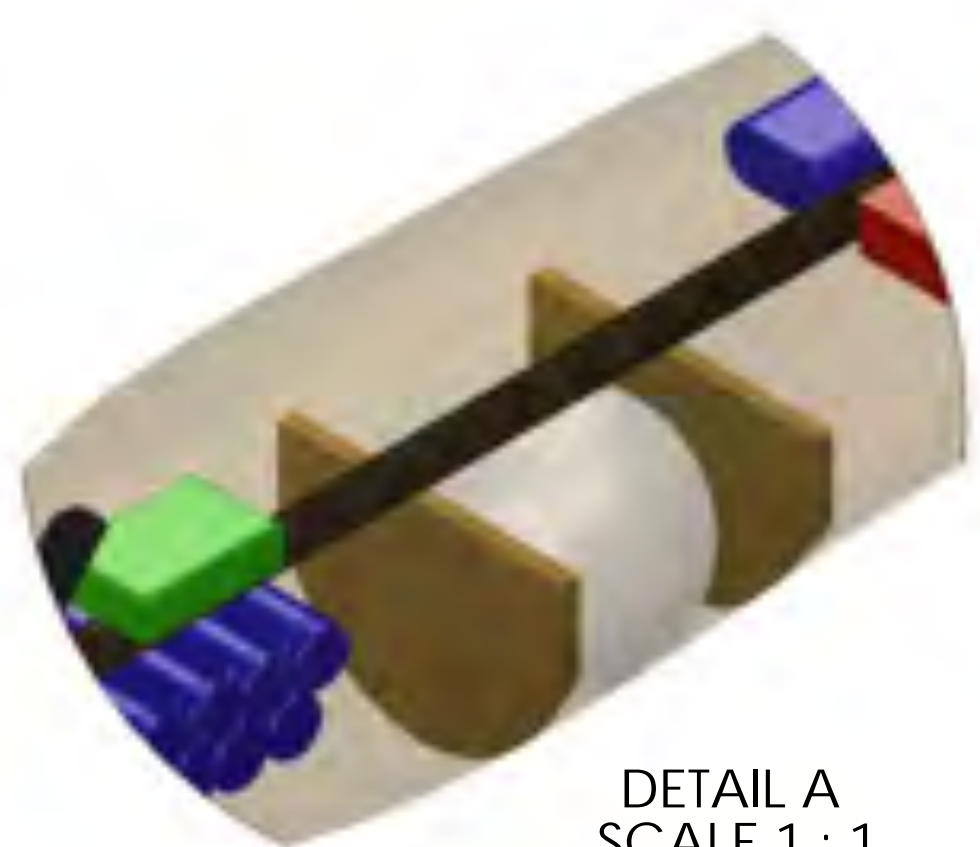
A

A

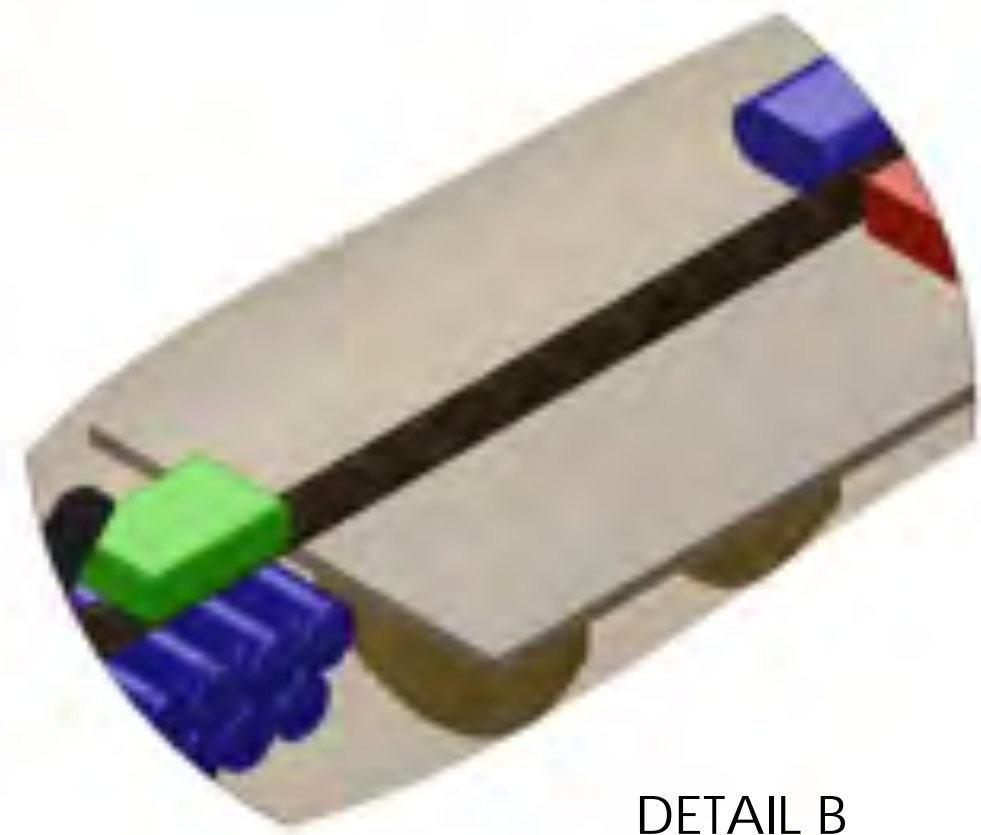


Scale: 1:2

B
A



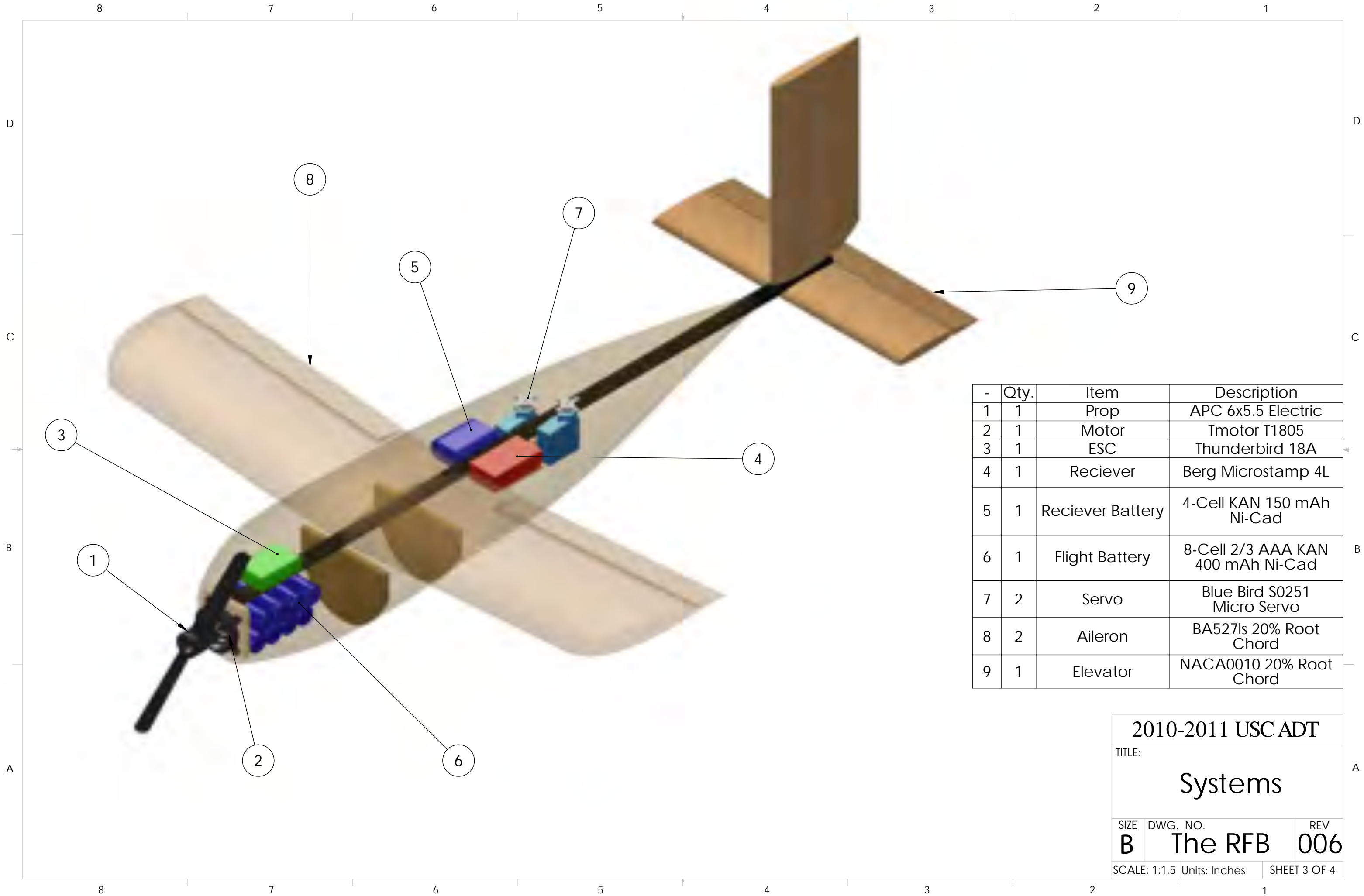
DETAIL A
SCALE 1 : 1
Golf Ball Payload



DETAIL B
SCALE 1 : 1
Steel Plate Payload

| | | |
|--------------------|------------------|--------------|
| 2010-2011 USC ADT | | |
| TITLE: Payloads | | |
| SIZE B | Entry The RFB | REV 006 |
| SCALE: Noted | Units: Inches | SHEET 2 OF 4 |

8 7 6 5 4 3 2 1



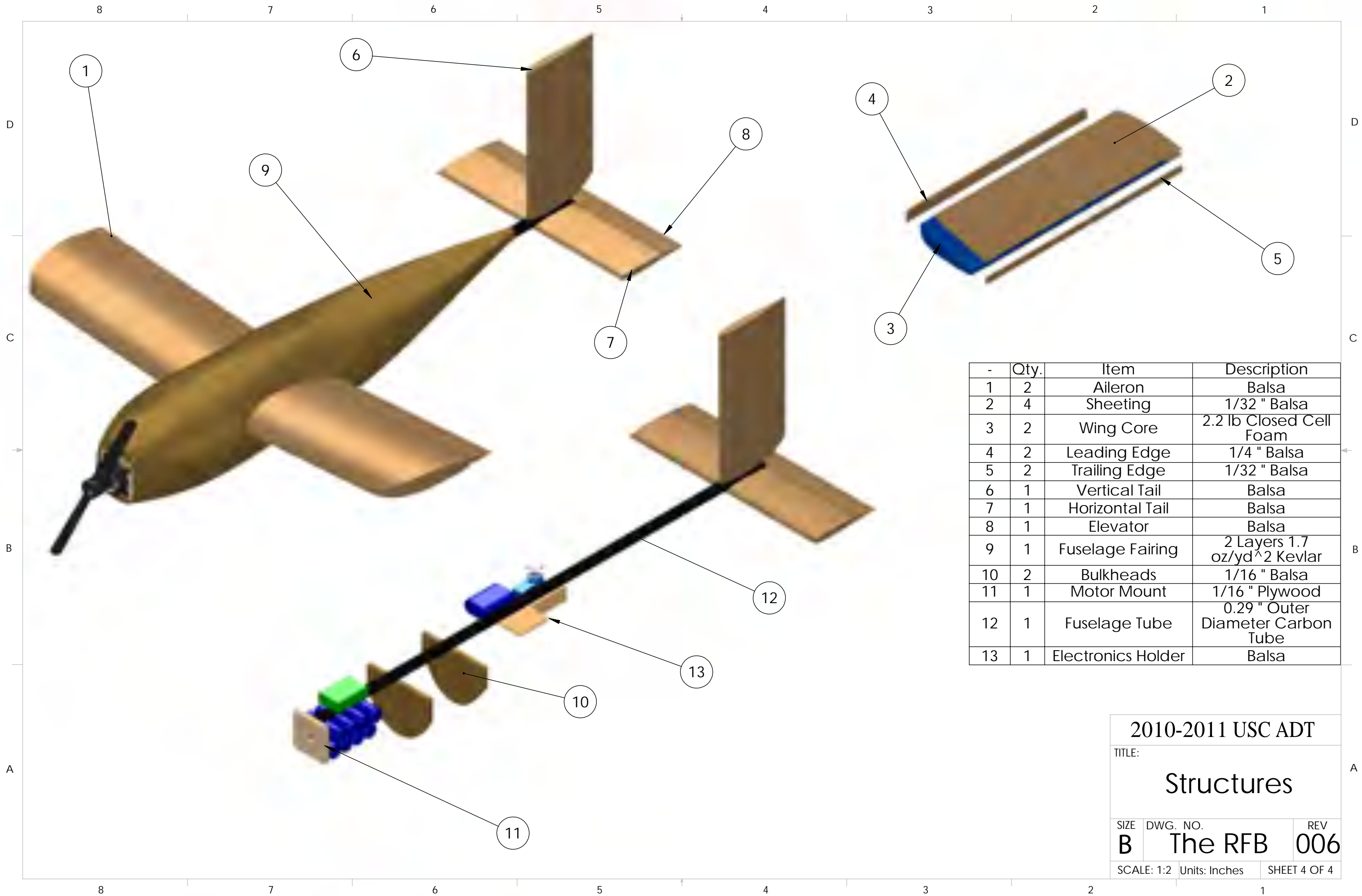
| - | Qty. | Item | Description |
|---|------|------------------|-----------------------------------|
| 1 | 1 | Prop | APC 6x5.5 Electric |
| 2 | 1 | Motor | Tmotor T1805 |
| 3 | 1 | ESC | Thunderbird 18A |
| 4 | 1 | Reciever | Berg Microstamp 4L |
| 5 | 1 | Reciever Battery | 4-Cell KAN 150 mAh Ni-Cad |
| 6 | 1 | Flight Battery | 8-Cell 2/3 AAA KAN 400 mAh Ni-Cad |
| 7 | 2 | Servo | Blue Bird S0251 Micro Servo |
| 8 | 2 | Aileron | BA527ls 20% Root Chord |
| 9 | 1 | Elevator | NACA0010 20% Root Chord |

2010-2011 USC ADT

TITLE:
Systems

| | | |
|----------|----------------|------------|
| SIZE | DWG. NO. | REV |
| B | The RFB | 006 |

SCALE: 1:1.5 Units: Inches SHEET 3 OF 4



| - | Qty. | Item | Description |
|----|------|--------------------|--|
| 1 | 2 | Aileron | Balsa |
| 2 | 4 | Sheeting | 1/32 " Balsa |
| 3 | 2 | Wing Core | 2.2 lb Closed Cell Foam |
| 4 | 2 | Leading Edge | 1/4 " Balsa |
| 5 | 2 | Trailing Edge | 1/32 " Balsa |
| 6 | 1 | Vertical Tail | Balsa |
| 7 | 1 | Horizontal Tail | Balsa |
| 8 | 1 | Elevator | Balsa |
| 9 | 1 | Fuselage Fairing | 2 Layers 1.7 oz/yd ² Kevlar |
| 10 | 2 | Bulkheads | 1/16 " Balsa |
| 11 | 1 | Motor Mount | 1/16 " Plywood |
| 12 | 1 | Fuselage Tube | 0.29 " Outer Diameter Carbon Tube |
| 13 | 1 | Electronics Holder | Balsa |

2010-2011 USC ADT

TITLE:
Structures

| | | |
|--------------------------|----------------------------|-------------------|
| SIZE B | DWG. NO. The RFB | REV 006 |
| SCALE: 1:2 Units: Inches | | SHEET 4 OF 4 |



6. Manufacturing Plan and Processes

The team examined several different methods and processes that would provide the desired characteristics for each major component of the entire aircraft – wing, empennage, and fuselage. Each major component underwent a downselect to determine its best-suited manufacturing technique.

6.1 Manufacturing Techniques

- **Solid Balsa Wood** – A solid piece of balsa wood is sanded with guides serving as female mold of the airfoil shape. This method serves as the baseline technique against which the other techniques are compared in the downselect.
- **Balsa Wood Build-up** – The spars use spruce pine or basswood with balsa ribs and shear-webs. Other areas carrying high loads are reinforced by Spruce, plywood, or composites. The structure is then covered with ParkKote Lite, a Mylar based skin material. For the fuselage, balsa bulkheads define the shape, with plywood bulkheads at the wing interface. The skin of the fuselage is either balsa sheet or ParkKote. For balsa built-up parts, a reusable jig must be constructed for alignment of components during the build.
- **Fiberglass-Over-Foam** – A foam core is cut by a hot wire or sanded to the desired shape and then covered with fiberglass. The fiberglass skin carries the main loads of the structure, and the foam core usually remains as part of the structures to aid in maintaining rigidity and shape. This method is common for manufacturing wings but is less common for fuselages since the foam core must be removed to make room for the payloads and propulsion components.
- **Balsa-Over-Foam** – This method is similar to the Fiberglass-Over-Foam method, but the foam core is covered with balsa. The intent is that the balsa skin carries the majority of the loads, but in this case the foam carries some of the shear forces in addition to creating the shape of the airfoil. Since the balsa is rigid by itself, some of the foam can be removed to save weight without adversely affecting the structural integrity of the wing.
- **Monocoque** – A monocoque part can be made using two methods. In the first method, a prototype of the component is constructed with fiberglass over shaped foam, or 3D printed material. The prototype is painted with surface coat and heavy fiberglass is laid up over it, creating a female mold. In the second method, a female mold is made directly from 3D printed material, polished, and used to lay up a part.
- **Balsa & Composite Hybrid** – Composites and balsa built-up sections are used. Composites are used in areas of high stress concentration, such as spars, while balsa ribs keep the shape of the part in areas that do not demand structural strength. Weight is conserved by using balsa in these areas and by utilizing the great strength-to-weight ratio of composite materials.
- **Carbon Tube Hybrid** – For the fuselage, a carbon tube would act as the spine joining the wing, fuselage and empennage together. This technique reduces the structural requirements of the fuselage and ensures the correct alignment of the empennage after several landings.



6.2 Figures of Merit

Qualitative analysis of each manufacturing technique was completed with a FOM analysis. Pugh's method was used for the downselect method. The FOMs were the following:

- **Skill Level** – When deciding on the manufacturing technique, the skills required and experience of team members in the various techniques must be considered. The effect of skill level is two-fold: if there are only a few team members skilled in a particular technique then time must be spent training others; if there are no team members sufficiently experienced in a particular technique then a substantial amount of time must be spent developing procedures and skills. A score of 1 indicates that no training or development time is required, 0 indicates that there is sufficient skills on the team already but some training is required, and -1 indicates a skills shortage requiring notable training and development time.
- **Manufacturing Time** – The manufacturing time for a given method was based on previous experience. The manufacturing time FOM is primarily a function of the amount of tooling required and cure time in addition to time efficiency in terms of the man-hours required per part: -1 indicates substantial tooling preparation and cure times leading to reduced time efficiency, 0 indicates an efficient but still labor intensive technique while 1 indicates a partially automated process with a very high time efficiency.
- **Weight** – The most important factor in Total Flight Score as shown in § 3.3. This FOM is relative to the baseline technique.
- **Specific Strength** – Each part must be able to survive expected loads, especially since Mission 2, a heavy lift mission, is the most important of the three missions. The specific strength measures the ultimate stress of the material or composite in relation to its density. The specific strength is an effective normalized method parameter with which to compare different materials.
- **Reparability** – The ability to repair any parts in a short time frame is important in a competition scenario. If a part cannot be easily repaired or must be rebuilt entirely if damaged then this will adversely affect the team's performance in the competition, as it will be necessary to submit to new technical inspection after each repair. A score of 1 indicates the possibility of quick repairs with minimal change to aircraft performance, 0 indicates repairs that are time consuming or may be detrimental to aircraft performance, and -1 indicates the necessity for a complete rebuild of the part or intolerable loss of aircraft performance.
- **Durability** – Certain components will experience substantial mechanical wear in normal use, such as the fuselage which must also serve as a skid plate during landing. This measures the ability of the material or composite to resist such wear relative to the baseline material.
- **Internal Volume and Access** – This is a consideration of the amount of internal volume created by each technique, which is especially important for the fuselage. These are considered relative to the baseline technique.



6.3 Manufacturing Downselects

Using the FOM-based downselects, the manufacturing method for each major component of the airplane was determined from the list of main construction techniques outlined in § 6.1. Construction methods that were deemed appropriate for a particular component are described in the following sub-sections.

6.3.1 Fuselage

6.3.1.1 Construction Method

The main function of fuselage was to hold the payloads and internal electrical systems, provide a streamlined body that incorporated other sub-components, and distribute the loads. The fuselage had to be constructed so that it could withstand payload loading, unloading, and tough landings. The downselect in Table 18 reflects these requirements and displays the best choice for the fuselage to be a carbon tube hybrid.

| Figure of Merit | Weight Factor | Balsa Build-Up | Fiberglass Over-Foam | Monocoque | Balsa/Composite Hybrid | Carbon Tube Hybrid |
|-----------------|---------------|----------------|----------------------|-----------|------------------------|--------------------|
| Skill Level | 12 | 1 | 0 | -1 | 1 | 1 |
| MFTG Time | 8 | 0 | -1 | -1 | -1 | -1 |
| RAC (Weight) | 30 | 1 | -1 | 0 | 1 | 1 |
| Specific Str. | 15 | 0 | -1 | -1 | 0 | 1 |
| Reparability | 5 | 1 | -1 | -1 | 0 | 1 |
| Durability | 10 | -1 | 0 | 1 | 1 | 1 |
| Access | 20 | 0 | -1 | 1 | 0 | 1 |
| TOTAL | 100 | 37 | -78 | -10 | 44 | 84 |

Table 18: Fuselage manufacturing downselect.

6.3.1.2 Material Selection

The downselect in Table 18 shows that a carbon tube hybrid fuselage will be used, but this still leaves a question of the material to be used in the construction of the aero-fairing to contain the propulsion systems and payloads. The primary requirements of this material are that it must withstand the mechanical wear from landing and that it has as minimal effect on the RAC as possible.

The composite material choices for the fuselage skin were the following:

- **Kevlar** – One and two layers of 1.7 oz/yd² and 3.4 oz/yd² Kevlar bi-directional cloth were considered. One layer of 3.4 oz/yd² Kevlar was used as the baseline for the down select.
- **Carbon** – One and two layers of 2.3 oz/yd² Carbon fiber bi-directional cloth were considered.
- **Fiberglass** – One layer of 5.6 oz/yd² fiberglass bi-directional cloth was considered.

The FOMs for material selection were the following:

- **Weight** – The weight of the skin material was decided to have the largest weight factor because of the RAC's contribution to Total Flight Score.
- **Conformation** – Each sample was rated for its conformation to a fuselage mold with complex curves. This is important from a manufacturing point of view since certain materials could



preclude the use of complex shapes for the fuselage, which will adversely affect aircraft performance.

- **Wear** – Samples of each skin option were made and were dragged along the ground under 3 lb of weights to simulate loaded mission landing. The wear of the material was compared by inspecting for tears and holes.

The optimum choice for composite material was selected through a downselect, shown in Table 19. One layer of 1.7 oz/yd² Kevlar were chosen as the fuselage skin.

| Figure of Merit | Weight Factor | Kevlar, 1 ply, 1.7oz/yd ² | Kevlar, 2 ply, 1.7oz/yd ² | Kevlar, 1 ply, 5 oz/yd ² | CF, 1 ply, 2.3oz/yd ² | CF, 2 ply, 4.6 oz/yd ² | FB, 1 ply, 5.6oz/yd ² |
|-----------------|---------------|--------------------------------------|--------------------------------------|-------------------------------------|----------------------------------|-----------------------------------|----------------------------------|
| RAC (Weight) | 50 | 1 | 0 | 0 | 0 | -1 | -1 |
| Conformation | 30 | 1 | 1 | -1 | 1 | 0 | 0 |
| Wear | 20 | 0 | 0 | 0 | -1 | -1 | -1 |
| TOTAL | 100 | 80 | 30 | -30 | 10 | -70 | -70 |

Table 19: Fuselage skin material downselect.

6.3.2 Wing

Since the airplane was designed to be small enough to fit inside the suitcase without disassembling the wings, the wings had no joint penalties. Initially balsa build-up was chosen as the most viable manufacturing process for its low weight and familiarity and simplicity. Moreover, high-weight and time-consuming methods such as molded composite and fiberglass over foam were ruled out to maintain a lightweight and simple design. However, during further development in the detailed phase, hybrid processes such as balsa over foam were suggested that would provide a viable light-weight and high specific strength solution. Table 20 displays the optimum choice for wing construction technique is balsa-over-foam.

| Figure of Merit | Weight Factor | Solid Balsa | Balsa Build-Up | Fiberglass-Over-Foam | Balsa-Over-Foam | Monocoque | Balsa/Composite Hybrid |
|-----------------|---------------|-------------|----------------|----------------------|-----------------|-----------|------------------------|
| Skill Level | 12 | 1 | 1 | 0 | 1 | -1 | 0 |
| MFTG Time | 9 | 0 | 0 | -1 | 1 | -1 | -1 |
| RAC (Weight) | 30 | 1 | 1 | -1 | 1 | 0 | 0 |
| Specific Str. | 27 | 0 | 0 | 1 | 0 | 1 | 1 |
| Reparability | 3 | 0 | -1 | -1 | 0 | -1 | 0 |
| Durability | 12 | 0 | -1 | -1 | 0 | 1 | 1 |
| TOTAL | 100 | 42 | 27 | -27 | 51 | 15 | 30 |

Table 20: Wing manufacturing downselect.



6.3.3 Empennage

The tail surfaces were initially chosen to be constructed out of solid balsa in the preliminary design plane, RFB 004. This method was maintained for the detailed design plane, RFB 006, since the tail surfaces, being so small, would not see any weight-savings by being constructed of balsa-over-foam as the wing was, and they would be easier and more efficient to fabricate using solid balsa. Table 21 indicates that the best choice for empennage construction technique is the solid balsa.

| Figure of Merit | Weight Factor | Solid Balsa | Balsa Build-Up | Fiberglass-Over-Foam | Balsa-Over-Foam | Monocoque | Balsa/Composite Hybrid |
|-----------------|---------------|-------------|----------------|----------------------|-----------------|-----------|------------------------|
| Skill Level | 12 | 1 | 1 | 0 | -1 | -1 | 0 |
| MFTG Time | 9 | 1 | 0 | -1 | 1 | -1 | -1 |
| RAC (Weight) | 30 | 1 | 1 | -1 | 1 | 0 | 0 |
| Specific Str. | 27 | 0 | 0 | 1 | 0 | 1 | 1 |
| Reparability | 3 | 0 | -1 | -1 | 0 | -1 | 0 |
| Durability | 12 | 0 | -1 | -1 | 0 | 1 | 1 |
| TOTAL | 100 | 51 | 27 | -27 | 27 | 15 | 30 |

Table 21: Empennage manufacturing downselect.

6.3.4 Manufacturing Summary

The following table portrays a summary of the manufacturing techniques used on each major component of the aircraft.

| Component | Manufacturing Technique |
|-----------|--|
| Fuselage | Wrapped carbon fiber tube fuselage with molded composite aero fairing. Layup schedule of the fuselage is as follows: 2 layers of bi-directional 1.7 oz/yd ² kevlar. Forward bulkhead 1/16 in plywood, aft bulkheads 1/16 in balsa wood. |
| Wing | 2.2 pcf insulation foam core, 60% solidity, with balsa leading and trailing edges, 1/32 in balsa skins. Solid balsa control surfaces. |
| Empennage | Solid balsa with solid balsa control surfaces. |

Table 22: Manufacturing summary.

6.4 Manufacturing Schedule

The manufacturing schedule was created to ensure that each major component of the aircraft was delivered on time. Keeping to the schedule was crucial to allow ample time to assemble each component in the final flying aircraft and to provide adequate time for flight testing. The manufacturing schedule is shown in Figure 33.



Figure 33: Manufacturing schedule.

7. Testing Plan

A complete test plan was implemented in order to verify predictions from PlaneSizer and the other analytical tools used. The test program included laboratory and flight tests during the entire development of the competition aircraft.

7.1 Schedule

A schedule of testing was developed and maintained to coordinate the test program with the design and building phases of the project, shown in Figure 34.

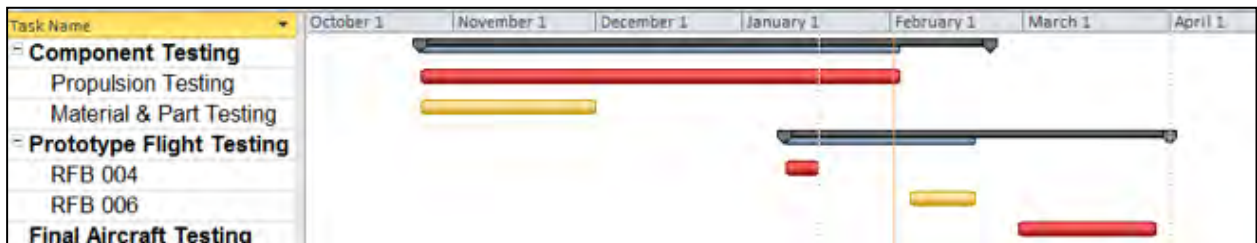


Figure 34: Testing schedule.



7.2 Subsystems Testing

7.2.1 Structures

Though foam was chosen as the wing structure from § 6.3.2, further specific decisions had to be made about the details of the foam wing. For example, to save weight, it would seem profitable to carve out blocks of the foam and make pseudo “ribs” out of the remaining foam. However, taking out the foam would most likely alter the structure of the foam. Therefore, several variations of the basic foam wing were chosen to be three-point tested:

- Solid Balsa
- Solid Foam
- Solid Foam with Carbon Spar with Monokote
- Solid Foam with Balsa Wood Sheeting
- Ribbed Foam with Carbon Spar and Monokote

The strongest variation of the foam wing could then be chosen to ensure the withstanding of possible flight loads.

7.2.2 Propulsion

As the high-scoring propulsion package was chosen based on the MDO’s output, it was necessary to test the propulsion system to ensure real-world performance matched the MDO’s predicted result. Propulsion components were static tested and flight tested, with component testing primarily emphasizing battery performance, as past experience has shown that real-world battery performance often differs from the manufacturer’s claims, and is the most significant detriment to predicted versus real-world performance. Airborne testing of the MDO output max performance propulsion system commenced with flight testing of the RFB 006 airframe, in order to validate the performance claims of the MDO’s output.

7.3 Flight Testing

Prototype testing consisted of flying two iterations of the aircraft, RFB 004 and RFB 006. Both of these airplanes were used as platforms for testing aerodynamics, stability and control, and propulsion systems, specifically at very low Reynolds numbers due to the small size of the aircraft. Constructing these iterations also gave the opportunity to refine manufacturing techniques in building aircraft components at such a small scale. This experience proved to be invaluable since all of the aircraft constructed in previous years were much larger and small mistakes, such as miniscule ripples in the wing, were less noticed in the overall performance of the aircraft.

Onboard testing hardware was not used due to the small size and light weight of the aircraft. For example, the onboard testing hardware available would have increased RFB 006’s target weight by 50% and would have significantly affected the performance of the airplane. Therefore, flight test performance results were gathered primarily through observations and pilot input. The team used a preflight checklist to ensure the safe operation of all airplane components prior to flight. This checklist is shown in Table 23.

| PRE-FLIGHT CHECKLIST | |
|------------------------|---|
| Action | Description |
| Remove Fuse | <input type="checkbox"/> Ensure aircraft is not armed |
| Check CG & Weight | <input type="checkbox"/> Ensure proper CG location <input type="checkbox"/> Record total weight of aircraft |
| Check ESC | <input type="checkbox"/> Secure to airframe <input type="checkbox"/> Plug in motor |
| Check Batteries | <input type="checkbox"/> Verify packs are peaked <input type="checkbox"/> Plus into ESC <input type="checkbox"/> Secure to airframe |
| Check Payloads | <input type="checkbox"/> Ensure proper payloads installed <input type="checkbox"/> Secure to airframe |
| Check Control Surfaces | <input type="checkbox"/> Secure mechanical connections <input type="checkbox"/> Secure electrical connections |
| Check Rx Connections | <input type="checkbox"/> Ch. 1 – Aileron <input type="checkbox"/> Ch. 2 – Elevator <input type="checkbox"/> Ch. 3 – Throttle <input type="checkbox"/> Ch. 4 – Receiver Battery |
| Check Failsafe | <input type="checkbox"/> Switch off transmitter & verify failsafe functionality |
| Arm | <input type="checkbox"/> Clear prop disc <input type="checkbox"/> Insert fuse |
| POST-FLIGHT CHECKLIST | |
| Disarm | <input type="checkbox"/> Remove fuse <input type="checkbox"/> Turn off Tx <input type="checkbox"/> Disconnect batteries |
| Check Weight | <input type="checkbox"/> Record total weight of aircraft |

Table 23: Pre- and post-flight checklist.

8. Performance Results

Once the tests were completed, the data was compiled and analyzed, and designs were adjusted accordingly to make necessary improvements. This section depicts performance results of the component and flight testing described in § 7 as well as the corresponding alterations.

8.1 Subsystems

8.1.1 Structures

The structures team performed three-point testing on different sections of wings as described in § 7.2.2. Of the five tested sections, the solid foam performed so inferior to the other four that its results are not listed in the following tables and graphs below. The candidates tested are pictured below in Figure 35.

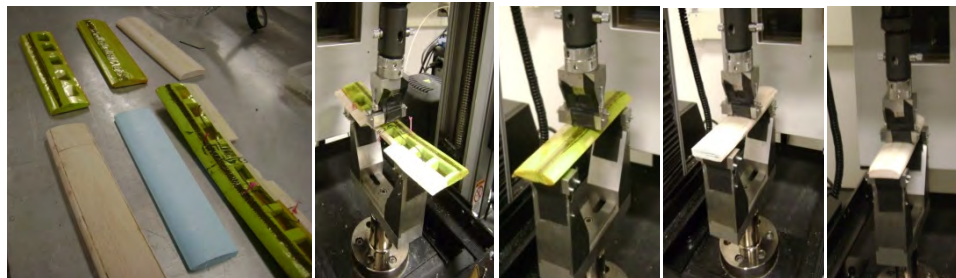


Figure 35: Wing test pieces (left to right: all candidates, ribbed foam with carbon spar and monokote, solid foam with carbon spar and monokote, solid foam with balsa wood sheeting, solid balsa).



The results from the three-point testing are shown below in Figure 36 and Table 24. The results suggest that balsa sheeted foam is the best candidate for the wing build up, as it balances weight and specific strength. Even though the maximum loading per unit weight of solid balsa is superior to that of the other tested candidates, the overall weight of a solid balsa piece is greater than the other candidates, and upon fabricating the different test pieces, the balsa-over-foam method proved easier to manufacture and yielded a more accurately shaped wing than the solid balsa method. Since the testing showed that all candidates met and surpassed structural requirements, the lightest one was chosen. Therefore balsa-over-foam method is the chosen fabrication method for the final competition plane wing.

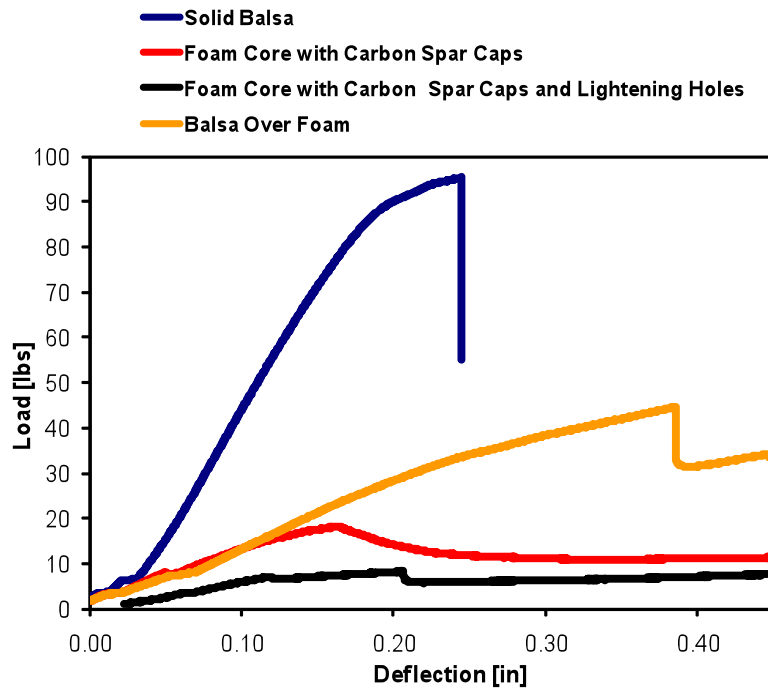


Figure 36: Three-point wing section testing results.

| Wing Build-Up Method | Ribbed Foam with Carbon Spar and Monokote | Solid Foam with Carbon Spar and Monokote | Solid Foam with Balsa Wood Sheeting | Solid Balsa |
|---------------------------|---|--|-------------------------------------|--------------|
| Weight (lb) | 0.022 | 0.029 | 0.035 | 0.047 |
| Max. Loading (lbs) | 8.3 | 18.3 | 44.6 | 95.4 |

Table 24: Wing section testing results: wing section weight and maximum loading before breaking.

8.1.2 Propulsion

Battery discharge performance was tested in order to characterize a reasonable expectation for actual performance vs. manufacturer claims. A major problem discovered with the small battery cells for this size airplane is a significant performance loss due to internal resistance. Internal resistance causes the pack's voltage to drop as current is increased, which impacts the maximum power output of the cells.

Airborne battery testing was commenced using the test bed airframe in Figure 37, which was large enough to carry the data logging hardware that was too heavy to install on the RFB 004 and 006 airframes.



Figure 37: Test bed airplane used for airborne battery testing.

A battery discharge curve captured using Castle Creations ICE data onboard the test bed airframe is displayed in Figure 38, showing the substantial battery voltage drop with current, typical for these small cells. The charged no-load voltage of the 11 cell pack tested was 15 V, however, once stabilized in the discharge curve, the pack voltage had dropped to 10 V with 7 A of current. This result was typical for all tested cells. Another performance detriment observed in testing was poor capacity; that is, due to the voltage decrease under load, the total mAh available were substantially less than the manufacturer's advertised capacity. This result appears typical for small NiMH cells being taxed under high discharge current, with tested capacities being as low as 60% of the manufacturer's claim. The integrated discharge curve in Figure 38 yields only 250 mAh of capacity compared to the manufacturer's stated capacity of 400 mAh. Based on the result of this testing, conservative values of 60% of the manufacturer's claimed voltage and battery capacity were used throughout the propulsion performance section of the MDO, to ensure that the resultant high-scoring propulsion package was indeed feasible in the real world.

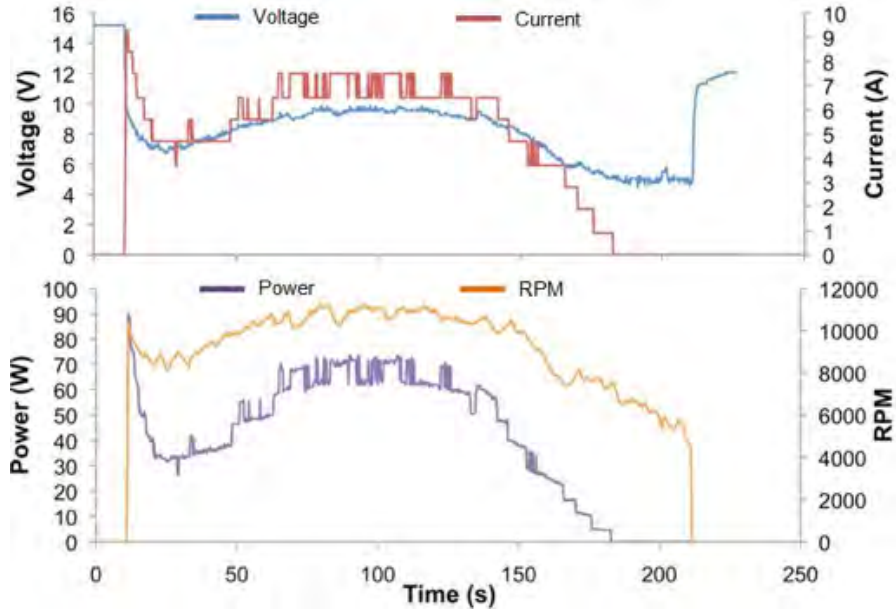


Figure 38: Airborne test data for 11S KAN 400 2/3AAA battery.

The MDO's best performing propulsion package was installed on RFB 006 for flight testing. Qualitatively, the empty airplane had ample power, acceleration, climb rate, and partial-throttle duration, although a quantitative analysis could not be completed due to the aircraft's stability issues at high speed which is where the propulsion system would have been operating at the peak of its ability. At the time of this writing detailed performance analysis of the final propulsion package will be forthcoming after test flights of the next airframe iteration.

8.2 Flight Testing

The RFB 006 prototype was the first aircraft iteration flown after Critical Design Review. As mentioned in § 5 and § 5.3.2, this airplane had a smaller span and AR than RFB 004 had and was flown with ailerons and elevator but without a rudder. The empty aircraft weight pre-flight was 0.48 lbs, which was slightly heavier than the design weight portrayed in § 5.5. Most of the excess weight resulted from an oversized receiver battery and possibly an overly-robust tail.

RFB 006 initially flew very well in both a trim flight and a Mission 1 simulation. The aircraft was highly stable and held its turns very well without tip stalling, which had been a problem with RFB 004. RFB 006 flew four laps in the Mission 1 simulation with a recorded speed of 67 ft/s (estimated from video footage). However, the airplane was only flown at a 55% throttle setting due to increases in Dutch roll characteristics at higher velocities. The aircraft was also overly sensitive to aileron inputs and lagged in response to elevator inputs. Therefore, the right aileron was removed and an elevator extension was added.

Troubles arose when RFB 006 was loaded with a payload for the first time. The aircraft then developed a severe tip stall problem while attempting to roll. It was determined that this resulted from the

combination of the heavy loaded weight with only a left wing aileron. While attempting to turn right with a payload, the single aileron had to be positioned at its maximum downward deflection to produce an acceptable turning radius. At maximum downward deflection, the aileron stalled the left wing causing a roll reversal into a nose-over dive. Essentially, pilot input would stall the left wing when attempting to roll right. The success of the first two flights could not be repeated after a series of crashes which altered the aircraft's geometry. The lessons learned from the RFB 006 flight test were are shown in Table 25.

| Issue | Solution |
|--|--|
| Soft elevator response | Increase elevator effectiveness |
| Dutch roll at high throttle settings | Increase directional stability |
| Tip stall while carrying payload | Fly with two ailerons |
| Deteriorated performance after hard landings | Increase robustness of fuselage and internal bulkheads |

Table 25: Problems encountered in RFB 006 flight test and corresponding solutions.



Figure 39: RFB 006 in Flight Tests.



9. References

- ¹ "2010/11 Rules and Vehicle Design." AIAA DBF Homepage. 23 Sept. 2010. 06 Oct. 2010
<http://www.aiaadb.org/2011_files/2011_rules.htm>
- ² Ullman, David G. *The Mechanical Design Process*. 1992. Ed. Jonathan Plant and Amy Hill. 3rd ed. New York: McGraw-Hill Higher Education, 2003.
- ³ "Tail Design and Sizing." Stanford University. 28 Feb. 2010. 19 Jan. 2011.
<<http://adg.stanford.edu/aa241/stability/taildesign.html>>.
- ⁴ "Longitudinal Static Stability." 3 Feb. 2011. <<http://adg.stanford.edu/aa241/stability/staticstability.html>>.
- ⁵ Roskam, J. *Airplane Flight Dynamics and Automatic Flight Controls: Part 1*. 5. Lawrence, KS: Design Analysis Research Corporation, 2007.
- ⁶ Drela, Mark and H. Youngren. "Athena© Vortex Lattice Program." 23 Aug. 2010. <<http://web.mit.edu/drela/Public/web/avl/>>.
- ⁷ Drela, Mark. "XFOIL Subsonic Airfoil Development System." 23 Aug. 2010. <<http://raphael.mit.edu/xfoil/>>.
- ⁸ "XFLR5." 23 Aug. 2010. <<http://xflr5.sourceforge.net/xflr5.htm>>.
- ⁹ Weather Underground. 30 January, 2011. <<http://www.wunderground.com/>>.
- ¹⁰ McArthur, John. "Aerodynamics of Wings at Low Reynolds Numbers: Boundary Layer Separation and Reattachment." Diss. University of Southern California, 2008. Print.
- ¹¹ Hoerner, Sighard. "Fluid-Dynamic Drag: Practical Information on Aerodynamic Drag and Hydrodynamic Resistance." Albuquerque, 1965.
- ¹² Page, Mark. "Model Airplane Drag Cook-book." Internal Document. 2008.
- ¹³ Mark Drela and Harold Youngren, "AVL 3.26 User Primer," Massachusetts Institute of Technology, 28 Feb. 2010 <http://web.mit.edu/drela/Public/web/avl/avl_doc.txt>.
- ¹⁴ MIL-F-8785C, *Flying Qualities of Piloted Airplanes*, Military Specification, 1980.

The logo features a stylized black and yellow shape resembling a wing or a flame, with yellow accents on the black background.

PURDUE

AERONAUTICS
& ASTRONAUTICS



AIAA Design Build Fly
Team **Golfstream**



Table of Contents

| | |
|--|----|
| 1.0 Executive Summary | 3 |
| 2.0 Management Summary | 5 |
| 2.1 Design Team Organization | 5 |
| 2.2 Milestone Chart | 5 |
| 3.0 Conceptual Design | 6 |
| 3.1 Mission Requirements | 7 |
| 3.2 Translating Mission Requirements to Design Requirements | 8 |
| 3.3 Concepts and Configurations | 11 |
| 4.0 Preliminary Design | 17 |
| 4.1 Models | 18 |
| 4.2 Design Trades | 23 |
| 4.3 Aerodynamics Results | 25 |
| 4.4 Stability and Controls Results | 29 |
| 4.5 Structural Model Results | 32 |
| 4.6 Propulsion Model Results | 33 |
| 4.7 Estimated Aerodynamic Characteristics | 35 |
| 4.8 Estimated Mission Performance | 37 |
| 5.0 Detail Design | 37 |
| 5.1 Dimensional Parameters | 37 |
| 5.2 Structural Characteristics and Capabilities | 38 |
| 5.3 System Design, Component Selection, Integration, and Architecture | 38 |
| 5.4 Propulsion System Analysis | 39 |
| 5.5 Weight and Balance Table | 40 |
| 5.6 Mission Performance | 40 |
| 5.7 Flight Performance | 41 |
| 5.8 Drawing Package | 41 |
| 6.0 Manufacturing Plan | 46 |
| 6.1 Prototype Construction | 46 |
| 6.2 Material Analysis and Manufacturing Selection | 46 |
| 6.3 Manufacturing Milestones | 47 |
| 7.0 Testing | 48 |
| 7.1 Objectives | 48 |
| 7.2 Master Test Schedule | 50 |
| 8.0 Performance Results | 51 |
| 8.1 Subsystem Performance | 51 |
| 8.2 Aircraft Flight Performance | 55 |
| 9.0 Glossary of Variables | 57 |
| 10.0 References | 58 |



1.0 Executive Summary

This report presents the design, manufacturing, and testing processes conducted by Team Golfstream of Purdue University in preparation for the 2010-2011 AIAA/Cessna/RMS Student Design/Build/Fly Competition located in Tucson, AZ. The winner of this competition is the team that achieves the highest overall score, which is a combination of the written design report score and the total flight score. Total flight score is the sum of the three individual mission scores. The first mission is a dash flight where score is based on the number of laps completed in a four minute time span. Maximizing score in mission one requires a high flight velocity. The second and third missions are three-lap payload flights, requiring the aircraft to internally carry steel bars and golf balls, respectively. Maximizing score in missions two and three requires a large payload capacity. All mission scores are summed and then divided by the square root of the rated aircraft cost (RAC). Rated aircraft cost is evaluated as the maximum empty flight weight of the aircraft, so a low weight is desirable. Additionally, the aircraft must be hand-launched and all aircraft components must fit inside a standard, FAA approved carry-on suitcase¹.

A scoring analysis was performed to identify how to maximize score based on the key mission requirements. From this analysis, it was determined that minimizing the rated aircraft cost would be the most important factor in maximizing total flight score. This was accomplished by maximizing the aerodynamic efficiency of the aircraft to reduce battery weight. A flying wing design was chosen because of its inherent high lift to drag ratio and low overall weight. A high lift to drag ratio would help increase the system efficiency, which reduces battery weight. Swept back wings with winglets were used to provide pitch and yaw stability. A fuselage was mounted underneath the wing to utilize the pendulum stability usually attributed to high-wing configurations. The fuselage was designed using carbon fiber and acts as a skid during landing, eliminating the additional weight and drag penalty associated with landing gear.

To develop an aircraft that would yield the maximum flight score, the spiral design methodology² shown by the schematic in Figure 1.1 was used. Each loop in the spiral design process represents a single iteration, during which the Raymer three phase design approach³ was taken. This allowed for risk evaluation and analysis before proceeding to the next design iteration². Each successive iteration advanced the aircraft toward an optimized design based on mission requirements. A series of four iterations were performed in this manner before a final detail design was generated.

The dimensions of this final aircraft are shown in Table 1.1. The aircraft uses a tractor propulsion system consisting of a Neu Neutrino 1210 brushless out-runner motor with a six-cell, 400 mAh NiMH battery pack and a 5.5x3.0 in. propeller.

Table 1.1: Aircraft geometry.

| Wingspan (in) | Root Chord (in) | Tip Chord (in) | Mean Aerodynamic Chord (in) | Quarter Chord Sweep Angle (Degrees) |
|---------------|-----------------|----------------|-----------------------------|-------------------------------------|
| 20 | 4.90 | 2.45 | 4.20 | 30 |

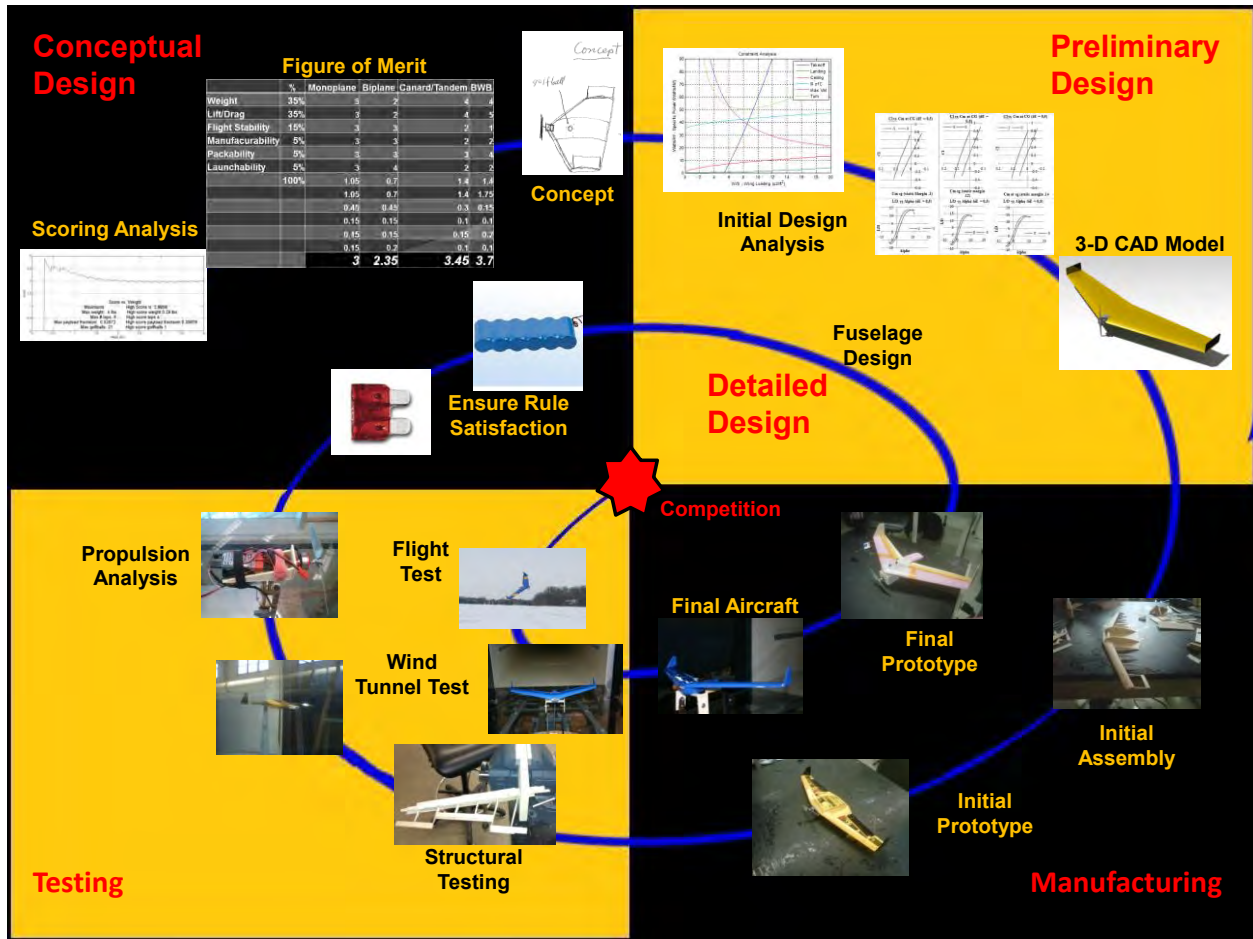


Figure of Merit

| | % | Monoplane | Biplane | Canard/Tandem | BWB |
|-------------------|-----|-----------|---------|---------------|------|
| Weight | 35% | 3 | 2 | 4 | 4 |
| Lift/ Drag | 35% | 3 | 3 | 4 | 4 |
| Flight Stability | 15% | 3 | 3 | 2 | 1 |
| Manufacturability | 5% | 3 | 3 | 2 | 2 |
| Packability | 5% | 3 | 3 | 3 | 4 |
| Launchability | 5% | 3 | 3 | 2 | 2 |
| 100% | | 1.92 | 0.7 | 1.4 | 1.4 |
| | | 0.40 | 0.40 | 0.3 | 0.15 |
| | | 0.15 | 0.15 | 0.1 | 0.1 |
| | | 0.15 | 0.15 | 0.15 | 0.2 |
| | | 0.15 | 0.2 | 0.1 | 0.05 |
| | | 3 | 2.35 | 3.45 | 3.7 |

Figure 1.1: Spiral design schematic.

Flight and wind tunnel tests were performed on the final aircraft design, and performance characteristics for each mission were found. These performance characteristics are outlined in Table 1.2. Since score is calculated by dividing total mission score by rated aircraft cost, score is maximized through decreasing rated aircraft cost, or minimizing weight. To be competitive and increase total mission score, the aircraft must have high flight velocity for mission one and high payload capacity for missions two and three.

Table 1.2: Mission performance and capabilities.

| Mission One | | Mission Two | | Mission Three | |
|------------------------|-------|----------------------|-------|---------------------------|-------------|
| Cruise Velocity (ft/s) | 36 | | | | |
| Turn Velocity (ft/s) | 37 | | | | |
| Takeoff Weight (lbs) | 0.300 | | | Takeoff Weight (lbs) | 0.400 |
| Laps in 4:00 (min) | 4 | Takeoff Weight (lbs) | 0.400 | Number of Golf Balls | 1 |
| Estimated Max. Laps | 8 | Payload Weight (lbs) | 0.100 | Estimated Max. Golf Balls | 20 |
| Score | 0.50 | Score | 0.75 | Score | 0.10 |
| | | | | Total Score | 2.46 |

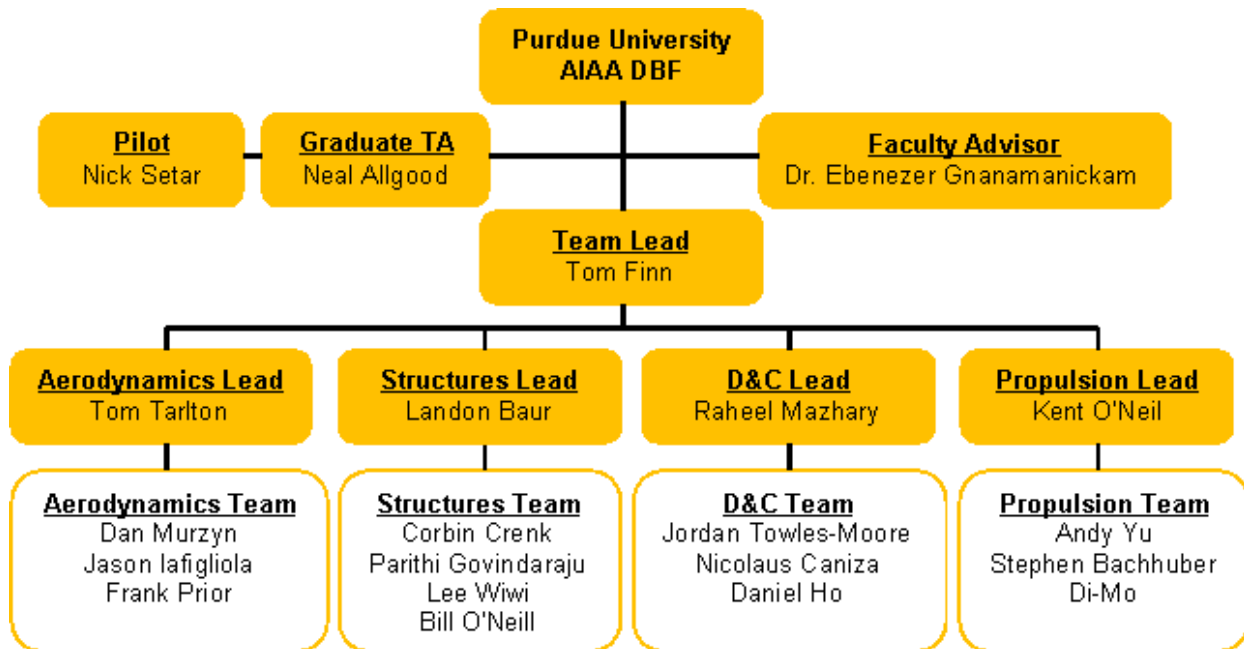


2.0 Management Summary

Team Golfstream is comprised of Purdue University students with different backgrounds and experience levels who share a common interest in aeronautics. During the first few weeks, the members familiarized themselves with the contest rules and analyzed the scoring system. Team members were then divided into sub-groups based on experience levels and areas of interest.

2.1 Design Team Organization

The focus areas of the sub-groups were: aerodynamics, structures, dynamics and controls, and propulsion. These sub-groups worked to optimize the aircraft with respect to their focus area in conjunction with the overall team goals. Keeping team efficiency and communication in mind, each team was assigned a team leader. Figure 2.1 illustrates the team organization.



Special thanks to Dillon McKenzie-Veal for CAD help.

Figure 2.1: Team organizational chart.

2.2 Milestone Chart

To streamline the design process, a Gantt chart was used to identify milestones to aid in keeping the team on schedule. Figures 2.2 and 2.3 present the corresponding charts outlining the fall and spring semesters.

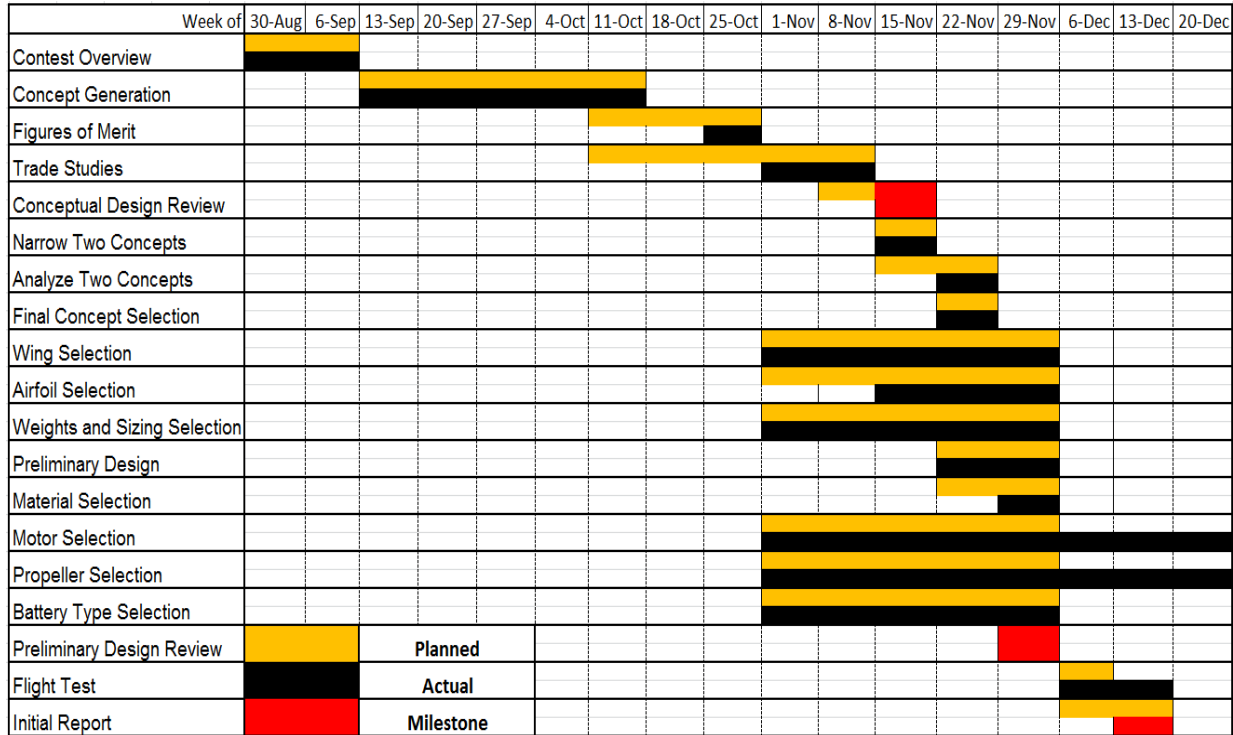


Figure 2.2: Fall milestone chart.

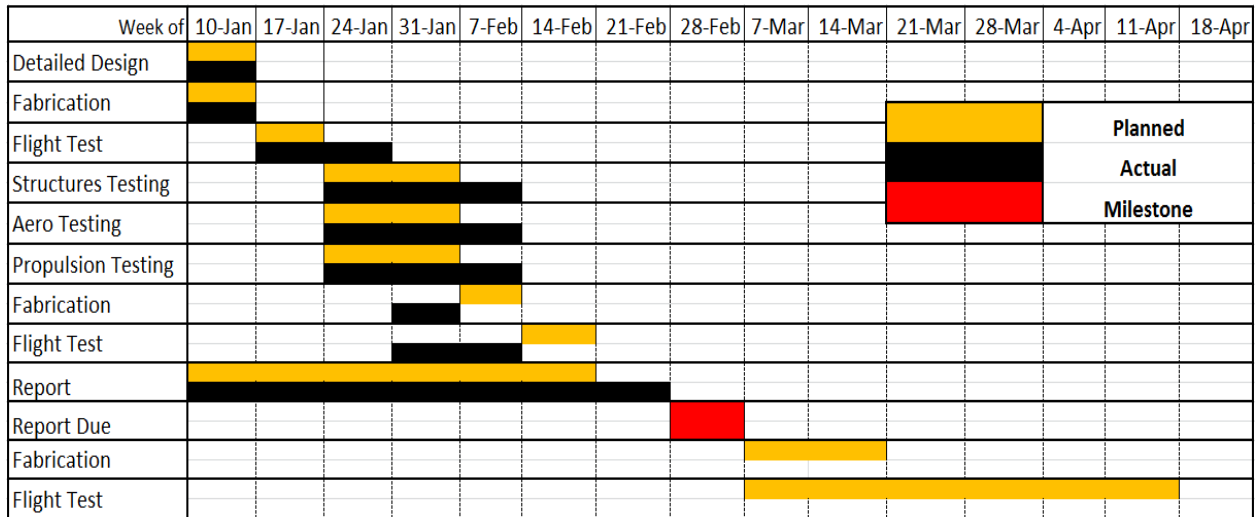


Figure 2.3: Spring milestone chart.

3.0 Conceptual Design

Conceptual design involved analyzing mission requirements, scoring equations, and design constraints to determine the aircraft configuration that would yield the maximum score.



3.1 Mission Requirements

The AIAA Design/Build/Fly Competition for 2010/11 consists of three flight missions. Requirements for these missions and competition constraints are given in the contest rules for the 2010/11 AIAA DBF competition¹. The goal of the competition is to successfully complete the missions, achieving a maximum total score while adhering to all competition rules.

3.1.1 Aircraft and Payload Requirements

The theme for this year's competition is a "Soldier Portable UAV," or unmanned aerial vehicle. Any aircraft configuration deemed ideal for scoring other than rotary wing or lighter-than-air may be used. Contest specified aircraft and payload requirements are as follows:

- Maximum battery weight of 0.75 lbs (only NiMH or NiCd batteries).
- 20 Amp fuse limit.
- The aircraft must be hand-launched for takeoff.
- A suitcase must contain the whole aircraft and tools necessary for assembly, except the transmitter.
- The sum of the suitcase's external dimensions (length, width, and height) is 45 in., with a maximum dimension of 22 in.
- All payloads are internally stored. Mission two uses steel bars and mission three uses golf balls.
- The steel bars are 3x4 in., with the thickness determined by the team.

3.1.2 Mission Profiles

Each team will attempt to complete the three missions with a maximum of four total flight attempts. The aircraft must be assembled and inspected within a five minute time span before each mission is attempted. The mission course is shown in Figure 3.1. The aircraft will be hand-launched, fly the 500 ft upwind leg, fly the 1000 ft downwind leg with a 360° turn, and fly the last 500 ft leg to complete one lap. Each mission must be completed before the next mission can be attempted. The aircraft must land on the runway without sustaining any major damage for an attempt to be counted as successful.

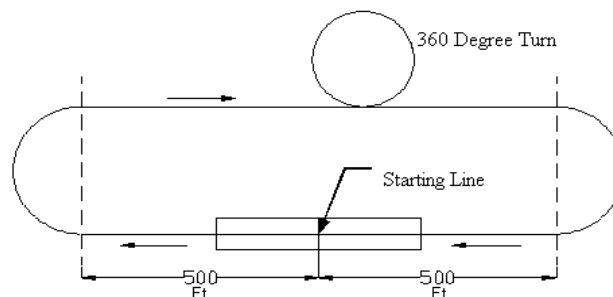


Figure 3.1: Course layout¹.



Each mission was designed to simulate a potential assignment for a soldier portable UAV. Mission one is a dash flight to complete the maximum number of laps within a four minute time limit. Mission two is a three lap payload flight with the team supplied steel bar. Mission three is a three lap payload flight with the competition supplied golf balls. The team selects the number of golf balls to be carried. Loading time is not a variable in the scoring equations, and flight time only factors into the score for mission one.

3.1.3 Scoring

Scoring equations were analyzed to determine the factors with the largest influence on overall flight score. In these equations, weight is measured using pounds, as specified by competition rules.

$$\text{Mission 1 Score} = N_{\text{laps}} / N_{\text{max}}$$

- N_{laps} is the number of completed laps flown.
- N_{max} is the maximum number of successful laps flown by any team for mission one.

$$\text{Mission 2 Score} = 3 * \text{Payload_Weight} / \text{Flight_Weight}$$

- Payload_Weight is the weight of the steel bar carried.
- Flight_Weight is the aircraft weight immediately after a successful flight.

$$\text{Mission 3 Score} = 2 * N_{\text{balls}} / N_{\text{max}}$$

- N_{balls} is the number of golf balls carried.
- N_{max} is the maximum number of golf balls successfully carried by any team for mission three.

$$\text{Total Flight Score} = \text{Mission 1} + \text{Mission 2} + \text{Mission 3}$$

$$\text{Total Team Score} = \text{Written Report Score} * \text{Total Flight Score} / \sqrt{\text{RAC}}$$

$$\text{RAC} = \text{Max}(\text{EW}_1, \text{EW}_2, \text{EW}_3)$$

- Rated aircraft cost (RAC) is the maximum empty weight of the aircraft recorded immediately after a successful scoring flight, where EW_n is the post-flight weight with the payload removed¹.

3.2 Translating Mission Requirements to Design Requirements

An initial scoring analysis was performed by perturbing baseline scoring parameters. This analysis proved inconclusive, as the sensitivity changed drastically with the RAC. This simplistic scoring analysis was replaced by an in-depth scoring analysis that sought to eliminate design variables. This scoring analysis takes into account all potential scoring scenarios for various configurations. Since this year's competition has a 20 Amp fuse and a 0.75 lb battery pack limit, it was evident that the aircraft would be smaller than previous competitions. Scores from missions one and three are nondimensionalized by the best competition values, so baseline estimates of these maximum values were made. To determine the



maximum score for mission two, a new variable, payload weight fraction, was defined as the payload weight divided by the flight weight. Historical data for payload weight fractions was researched using past DBF reports; however, no conclusive trend was found. Additionally, all historic data was obtained from aircraft much larger than this year's expected size¹.

Concerns arose over how the payload weight fraction may scale as the aircraft's empty weight approaches the minimum feasible weight limit. For instance, some quantities such as glue and wood only scale in discrete values. To more accurately estimate how payload weight fraction changes with the aircraft's empty weight, a smaller version of Purdue's 2009-2010 DBF competition aircraft was built and flown. In Figure 3.2, a trend was developed between last year's 5.7 lbs aircraft and this smaller 7 oz version. It was hypothesized that an aircraft could become so small that it could no longer carry a payload. Based on this hypothesis, a point is placed at the origin, representing a very small aircraft incapable of carrying a payload. This point was critical in generating a curve fit to estimate how payload fraction may vary with lightweight aircraft. Although this is a small sample size from which to draw a trend, these mark actual experimental data points and served as a starting point for the analysis. Using the curve fit from Figure 3.2, the maximum payload weight can be estimated from the associated rated aircraft cost, eliminating one scoring variable. The number of variables was further reduced by assuming that carrying more golf balls would not increase the profile drag. Therefore, the number of golf balls could be calculated based on the payload weight fraction. Score can be estimated by number of laps, rated aircraft cost, payload weight fraction, and maximum baselines.

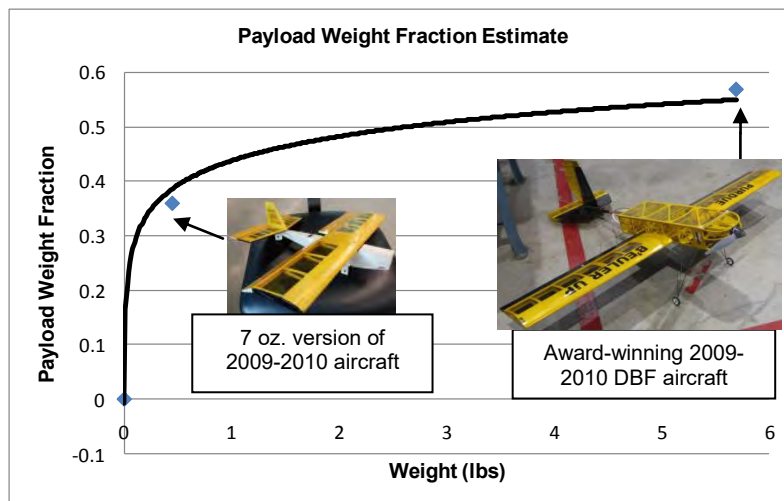


Figure 3.2: Payload weight fractions from Purdue aircraft.

A rudimentary Monte Carlo simulation was conducted using potential aircraft for all cases. This is a type of computational method that relies on taking repeated random samples to compute results. In this case, random baseline values were used to represent all conceivable planes and scenarios. Based on this simulation, Figures 3.3, 3.4, and 3.5 were generated.

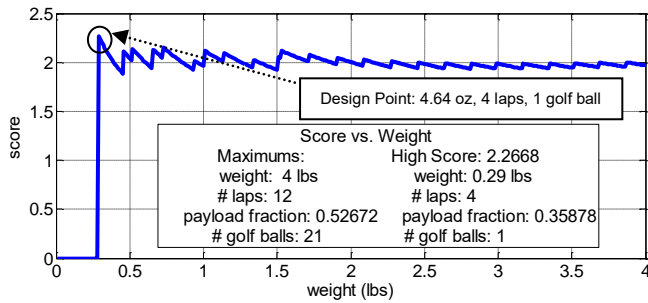


Figure 3.3: Score scenario.

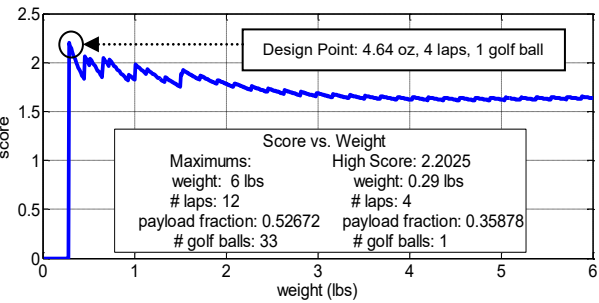


Figure 3.4: Score scenario.

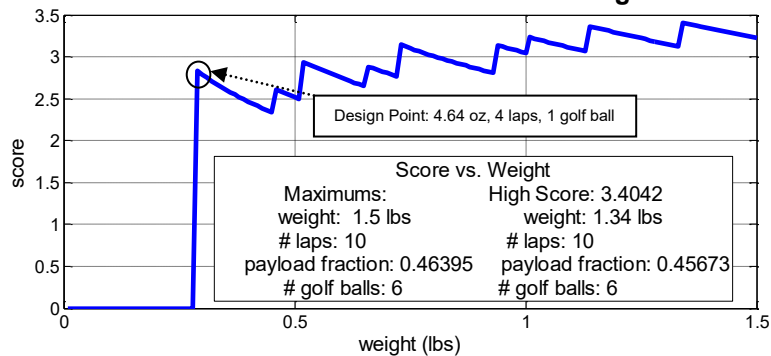


Figure 3.5: Score scenario.

Figures 3.3 and 3.4 describe scenarios where the winning aircraft weighs 4.64 oz, flies four laps, and carries one golf ball. For both scenarios, the maximum number of laps was 12 and the maximum number of golf balls was 21 and 33, respectively. This illustrates that, for most cases, a lower RAC is more important than carrying the most golf balls or flying the most laps. One scenario in which this is not the case is depicted in Figure 3.5, where the winning aircraft weighs 21.4 oz, carries six golf balls, and flies 10 laps. These also represent the maximum values for each scoring variable. As long as one team successfully flies a large number of golf balls, the lightest aircraft will score highest. This trend breaks down when all competition aircraft are relatively light and fly a comparable payload. In this case, the lightest aircraft scores high, but not the highest.

Using this information, building the lightest possible aircraft became the priority. The target weight of the aircraft was increased from 4.64 oz to 4.80 oz to allow for a 0.16 oz margin of error during manufacturing. This dictated building a 4.80 oz aircraft that could complete four laps, carry one golf ball, and carry one steel bar weighing the equivalent of a golf ball.

3.2.1 Translating Mission Requirements to Design Requirements Summary

- Aircraft Assembly – Create a design solution that can be assembled within five minutes while remaining as light as possible.
- Mission One: Dash to Critical Target – Create a design solution to successfully and timely complete an unloaded flight with the minimum possible weight.



- Mission Two: Ammo Re-Supply – Create a design solution that successfully carries one steel bar equivalent to a golf ball in weight for three laps.
- Mission Three: Medical Supply Mission – Create a design solution that carries one golf ball for three laps.
- Manufacturing – Produce a 4.80 oz aircraft that is easy to manufacture and repair.

3.3 Concepts and Configurations

The initial scoring analysis established that the aircraft needed to be as lightweight as possible. The aircraft must also be designed to fly all missions in accordance with the competition rules. Combining the need for a lightweight aircraft along with scoring in all missions, a payload of one golf ball for mission three and its equivalent weight in steel for mission two was decided.

3.3.1 Brainstorming

A comprehensive conceptual design process was necessary to ensure a successful aircraft, as design changes are more costly later in the design process. An objective tree, a morphological matrix, and a house of quality (HOQ) were used to translate the mission requirements into design requirements, as shown in Figure 3.6 and Table 3.1.

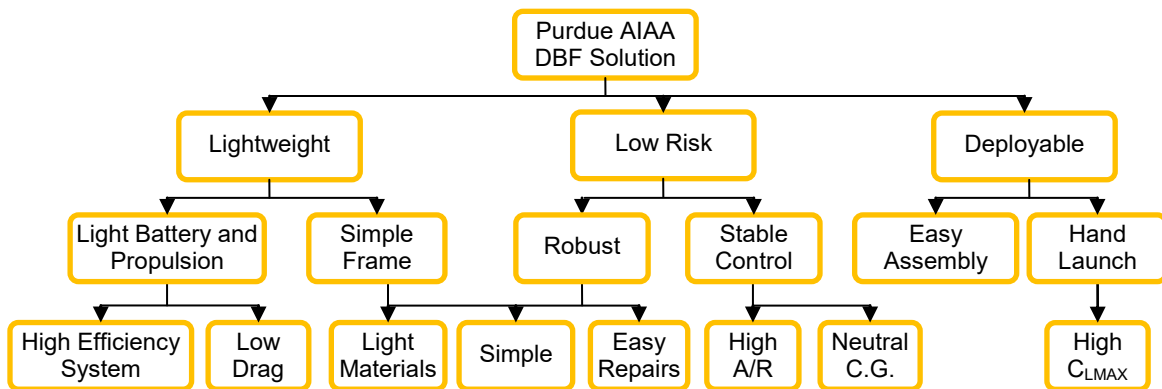


Figure 3.6: Objective tree.

The HOQ was used to assign numerical values to mission requirements based on the design constraints from the objective tree. Table 3.1 shows how the importance of each item was ranked based on the scoring analysis. Initially, missions two and three were treated separately, but as the process progressed, it was determined that the two missions could be combined, as they were similar in scoring.



Table 3.1: House of quality.

| Customer Requirements (What) | | Design Requirements (How) | Importance | + | | + | | - | | - | |
|------------------------------|----------------|---------------------------|------------|--------------|------------|--------------|------------------|--------------|--------------|-----------------|---|
| | | | | Aspect Ratio | Lift/ Drag | Power/Weight | Prop. Efficiency | Empty Weight | Wing Loading | Cruise Velocity | Stall Velocity |
| Mission 1 | High Speed | 0.18 | 7 | 8 | 9 | 6 | 6 | 2 | 9 | 4 | Very Important Moderately Important Somewhat Important Least Important |
| | Light Weight | 0.08 | 4 | 8 | 7 | 8 | 9 | 7 | 3 | 4 | |
| Mission 2&3 | Light Weight | 0.14 | 4 | 8 | 7 | 8 | 9 | 7 | 3 | 4 | |
| | Carry Capacity | 0.12 | 6 | 9 | 8 | 9 | 8 | 4 | 8 | 2 | |
| General | Stable | 0.06 | 9 | 6 | 1 | 0 | 4 | 6 | 1 | 8 | |
| | Robust | 0.08 | 5 | 1 | 3 | 1 | 3 | 2 | 1 | 6 | |
| Absolute Importance | | | 6 | 9 | 8 | 7 | 9 | 2 | 4 | 2 | |

Multiple conceptual designs were generated based on the HOQ analysis. Figure 3.7 shows sketches that depict various potential aircraft configurations. Using the importance rankings in Table 3.1, aircraft design features were then determined using figures of merit (FOM).

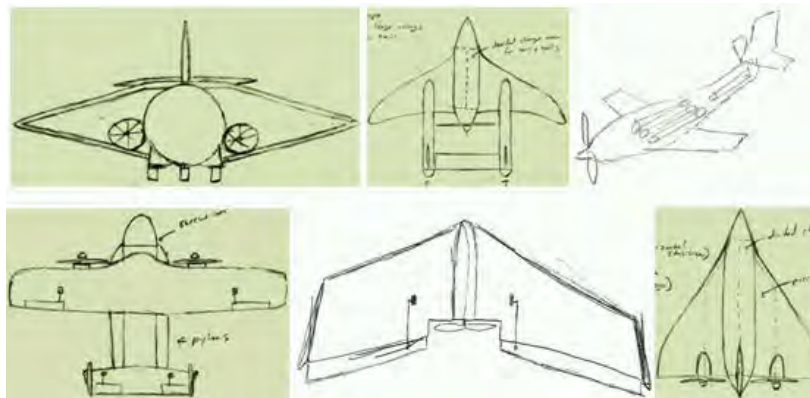


Figure 3.7: Conceptual design sketches.

3.3.2 Aircraft Configuration

Figures of merit were used to determine the appropriate design configurations based on previously determined design requirements. Several possible aircraft configurations and concepts were analyzed. In an effort to remove the subjective nature of the figure of merit analysis, trade studies and historical data were utilized. The findings of these studies for each configuration were then used to assign the numerical values of each performance factor. The scoring analysis and other design constraints were considered when allocating the percentage weights of each performance factor. The following outlines the considerations for weighting used in this analysis.

- Weight was shown to be the most crucial factor in the scoring analysis.
- Lift to drag is critical for speed, range, efficiency, and payload capacity.
- Flight stability is an important factor, but less significant than weight or lift to drag.
- Manufacturability is a concern because a simple, reliable, and repairable design is important.

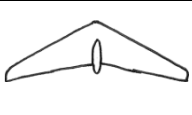


- Packability will be a small factor, since the aircraft should fit into the suitcase in one piece.
- Launchability is moderately important.
- Weight balance is a concern for configurations that may alter the location of heavier components.
- Landing without sustaining damage to the aircraft is required for a successful mission.
- Thrust must be adequate to overcome drag at the desired flight conditions.
- Drag effects influence the size of the propulsion system and the efficiency of the aircraft.
- Assembly time is a small concern because the allotted five minutes should be more than adequate.

3.3.3 Wing Configuration

The wing configuration is the most significant characteristic of an aircraft concept, as it has the largest influence on flight performance. A range of wing configurations, including a monoplane, biplane, canard/tandem wing, and flying wing, were considered. A figure of merit analysis was performed to find the configuration that best met design requirements. Numerical values were assigned based on the results of a theoretical aerodynamic trade study. The conclusions of this analysis are in Table 3.2.

Table 3.2: Wing configuration FOM.

|  | |  |  |  |  |
|---|--------|---|---|---|---|
| Merit | Weight | Monoplane | Biplane | Canard/Tandem Wing | Flying Wing |
| Weight | 35% | 3 | 2 | 4 | 4 |
| Lift/Drag | 35% | 3 | 2 | 4 | 5 |
| Flight Stability | 15% | 3 | 3 | 2 | 1 |
| Manufacturability | 5% | 3 | 3 | 2 | 2 |
| Packability | 5% | 3 | 3 | 3 | 4 |
| Launchability | 5% | 3 | 4 | 2 | 2 |
| Total | 100% | 3 | 2.35 | 3.45 | 3.7 |

The following provides an explanation of the considerations in Table 3.2.

- Monoplane – The monoplane configuration is the most general aircraft configuration. This is used as the baseline for comparison.
- Biplane – The biplane was considered to have more lift for a given wing span than the monoplane. Additionally, braces placed between wings can allow for a strong, lightweight structure. The biplane configuration, however, has more drag than the monoplane due to bracing structure, which leads to adverse aerodynamic effects due to the close proximity of the wings.
- Canard/Tandem Wing – Canard/tandem wings use a lifting wing in front of the main wing for stability. This offers greater overall lift when compared to a monoplane, as the control surface also produces lift. With this configuration, the main wing is positioned in the downwash induced by the canard or forward wing. This can increase the induced drag from the main wing, which decreases the overall lift



to drag performance. Furthermore, the canard/tandem wing configuration can suffer from a high stall speed due to the canard/forward wing stalling before the main wing.

- Flying Wing – The flying wing configuration is expected to have the best lift to drag ratio because of the minimal wetted and frontal area. The flying wing is also expected to be the lightest, as this configuration does not require structure for the tail section. Since pitch and yaw stability must come from either the wing itself or surfaces attached to it, there are stability issues associated with this configuration. This reduces the moment arm of these control surfaces, reducing control authority.

The flying wing configuration was chosen due to its favorable lift to drag ratio and low weight. Stability concerns were noted and addressed during the preliminary and detailed designs.

3.3.4 Vertical Stabilizer Configuration

Next, a range of vertical stabilizer configurations were considered. This included no stabilizer, a single central stabilizer mounted to the wing, a stabilizer mounted to a boom, or winglets. Numerical values were assigned based on a theoretical stability analysis conducted for the various configurations and their associated sizing. The figure of merit study is shown in Table 3.3.

Table 3.3: Vertical stabilizer configuration FOM.

|  | |  |  |  |  |
|--|--------|--|--|---|--|
| Merit | Weight | None | Single Central | Single Boom | Winglets |
| Manufacturability | 35% | 5 | 3 | 2 | 4 |
| Stability | 50% | 1 | 3 | 4 | 4 |
| Drag Effects | 15% | 4 | 3 | 3 | 5 |
| Total | 100% | 2.85 | 3 | 3.15 | 4.15 |

The following provides an explanation of the considerations in Table 3.3.

- None – A flying wing with no vertical stabilizer will have no yaw control; yaw stability must come from other features.
- Single Central – A central vertical stabilizer will be located close to the center of gravity (C.G.) of the aircraft. This requires a larger stabilizer, which will increase weight and drag.
- Single Boom – A stabilizer mounted on a boom adds weight due to the boom structure, but the stabilizer is smaller due to a larger moment arm.
- Winglets – Winglets act as a pair of vertical tails, providing stability in the yaw direction. This effect is increased with wing sweep as the winglets move further aft. Additionally, winglets can reduce induced drag.

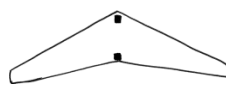
From the above considerations, winglets were chosen because they would provide the necessary control with the smallest weight and drag penalty.



3.3.5 Landing Gear Configuration

Competition rules stipulate that the aircraft must land on the paved runway without sustaining significant damage. Furthermore, the landing gear configuration must facilitate a hand-launched takeoff. For these reasons, several landing gear configurations were considered. These include tricycle and bicycle landing gear, as well as a landing skid. The tail dragger configuration was omitted due to the lack of a tail. Table 3.4 illustrates the FOM for the landing gear configurations considered.

Table 3.4: Landing gear configuration FOM.

|  | |  |  |  |
|---|--------|---|--|---|
| Merit | Weight | Tricycle | Bicycle | Skid |
| Manufacturability | 10% | 3 | 2 | 4 |
| Weight | 50% | 1 | 2 | 5 |
| Ground Handling | 40% | 5 | 2 | 2 |
| Total | 100% | 2.8 | 2 | 4.5 |

The following provides an explanation of the considerations in Table 3.4.

- Tricycle – The tricycle configuration was used as the baseline design. Tricycle landing gear exhibits predictable and reliable ground handling.
- Bicycle – Poor ground handling characteristics eliminated this design.
- Skid – The aircraft will land on a reinforced skid attached to the bottom of the aircraft. This minimizes weight and drag by adding minimal material.

Weight is the driving factor in this design and played a large role in this analysis. The FOM for landing gear led to a skid type configuration.

3.3.6 Motor Location

Motor location is important, as the propulsion system is the heaviest aspect of the aircraft. Positioning the motor has a large influence on the C.G. and maintaining a positive static margin for the aircraft. Table 3.5 illustrates the FOM for motor configurations considered.

Table 3.5: Motor configuration FOM.

|  | |  |  |  |
|---|--------|---|--|---|
| Merit | Weight | Tractor | Pusher | Twin Tractor |
| Weight | 45% | 3 | 3 | 1 |
| Weight Balance | 15% | 3 | 2 | 4 |
| Thrust | 25% | 3 | 3 | 4 |
| Launchability | 15% | 3 | 2 | 3 |
| Total | 100% | 3 | 2.7 | 2.5 |

The following provides an explanation of the considerations in Table 3.5.



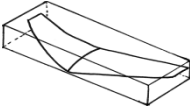
- Single Tractor – The single tractor system benefits from high propeller efficiency, as well as keeping the C.G. ahead of the aerodynamic center.
- Single Pusher – The single pusher configuration shifts the C.G. aft, and hand-launch ability becomes an issue, as the launcher’s hand is directly in front of the propeller arc during the launch. Additionally, the propeller efficiency is decreased due to the wake of the aircraft wing.
- Twin Tractor – The twin tractor system provides an increase in thrust, but the additional motor and required electronics increases the propulsion system weight.

The figure of merit analysis shows that a single tractor motor is the best option for the aircraft, as this solution gives the best combination of the desired merits.

3.3.7 Suitcase Fit

The aircraft must fit into a standard carry-on suitcase, so packing configurations were drafted and analyzed. The compared configurations are displayed in Table 3.6.

Table 3.6: Wing packing configuration FOM.

|  | |  |  |  |  |
|---|--------|---|---|--|---|
| Merit | Weight | One Piece | Hinged Wings | Two Piece | Three Piece |
| Manufacturability | 30% | 5 | 3 | 4 | 3 |
| Weight | 60% | 5 | 2 | 3 | 1 |
| Assembly Time | 10% | 5 | 4 | 3 | 2 |
| Total | 100% | 5 | 2.5 | 3.3 | 1.7 |

The following provides an explanation of the considerations in Table 3.6.

- One Piece – The aircraft remains as a single piece and fits into the suitcase as a single unit. This solution produces the minimum weight of any configuration.
- Hinged Wings – This provides a simple and quick solution for assembly, but penalizes the scoring with higher weight. It also greatly increases manufacturing complexity.
- Two Piece – This configuration is adequate in maximizing space utility, but requires some assembly time. The joints also require extra support, which increases weight.
- Three Piece – This is the least ideal setup compared to the others, as it requires more support for the joints and adds extra weight. The joints also reduce internal volume for payload capacity.

Although all of these concepts are capable of satisfying the five minute assembly time, weight is the ultimate influence. Joints require additional support, which increases weight and are structural weak points. A single piece wing eliminates the need for joints and simplifies storage in the suitcase.



3.3.8 Morphological Matrix

Figures of Merit were used to select the configurations that demonstrated the most favorable characteristics. A morphological matrix documenting the selected configuration is shown in Table 3.7.

Table 3.7: Morphological matrix.

| Components | Configurations | | | |
|---------------------|-----------------------|--------------|--------------|-------------|
| Wing Configuration | Monoplane | Biplane | Canard | Flying wing |
| Vertical Stabilizer | None | Central | Boom | Winglets |
| Landing Gear | Tricycle | Bicycle | Skid | |
| Motor Configuration | Tractor | Pusher | Twin tractor | |
| Packaging | One piece | Hinged wings | Two piece | Three piece |

3.3.9 Review of Conceptual Design

The final conceptual design is a swept, flying wing aircraft with a single tractor motor and winglets, as seen in Figure 3.8.

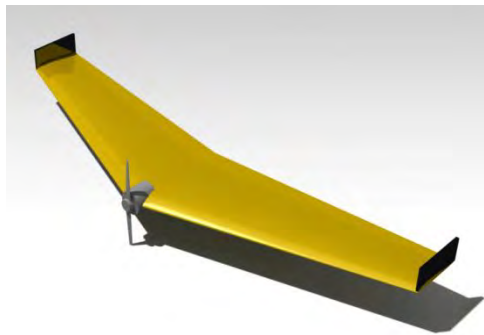


Figure 3.8: Conceptual design.

4.0 Preliminary Design

The chosen aircraft concept was a flying wing with a single tractor motor and winglets, as shown in Figure 3.8. The spiral design methodology was used to develop a concept and converge on a final design. With this method, a design was progressed through the conceptual design, preliminary design, and manufacturing phases. The resulting solution was then tested and compared to design requirements. Using test data and further analysis, a revised design concept was then proposed and the process was repeated. The aircraft design was iterated in this fashion until a maximum scoring aircraft was achieved.

Within the paradigm of the spiral design approach, preliminary design is where specific aircraft parameters are analyzed and defined. To reach decisions on the specifics of the aircraft design, several computational models were used to ensure the resulting aircraft demonstrates desired characteristics. The various sub-phases of the preliminary design process are shown in Figure 4.1.

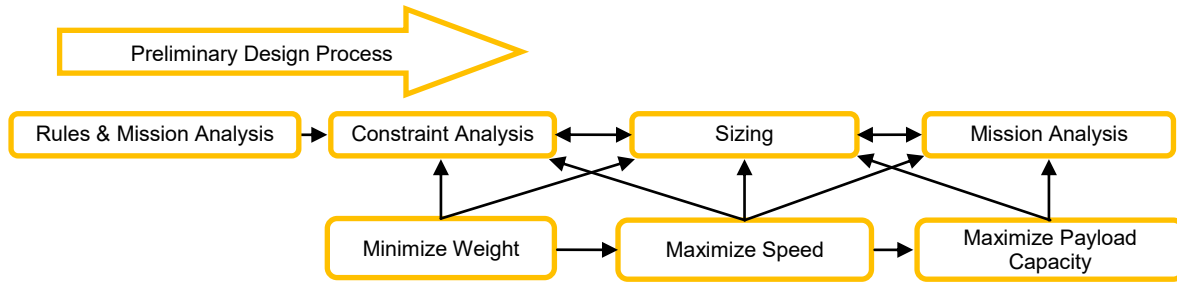


Figure 4.1: Preliminary design process.

4.1 Models

Computational models were used to carry out design constraint analyses on the mission performances and determine how they affect the total score. The computational models used were either Purdue legacy models, freshly developed tools, or a combination of the two. Initially, a constraint and scoring analysis was performed to establish preliminary design space and the resulting aircraft parameters. A preliminary design point was chosen and these values were then used in the aerodynamics, dynamics and controls, structures, and propulsion analyses.

4.1.1 Constraint Model

A constraint analysis model was used to translate design requirements into a bounded design space. Previous Purdue DBF aircraft and contest rules were examined to determine aircraft and mission specific parameters such as aspect ratio and payload weight fraction. These were then used in lift, speed, and power equations to generate specific power and wing loading for different phases of flight. The process used to define aircraft sizing constraints is shown in Figure 4.2.

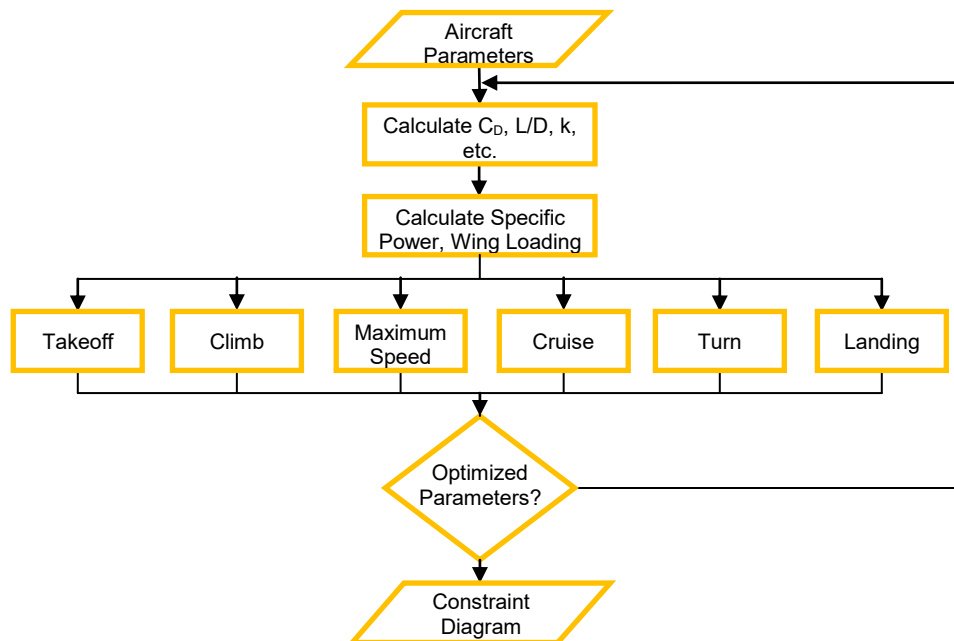


Figure 4.2: Constraint model.



4.1.2 Mission Model

A mission model was created to estimate the power and energy requirements of each mission. To do this, missions were broken down into the distance and time for takeoff, climb, cruise, maximum speed, and turns. The predicted power requirements for each flight phase were found and integrated over time to determine total energy required. The maximum power required and total energy required then served as the lower bounds for motor and battery selection, respectively. Figure 4.3 illustrates the process used for mission modeling³.

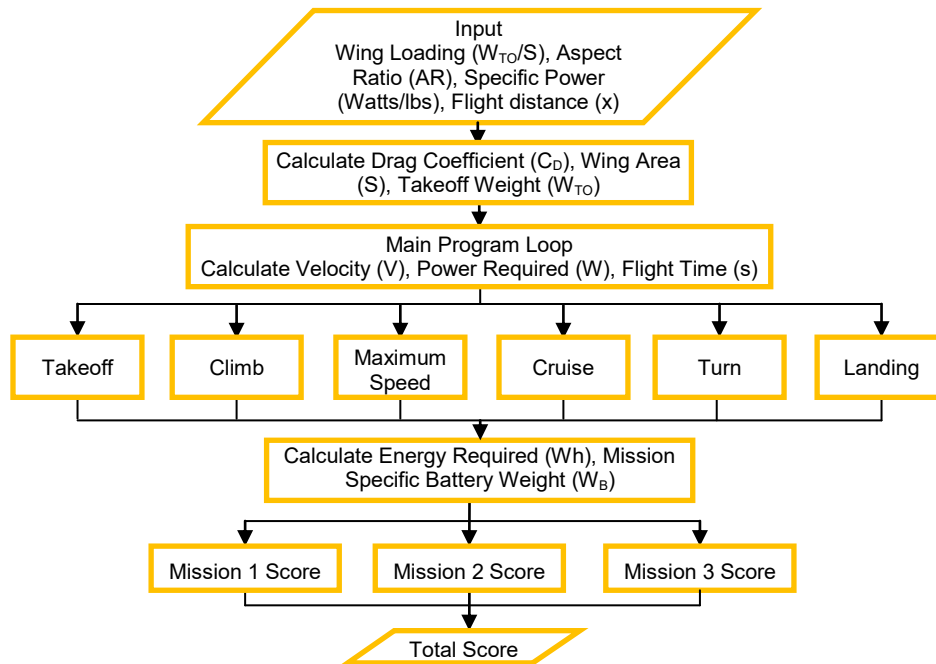


Figure 4.3: Mission model.

4.1.3 Aerodynamics Model

In order to define the wing so that it would exhibit the desired characteristics, a multistep approach was taken. Aspect ratio, wing area, and wing span were based on the constraint sizing analysis. From these requirements, lift coefficients were determined for the 2-D airfoil section. This data and additional requirements for stability and drag culminated in an ideal airfoil. Wing planform was then investigated to find the geometry that provided the highest lift to drag performance and acceptable stability characteristics. Figure 4.4 illustrates this process.

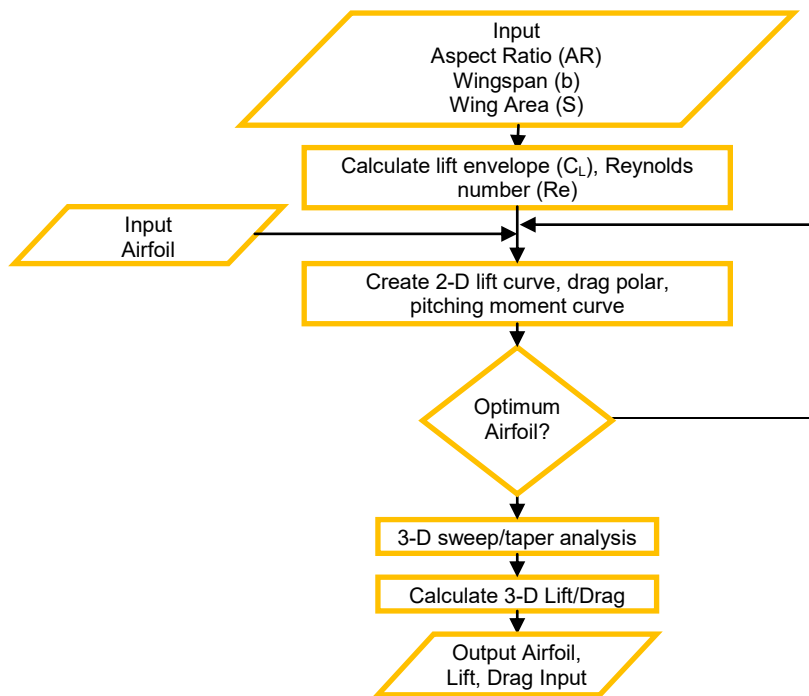


Figure 4.4: Aerodynamics model⁴.

4.1.4 Stability and Controls Model

One of the main concerns with a flying wing design is stability; therefore an extensive analysis on both the longitudinal and lateral stabilities of the aircraft was conducted. To simplify the preliminary analysis, it was assumed that these two stabilities were uncoupled and two separate analyses were conducted.

Due to the lack of a vertical tail structure, the lateral stability of the aircraft was a concern. Winglets were optimized to produce a desired correcting force without compromising maneuverability. The winglet design was configured to decrease induced drag. Winglet analysis was based off of a vertical tail analysis. Specifically, the size of each winglet was determined by halving the vertical tail size obtained from the vertical stabilizer analysis outlined by Raymer³. Figure 4.5 demonstrates the process used to determine winglet sizing.

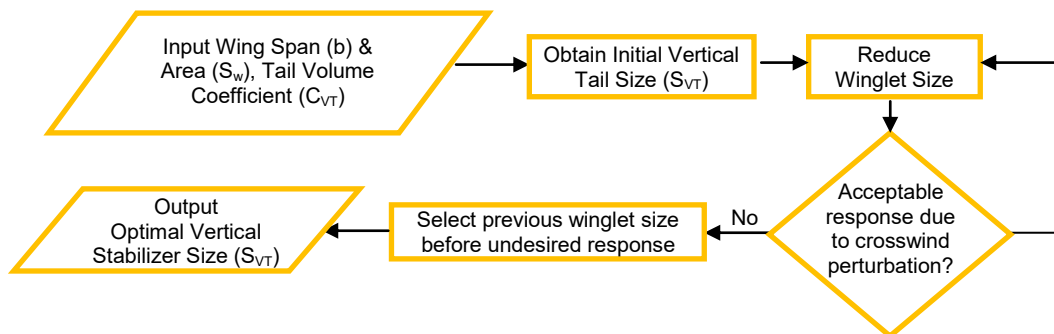


Figure 4.5: Winglet sizing model.



Longitudinal stability is difficult to achieve without the horizontal stabilizer. Subsequently, static margin (S.M.) was closely studied to ensure adequate stability and control. Static margin is based on the location of the C.G. relative to the aerodynamic center. Changing the C.G. location is most easily accomplished by altering the arrangement of the electrical components within the fuselage. The key part of this analysis is determining the optimum component locations to achieve the desired C.G. location. This process is outlined in Figure 4.6.

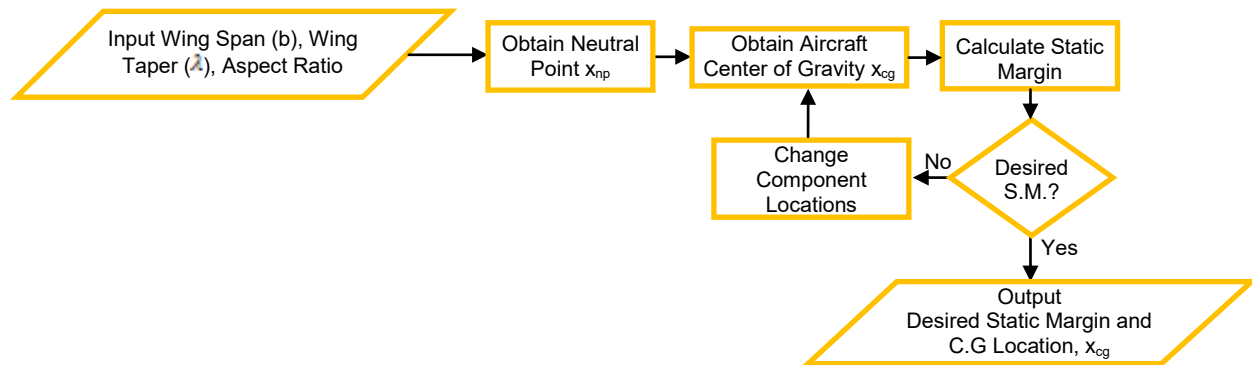


Figure 4.6: Static margin model.

The initial stability and control analysis was performed using a *MATLAB* program named *Flat Earth*⁵. This is a program developed by Dr. Andrisani, a professor at Purdue University, and his students. It gathers the relevant parameters of an aircraft and computes its stability derivatives by solving the equations of motion with numerical integration techniques. In addition, *Simulink* was used to predict the dynamics of the aircraft given perturbations in the control surfaces or external forces.

4.1.5 Structural Model

Structural modeling analyzed the properties of different materials commonly used in model aircraft. It was then determined how the structure could be designed to minimize weight while maintaining necessary structural integrity. Strength and density properties were analyzed to determine the ideal material for each aircraft component. Preliminary results from the constraint and aerodynamic models for span, aspect ratio, and airfoil thickness were used as input parameters. Calculations for stress and moment of inertia were then iterated for spars of different shapes and cross section dimensions. Structural weight was calculated from the density and volume of materials used. Weight from glue joints was ignored in this model. Figure 4.7 illustrates the process used to determine the optimum wing spar dimensions. The focus was to minimize weight to maximize overall score.

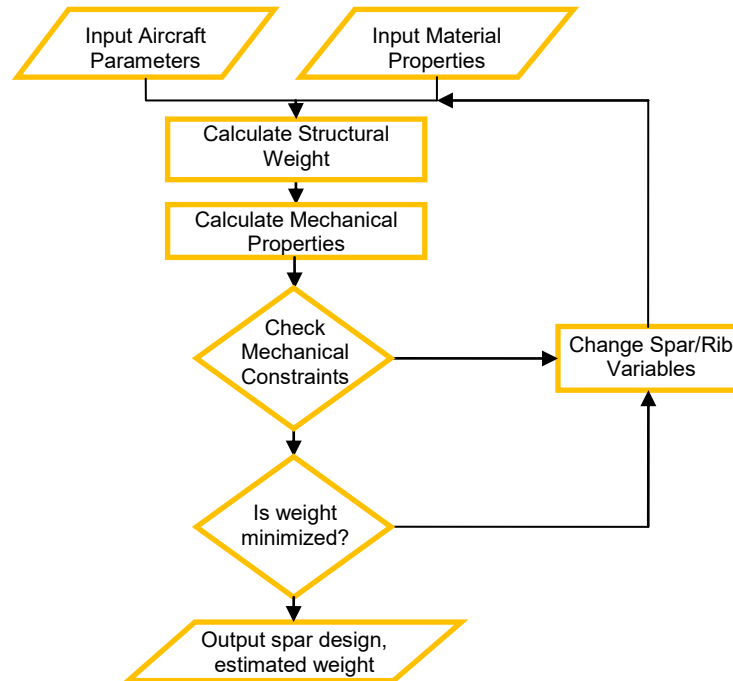


Figure 4.7: Structural model.

4.1.6 Propulsion Models

An efficient and lightweight motor, propeller, and battery combination was needed to maximize the overall score for the competition. The motor and propeller efficiency curves were calculated from aerodynamic data and specifications provided by manufacturers. The aerodynamic data was derived from experimentation and the Goldstein method⁶. Total efficiency was calculated from the propeller and motor curves. The power outputs of motors with ideal efficiencies were used to determine system voltage, flight time, and required battery capacity. From the battery and motor choices, the system weight was calculated. This process was repeated until the best motor and propeller combination was found.

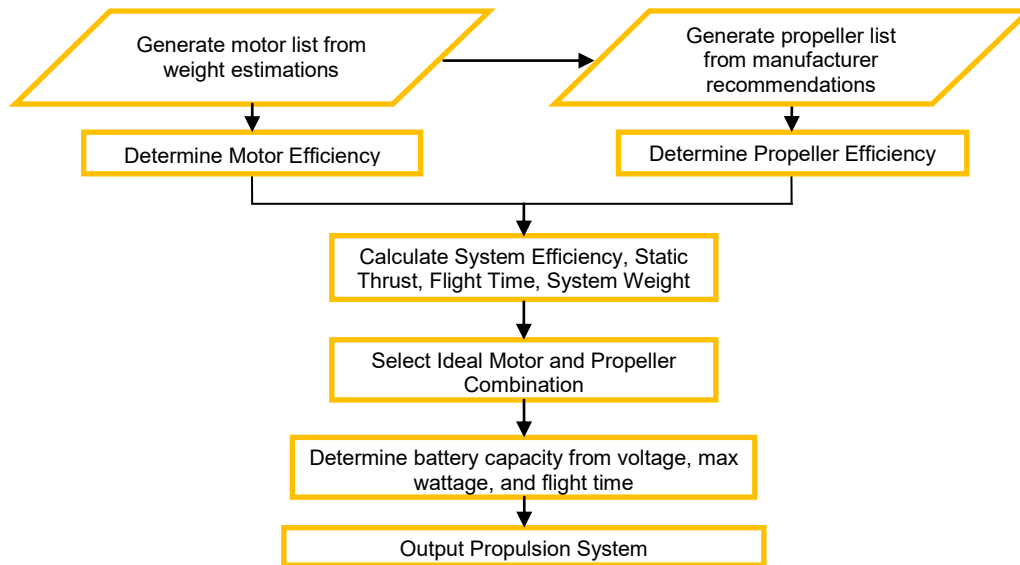


Figure 4.8: Propulsion model.

4.2 Design Trades

The constraint and mission modeling processes were performed to provide preliminary aircraft parameters. Each subsystem was then analyzed to further define aircraft parameters and develop theoretical performance expectations.

4.2.1 Constraint Model Results

The constraint model used mission requirements to find the design space based on specific power and wing loading. This design space, shown in green, is depicted in Figure 4.9.

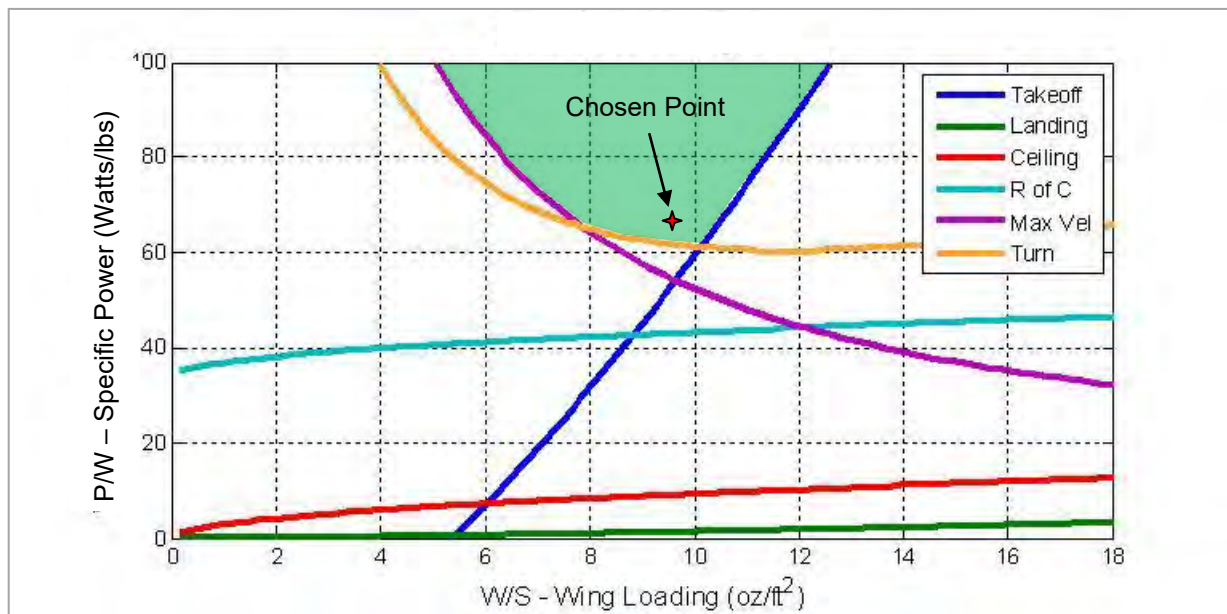


Figure 4.9: Constraint analysis.



The shape of the constraint curves show that the ideal design space is restricted by the takeoff, maximum velocity, and turn phases of flight. Due to the hand-launch requirement, tests were performed to determine the maximum possible takeoff speed. A maximum launch speed of 28 ft/s was found and used for modeling the takeoff curve.

The results of the constraint analysis, combined with other aircraft parameters, were then used to determine which constraint values gave the maximum score. This score corresponded to a specific power of 65 Watts/lbs and a wing loading of 9.4 oz/ft².

4.2.2 Mission Model Results

All three missions were simulated to determine the minimum energy required, which was then used to determine the minimum battery weight. Mission one, the dash flight, requires the most total energy because it has a higher flight speed and flies a greater distance. The results of mission one's flight simulation can be seen in Table 4.1.

Table 4.1: Energy use breakdown by flight leg, mission one.

| Leg | Power Required (watt) | Velocity (ft/s) | Time (s) | Distance (ft) | Energy Used, Leg (W*h) |
|------------|-----------------------|-----------------|----------|---------------|------------------------|
| Takeoff | 23.0 | 31.55 | 0.8 | 17 | 0.005 |
| Climb | 24.7 | 33 | 7.2 | 238 | 0.049 |
| Max. Speed | 32.9 | 40 | 193.6 | 7745 | 1.769 |
| Turn | 30.7 | 36 | 27.4 | 986 | 0.151 |
| Total | N/A | N/A | 229.0 | 8986 | 2.056 |

The total energy needed to complete four laps for mission one was found to be 2.056 W*h, which was used as a minimum value for propulsion analysis modeling. In this analysis, one assumption made was that voltage remained constant as the battery drained, so conversions from watt-hours to milliamp-hours used nominal voltage discharge for an approximation. Propulsion efficiency was based on that of previous Purdue DBF aircraft and may deviate for smaller scales.

Using the results from the constraint and mission model analysis, in conjunction with their respective inputs, initial aircraft sizing parameters were established. Further performance analysis models were based on the parameters outlined in Table 4.2.



Table 4.2: Aircraft sizing parameters.

| Summary | |
|------------------------------------|-------|
| Aspect Ratio | 5.44 |
| Wing Area (in. ²) | 73.5 |
| Wingspan (in) | 20 |
| Payload Weight (lbs) | 0.100 |
| Empty Weight (lbs) | 0.174 |
| Total Battery Weight (lbs) | 0.126 |
| Takeoff Weight M1 (lbs) | 0.300 |
| Takeoff Weight M3 (lbs) | 0.400 |
| Total Energy Required (Watt-hours) | 2.056 |

4.3 Aerodynamics Results

Aerodynamic results were determined through the use of analytical models and traditional calculations based on empirical trend fits. These results are outlined in the following section.

4.3.1 Coefficient of Lift Envelope Calculations

It was important to find the lift coefficient (C_L) envelope that would generate the necessary lift for each mission based on the preliminary aircraft dimensions. This lift envelope was then used to eliminate airfoils from consideration. From the constraint analysis and mission models, flight speed, wing loading, and flight weight were determined. These values were then used in the equation below to calculate the required C_L envelope for missions two and three, as these had higher lift requirements. The results can be seen in Table 4.3.

$$C_L = \frac{L}{\left(\frac{1}{2} \rho u^2 S\right)}$$

Table 4.3: Estimated and calculated flight values.

| | ρ (slug/ft ³) | u (ft/s) | S (ft ²) | L (oz) | C_L |
|---------|--------------------------------|----------|----------------------|--------|-------|
| Takeoff | 0.002208 | 28 | 0.51 | 7.0 | 1.01 |
| Cruise | 0.002208 | 36 | 0.51 | 7.0 | 0.61 |

4.3.2 Airfoil Selection

Following the coefficient of lift envelope calculations shown above, a range of airfoils and their lift characteristics were investigated. A total of 53 different airfoils were compared during this analysis. The airfoils that best met the C_L requirements and further demonstrated other desired characteristics were chosen for additional comparison. The most notable of these other characteristics is the airfoil pitching moment coefficient (C_m). Since the aircraft will rely solely on the main wing for pitch control, the moment created from the wing must allow for stable, level flight. For any aircraft to have positive static stability, it must have a positive static margin. In steady level flight, this would require that the C_m about the aerodynamic center have a positive value. This narrowed the eligible airfoils to only those with small camber, and included airfoils that exhibited reflex. Some of the airfoil designs that were compared



included: Martin Hepperle, Eppler, and NACA series. Airfoils were analyzed using *XFLR5*⁷ for 2-D viscous flow over a range of angles of attack. Aerodynamic characteristics such as C_l and C_m vs. α as well as the drag polars were recorded and then compared. To estimate Reynolds number, an assumption of flight conditions was made based on mission modeling. Table 4.4 shows the assumed flight conditions of Tucson, AZ.

Table 4.4: Assumed flight conditions.

| Tucson Flight Conditions | |
|----------------------------------|----------|
| Dynamic viscosity (slugs/ft*s) | 3.69E-07 |
| Density (slugs/ft ³) | 0.002208 |
| Chord length (ft) | 0.3175 |
| Cruise speed (ft/s) | 36 |
| Reynolds number | 66420 |

From the *XFLR5* analysis, the list of airfoils was narrowed down to five. C_l , C_d vs. C_l , and C_m plots of these airfoil characteristics are shown in Figures 4.10, 4.11, and 4.12.

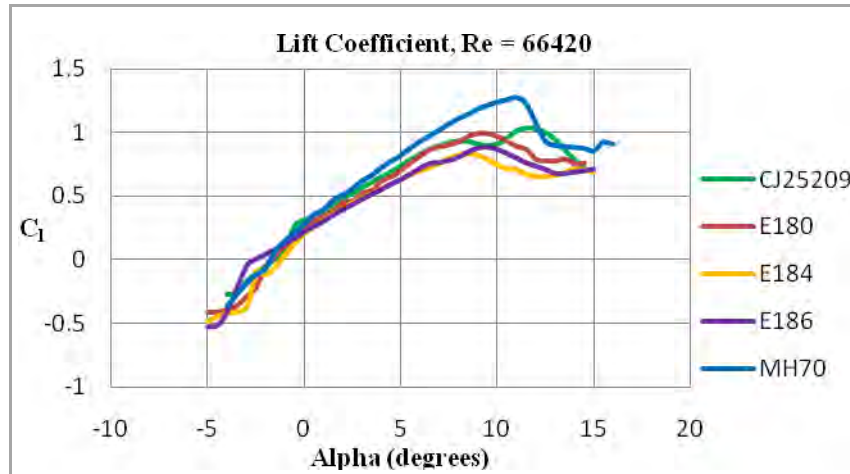


Figure 4.10: Lift curve comparison.

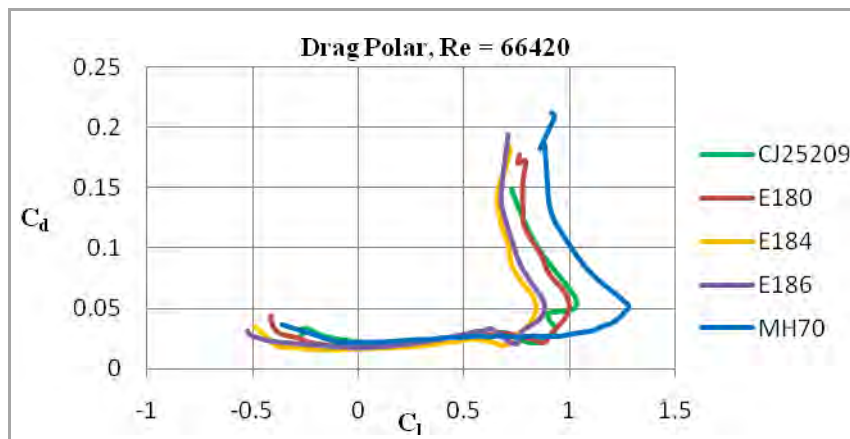


Figure 4.11: Drag polar comparison.

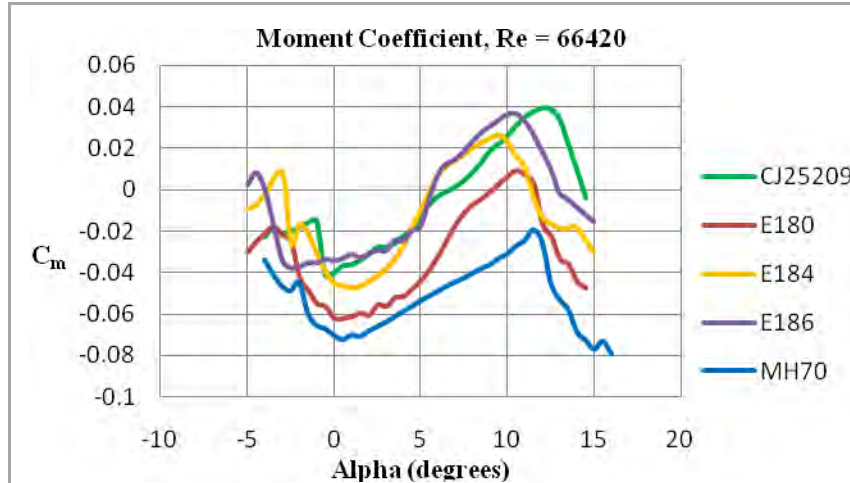


Figure 4.12: Pitching moment coefficient comparison.

Figures 4.10, 4.11, and 4.12 show that these airfoils meet the C_l requirements for cruise outlined in Table 4.3. Furthermore, the CJ25209 and the Martin Hepperle 70 (MH70) are shown to have the highest lift and also meet the C_l takeoff requirements. A higher lift coefficient will increase the aircraft's total lift, increasing the aircraft payload potential. This higher payload potential would then increase the score for missions two and three. From the drag polar, it can be seen that the MH70 has a higher lift to drag ratio than the CJ25209. This is beneficial since a higher lift to drag ratio reduces the amount of power required, increases aerodynamic efficiency, and reduces battery and overall flight weight. Overall, the MH70 airfoil has a higher $C_{l_{max}}$, higher lift to drag ratio, and a desired C_m curve based on the criteria outlined above. The MH70 was chosen for these reasons; its geometry is shown in Figure 4.13.

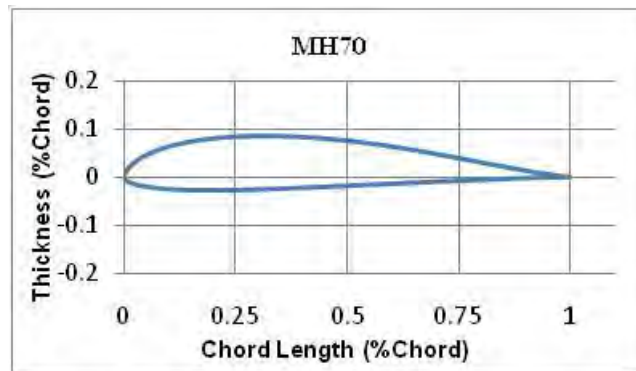


Figure 4.13: 2-D geometry of the MH70 airfoil.

4.3.3 Sweep and Taper Analysis

Following the airfoil selection, the planform shape and its effects on lift, drag, and stability were investigated. It was noted that with a flying wing, the elevators are on the main lifting plane. This means the elevator deflection required to create a pitch up moment also reduces the wing's lift for a given angle of attack. Although this is similar to a conventional aircraft, the effects are more pronounced due to the close proximity of the elevators to the center of gravity. The elevator acts like a negative flap by



decreasing camber, which dramatically decreases the lift on the entire wing. This makes it important to also account for the effects of the elevators when investigating different wing planforms.

To better understand the lift and drag performance of different sweep and taper combinations, *XFLR5* was used to create C_L vs. C_M plots for elevator deflection angles of ± 5 degrees. The maximum static margin was then chosen for each sweep and taper combination so that, for an elevator deflection of 5 degrees, the steady state C_L value was maximized. This was done to find the highest C_L values that could be achieved by the aircraft and their associated stability.

Wing sweep was varied from 20 to 40 degrees in 10 degree increments for an initial taper ratio of 0.5. The resulting performance for the different wing sweeps is shown in Table 4.5.

Table 4.5: Effects of sweep.

| Effect of Sweep for Taper Ratio = 0.5 | | | |
|--|-------|-------|------|
| Sweep (degrees) | 20 | 30 | 40 |
| $C_{L_{max}}$ | 0.8 | 0.75 | 0.7 |
| Lift to Drag | 14.04 | 13.99 | 13.9 |
| Static Margin (% MAC) | 12 | 16 | 20 |

While low sweep angles provided the highest lift for the best lift to drag ratio, higher sweep angles could afford a larger static margin due to the increase in elevator control authority, providing higher stability. Based on these trends, it was determined that the desired choice would be the lowest wing sweep possible that still allowed for an adequate static margin. Initially, a static margin of 12% mean aerodynamic center (MAC) was deemed acceptable by the dynamics and controls analysis. This resulted in a wing sweep of 20 degrees to be chosen. Flight tests later showed that this configuration provided inadequate control and stability. The next design iteration addressed this issue by increasing wing sweep to 30 degrees. This allowed for a static margin of 16% MAC with a $C_{L_{max}}$ of 0.75.

With a sweep angle chosen, the effects of taper ratio were then investigated. Taper ratio was varied from 0.33 to 1, and the same analysis was performed. The results are shown in Table 4.6.

Table 4.6: Effects of taper.

| Effect of Taper for Sweep = 30 degrees | | | |
|---|------|------|------|
| Taper Ratio | 0.33 | 0.5 | 1 |
| $C_{L_{Max}}$ | 0.7 | 0.75 | 0.76 |
| Lift to Drag | 13.8 | 14 | 14.1 |
| Static Margin (% MAC) | 12 | 16 | 18 |

From Table 4.6, it can be seen that as taper ratio is decreased from 1 to 0.5, lift to drag increases as well as $C_{L_{max}}$ performance. As the taper ratio is further decreased from 0.5 to 0.33, however, the achievable $C_{L_{max}}$ and L/D remain approximately constant. This means that the only notable difference between a taper ratio of 0.5 and 0.33 was the slightly higher static margin that could be set for the smaller taper



ratio. From these results, a taper ratio of 0.5 was ultimately selected as this would simplify manufacturing and have minimal effects on lift and drag characteristics.

Based on these analyses, a wing sweep of 30 degrees and a taper ratio of 0.5 were chosen. The performance of this configuration is shown in Figure 4.14. The C_M is revolved about the static margin of 16% MAC, meaning all steady state values lie on the y-axis. Moment coefficient curves were not created for near stall conditions as the numerical method used in *XFLR5* failed to converge at these points.

4.4 Stability and Controls Results

The first design iteration had a sweep angle of 20 degrees which was determined from the aerodynamic analysis. Flight testing concluded that the aircraft was unstable and exhibited inadequate elevon control authority. This led to a redesign that increased the wing sweep to 30 degrees and the static margin to 16% MAC. Subsequently, the aircraft's yaw stability benefited from having a longer winglet moment arm. The elevons also had a greater moment to control the pitch and roll of the aircraft.

4.4.1 Elevon Sizing

The control surface design for a tailless aircraft is paramount, due to the pitch instability issues associated with such aircraft. Elevons were chosen instead of individually actuated elevators and ailerons to minimize the mechanical weight associated with the number of servos. Full span elevons were chosen to maximize the effect of the control surfaces and decrease the manufacturing difficulty. The chord of the elevons was determined from a suggested range based on the percentage of local wing chord⁸. The first flying prototype used elevons that were 20% of the local wing chord. Based on pilot feedback, the size of the elevons was decreased on subsequent models. The chord of the final elevons is 13.5% of the local wing chord. The dimensions are illustrated in the drawing package in section 5.8. This resulted in the trim diagram shown in Figure 4.14.

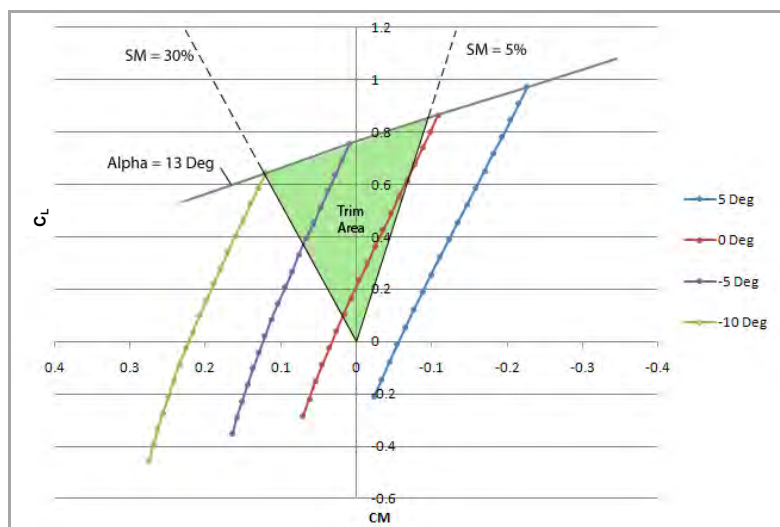


Figure 4.14: Trim diagram for 30 degree sweep, taper ratio of 0.5, and 15% static margin.



4.4.2 Winglet Sizing

A vertical tail sizing analysis was used to determine initial winglet dimensions. Aspect and taper ratios were chosen as 1.3 and 0.3, respectively. These values were determined from the range recommended by Raymer for vertical tail sizing³. Each winglet was approximated to be half of the vertical tail area. A vertical tail size of about 12 in.² was obtained using the following equation.

$$S_{VT} = \frac{C_{VT} b_w S_w}{L_{VT}}$$

This approach is typically used with conventional aircraft, but used here to obtain an initial value to begin the design process. Using the aforementioned *Flat Earth* simulations, the stability of the aircraft was estimated for various winglet sizes. Historical data suggested that 12 in.² is an overly conservative size for yaw stability for planes of this configuration. To more closely match historical winglet sizing, the area was reduced to analyze the trade-off between weight and lateral stability. By introducing a crosswind perturbation into the analysis, and assuming no pilot input, the yaw responses were obtained. The settling time of these responses is an indication of the stability of the aircraft. As the settling time increases, the aircraft will take longer to return to the steady state, indicating less stability. A longer settling time does not necessarily mean that the aircraft is impossible to fly, but rather it is harder for the pilot to control. Therefore, the lower limit of the vertical stabilizer sizing is dependent on the pilot's preference. Figure 4.15 shows the correlation between vertical stabilizer sizing and settling time.

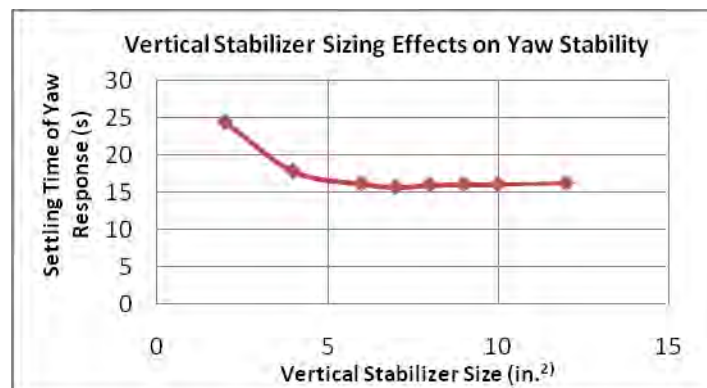


Figure 4.15: Vertical tail/winglet sizing effects on yaw stability.

Figure 4.15 shows yaw stability is insensitive to reductions in the vertical stabilizer size from 12 to 6 in.². This suggests that there is no need to have a vertical stabilizer as large as 12 in.² while the lower limit for size should be around 6 in.². Given the length of the tip chord combined with the suggested aspect and taper ratios, a vertical stabilizer size of 9 in.², or winglet sizes of 4.5 in.², was chosen. This was deemed reasonable as it is a significant reduction from the initial size 12 in.² while maintaining a safety factor of 1.5. This analysis was used to understand the general stability trends as winglet area is varied.

This winglet was used for the first few design iterations of the aircraft and proved to provide sufficient stability. Subsequent iterations of the spiral design focused on designing the winglets to improve the



aerodynamic efficiency of the aircraft while maintaining yaw stability. To this end, Whitcomb's classical winglet was studied to decrease drag. Testing outlined in section 8.1.2 details the performance of both winglet designs. Whitcomb's design is illustrated in Figure 4.16.

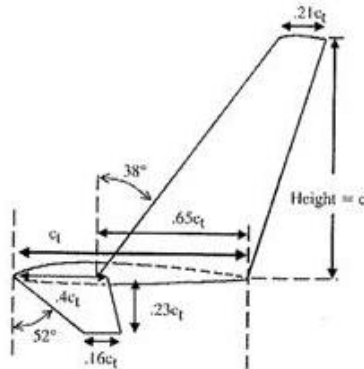


Figure 4.16: Whitcomb's proposed winglet design³.

This design produces winglets with a total vertical surface of 6.13 in.². The areas of these winglets lie at the lower limit of the recommended range, as shown in Figure 4.16.

4.4.3 Static Margin

Static margin is an important parameter for the aircraft's longitudinal static stability. The absence of a horizontal tail limits the range of neutral point locations, decreasing the range for stable C.G. locations.

This analysis assumes that the aircraft is in power-off condition, which is acceptable because a horizontal thrust force has a negligible contribution to the static margin. The effects of the fuselage were also assumed to be insignificant. By modeling the aircraft as a flying wing without a horizontal stabilizer, the aircraft's neutral point coincides with the aerodynamic center of the wing. Given the wing geometry, the aerodynamic center can be computed using the following equations given by Raymer³.

$$x_{ac_w} = yMAC \tan(\phi_{L_e}) + 0.25MAC; \quad yMAC = \frac{b(1+2\lambda)}{6(1+\lambda)}; \quad MAC = \frac{2}{3}\lambda \frac{(1+\lambda+\lambda^2)}{1+\lambda}$$

Based on these equations, the location of the aerodynamic center was determined to be 3.81 in. aft of the leading edge of the root chord.

According to Nickel and Wohlfahrt, the static margin of a stable, tailless aircraft should be between 15% and 20% MAC⁹. Based on the desired static margin, the location of the center of gravity can be calculated from the following equation⁴.

$$x_{cg} = \frac{SM * MAC}{x_{AC}}$$

Based on the desired static margin, and the location of the aerodynamic center, the location of the center of gravity needs to be between 3.04 and 3.24 in. aft of the leading edge. The C.G. location is more sensitive than the neutral point simply because it changes significantly with component placement in the



fuselage. Since the location of the payload will have a significant effect on the C.G. and therefore static margin of the aircraft, it is desirable to place all payloads directly at the C.G. of the aircraft. This was considered when designing the component layout of the aircraft system and would prevent the static margin from changing significantly between missions.

4.5 Structural Model Results

Structural differences between flying wings and conventional designs limited the possible wing configurations. To conserve weight and improve aerodynamic characteristics, a central fuselage structure was not desired. Unfortunately, the wing did not provide adequate space to house the electronics and payload; therefore, a fuselage was necessary. Some electrical components, such as servos, could still be stored within the wing to minimize fuselage size.

Stress calculations were performed to determine the minimum structural weight required to build a wing using ribs and spars of different materials. Simple beam theory and the equations below were used for the stress analysis of multiple spar configurations¹⁰.

$$\sigma = \frac{My}{I}; I = \frac{bh^3}{12}$$

Assumptions were made to simplify the process of determining the ideal spar design. One assumption was considering the spar as a rectangular cantilever beam. Loads were placed on the wingtips to simulate the required wingtip test. This wingtip test was a simple analysis that approximates distributed loading seen during a 2.5 G turn¹¹. Max stress was determined for a variety of spar configurations. Research found that the ultimate tensile strength of RC grade balsa was about 770 psi¹². Results of the model can be seen in Table 4.7.

Table 4.7: Spar results.

| Spar Type | Max Stress (psi) | Weight (oz) | % Ultimate Stress |
|-----------|------------------|-------------|-------------------|
| Solid | 638.66 | 0.053 | 83.16 |
| Box | 683.55 | 0.037 | 89.00 |
| I-Beam | 683.55 | 0.037 | 89.00 |

A box spar was chosen over an I-beam because it provided the same strength and was easier to manufacture. The shear web's placement on the backside of the spar rather than between the spar caps provided a larger surface area for glue. A D-tube structure was also created by wrapping balsa sheeting around the leading edge, covering the top and bottom of the wing. This D-tube, shown in Figure 4.7, creates a closed structure which provides additional torsional rigidity.

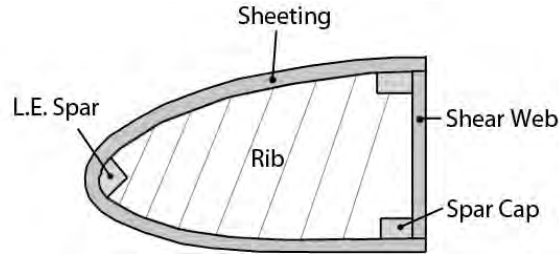


Figure 4.17: D-tube structure.

Once the spar was designed, the ribs needed to be positioned along the wing span. Rib spacing is generally one third of the chord length, which equates to 1.63 in. between ribs and a total of 12 ribs. Once ribs were placed, they were optimized to minimize weight while meeting strength and stiffness requirements.

4.6 Propulsion Model Results

The propulsion system, as shown in Figure 4.18, was selected by choosing a complementing motor, battery, speed controller, and propeller that would complete all missions for the lightest weight.



Figure 4.18: Propulsion system diagram.

Battery packs were selected by analyzing cell configurations that would minimize weight while meeting the 32 Watt design requirement from the constraint analysis. NiMH batteries have an energy density ranging from 27-55Wh/lb, which is significantly greater than the energy density of (NiCd) batteries which range from 20-36Wh/lb¹³. Based on the average energy densities shown in Figure 4.19, NiMH batteries were chosen.

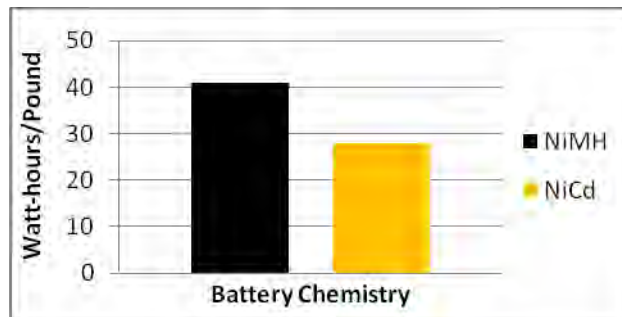


Figure 4.19: Battery chemistry comparison.

A comparison of battery packs ranging from 1.2 to 12 V was performed based on the estimation of energy needed from section 4.2.2 and an allotted flight time of 4.5 minutes. This time was based on the time requirement for mission one and an additional factor of safety for landing. The top three performing battery packs are displayed in Table 4.8.



Table 4.8: Battery pack comparison.

| Cells | Voltage (V) | Capacity (mAh) | Cell Type (mAh) | Cell Weight (oz) | Battery Weight (oz) | Discharge Rate (Amps) |
|-------|-------------|----------------|-----------------|------------------|---------------------|-----------------------|
| 1 | 1.2 | 1851.85 | 2200 | 1.53 | 1.53 | 24.69 |
| 2 | 2.4 | 925.93 | 1500 | 0.81 | 1.62 | 12.35 |
| 6 | 7.2 | 308.64 | 400 | 0.27 | 1.62 | 4.12 |

Using weight as the main constraint, one 2200 mAh cell was the lightest option; however, this combination was eliminated because the discharge rate exceeds the 20 amp fuse limit. The next lightest combination was either a two-cell 1500 mAh pack or a six-cell 400 mAh pack.

Possible motors were chosen based on the 32 Watt power requirement. Twelve motors, including both in-runners and out-runners, were initially analyzed to determine the ideal motor for this application. The list of motors shown in Table 4.9 was narrowed down to three based on weight and efficiency.

Table 4.9: Motor comparison.

| Motor | Type | Weight (oz) | Kv (RPM/volt) | R_m (Ohms) | I_o (Amps) | Continuous Power (W) |
|---------------------------------|------------|-------------|---------------|--------------|--------------|----------------------|
| E-Flight Park 250 ¹⁴ | Out-Runner | 0.49 | 2200 | 0.25 | 0.45 | 50 |
| Neu Neutrino 1210 ¹⁵ | Out-Runner | 0.49 | 1850 | 0.21 | 0.4 | 75 |
| Neu Proton 507 ¹⁵ | In-Runner | 0.52 | 5300 | 0.18 | 0.42 | 50 |

Efficiency curves were generated for each of the motors based on these specifications and the two potential battery packs. It was found that all motors were more efficient with the six-cell battery pack as opposed to the two-cell battery pack. Therefore, the six-cell 400 mAh battery pack was chosen as the main propulsion pack. Though the Neu Proton 507 has the highest overall efficiency, the higher Kv value of this motor would require a gear box to adjust the propeller efficiency to an acceptable level. A gearbox adds weight and complexity, so the Neu Proton 507 was eliminated from consideration. The Neutrino and the Park 250 have identical weights, but the Neutrino has a higher efficiency. Based on this analysis, the Neu Neutrino 1210 is the most ideal motor for this application with a maximum efficiency of 79.5%. The efficiency and power output of the E-flite Park 250 and Neu Neutrino 1210 are compared in Figure 4.20.

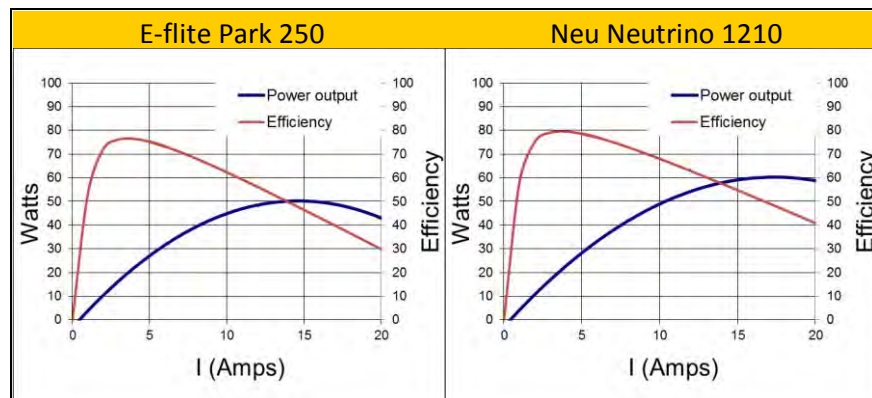


Figure 4.20: Motor efficiency trends.



For the preliminary design, a propeller was chosen utilizing eCalc, an online propeller efficiency calculator, with inputs from the Neutrino and the six cell 400 mAh battery pack¹⁶. Table 4.10 compares a list of commercially available propellers which were used to calculate propulsion system efficiency.

Table 4.10: Propeller comparison.

| Diameter x Pitch (in.) | Static Thrust (oz) | Efficiency (%) | Flight Time (min) |
|------------------------|--------------------|----------------|-------------------|
| 5.5x2.5 | 5.94 | 85.1 | 6.84 |
| 5.5x2 | 4.92 | 84.7 | 8.06 |
| 4.6x3 | 4.49 | 83.2 | 10.17 |
| 5x3 | 5.53 | 84.8 | 7.92 |

Based on the results from eCalc, the ideal propeller for the propulsion system is a 5.5x3.0 propeller. Of the considered propellers, the 5.5x3.0 provided the highest thrust and overall system efficiency while allowing for the desired flight time. Further analysis using a blade element momentum theory code based on Goldstein's propeller theory⁶ and wind tunnel and flight testing will be used to verify these results.

4.7 Estimated Aerodynamic Characteristics

Airfoil analysis in section 4.3.2 concluded that the MH70 airfoil provided the best 2-D aerodynamic performance. It was then important to find the lift and drag for the entire aircraft for the expected flight conditions. The following relations were used to estimate the drag coefficient.

$$C_D = C_{D0} + C_{D2}C_L^2 + C_{Di}$$

The first two terms on the right-hand-side of this equation describe the aircraft's profile drag, and the third term describes its induced drag, C_{Di} . C_{Di} can be estimated by the equation below.

$$C_{Di} = \frac{C_L^2}{\pi A R e}$$

XFLR5 was used to theoretically calculate the C_L vs. alpha curve, the drag polar, and the wing efficiency factor of the 3-D wing. Screen shots from this analysis are shown in Figure 4.21.

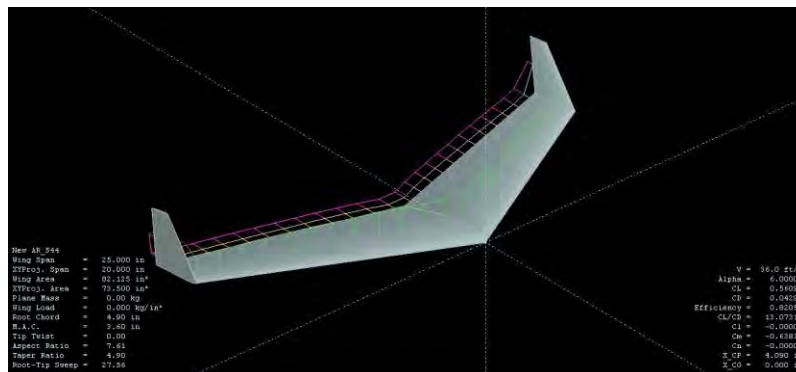


Figure 4.21: XFLR5 analysis.

The freestream velocity was set to 36 ft/sec based on estimations from Table 4.4. This corresponded to a Reynolds number of 66420. The results of this analysis are shown in Figures 4.22 and 4.23. It is



important to note that the *XFLR5* simulation is based on the wing only, and does not include the effects of the fuselage or winglets.

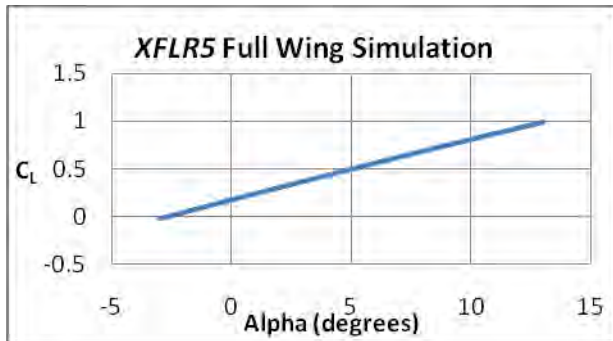


Figure 4.22: C_L vs alpha of the complete wing.

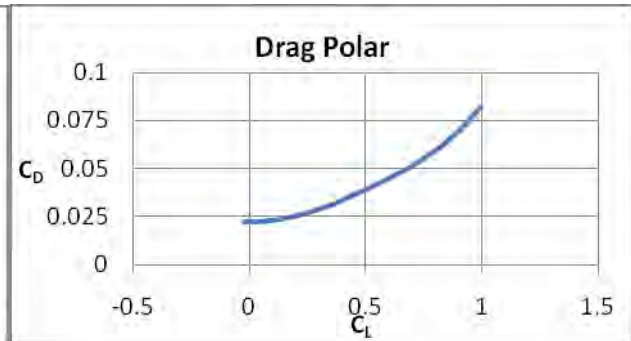


Figure 4.23: Drag polar of the complete wing.

The constants necessary to predict the aircraft's drag performance were then derived from Figures 4.22 and 4.23. The coefficient of profile drag, C_{D_0} , was determined to be 0.022 by the point at which C_L equals zero. C_{D_2} was calculated to be 0.026 by using a second order curve fit on the existing drag polar. Only the C_D region prior to the stall angle of attack was used to create this curve fit. The span efficiency factor was then determined to be 0.98 using *XFLR5* simulations. Wing loading was used in conjunction with wing area and estimated cruise speed to calculate a $C_{L_{req}}$ of 0.45 for mission one and 0.60 for mission two, respectively. C_{D_0} for the fuselage and winglets was estimated using surface area, form factor, and skin friction coefficients. The drag estimates computed for each mission are displayed in Table 4.11.

Table 4.11: Drag estimates for each mission.

| | Mission One | Mission Two | Mission Three |
|-----------------------------------|--------------|--------------|---------------|
| C_{D_0} Wing | 0.022 | 0.022 | 0.022 |
| C_{D_0} Winglet | 0.005 | 0.005 | 0.005 |
| C_{D_0} Fuselage | 0.010 | 0.010 | 0.010 |
| Total C_{D_0} | 0.037 | 0.037 | 0.037 |
| C_{Di} Wing | 0.013 | 0.024 | 0.024 |
| Total C_{Di} | 0.013 | 0.024 | 0.024 |
| Total C_D | 0.058 | 0.069 | 0.069 |

Total drag and lift for each mission were then found using the C_D values, C_L values, flight velocities, and wing area. The higher drag in missions two and three are partially attributed to the higher lift required to carry the payload. The values in Table 4.12 show the expected cruise conditions for each mission.

Table 4.12: Total lift and drag for missions one, two, and three.

| | Mission One | Mission Two | Mission Three |
|-------------------------|-------------|-------------|---------------|
| Average Total Drag (oz) | 0.752 | 0.896 | 0.896 |
| Alpha (degrees) | 4.5 | 6.5 | 6.5 |
| Total Lift (oz) | 4.80 | 6.40 | 6.40 |



Table 4.13 illustrates the important stability derivatives of the aircraft. The computed derivatives indicate a stable system. It should be noted that δa refers to deflections of the elevons in the opposite directions while δe corresponds to elevon deflections in the same directions.

Table 4.13: Stability derivatives.

| | | | | | | | |
|------------------|-------|------------------|--------|------------------|--------|--------------|--------|
| $C_{L\alpha}$ | 3.657 | $C_{M\alpha}$ | -0.579 | $C_{n,\delta a}$ | -0.016 | $C_{n\beta}$ | 0.028 |
| $C_{L,\delta e}$ | 1.250 | $C_{M,\delta e}$ | -1.180 | $C_{l,\delta a}$ | 0.203 | $C_{l\beta}$ | -0.246 |

4.8 Estimated Mission Performance

Combining all the preliminary design models resulted in a unified design for the aircraft. Estimations were also made for each mission's performance, resulting in a total flight score of 2.46. These estimations for mission performance are shown in Table 4.14.

Table 4.14: Estimated mission performance.

| Mission One | | Mission Two | | Mission Three | |
|------------------------|-------|------------------------|-------|--------------------------|-------------|
| Cruise Velocity (ft/s) | 42 | | | Cruise Velocity (ft/s) | 36 |
| Turn Velocity (ft/s) | 37 | Cruise Velocity (ft/s) | 36 | Turn Velocity (ft/s) | 36 |
| Flight Time (s) | 239 | Turn Velocity (ft/s) | 36 | Flight Time (s) | 180 |
| Takeoff Weight (lbs) | 0.300 | Flight Time (s) | 180 | Takeoff Weight (lbs) | 0.400 |
| Laps | 4 | Payload Weight (lbs) | 0.100 | Number of Golf Balls | 1 |
| Max. Laps | 8 | Takeoff Weight (lbs) | 0.400 | Max. Golf Balls | 20 |
| Score | 0.50 | Score | 0.75 | Score | 0.10 |
| | | | | Max. Empty Weight | 0.300 |
| | | | | Total Score | 2.46 |

5.0 Detail Design

After progressing through four iterations of designing, building, and testing, a detailed final design was converged upon. The final dimensions of the aircraft, as well as associated characteristics, are documented in this section.

5.1 Dimensional Parameters

The dimensional parameters for the final aircraft design can be seen in Table 5.1.

Table 5.1: Aircraft dimensions.

| Wing | | Winglets | | Elevons | |
|-------------------------------|------|------------------|------------|---------------------------------|-------|
| Span (in.) | 20 | Height (in.) | 2.49 | Span (in.) | 9.15 |
| Root Chord (in.) | 4.9 | Root Chord (in.) | 2.45 | Chord (% Chord) | 13.5 |
| Tip Chord (in.) | 2.45 | Tip Chord (in.) | 0.50 | Elevon Area (in. ²) | 12.32 |
| ¼ Chord Sweep (degrees) | 30 | Airfoil | Flat Plate | Max Deflection (degrees) | 25 |
| Wing Area (in. ²) | 73.5 | Fuselage | | | |
| Aspect Ratio | 5.44 | Length (in.) | 8.06 | | |
| Taper Ratio | 0.5 | Width (in.) | 3.25 | | |
| Airfoil | MH70 | Height (in.) | 1.03 | | |



5.2 Structural Characteristics and Capabilities

An aircraft structure must be as light as possible while still meeting strength and rigidity requirements. Focus was placed on two key areas to minimize structural weight: wings and fuselage. Experimental tests and analysis identified areas of improvement for these structures. These tests results are in Section 8.1.3.

5.2.1 Wing

One of the necessary requirements of the wing structure is to withstand a simulated 2.5 G wingtip test during technical inspection, representative of a distributed load seen in flight. This corresponds to a bending moment at the root chord of 60 oz-in. A D-tube at the leading edge was used in the final design to provide the required bending and torsional strength. The spar caps configuration consisted of a base of 3/32 in. and a height of 1/8 in. A shear web of 1/16 in. balsa connected the spar caps. Caps were placed over the ribs to provide surface area for applying mylar covering. The grain for the spar caps was oriented spanwise to match the direction of the compressive and tensile loads. The grain for the shear web was oriented vertically to provide greater stability for the spar caps and minimizes crack propagation in case of failure. A longeron provided an attachment point for the elevons. This also provided additional bending and torsional strength to the wing. The final spar configuration was chosen based on the experimental results shown in Section 8.1.3. This design failed at a load equivalent to 3.5 G.

5.2.2 Fuselage

The requirement for a hand-launched aircraft eliminated the need for landing gear for takeoff, allowing for the possible use of a landing skid. To save weight, reduce drag, and maintain simplicity, a decision was made to use a skid configuration for landing. The fuselage provided a suitable platform to act as the landing skid. Additionally, it supported the payload and housed the electronics. Fiberglass, carbon fiber, and built-up balsa fuselages were considered for weight reduction. Following a trade study, carbon fiber was ultimately chosen due to its low weight and durability. The final fuselage design consists of a single piece carbon fiber shell of 1/32 in. uniform thickness. The single piece fuselage structure eliminated failure due to joints and reduces the construction complexity. The molded shell allowed for minimal internal structure while providing a higher payload volume. The durable nature of carbon fiber composites also prevented structural damage upon landing. The carbon fiber fuselage has demonstrated more than adequate structural integrity and resistance to abrasion during numerous hard landings on asphalt. Additionally, the composite structure appeared to flex and absorb impact loads instead of cracking, as was apparent with the initial mylar-covered balsa prototype fuselage.

5.3 System Design, Component Selection, Integration, and Architecture

The designed aircraft contains multiple systems that, once integrated, make it a simple, sturdy, and lightweight aircraft. The wing was constructed as a single piece to reduce weight and assembly time. Furthermore, the 20 in. span fits within the dimensional constraints of the case, making storage and



removal of the aircraft simple and efficient. The only required assembly is the attachment of the fuselage to the wing. A small tab at the front of the fuselage fits into a slot along the bottom of the leading edge. The wing is fitted with two blind nuts that line up with holes drilled through the fuselage. To secure the fuselage to the wing, two nylon bolts are inserted through the fuselage and into the blind nuts. The receiver chosen was the Spektrum AR6255, which was the lightest 2.4 GHz receiver on the market to meet the failsafe requirements. Blue Arrow S0361 servos were selected for being the lightest servos available on the market to provide adequate torque. A Castle Creations Phoenix 10 speed controller was chosen for being the lightest, fully programmable speed controller available on the market.

The carbon fiber fuselage encloses the receiver, speed controller, batteries, and payload. The use of carbon fiber minimizes weight and maximizes the internal payload volume by eliminating the need for internal supporting structures. The electrical components are secured internally with lightweight Velcro, making alterations simple. The steel bar sits inside a recess in the fuselage, and is sandwiched between the fuselage and the wing. This secures the steel bar from all sides. The golf ball is confined by cleats in the fuselage structure. When bolted together, the fuselage forms a secure housing for the payloads.

To illustrate the aircraft architecture, Figure 5.1 was created to display the system design and integration. The figure is color coded to organize components into subgroups based on component responsibilities.

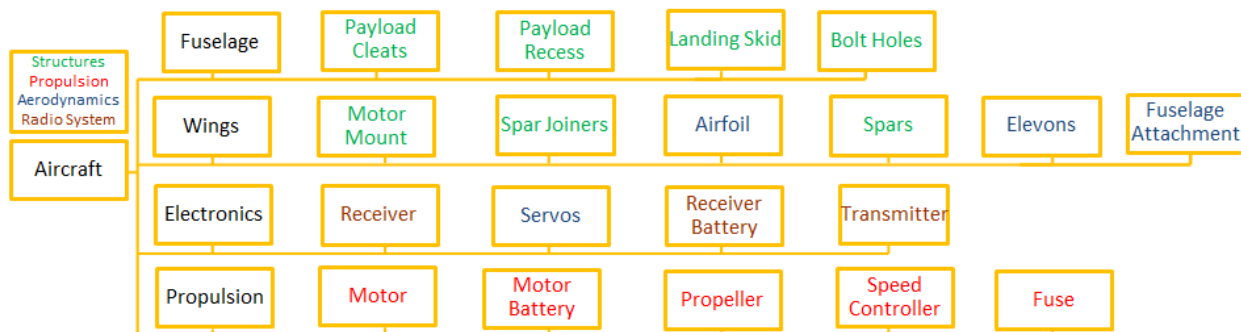


Figure 5.1: Aircraft architecture tree.

5.4 Propulsion System Analysis

The primary goal of the detailed propulsion design was to maximize the overall system efficiency while maintaining the required amount of thrust. The advance ratio, J , which is the ratio of the flight speed to rotational velocity of the propeller, was varied to study its effect on system efficiency. Using blade element momentum theory and specifications provided by the manufacturer, thrust, power, and propeller efficiency were calculated for a variety of commercially available propellers. The analysis showed that the propeller best suited for this system is the APC 5.5x3, yielding an overall system efficiency of 39.1% at an advance ratio of 0.4. The efficiency trends are displayed in Figure 5.2. These trends were further analyzed and validated using flight and wind tunnel testing. Specific numbers can be found in Section 8.1.4.

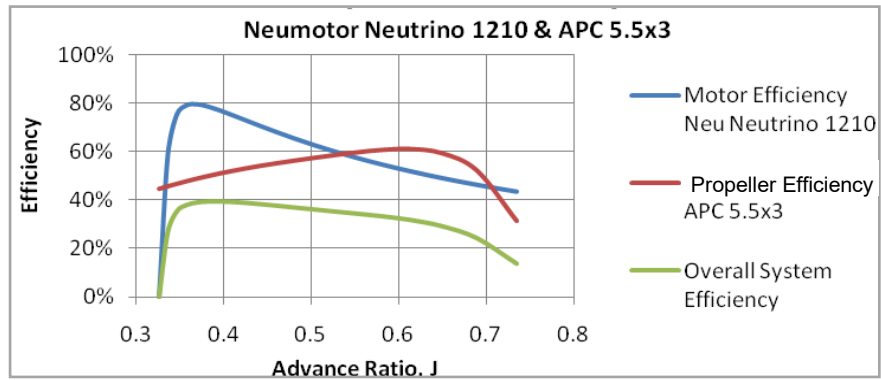


Figure 5.2: Propulsion efficiency.

5.5 Weight and Balance Table

The weight and balance table was tabulated based on component weights and a distance from the front of the motor mount, which served as a datum. The calculated C.G. of the aircraft for each mission was between the forward and aft limits of 3.04 and 3.24 in., respectively. This is shown in Table 5.2.

Table 5.2: Weight and balance table.

| | | Mission One | | | Mission Two | | | Mission Three | | |
|-------------------------|----------------------|-------------|-------------------------------|-----------------|-------------|-------------------------------|-----------------|---------------|-------------------------------|-----------------|
| Component | | Weight (oz) | Component C.G. Location (in.) | Moment (oz-in.) | Weight (oz) | Component C.G. Location (in.) | Moment (oz-in.) | Weight (oz) | Component C.G. Location (in.) | Moment (oz-in.) |
| Structures | Wing Structure | 0.14 | 3.38 | 0.47 | 0.14 | 3.38 | 0.47 | 0.14 | 3.38 | 0.47 |
| | Fuselage | 0.29 | 3.20 | 0.93 | 0.29 | 3.20 | 0.93 | 0.29 | 3.20 | 0.93 |
| | Winglets | 0.03 | 7.81 | 0.23 | 0.03 | 7.81 | 0.23 | 0.03 | 7.81 | 0.23 |
| | Monokote | 0.02 | -- | -- | 0.02 | -- | -- | 0.02 | -- | -- |
| Propulsion | Motor | 0.50 | -0.32 | -0.16 | 0.50 | -0.32 | -0.16 | 0.50 | -0.32 | -0.16 |
| | Battery | 1.80 | 4.73 | 8.51 | 1.80 | 4.73 | 8.51 | 1.80 | 4.73 | 8.51 |
| | Speed Controller | 0.22 | 2.25 | 0.50 | 0.22 | 2.25 | 0.50 | 0.22 | 2.25 | 0.50 |
| | Electrical Fuse | 0.02 | 2.00 | 0.04 | 0.02 | 2.00 | 0.04 | 0.02 | 2.00 | 0.04 |
| | Propeller | 0.15 | -0.68 | -0.10 | 0.15 | -0.68 | -0.10 | 0.15 | -0.68 | -0.10 |
| Control System | Elevons | 0.03 | 6.30 | 0.19 | 0.03 | 6.30 | 0.19 | 0.03 | 6.30 | 0.19 |
| | Receiver | 0.19 | 1.88 | 0.36 | 0.19 | 1.88 | 0.36 | 0.19 | 1.88 | 0.36 |
| | Receiver Battery | 0.36 | 2.41 | 0.87 | 0.36 | 2.41 | 0.87 | 0.36 | 2.41 | 0.87 |
| | Servos | 0.26 | 4.05 | 1.05 | 0.26 | 4.05 | 1.05 | 0.26 | 4.05 | 1.05 |
| Payload | Golf Ball/Steel Bars | | | | 1.60 | 3.30 | 5.28 | 1.60 | 2.97 | 4.75 |
| | Total | 4.01 | -- | 12.89 | 5.61 | -- | 18.17 | 5.61 | -- | 17.64 |
| C.G. of Aircraft (in.): | | 3.21 | | | 3.24 | | | 3.14 | | |

5.6 Mission Performance

With the final aircraft dimensions defined, the expected performance for each mission was evaluated. The scores are summarized along with the flight performance data in Table 5.3.



5.6.1 Mission One – Dash to Critical Target

In mission one, score is based on the number of laps completed in the allotted four minute time span. For an estimated cruise velocity of 42 ft/s and a turning G load factor of 3 Gs, it will be possible for the aircraft to complete four laps. Since the score calculation for this mission requires the maximum laps achieved by any competing aircraft, an exact score cannot be calculated. Assuming that the maximum number of laps completed will be eight, score is estimated to be: $M1 = 4/8 = 0.5$.

5.6.2 Mission Two – Ammo Re-supply

Mission two is a three-lap payload flight where score is based on payload weight fraction. The final aircraft design allows a steel bar of 0.1 lbs to be carried, resulting in a flight weight of 0.400 lbs. The score for mission two is estimated to be: $M2 = 3*(0.1/0.4) = 0.75$.

5.6.3 Mission Three – Medical Supply

Mission three is a three-lap payload flight where score is based on the number of golf balls carried. Since the score calculation for this mission is nondimensionalized by the maximum number of golf balls carried by any competing aircraft, an exact score cannot be calculated. Assuming that the maximum number of golf balls carried is 20, score is estimated to be: $M3 = 2*(1/20) = 0.1$.

5.7 Flight Performance

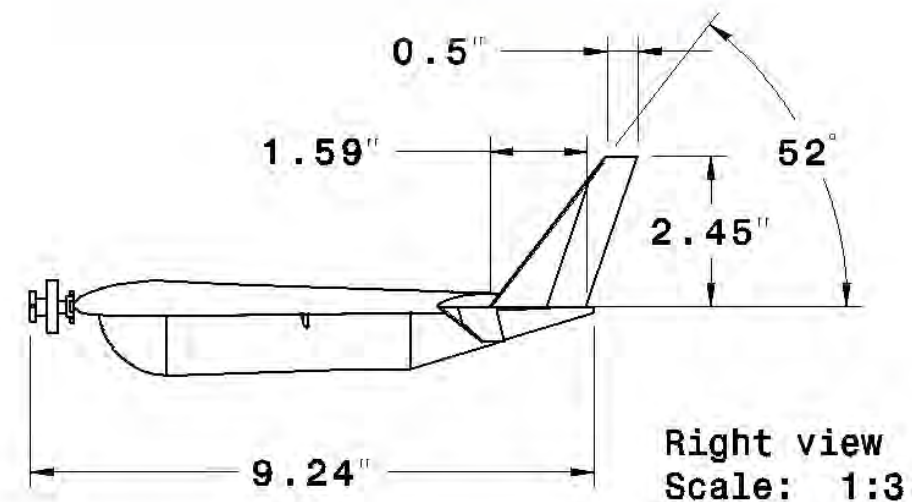
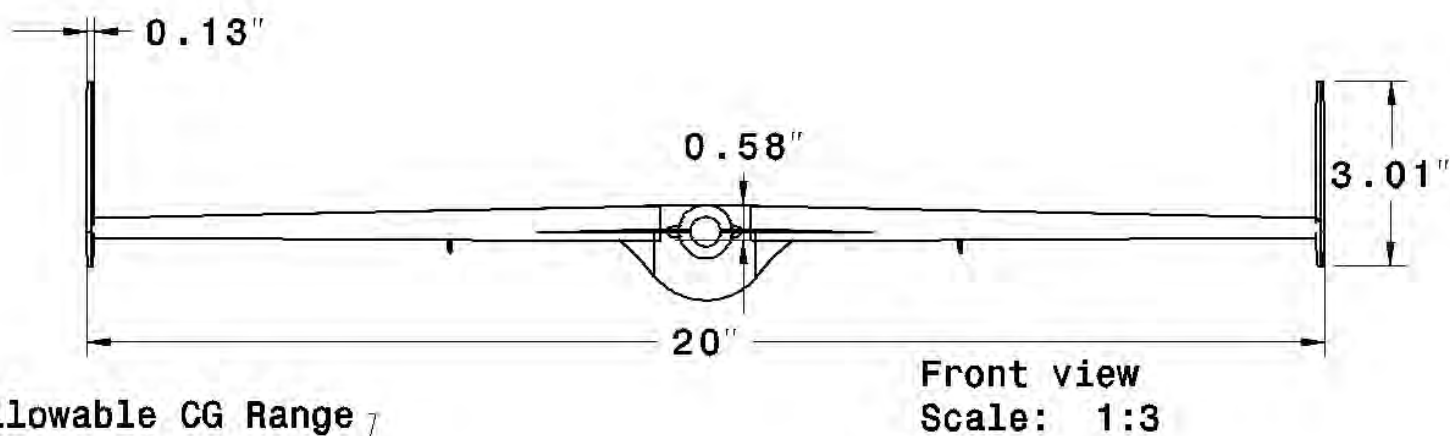
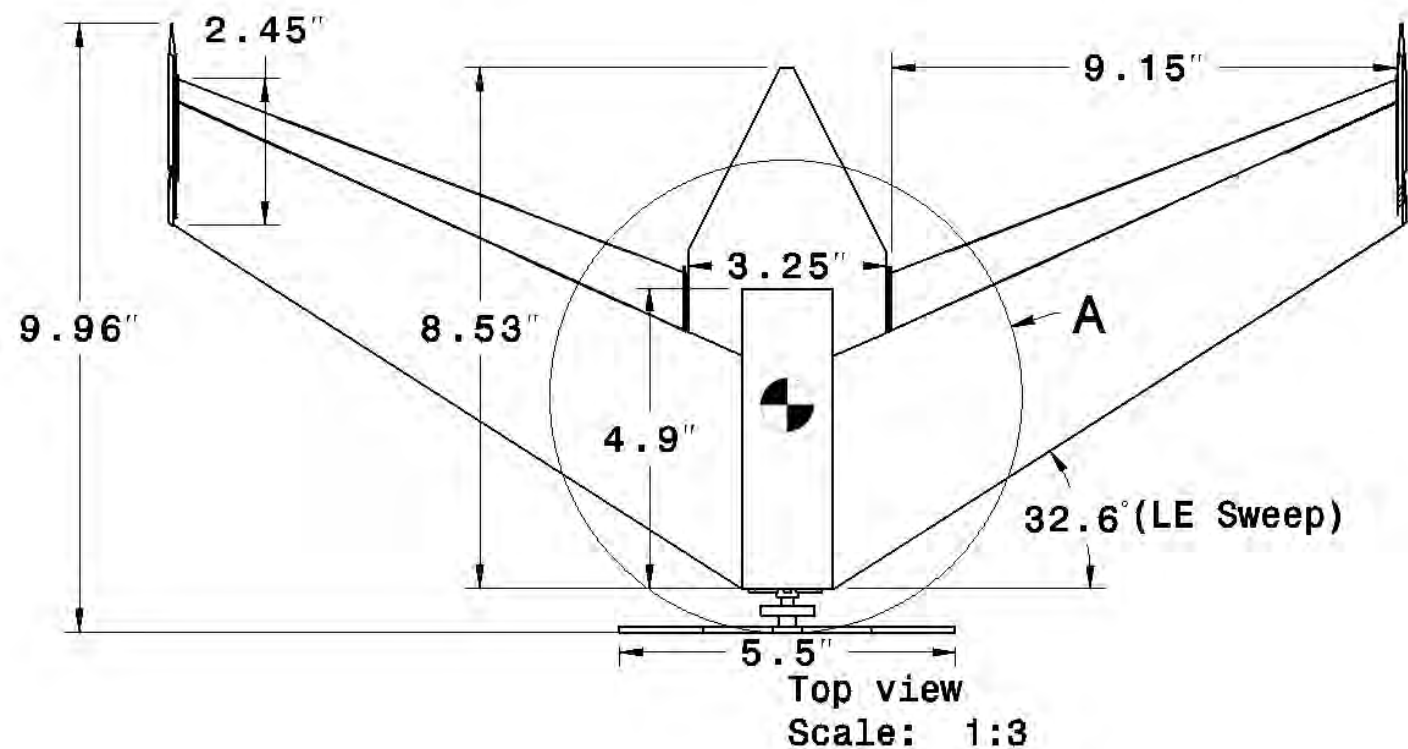
Dimensional parameters and mission profile predictions for the final competition aircraft are summarized in Table 5.3.

Table 5.3: Flight performance.

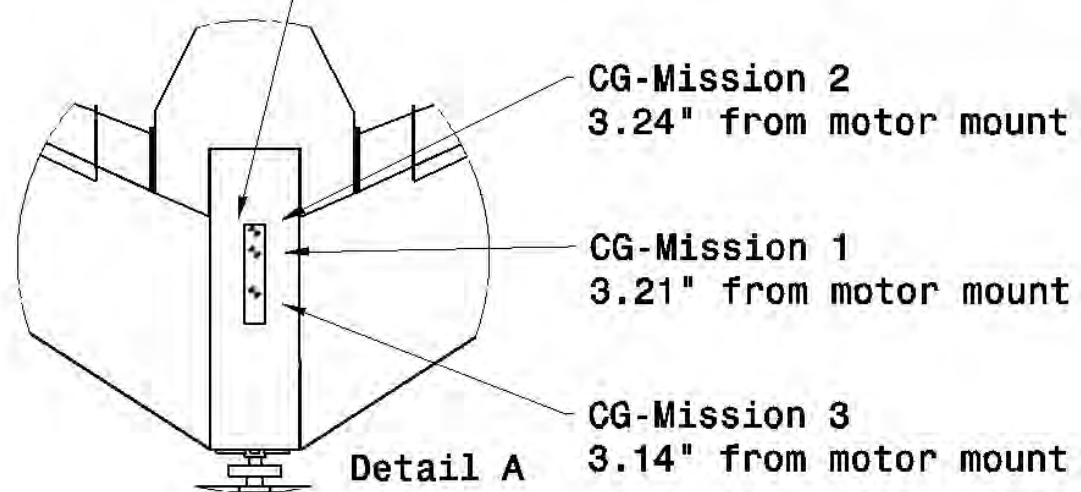
| Aircraft Parameters | | Mission Parameters | Mission One | Mission Two | Mission Three |
|-------------------------|-------|---------------------|-------------|-------------|---------------|
| L/D max | 13.5 | Takeoff Weight (oz) | 5 | 6.6 | 6.6 |
| C_{L0} | 0.17 | Payload (oz) | 0 | 1.6 | 1.6 |
| C_{Lmax} | 1.1 | Stall Speed (ft/s) | 23.4 | 26.9 | 26.9 |
| C_{D0} | 0.058 | Climb Rate (ft/s) | 25 | 25 | 25 |
| Max Thrust (oz) | 4 | Cruise Speed (ft/s) | 40 | 36 | 36 |
| Max Speed (ft/s) | 47 | Mission Score | 0.50 | 0.75 | 0.10 |
| Max Range (ft) | 11000 | Total Score | 2.46 | | |
| Max Takeoff Weight (oz) | 6.6 | | | | |
| Max Payload (oz) | 1.6 | | | | |
| Flight Weight (oz) | 5 | | | | |

5.8 Drawing Package

The drawing package was created from the aircraft design parameters and selected component configurations discussed in preliminary and detail design. *CATIA* was used as the computer aided design (CAD) package for designing components and configurations. The created drawings were used by the team for manufacturing parts and estimating the C.G. of the aircraft. The following images document the aircraft designed by Team Golfstream for the 2010-2011 DBF competition.



Allowable CG Range



Purdue University
TEAM GOLFSTREAM



DRAWN BY:
J. Towles-Moore

APPROVED BY:
T. Finn

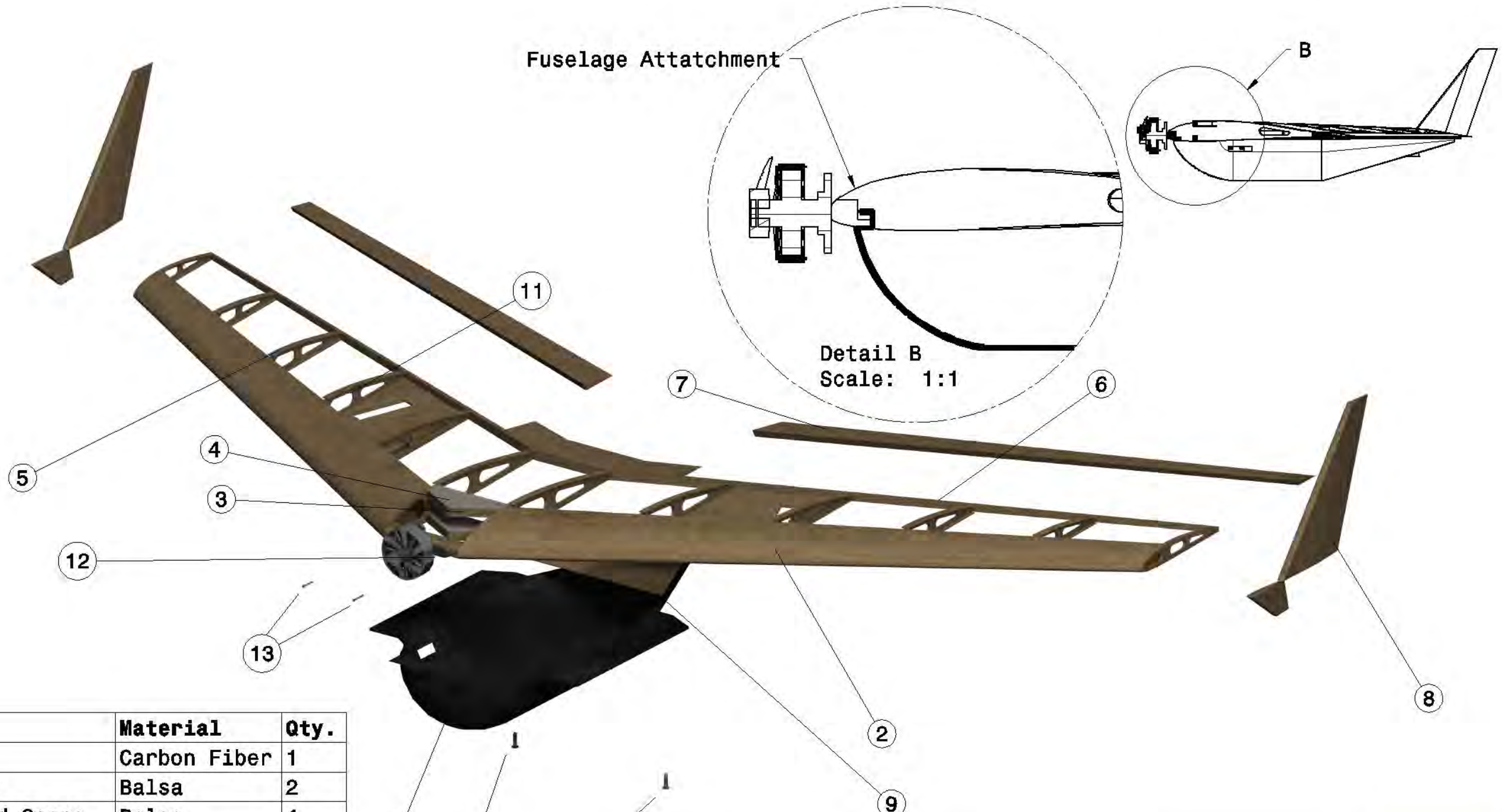
AIRCRAFT THREE-VIEW

UNLESS OTHERWISE SPECIFIED ALL DIMENSIONS ARE GIVEN IN INCHES

| SCALE: | DRAWING NO. | REVISION |
|--------|-------------|----------|
| 1:3 | 2011-001 | A |

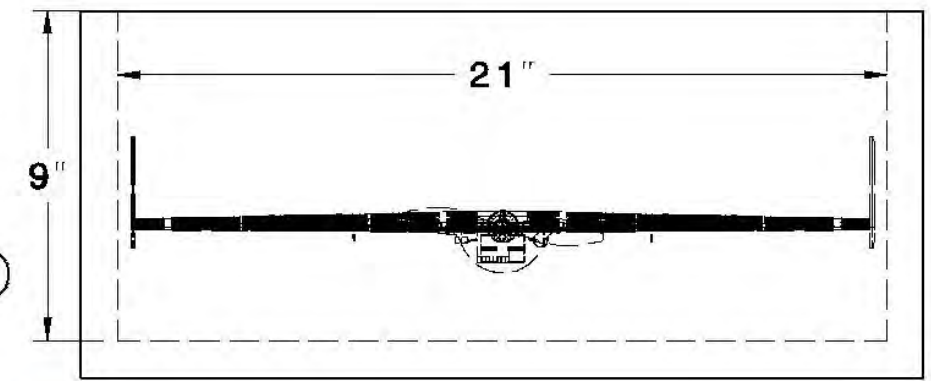
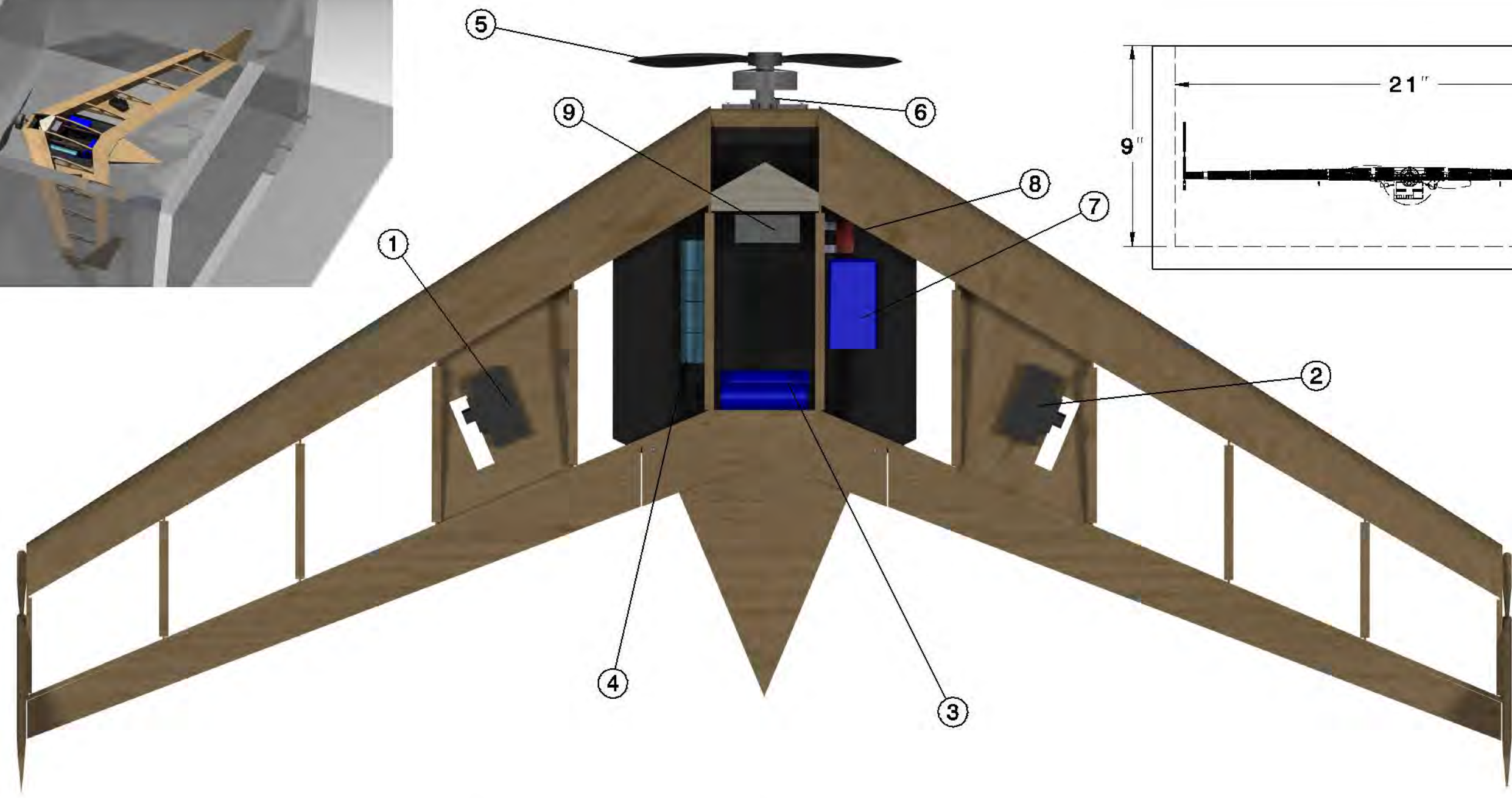
ANGLE TOLERANCE: 30'
DIMENSION TOLERANCE: .04

| DATE OF APPROVAL | REPORT PAGE | PAGE 1 OF 4 |
|------------------|-------------|-------------|
| 02/22/2011 | 42 OF 58 | |



| Part | Name | Material | Qty. |
|------|---------------------|--------------|------|
| 1 | Fuselage | Carbon Fiber | 1 |
| 2 | Leading Edge | Balsa | 2 |
| 3 | Quarter Chord Spars | Balsa | 4 |
| 4 | Spar Plates | Balsa | 4 |
| 5 | Ribs | Balsa | 12 |
| 6 | Trailing Edge Spar | Balsa | 2 |
| 7 | Ailerons | Balsa | 2 |
| 8 | Winglets | Balsa | 2 |
| 9 | Fuselage Cover | Balsa | 1 |
| 10 | Fuselage Bolts | Nylon | 2 |
| 11 | Servo Mounts | Balsa | 1 |
| 12 | Motor Mount | Balsa | 1 |
| 13 | Motor Mount Screws | Steel | 2 |

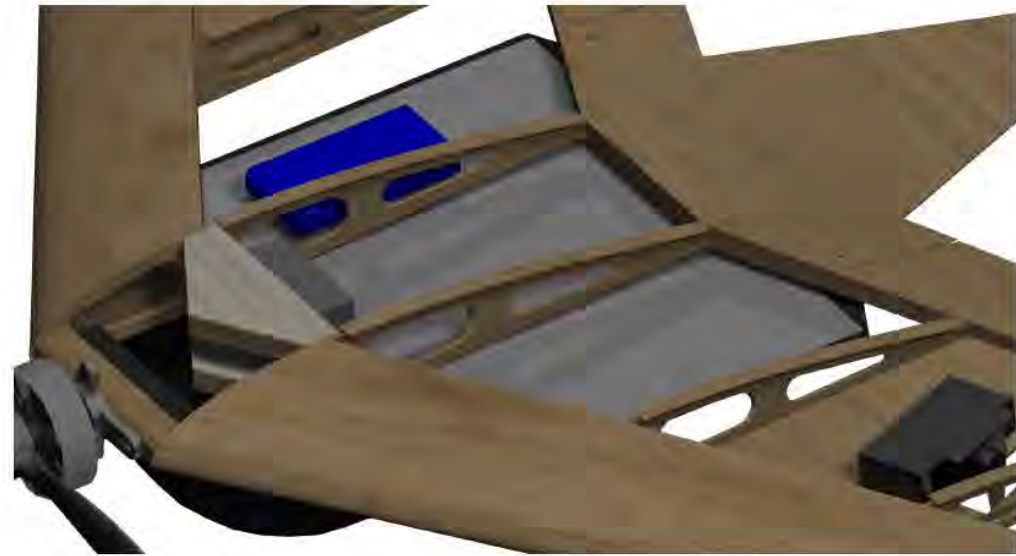
| | | | |
|---|--|---|--------------------------------|
| Purdue University TEAM GOLFSTREAM | |  | |
| DRAWN BY: W. O'Neil | | <h1>Structural Layout</h1> | |
| APPROVED BY: T. Finn | | | |
| UNLESS OTHERWISE SPECIFIED ALL DIMENSIONS ARE GIVEN IN INCHES | | SCALE: 1:2 | DRAWING NO. 2011-002 |
| | | REVISION A | |
| ANGLE TOLERANCE: -- DIMENSION TOLERANCE: -- | | DATE OF APPROVAL 02/22/2011 | REPORT PAGE 43 OF 58 |
| | | PAGE 2 OF 4 | |



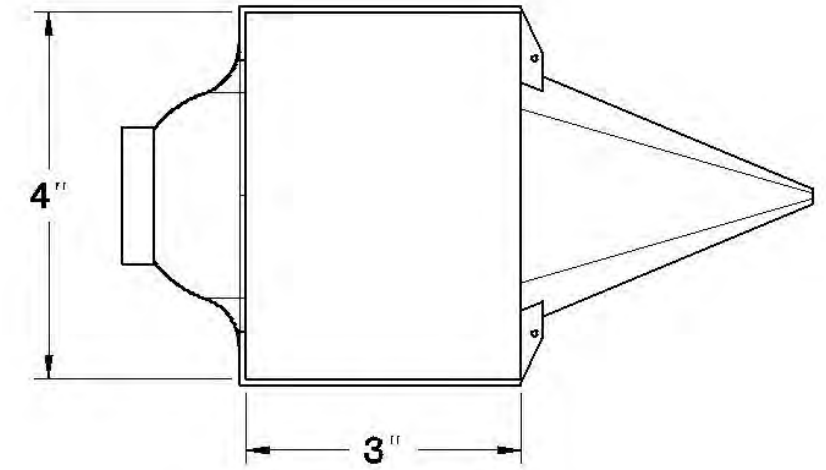
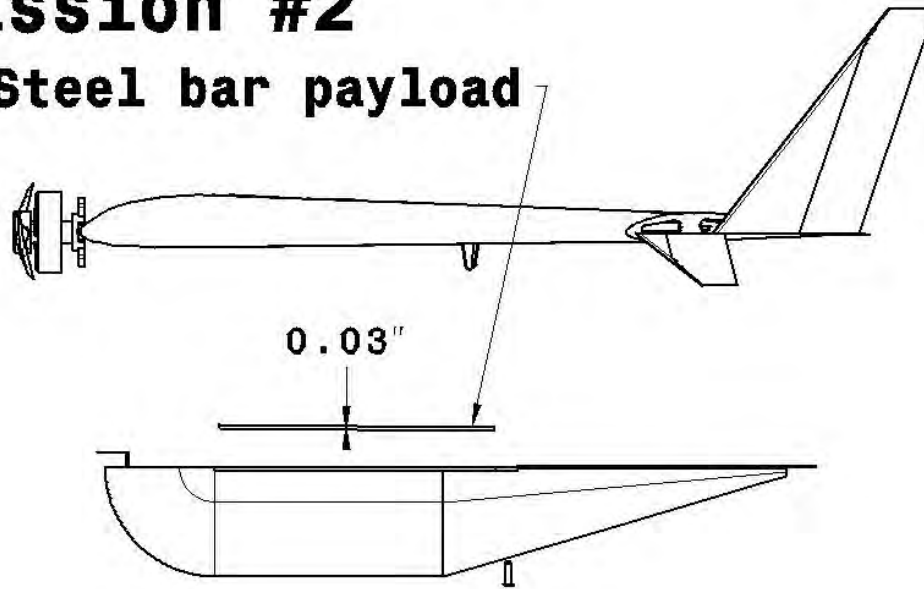
| SYSTEMS COMPONENTS | | | |
|--------------------|--------------------|-----------------------------|------|
| Item | Part | Source | Qty. |
| 1 | Left Elevon Servo | Blue Arrow S0361 | 1 |
| 2 | Right Elevon Servo | Blue Arrow S0361 | 1 |
| 3 | Propulsion Battery | KAN 400 mAh 2/3 AAA Cells | 6 |
| 4 | Receiver Battery | KAN 125 mAh 1/4 AAA Cells | 4 |
| 5 | Propeller | APC 5.5X3 | 1 |
| 6 | Motor | Neu Neutrino 1210 | 1 |
| 7 | Speed Controller | Castle Creations Phoenix 10 | 1 |
| 8 | Fuse | ATO 20 Amp Mini | 1 |
| 9 | Receiver | Spektrum AR6255 | 1 |

Purdue University
TEAM GOLFSTREAM

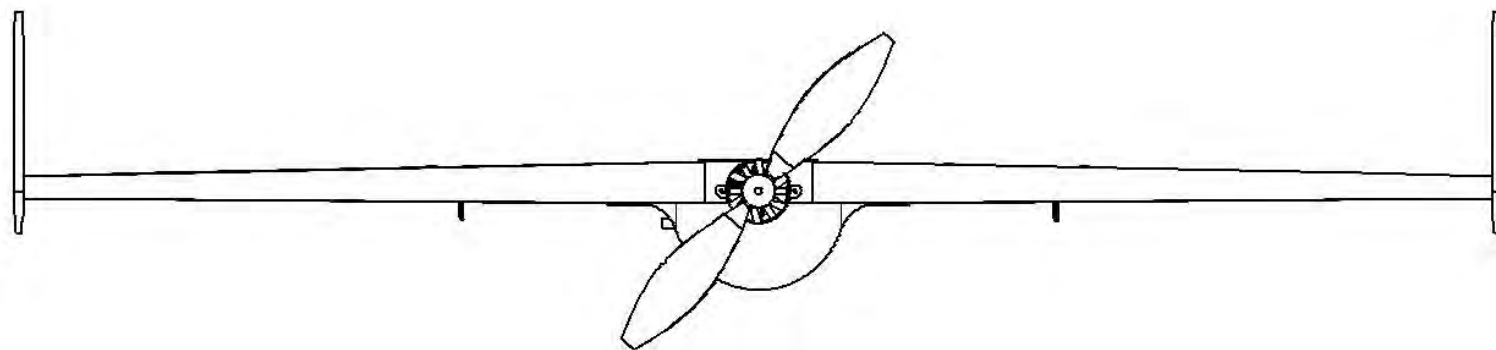
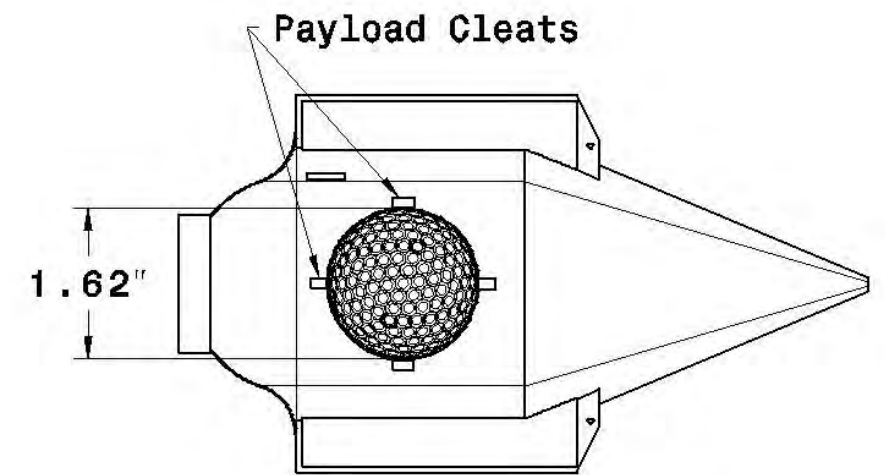
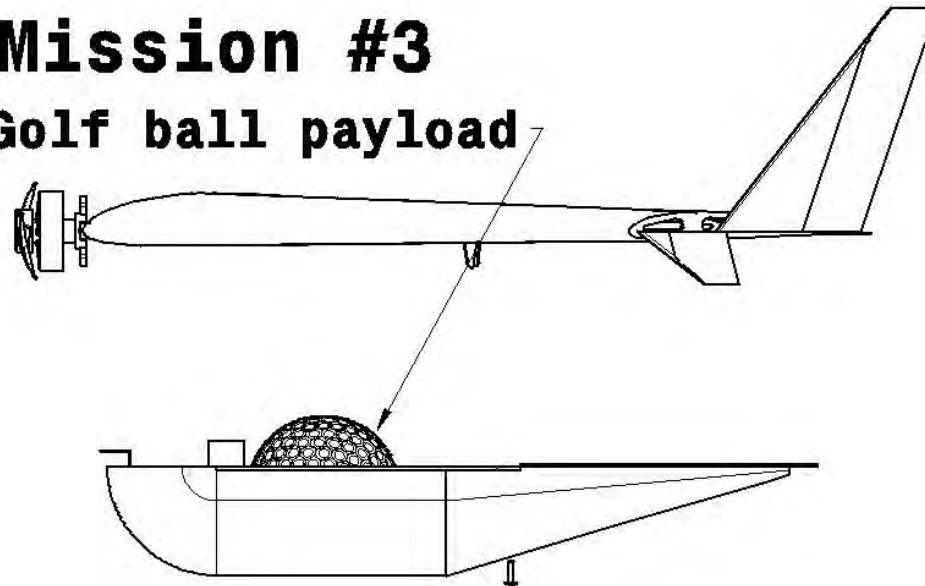
| | | | |
|---|--------------------------------|-------------------------|-------------|
| DRAWN BY: W. O'Neill | | <h1>Systems Layout</h1> | |
| APPROVED BY: T. Finn | | | |
| UNLESS OTHERWISE SPECIFIED ALL DIMENSIONS ARE GIVEN IN INCHES | | | |
| SCALE: 1:2 | DRAWING NO. 2011-003 | REVISION A | |
| ANGLE TOLERANCE: -- DIMENSION TOLERANCE: -- | DATE OF APPROVAL 02/22/2011 | REPORT PAGE 44 OF 58 | PAGE 3 OF 4 |



Mission #2
Steel bar payload



Mission #3
Golf ball payload



Purdue University
 TEAM GOLFSTREAM



DRAWN BY:
 W. O'Neill
 APPROVED BY:
 T. Finn

Payload Accommodation

UNLESS OTHERWISE
 SPECIFIED ALL
 DIMENSIONS ARE
 GIVEN IN INCHES

| SCALE: | DRAWING NO. | REVISION |
|--------|-------------|----------|
| 1:2 | 2011-004 | A |

| ANGLE TOLERANCE: -- | DATE OF APPROVAL | REPORT PAGE | PAGE 4 OF 4 |
|-------------------------|------------------|-------------|-------------|
| DIMENSION TOLERANCE: -- | 02/22/2011 | 45 OF 58 | |



6.0 Manufacturing Plan

6.1 Prototype Construction

Throughout the iterative spiral design process, several different working prototypes were fabricated. In each case, a CAD model of the new aircraft was created using *CATIA*. These CAD models were used to create templates for manufacturing aircraft parts of all prototypes. For the first prototype, the aircraft was fabricated using a built-up balsa structure. Subsequent prototypes were constructed from Foamular 250 extruded polystyrene foam and machined using a computer numerical control (CNC) hotwire cutter. This method was adopted to reduce the time spent on manufacturing, allowing for more design iterations. When the prototype was deemed to be a practical and efficient design, they were once again manufactured using balsa wood to better represent the final competition aircraft.

6.2 Material Analysis and Manufacturing Selection

Selecting the correct building materials and manufacturing techniques was paramount to manufacturing since this would directly impact structural integrity and weight. For this reason, several types of materials and manufacturing processes were considered and evaluated.

6.2.1 Material Selection

Balsa, foam, and carbon fiber were considered for the construction of the aircraft, as listed in Table 6.1.

- **Foam Build-up** – Using a lightweight foam material, aircraft wings can be cut out rapidly with either a CNC hotwire or 5-axis CNC mill. Using this material, the amount of manual fabrication can be reduced, allowing more test aircraft to be built and flight tested over a short period. A drawback to this material is that a solid foam wing can lead to a heavier overall design. A prototype was built using this material to determine the approximate flight weight associated with this method. The overall weight of this prototype was 7.2 oz.
- **Balsa Build-up** – By using balsa, which has superior strength to weight properties, more efficient structural geometries can be created. This material allows for a stronger and lighter airframe but also takes much more time to manufacture. A prototype was built using this material to determine the approximate flight weight. The prototype weighed a total of 6.0 oz.
- **Carbon Fiber** – Carbon fiber offers extreme strength and rigidity; however it is heavier and more difficult to shape than balsa or foam.

Table 6.1: Materials selection FOM.

| Merit | Weight | Balsa Build-up | Pink Foam | Carbon Fiber |
|-------------------|--------|----------------|-----------|--------------|
| Weight | 50% | 4 | 3 | 2 |
| Manufacturability | 20% | 3 | 4 | 2 |
| Repairability | 15% | 3 | 5 | 4 |
| Durability | 15% | 3 | 2 | 5 |
| Total | 100% | 3.5 | 3.35 | 2.75 |



The balsa build-up method was chosen because it offered many advantages over the foam method. While a foam aircraft could be built in a shorter time frame, the superior structural strength and weight savings made the balsa build-up method the preferred choice.

6.2.2 Manufacturing Methods

Several potential methods were considered for cutting the two-dimensional balsa profiles; CNC milling, water jet cutting, laser cutting, and cutting by hand. The ideal method should be both accurate and efficient, given time and money constraints. Table 6.2 was created to aid this decision.

Table 6.2: Manufacturing methods FOM.

| Merit | Weight | CNC | Water Jet | Laser Cutter | Hand Cut |
|---------------|--------|-----|-----------|--------------|----------|
| Accuracy | 50% | 3 | 4 | 5 | 1 |
| Time | 20% | 2 | 3 | 5 | 1 |
| Accessibility | 20% | 4 | 2 | 3 | 5 |
| Cost | 10% | 3 | 2 | 3 | 5 |
| Total | 100% | 3 | 3.2 | 4.4 | 2.2 |

The laser cutting method was chosen as the best method to manufacture the individual components because it can accurately cut out multiple parts in a short amount of time.

A wood jig was constructed that secured the wing cross sections while building the aircraft. This jig was used to ensure that the balsa wing ribs were accurately positioned. Once the ribs were in place, the upper spar cap was glued into place to secure the ribs. The wing assembly was then removed from the jig and the lower spar cap, leading edge spar, shear webs, and balsa sheeting were added to complete the wing structure. This process was repeated for the other wing half.

The two wing halves were then connected by gluing their respective quarter-chord spars together. To increase the strength of the glue joint, a small piece of balsa was used to span the joint. The motor mount was formed by gluing a piece of plywood to the front of the aircraft. MonoKote was used to cover the wing and form the elevon hinge joints. Once the wing was finished, an aerodynamic fuselage design was modeled using *CATIA*. The 5-axis CNC mill used this model to cut out a female mold from a solid block of foam. The female mold was then used to lay up a carbon fiber sheet. Epoxy resin was applied to the carbon fiber mold and vacuum bagged until the mold was set. The resulting carbon fiber fuselage was removed from the mold and modified to use two nylon bolts to attach to the wing structure. The fuselage has sufficient interior room to hold all payloads and electronics while creating a durable, lightweight surface to land on.

6.3 Manufacturing Milestones

Figure 6.1 summarizes the manufacturing timeline of the aircraft prototypes and the plans for future iterations. Final construction refers to assembling and fitting the aircraft with all necessary electronics.



adjusted to minimize drag while maintaining acceptable yaw stability. In the second test, the elevons were tested to ensure adequate pitch and roll authority were achieved while keeping a minimal overall weight. All tests utilized the wind tunnel apparatus pictured in Figure 7.1.

7.1.3 Structures

Loading tests were performed on key aircraft structures to verify that failure loads exceeded design requirements. The wing structure was tested by fixing the wing spar at the root and applying a load at the tip until failure occurred. The same apparatus was used to test torsional strength of the D-tube and glue joint strength at the union of the wing halves. These tests identified potential failure points and design revisions were made accordingly. Figure 7.2 illustrates the apparatus used for the structural tests.



Figure 7.2: Structural test apparatus.

7.1.4 Propulsion

A series of propulsion tests were executed to evaluate the performance of various motor, battery, and propeller combinations. A wind tunnel and force balance were used to measure the thrust produced at various flight speeds. Voltage and current draw of the propulsion system was measured during flight tests using an Eagle Tree telemetry system. Figure 7.3 illustrates the apparatus and setup used for wind tunnel propulsion testing.



Figure 7.3: Propulsion test setup.

7.1.5 Flight Testing

A series of flight tests were completed to evaluate the system performance of each completed prototype. Several parameters were measured and recorded for each flight test. These include cruise speed, stall speed, flight time, and power consumption. After basic flight characteristics were evaluated, each mission was then simulated. Areas of improvement were identified through these flight analyses and were



addressed in subsequent iterations. Figure 7.4 displays an example of a flight test checklist that was filled out to document each flight.

| | | | | | | | | | | |
|--|--|---------------|---------------------|----------|-------------------|---------------------|-------------|--------------------|---------------------|----------|
| Pilot | Nick Setzer | | Flight # | 8- | | Startup Procedure | | Shutdown Procedure | | |
| Date | 2/05/2011 | | Flight Time | 4:16 min | | CG Check | ✓ | | Propulsion | ✓ |
| Mission Objectives: | To obtain experimental values for the mAh, amperage, wattage, and voltage during Mission 2 using an Eagle Tree | | | | | Transmitter Program | ✓ | | Receiver | ✓ |
| | | | | | | Antenna | ✓ | | Transmitter | ✓ |
| Weather Conditions | | | | | | Transmitter ON | ✓ | | Battery Post Flight | |
| Wind Velocity (MPH) 11 (WSW) Temperature (°F) 34 | | | | | | Receiver ON | ✓ | | Heat | Voltage |
| Pre-Flight | | | | | | Motor ON | ✓ | | Transmitter | cold 5.5 |
| | | | | | | Static Test | ✓ | | Receiver | cold 4.8 |
| | | | | | | Radio | | Propulsion | warm 8.1 | |
| Secure | ✓ | | ✓ | | ✓ | | Range Check | ✓ | | |
| Batteries | Type: N, MH | Cell Count: 7 | Capacity (mAh): 400 | | Directional Check | | ✓ | | | |
| Pilot Comments | quick, adequate power, maneuverable, good handling/stall characteristics | | | | | | | | | |

Figure 7.4: Flight test checklist.

Figure 7.5 is an image taken during actual flight testing. The prototype shown in the image is the same aircraft that is referenced in Figure 7.4.



Figure 7.5: Flight test photo.

7.2 Master Test Schedule

To ensure that all test objectives were accomplished on time, two test schedules were created. Table 7.1 shows test objectives for each aircraft subsystem along with corresponding start and end dates.

Table 7.1: Master test schedule.

| Test Area | Test | Objective | Start Date | End Date |
|-----------------------|------------------------|---|------------|-----------|
| Aerodynamics | Wind Tunnel | Obtain lift, drag, pitching, and stall characteristics | 1/24/2011 | 2/15/2011 |
| Dynamics and Controls | Elevon Sizing | Find the minimum size needed for appropriate control authority | 1/31/2011 | 2/14/2011 |
| | Winglet Sizing | Find the minimum size needed for yaw stability | 1/31/2011 | 2/14/2011 |
| Structures | Spar Testing | Determine spar dimensions for 2.5 G load | 1/24/2011 | 2/12/2011 |
| | Glue Joint | Determine glue joint strength | 1/24/2011 | 2/12/2011 |
| | Wing Testing | Determine torsion strength and wing loading | 1/24/2011 | 2/12/2011 |
| Propulsion | Propeller | Determine correct sizing and propeller shape | 1/24/2011 | 2/14/2011 |
| | Motor | Determine what motor produces necessary thrust | 1/24/2011 | 2/14/2011 |
| | Battery | Test various battery sizes for thrust alterations | 1/24/2011 | 2/14/2011 |
| Flight Test | Flight Data | Obtain flight data such as voltage, amperage, and wattage of aircraft | 1/24/2011 | 2/13/2011 |
| | Mission Simulations | Simulate each mission for competition | 1/24/2011 | 4/10/2011 |
| | Flight Characteristics | Determine necessary design changes for improved handling | 1/24/2011 | 4/10/2011 |



The flight test schedule, arranged by aircraft iteration, is shown in Table 7.2. This table displays the payload, flight objectives, and flight dates.

Table 7.2: Flight test schedule.

| Flight | Aircraft (Prototype) | Payload | Objective | Date |
|--------|----------------------|------------|-------------------------|-----------|
| 1 | Original Design (1) | None | First Test Flight | 1/17/2011 |
| 2 | Original Design (1) | None | First Successful Flight | 1/22/2011 |
| 3 | Foam Wing (2) | None | Familiarization Flight | 1/29/2011 |
| 4 | Foam Wing (2) | Golf Ball | Mission Three | 1/29/2011 |
| 5 | Balsa Build-up (3) | None | Mission One | 2/04/2011 |
| 6 | Balsa Build-up (3) | None | Mission One | 2/04/2011 |
| 7 | Balsa Build-up (3) | None | Familiarization Flight | 2/05/2011 |
| 8 | Balsa Build-up (3) | Eagle Tree | Mission One | 2/05/2011 |
| 9 | Balsa Build-up (3) | None | Mission One | 2/05/2011 |
| 10 | Balsa Build-up (3) | None | Mission One | 2/05/2011 |
| 11 | Balsa Build-up (3) | Golf Ball | Mission Three | 2/13/2011 |
| 12 | Balsa Build-up (3) | Golf Ball | Mission Three | 2/13/2011 |

8.0 Performance Results

In order to confirm the expected results obtained from the design process, a variety of tests were completed to measure actual aircraft performance. The results of these tests were applied to the final design and were a crucial part in the optimization of the aircraft.

8.1 Subsystem Performance

Based on test plans outlined in section 7, performance data of each key subsystem was obtained through experimentation and flight testing. These results are compared to the predictions in sections 4 and 5.

8.1.1 Aerodynamic Performance

The aerodynamic performance estimates of the entire aircraft were validated using extensive wind tunnel experimentation and flight testing. The prototype aircraft was tested at Purdue University's subsonic Boeing Wind Tunnel to evaluate the aerodynamic characteristics of the integrated assembly and serve as a basis of comparison with theoretical data. The data obtained from wind tunnel testing corresponds to a Reynolds number of 66420, which encompasses the estimated cruise velocity of 36 ft/sec and the expected flight conditions of Tucson, AZ. Figure 8.1 compares wind tunnel data to experimental data.

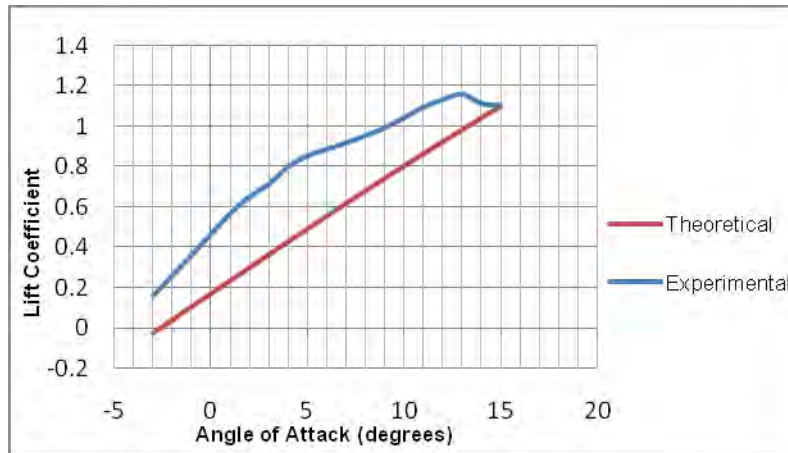


Figure 8.1: Lift coefficient vs. angle of attack.

Figure 8.1 shows the comparison between theoretical data obtained from *XFLR5* and experimental lift coefficient curves. *XFLR5* underestimates the lift generated by a 3-D wing with winglets, so a small discrepancy was expected. From this plot, it is shown that the selected wing satisfies the C_L envelope requirements outlined in section 4.3.1. The experimental results indicate a stall angle of 13 degrees and a constantly higher C_L value over the entire range of angle of attack.

In addition to lift coefficient, the drag polar was compared and is displayed in Figure 8.2. As with the lift, the *XFLR5* simulation underestimated the total drag on the airfoil.

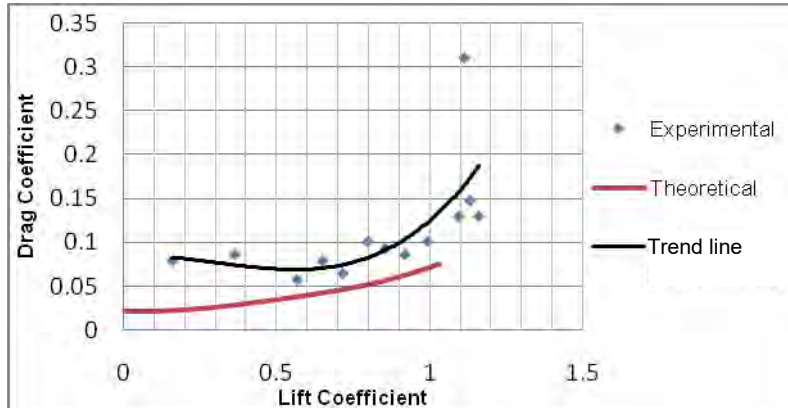


Figure 8.2: Drag polar.

This drag polar exhibits a sharp increase in drag at a C_L value of 1.16. This corresponds to the onset of stall from Figure 8.1. The drag is relatively low over the entire C_L flight envelope discussed in section 4.3. There is a noticeable fluctuation in the drag data points attributed to the accuracy of the instrumentation measuring small magnitude drag forces. Other errors are attributed to the design of the mounting apparatus. Since the aircraft is mounted on a small flat plate for wind tunnel testing, additional lift and drag are generated, primarily at nonzero angles of attack. This causes the experimental lift and drag to be slightly overestimated. The contributions of the mount were accounted for by running the wind tunnel



without the aircraft in the test section. Error is also present in the theoretical estimation obtained from the *XFLR5* software. The *XFLR5* simulations have difficulty simulating low Reynolds number flows, transition effects, and winglet contributions. Table 8.1 shows the theoretical and experimental drag and lift.

Table 8.1: Theoretical and experimental drag and lift.

| Model | C_{D0} | C_{Lmax} |
|--------------|----------|------------|
| Theoretical | 0.022 | 1.10 |
| Experimental | 0.055 | 1.16 |

The theoretical zero-lift coefficient of drag is less than half the experimental value. This is a result of the theoretical simulations run in *XFLR5*, assuming no fuselage. This assumption accounts for most of the error between these values, as the fuselage is the largest contributor to drag. The software program also does not accurately model the stall characteristics of a 3-D wing. Therefore, the maximum C_L will be lower than the experimental value because of the inherent inability of the simulation to predict the onset of stall.

8.1.2 Dynamics and Controls Performance

Section 4.4.2 called for a comparison between two different winglet designs. This was achieved with wind tunnel tests that were conducted to analyze how the aircraft performed with both winglets attached. The first winglet set, which was designed from theoretical analysis, has a planform area of 4.5 in.² while the other, based on a proposed design found in Raymer³, is sized at 3.07 in.².

The yaw stability of the aircraft with each winglet was compared. Measuring the aircraft yawing moment showed how well the aircraft adjusts to incoming flow as it stabilizes itself. At various sideslip angles, the yaw moment of the aircraft at a typical flight speed of 40 ft/s was measured. In addition, a third data set with no winglets was also tested to serve as a reference set. Figure 8.3 illustrates the results.

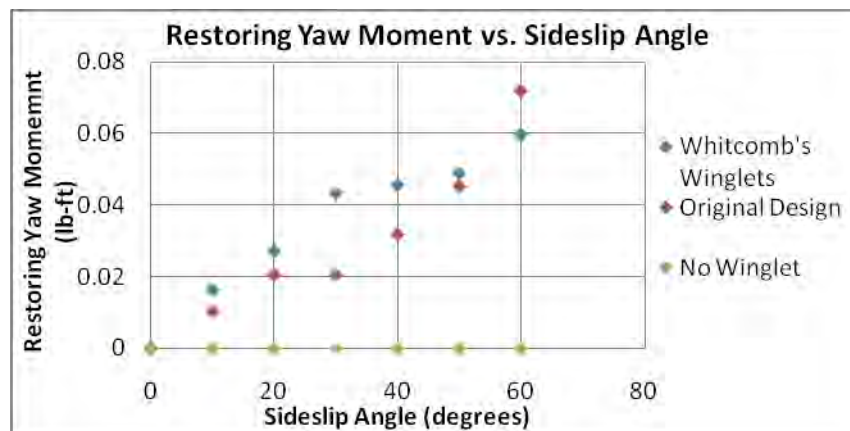


Figure 8.3: Yaw stability for winglets.

As expected, the aircraft did not demonstrate yaw stability without winglets. Although Whitcomb's proposed winglets were smaller in size, they generally exhibited a greater yawing moment than the original design. Since it is known that the original winglet design is sufficient for yaw stability for the aircraft, it can be inferred that Whitcomb's design will be also be sufficiently stable.



Wind tunnel testing showed that wings fitted with Whitcomb's winglets at cruise speed and no sideslip angle experienced a drag force of 0.17 lbs compared to 0.19 lbs drag that was experienced with the original winglets, which was a 12% improvement in the aerodynamic performance. Whitcomb's proposed winglet configuration was chosen for providing greater stability and higher aerodynamic efficiency.

8.1.3 Structures Performance

With the wing dimensions and planform finalized, wingtip tests were conducted in order to optimize the strength and size of individual structural components. Three different test wings were built and tested in order to determine the best component combination. The first two wings were constructed with large spars to decrease the influence of small scale manufacturing errors. One of the wings was built with balsa sheeting over the leading and trailing edges to form a D-tube structure, as seen in Figure 8.4, and the other consisted of only the balsa ribs and spars. The D-tube structure greatly increases the torsional rigidity and aerodynamic efficiency of the wing. The two constructed wings were loaded until failure, and then compared to estimate the additional structural bending contribution of the D-tube. It was found that the D-tube increased the ultimate load by a factor of 1.9. The third wing was constructed from updated dimensions based on analytical estimations adjusted with data from the previous testing. Without the D-tube structure, the wing failed at approximately 3.5 Gs as seen in Table 8.2. This wing exceeded the necessary structural requirement for the competition wingtip test without contributions of the D-tube. Using a D-tube, the current configuration is able to withstand approximately 6.65 Gs. Further testing will yield a fully optimized wing that will minimize structural weight and withstanding a 4.0 G load. This represents a 1.6 factor of safety.



Figure 8.4: Broken full wing with D-tube.

Table 8.2: Wingtip results.

| Build-up | Cap Height (in) | Cap Width (in) | Web Height (in) | Web Width (in) | Load at Failure (oz) | G Load |
|--------------------------|-----------------|----------------|-----------------|----------------|----------------------|--------|
| Wing With D-Tube | 1/4 | 1/8 | 13/28 | 1/16 | 36.7 | 11.1 |
| Wing No D-Tube | 1/4 | 1/8 | 13/28 | 1/16 | 19.0 | 5.8 |
| Wing No D-Tube | 3/32 | 1/8 | 13/28 | 1/16 | 11.7 | 3.5 |
| Current Wing with D-Tube | 3/32 | 1/8 | 13/28 | 1/16 | 22.0 | 6.65 |

8.1.4 Propulsion Performance

Validation of the theoretical propulsion model described in sections 4.6 and 5.4 was critical to ensure that the aircraft meets the original design requirements. To do this, extensive wind tunnel and flight testing



was conducted to compare thrust, current draw, voltage drop, and milliamp-hour use. Purdue's Boeing Wind Tunnel was used to simulate all three mission speeds. To do this, the wind tunnel velocity was set to the predicted flight velocity and the throttle was set so that the thrust equaled the drag, simulating steady-state flying conditions. An Eagle Tree telemetry system gathered all relevant propulsion data. This setup is shown in Figure 8.5.



Figure 8.5: Propulsion wind tunnel test.

This wind tunnel testing validated the battery model used in the propulsion analysis. The experimental voltage drop throughout the mission one test flight very closely matches the analytical model. The wind tunnel testing also showed that both eCalc and the blade element momentum theory models over predicted the amount of thrust generated by this propulsion system. A comparison of the analytical and experimental propulsion data is summarized in Table 8.3.

Table 8.3: Comparison of analytical and experimental propulsion data.

| | Mission One Propulsion Comparison | | |
|-----------------------|-----------------------------------|--------------|------------------------|
| | Analytical | Experimental | Percent Difference (%) |
| Current (Amps) | 4.07 | 2.33 | -74.67 |
| Power (Watts) | 29.70 | 16.78 | -77.00 |
| Thrust (oz) | 3.32 | 1.12 | -196.43 |

Though it is unclear why the analytical models inaccurately predicted the propulsion attributes, the unexpected decrease in current draw allows for a longer battery life that is well above the duration of mission one. Higher pitch propellers are currently being tested to increase the dynamic thrust in order to more closely match the required design thrust and power requirements without adding additional weight. Preliminary results indicate that the APC 5.5x5.5 in. propeller may closely match the analytical results of the APC 5.5x3.0 propeller. If this holds true, all mission goals will be met for the expected design weight.

8.2 Aircraft Flight Performance

The first test flights resulted in crashes due to stability and control issues. These issues were determined to be related to incorrect C.G. placement, wing sweep, and static margin⁹. Another unexpected failure occurred during landing when the main wing spars failed at the glue joints. Once these issues were



resolved by moving the C.G. forward, increasing the sweep to 30°, and adding bracing to the wing spar joints, a successful test flight was achieved.

Once a successful prototype was built, practice runs for mission one were completed with an Eagle Tree telemetry system onboard. The Eagle Tree telemetry system was used to record current draw, voltage, and cumulative mAh for further analysis of the propulsion subsystem. Figures 8.6 and 8.7 illustrate results obtained during these tests. From Figure 8.6, the maximum current draw was 5.2 Amps, which is much lower than the maximum allowable current draw of 20 Amps as defined by the contest rules¹.

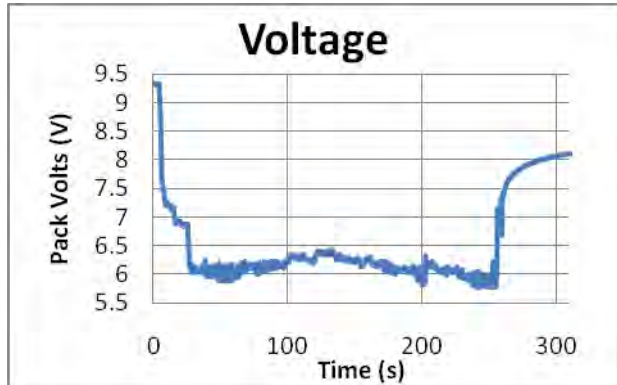
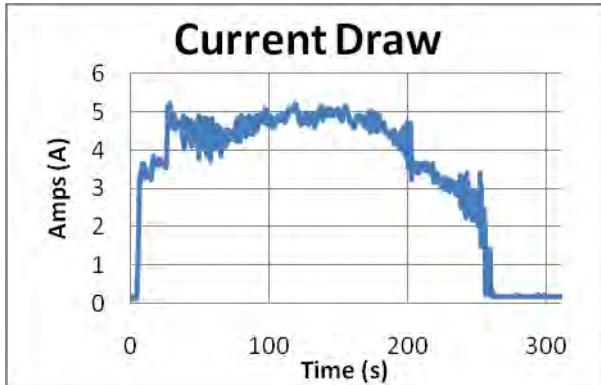


Figure 8.6: Current draw vs. time for mission one. Figure 8.7: Voltage vs. time for mission one.

Actual flight performance data for mission one is compared to the predicted performance in Table 8.4. A seven cell, 400 mAh NiMH battery was used for this flight test. It should be noted that this battery pack was used for testing and is not the pack to be used during competition. As seen in Table 8.4, this battery led to an actual velocity over 20% higher than the predicted velocity. However, even with this higher velocity, the actual time taken to complete four laps was 4:19. This discrepancy was attributed to lack of pilot familiarity with the aircraft, wide turns, and the practice course being longer than contest dimensions.

Table 8.4: Actual flight performance vs. predicted.

| Lap | Actual Time (s) | Actual Velocity (ft/s) | Predicted Velocity (ft/s) | Percent Difference |
|-----------|-----------------|------------------------|---------------------------|--------------------|
| 1 (Leg 1) | 25 | 50.4 | 40 | 20.6% |
| 1 (Leg 2) | 32 | 34.4 | 40 | -16.3% |
| 2 (Leg 1) | 20 | 63 | 40 | 36.5% |
| 2 (Leg 2) | 28.5 | 38.6 | 40 | -3.6% |
| 3 (Leg 1) | 20 | 63 | 40 | 36.5% |
| 3 (Leg 2) | 33 | 33.3 | 40 | -20.1% |
| 4 (Leg 1) | 22 | 57.3 | 40 | 30.2% |
| 4 (Leg 2) | N/A | N/A | 40 | N/A |
| Average | 25.8 | 48.6 | 40 | 21.5% |

Other results and observations from flight testing are listed in Table 8.5. Also listed are any comments relevant to the flight and any pertinent data gathered.



Table 8.5: Flight performance results.

| Flight Number | Objective | Results |
|---------------|-------------------------|---|
| 1 | First Test Flight | Crash due to instability |
| 2 | First Successful Flight | Solved most of the instability issues, crash landing |
| 3 | Familiarization Flight | Flew various maneuvers to test aircraft performance |
| 4 | Mission Three | Flew successfully with one golf ball and flight data recorder, |
| 5 | Mission Three | Flew mission two with new prototype loaded with one golf ball and flight recorder |
| 6 | Mission One | Flew four laps in 4:10 min, charger put 248 mAh into pack |
| 7 | Familiarization Flight | New day of test flying |
| 8 | Mission One | 4:19 min, four laps |
| 9 | Mission One | 4:35 min, four laps |
| 10 | Mission One | 2:56 min, four laps (3 cell lithium polymer pack) |
| 11 | Mission Three | One golf ball, three laps, 3:52 min |
| 12 | Mission Three | One golf ball, three laps, 3:45 min |

9.0 Glossary of Variables

| | | | |
|------------------|---|------------------------|--|
| L | Lift | q | Dynamic pressure |
| C_L | Whole aircraft coefficient of lift | $\phi_{L\epsilon}$ | Sweep angle at leading edge |
| ρ | Fluid density | λ | Taper ratio |
| u | Flow velocity | $C_{L\alpha}$ | Change in whole aircraft coefficient of lift with respect to angle of attack |
| S | Wetted area | x_{cg} | Location of center of gravity relative to leading edge |
| Re | Reynolds number | x_{acw} | Position of aerodynamic center of wing relative to leading edge |
| c | Chord length | x_{np} | Aircraft neutral point |
| μ | Dynamic viscosity | RMC | Root mean chord |
| A_{px} | Elevon power with respect to roll axis | MAC | Mean aerodynamic chord |
| A_{py} | Elevon power with respect to yaw axis | $C.G.$ | Center of gravity |
| a | Elevon power | SM | Static margin |
| $m1$ | Distance from C.G. to roll axis | y | Span-wise location |
| $m2$ | Distance from C.G. to yaw axis | σ | Stress |
| S_{VT} | Vertical tail size | M | Moment |
| C_{VT} | Vertical tail volume coefficient | I | Moment of inertia |
| b_w | Wing span | b | Width of rectangle |
| S_w | Wing area (planform area) | h | Height of rectangle |
| L_{VT} | Distance between aerodynamic center of wing and vertical tail | C_D | Drag coefficient |
| AR | Aspect ratio | C_{D0} | Profile drag |
| C_{Di} | Induced drag coefficient | C_{D2} | Quadratic drag coefficient |
| D | Drag | e | Span efficiency |
| $C_{L\alpha}$ | Change in lift with angle of attack | $C_{L,\delta\epsilon}$ | Change in lift with elevator deflection angle |
| $C_{M\alpha}$ | Change in pitch with angle of attack | $C_{M,\delta\epsilon}$ | Change in pitch with elevator deflection angle |
| $C_{n,\delta a}$ | Change in yaw with aileron deflection angle | $C_{l,\delta a}$ | Change in roll with aileron angle of attack |
| $C_{n\beta}$ | Change in yaw with sideslip | $C_{l\beta}$ | Change in roll with sideslip |



10.0 References

- ¹ AIAA Design/Build/Fly Competition -20010/11 Rules”, 7 Sept. 2010, <<http://www.aiaadbf.org/>>.
- ² Blanchard, B. S. and Fabrycky, W. J., “Bringing Systems Into Being,” *Systems Engineering and Analysis*, Fourth Edition, Prentice Hall, Upper Saddle River, NJ, 2006, p. 22-51.
- ³ Raymer, D.P. (2006). *Aircraft Design: A Conceptual Approach* (4th ed.). Washington, DC: AIAA, Inc.
- ⁴ Roskam, J. (1990). *Airplane Design: Part VI: Preliminary Calculation of Aerodynamic, Thrust, and Power Characteristics*. Ottawa, KS: Roskam Aviation and Engineering Corporation.
- ⁵ Andrisani, Dominick. (2006). *Flat Earth* [software]. Vers. 9.52. Indiana: Purdue University.
- ⁶ Sullivan, John P., “Advanced Theoretical Treatments of Propeller Aerodynamics”, Notes of Short Course presented at von Karmen Institute for Fluid Mechanics, Brussels, Belgium, May 1982
- ⁷ Drela, M., & Youngeron, H. (2010). *XFLR5* [software]. Massachusetts: MIT.
- ⁸ Gale, F. (1991). *Tailless Tale*. Olalla, WA: B²Streamlines.
- ⁹ Nickel, K. & Wohlfahrt, M. (1994). *Tailless Aircraft in Theory and Practice*. (E. M. Brown, Trans) Washington, DC: AIAA, Inc.
- ¹⁰ Gere, J., and Goodno, B. (2009). *Mechanics of Materials* (7th ed.). Mason, OH: Cengage Learning.
- ¹¹ Gaunt, J., Flores, J., & Perry, V. *Design, Fabrication, Structural Testing, and Numerical Analysis of a Small Scale Composite Wing*. California Polytechnic State University, San Luis Obispo.
- ¹² Houtzager, B., Overbeeke, R., & Vennix, R. (2009). *Mechanical, Physical, and Environmental Properties*. Retrieved from <http://www.matbase.com/matbase_material_properties_database.html>.
- ¹³ Buchmann, Ian. (2001). *Batteries –In a Portable World*. <<http://www.buchmann.ca/chap2-page2.asp>>.
- ¹⁴ (2011). *E-flite - Advancing Electric Flight*. <<http://www.e-fliterc.com>>.
- ¹⁵ (2010). *Castle Creations- World Class Brushless Motors*. <<http://www.castlecreations.com/products/neumotors/nm.html>>.
- ¹⁶ Muller, Markus. *eCalc –Online Propeller calculator*. < <http://www.ecalc.ch/indexcalc.htm>>.